

21

Final Report

Experimental and Theoretical Studies of Wave Propagation
in Granular, Rock and Porous Media

by

Martin H. Sadd
Arun Shukla

Prepared for

The U.S. Army Research Office

Under Contract No. DAAL03-86-K-0125

AD-A213 672

SDTIC
ELECTE
OCT 25 1989
D^{CS}D



Department of Mechanical Engineering & Applied Mechanics
University of Rhode Island
Kingston, RI 02881

DISTRIBUTION STATEMENT A
Approved for public release
Distribution Unlimited

August 1989

UNCLASSIFIED

MASTER COPY

FOR REPRODUCTION PURPOSES

SECURITY CLASSIFICATION OF THIS PAGE

REPORT DOCUMENTATION PAGE

1a. REPORT SECURITY CLASSIFICATION Unclassified		1b. RESTRICTIVE MARKINGS	
2a. SECURITY CLASSIFICATION AUTHORITY		3. DISTRIBUTION / AVAILABILITY OF REPORT Approved for public release; distribution unlimited.	
2b. DECLASSIFICATION / DOWNGRADING SCHEDULE		4. PERFORMING ORGANIZATION REPORT NUMBER(S)	
4. PERFORMING ORGANIZATION REPORT NUMBER(S)		5. MONITORING ORGANIZATION REPORT NUMBER(S) ARO 23328.10-65	
6a. NAME OF PERFORMING ORGANIZATION University of Rhode Island Mechanical Engineering Dept.	6b. OFFICE SYMBOL (if applicable)	7a. NAME OF MONITORING ORGANIZATION U. S. Army Research Office	
6c. ADDRESS (City, State, and ZIP Code) Wales Hall Kingston, RI 02881		7b. ADDRESS (City, State, and ZIP Code) P. O. Box 12211 Research Triangle Park, NC 27709-2211	
8a. NAME OF FUNDING / SPONSORING ORGANIZATION U. S. Army Research Office	8b. OFFICE SYMBOL (if applicable)	9. PROCUREMENT INSTRUMENT IDENTIFICATION NUMBER DAAL03-86-K-0125	
8c. ADDRESS (City, State, and ZIP Code) P. O. Box 12211 Research Triangle Park, NC 27709-2211		10. SOURCE OF FUNDING NUMBERS	
		PROGRAM ELEMENT NO.	PROJECT NO.
		TASK NO.	WORK UNIT ACCESSION NO.
11. TITLE (Include Security Classification) Experimental and Theoretical Studies of Wave Propagation in Granular, Rock and Porous Media.			
12. PERSONAL AUTHOR(S) Martin H. Sadd, and Arun Shukla			
13a. TYPE OF REPORT Final Report	13b. TIME COVERED FROM 7/1/86 TO 6/30/89	14. DATE OF REPORT (Year, Month, Day) 1989, August, 31	15. PAGE COUNT 132
16. SUPPLEMENTARY NOTATION The view, opinions and/or findings contained in this report are those of the author(s) and should not be construed as an official Department of the Army position, policy, or decision, unless so designated by other documentation.			
17. COSATI CODES		18. SUBJECT TERMS (Continue on reverse if necessary and identify by block number)	
FIELD	GROUP	SUB-GROUP	
		Wave Propagation, Granular Media, Microstructural Media, Dynamic Photomechanics, Distinct Element Method, Rock Mechanics & Porous Media. (JES)	
19. ABSTRACT (Continue on reverse if necessary and identify by block number) An experimental and theoretical study of wave propagation in granular, rock and porous media is described. The wave propagation is a result of explosive loadings of 50-100 μ s duration. Specific wave propagational variables include the wave speed, inter-granular contact forces (local wave amplitude) and wave spreading geometries. The relationship of the media microstructure to these propagational variables has been studied for a variety of granular and porous materials. micro seconds			
20. DISTRIBUTION / AVAILABILITY OF ABSTRACT <input type="checkbox"/> UNCLASSIFIED/UNLIMITED <input type="checkbox"/> SAME AS RPT. <input type="checkbox"/> DTIC USERS		21. ABSTRACT SECURITY CLASSIFICATION Unclassified	
22a. NAME OF RESPONSIBLE INDIVIDUAL		22b. TELEPHONE (Include Area Code)	22c. OFFICE SYMBOL

Table of Contents

Report Documentation Page	i
Table of Contents	ii
1. Statement of Problem	1
2. Summary of Results	4
3. List of Publications	10
4. List of Participating Scientific Personnel	12
5. Appendices: Reprints of Major Publications	13

	✓
	□
	□
Appendices	
A-1	



1. Statement of Problem

The completed research to be described in this report is concerned with the propagation of waves in geological materials. Since such materials are made up from sands, clays and rocks, they contain granular and porous microstructures. These local microstructures or fabric (as it is sometimes referred to) are a function of the geometry of the material distribution, and produce non-continuous fields of mass density, stress, strain, displacement, etc. These types of materials are therefore difficult to model using classical continuum mechanics such as elasticity, plasticity or viscoelasticity theories. One of the key features of this research was to investigate the effect of this microstructure on the propagation of waves produced by explosive loadings of short duration.

In many cases, geological materials will be composed of sands, gravel and/or crushed rock, and can therefore be categorized as a granular medium. Such a medium can be characterized, for modeling purposes, as a collection of distinct particles which can displace independently from one another and interact only through contact mechanisms. This type of media transmits mechanical loadings through discrete paths as determined by the geometry of the granular packing. For the case of porous media containing various distributions of open pores, a similar direction-oriented behavioral response will also occur.

In regard to wave propagation, our interest was involved with the transient dynamic behavior of such a structured medium when it is subjected to explosive

loadings of 50-100 μ s duration. Specific variables of interest included:

- wave speed
- inter-granular contact forces (local wave amplitude)
- wave spreading geometry

The goal of the research was to relate how the specific microstructure of the medium effects these wave propagational variables.

In order to conduct the investigation, both theoretical and experimental methods of study were employed. The theoretical work focused on two general methods which included the use of a new *microstructural continuum theory* for modeling, and a computational study using the so-called *distinct element method* to model the dynamic behavior of granular assemblies. The microstructural continuum theory which was used was the *distributed body theory* originally developed by Goodman and Cowin (see reference 29 in paper A in the Appendix). This particular theory assumes that the medium is distributed in space by an independent kinematical function called the volume distribution function, and thus this theory allows the medium to contain voids and other microstructures. In regard to the numerical modeling, the distinct element method was used to determine the motion of each granule in particular model assemblies. This computational scheme assumes that each granule may be modeled by rigid body dynamics with particle interactions having stiffness and damping properties. The predicted movements of the various granules are then the result of the propagation through the medium of disturbances which originated at the boundary loading points.

The experimental efforts employed the principles of dynamic photoelasticity along

with high speed photography to get the complete stress field information due to explosive loading in various granular assemblies. This technique gave complete details about the wave velocities, dynamic contact stresses and wave spreading during the particle contact interaction period. Assemblies containing particles of different size and arrangements were used in the experiments. A detailed investigation was conducted to study the influence of local microstructure on the wave propagation phenomenon. The experimental study also made use of electrical resistance strain gages to study wave propagation in real earth materials. A preliminary investigation was conducted to study dynamic load transfer in granular rock media.

2. Summary of Results

This section briefly describes the major results of the research program. References will be made to the reprints of our major papers which appear in the Appendix. Details of the particular results can be found in each of the papers.

Wave Propagation in Distributed Bodies Wave propagation studies have been conducted based upon a distributed body model of geological media. The distributed body model employs an independent kinematical volume distribution function which describes the way the material is distributed in space, and thus allows the theory to generate porous and granular microstructures. The theory uncouples the mass density of the granules from the mass density of the entire material, and allows compressibility due to both granule compressibility and void compaction. A one-dimensional theory of propagating singular surface acceleration waves has been developed for particular volume distribution functions which have application to geological materials. Three different volume distribution functions were developed producing periodic, exponential and a periodic-exponential material microstructures. A general computer code was developed to calculate the results predicted from the model for a variety of constitutive and microstructural model parameters. Results for the wave speed and amplitude behavior as a function of these model parameters are given in Figures 2-8 in Paper A in the Appendix. Specific relationships between the microstructure and the wave speed and attenuation have been determined, and these theoretical results are in general agreement with measured results.

Distinct Element Modeling of Wave Propagation in Granular Materials The distinct element model is a numerical scheme which uses Newtonian rigid-body mechanics to model the translational and rotational motion of each disk in a granular assembly. The method incorporates prescribed stiffness and damping at the contacts between each of the granules, and these model parameters were determined from calibration tests in the experimental segment of the research program. Ultimately the distinct element method establishes an explicit time-stepping scheme that enables the calculation of the inter-granule contact force between all granules at each of the selected time steps. The method is numerically efficient so that large numbers of granules may be analyzed in a given problem. The basic method is outlined in Paper B in the Appendix. Comparisons of the numerical results with those from dynamic photoelasticity are shown in Figures 4 and 5 in Paper B. These comparisons indicate reasonably good agreement between theoretical and experimental results for the assemblies which were studied. Inter-granular contact force distributions indicated the dependence of microstructure on the wave propagational characteristics, and it was discovered that the microstructural measure of the *branch angle* between local granules is an effective variable to use in establishing the connection between microstructure and wave propagation.

The Effect of Voids and Inclusions on Wave Propagation in Granular Materials Theoretical and experimental studies have been conducted on wave propagation in granular materials containing local discontinuities of voids and

inclusions. The granular medium was simulated by specific assemblies of circular disks, and the voids were created by removing particular disks from the assembly while inclusions were created by replacing certain disks with ones of a higher impedance material. The theoretical modeling employed the distinct element method, and the experimental study used the technique of dynamic photoelasticity. Comparisons were made between the computational and experimental data on the inter-granular contact forces around each void or inclusion, and these comparisons are shown in Figures 7-11 in Paper C in the Appendix. Both voids and inclusions produce local wave scattering through various reflection mechanisms, and the results seem to indicate that the inclusions produce higher local wave attenuation.

Experimental-Numerical Hybrid Technique of Load Transfer Coefficients for Wave Propagation Predictions in Granular Media Experimental studies on dynamic load transfer in granular media have been conducted through the use of dynamic photoelasticity. The experimental data collected allows the determination of the time dependent inter-granular contact loadings between the granules. This leads to the calculation of load transfer coefficients, i.e. the ratio of the maximum output contact load to the maximum input contact load, for various packing geometries. These coefficients were then used along with the principle of superposition to predict the peak inter-granular contact loads in several model granular assemblies. Results of the numerical hybrid scheme were then compared with experimental data for the assemblies investigated, see Figures

12-15 in Paper D in the Appendix.

Influence of Local Microstructure on Wave Propagation Phenomenon A

detailed experimental study was conducted to evaluate the effect of different microstructures or fabric of granular media on the wave propagation phenomenon. The granular media was simulated by circular disks made of photoelastic materials. Attention was focussed on the load transfer paths, wave velocities, wave attenuation and the dynamic stresses which are generated at the contacts due to the passage of stress waves. The details of the results are included in Paper E in the Appendix. Figures 2 through 7 contain photographs showing the full field description of the wave propagation process in different assemblies. The paper discusses the primary and secondary load transfer paths in different assemblies and clearly demonstrates the influence of the microstructure on the load transfer process.

Angular Dependence of Dynamic Load Transfer Process An experimental

investigation was conducted to evaluate the dependance of packing geometry on the dynamic load transfer in two dimensional granular chains. The results from these experiments are shown in Paper F in the Appendix. It was shown, that in two dimensional chains, rapid attenuation of load transfer occurs as the branch angle increases from 0 to 90 degrees. It was also observed that the wavelength of the loading pulse increases with the branch angle. These results are illustrated in the Figures 11 and 12 of Paper F.

Wave Propagation in Porous Media As a Function of Fluid Saturation

Dynamic photoelasticity was used to study wave propagation in a porous media as a function of fluid saturation. The porous media was modeled as a continuous solid containing particular arrays of holes or voids. The study investigated the wave propagation phenomenon from a microscopic point of view by going into the details of the geometric nature of the porous structure. The details of this study are given in Paper G in the Appendix. The results show the dependence of wave velocity and attenuation on the porosity as well as the microstructural arrangement of the pores.

Wave Propagation and Energy Transfer Across Contacts Between Large Bodies

This study experimentally investigated the formation of dynamic contacts between two bodies which are much larger than the wave length of the loading pulse. Results from this study are given in Paper H in the Appendix. Dynamic photographs provided full field information of diffraction, reflection and transmission process as a function of time. The results show that the individual wave types interact with the contact region in specific ways as determined by the reflection and refraction laws. It must be mentioned here that only qualitative treatment of the data was possible in this study. Initial attempts to quantitatively evaluate fringe pattern data were not successful.

Dynamic Load Transfer in Virgin and Damaged Rock Media Electrical resistance strain gages were used to study dynamic load transfer in a single chain assembly of disks fabricated from four different grades of white Vermont Marble.

The study was preliminary in nature and the results are given in Paper I in the Appendix. The results show the dependence of wave velocity on the microstructure of the rock. The effect of prior damage in rock grains on wave propagation phenomenon was also investigated.

3. List of Publications

1. Dynamic Photoelastic Investigation of Wave Propagation and Energy Transfer Across Contacts, A. Shukla and H.P. Rossmanith, *Journal of Strain Analysis*, Vol. 21, pp. 213-218, 1986.
2. Angular Dependence of Dynamic Load Transfer Due to Explosive Loading in Granular Aggregate Chains, A. Shukla, C.Y. Zhu and M.H. Sadd, *Journal of Strain Analysis*, Vol. 23, pp. 121-127, 1988.
3. Influence of the Microstructure of Granular Media on Wave Propagation and Dynamic Load Transfer, A. Shukla and C.Y. Zhu, *Journal of Wave-Material Interaction*, Vol. 3, pp. 249-265, 1988.
4. Wave Propagation in Distributed Bodies with Applications to Dynamic Soil Behavior, M.H. Sadd and M. Hossain, *Journal of Wave-Material Interaction*, Vol. 3, 1988.
5. Investigation of Dynamic Soil Structure Interaction Due to Explosive Loading, A. Shukla and Y. Xu, *Proc. Society of Experimental Mechanics, 1989 Meeting*, Cambridge, Massachusetts, 1989.
6. Wave Propagation in Porous Media as a Function of Fluid Saturation, A. Shukla and V. Paoletti, to appear in *Journal of Experimental Mechanics*, 1989.
7. Computational and Experimental Modeling of Wave Propagation in Granular Materials, M.H. Sadd, A. Shukla and H. Mei, *Proc. of the Fourth International Conference on Computational Methods and Experimental Measurements*, Capri, Italy, 1989.

8. The Effect of Voids and Inclusions on Wave Propagation in Granular Materials, M.H. Sadd, A. Shukla, H. Mei and C.Y. Zhu, **Micromechanics and Inhomogeneity-The Toshio Mura Anniversary Volume**, Springer-Verlag, New York, 1989.
9. The Use of Load Transfer Coefficients to Predict Dynamic Loads in Granular Assemblies, C.Y. Zhu, A. Shukla and M.H. Sadd, *Symposium on Wave Propagation in Granular Media, Proc. 1989 ASME Winter Annual Meeting*, San Francisco, California, 1989.
10. Dynamic Load Transfer Due to Explosive Loading in Virgin and Damaged Granular Rock Media, V. Prakash and A. Shukla, *Proc. of the Spring Conference on Experimental Mechanics*, Boston, pp.264-273, 1989.
11. Investigation of Dynamic Soil Structure Interaction Due to Explosive Loading, A. Shukla and Y. Xu, *Proc. of the Spring Conference on Experimental Mechanics*, Boston, pp. 238-243, 1989.
12. Dynamic Photoelastic Studies of Wave Propagation in Granular Media, A.Shukla, Invited Review Paper for *Journal of Optics and Lasers in Engineering*, 1990.

4. List of Participating Scientific Personnel

The participating scientific personnel on this project consisted of two professors and five graduate students. These individuals are listed below:

1. Professor Martin H. Sadd
2. Professor Arun Shukla
3. Mr. Vikas Prakash, M.S. Degree, May 1988.
4. Mr. Yi Xu, M.S. Degree, May 1988, Ph.D Degree in progress.
5. Mr. Hai Mei, M.S. Degree, May 1989.
6. Mr. Mohammad Hossain, M.S. Degree in progress.
7. Mr. Chang-Yi Zhu, Ph.D. Degree in progress.

5. Appendices: Reprints of Major Publications

Included in this appendice are reprints of the major publications which have resulted from the research project. Through brief summaries, reference is made to each of these papers in the main body of this report. These complete papers provide details of the research results.

WAVE PROPAGATION IN DISTRIBUTED BODIES WITH APPLICATIONS TO DYNAMIC SOIL BEHAVIOR

MARTIN H. SADD and MOHAMMAD HOSSAIN
Mechanical Engineering and Applied Mechanics
University of Rhode Island
Kingston, RI 02881-0805

ABSTRACT

A study is presented which models wave propagation through materials with microstructure. The specific microstructure of interest is that found in geological materials such as granular and rock media, and the modeling is carried out using the distributed body theory of Goodman and Cowin. Wave propagation is studied through the use of singular surface wave theory, and specific results for the wave speed and amplitude behavior are presented. Three different types of microstructure are modeled by using different volume distribution functions. Results of wave speed and amplitude attenuation are presented for various microstructural model parameters.

1. INTRODUCTION

Geological materials such as sands, clays and/or rocks are complex materials and have proven to be difficult to model using classical continuum mechanics. These types of materials may be classified as materials with microstructure since at the micro-level the mass density along with other important field variables are not continuous in the mathematical sense. Modeling of these materials using classical continuum mechanics (e.g. elasticity, plasticity, viscoelasticity, etc.) has progressed to a point where fundamentally new information will probably have to come from a theory incorporating microstructure in its basic framework. The work herein reported is concerned with the modeling of the dynamic response of such media. Of particular interest is the propagation of mechanical signals (i.e. wave propagation) through materials composed of granular, rock, porous and other discontinuous structures.

Studies of geological materials with microstructure started many years ago with research on granular materials modeled as aggregate assemblies of discs or spheres. The concept of modeling granular media as an array of elastic particles (e.g. spheres or discs) led to the initial attempts at predicting wave propagation through such media. Early work [1-6] employed a normal granular contact force concept. This initial work investigated the propagation velocity as a function of confining pressure, particle size and aggregate geometry. It was discovered, however, that the classical theory of contact due only to normal forces, does not in general accurately model real materials, and thus Duffy and Mindlin [7] proposed a theory for granular media which included both normal and tangential contact forces. This theory produced a non-linear and inelastic stress-strain relation.

More recent theories of granular media behavior have included statistical-stochastic approaches [8-13]. Cundall and Strack [14] proposed a numerical method called the distinct element technique for granular and rock assemblies, and this approach has been used for rubble screens [15]. Morland [16] considered a rock/granular media as a regularly jointed media and used an anisotropic elasticity approach. Particulate media has also been studied by Hill and Harr based upon a diffusion equation derived from probabilistic models [17]. Endochronic theories have been applied to granular soils [18-20], and mixture theories [21] also show some promise of modeling such media. Pore-collapse models originally developed by Carrol and Holt [22] have been used to study the dynamic response of porous and granular media.

With regard to experimental work, the method of photoelasticity has been employed to study load transfer in granular assemblies. Photoelasticity has been used to study static behavior [23-25]. Dynamic photomechanics studies of granular media have been performed [26-27]. Their technique employed the use of high speed photography to record wave propagation through an assembly of birefringent discs.

Some very interesting microstructural modeling has been done with the so-called "fabric tensor" theories for example [28]. This research has been investigating the construction of constitutive relations dependent upon fabric tensors which describe the important microstructural features of the particular material, e. g., distributions of contact normal vectors. At the present time, wave propagation theories using fabric tensors have not been developed.

Finally, granular and porous materials have been modeled by the so-called "distributed body" theory [29]. This particular theory assumes that the medium is distributed in space by an independent kinematical function called the volume distribution function. This theory has been applied to wave propagation studies and some success has been achieved in modeling particular situations. Based upon this success, the present work is concerned with applying distributed body theory to wave propagation in geological soil media with particular microstructures.

The purpose of the present work is to extend the preliminary developments of the distributed body theory for applications to geological materials. The paper starts with the basic ideas previously developed for one-dimensional acceleration waves propagating in a distributed body. Next, specific volume distribution functions are selected which show promise of modeling granular geological materials. Finally, a general computer code is developed which can calculate wave speed and amplitude behavior as a function of distance for all of the various distribution functions selected. Results from the code are shown to demonstrate the effects of the selected volume distribution function, the constitutive parameters, and the initial wave amplitude.

2. DISTRIBUTED BODY THEORY

The distributed body theory originally developed by Goodman and Cowin [29] was constructed to allow a continuum theory to be applied to materials with non-continuous fields of mass density, stress, body force, etc. Thus, the model could be used to describe the behavior of a wide variety of materials having granular and/or porous structures. Fundamental to the theory is the assumption that, at any point in the material, the overall mass density may be written as

$$\rho = v \gamma \quad (1)$$

where γ is the density of the granules (or matrix material) and $v = v(X,t)$ is referred to as the volume distribution function. This function describes the way the medium is distributed in space allowing for voids or other particular granular structures. Thus, this theory uncouples the mass density of the granules from the mass density of the entire material, and allows the compressibility due to both granule compressibility and void compaction. In general $0 < v \leq 1$, and v is related to the porosity n and void ratio e by the expressions

$$v = 1 - n = \frac{1}{1 + e} \quad (2)$$

Within a one-dimensional framework, the classical balance law of conservation of linear momentum reads

$$\rho_0 \ddot{x} = \frac{\partial T}{\partial X} + \rho_0 b \quad (3)$$

where T is the stress, b is the body force, x is the particle position, X is the reference position coordinate, and $()_0$ indicate values in the reference state. In addition to this classical balance law, the distributed body theory also requires an independent balance equation governing the volume distribution. In one dimension this second equation governing void change is given by

$$\rho_0 k \ddot{v} = \frac{\partial h}{\partial X} + \rho_0 g \quad (4)$$

where k is called the equilibrated inertia, h the equilibrated stress, and g the intrinsic body force. Physical interpretation of the micro-structural variables k , h and g is somewhat difficult to make. In general, these variables are related to the local contact mechanics at the granular level and can be related to particular self-equilibrated singular stress states from classical elasticity (e. g. double force systems, centers of

dilatation). It has been proposed [31] that k is related to the void mean surface area and to the number of voids present, h is a result of the interaction forces between neighboring voids and will vanish when the voids are sufficiently separated; and g is related to the coupling between the total deformation of the medium and the changes in void volume.

For granular geological materials, we assume that the media is composed of compressible granules at relatively high confining pressures so as to prevent material flow. For this case an appropriate constitutive formulation would read

$$T = T(v_0, v, \frac{\partial v}{\partial X}, \epsilon) \quad (5)$$

and hence the stress depends upon the reference and current volume distributions, the gradient of the volume distribution, and the strain ϵ . An explicit form of relation (5) which has been proposed [32] uses an even quadratic form in the gradient of v , i.e.

$$T = v \left[\Lambda(v_0, v, \epsilon) + 1/2 \alpha(v_0, v, \epsilon) \left(\frac{\partial v}{\partial X} \right)^2 \right] \quad (6)$$

The constitutive dependence on the gradient of the volume distribution $\partial v/\partial X$ is significant and allows an equilibrium stress to depend on this gradient. Since equation (6) involves the square of the gradient, it will be an *isotropic form* in that variable (required by material frame indifference) and, hence, the stress response will be independent of the sign of the gradient. Also, the presence of the gradient term allows the theory to predict a generalized Mohr-Coulomb failure criterion.

First and second order moduli defined by

$$E = \frac{\partial T}{\partial \epsilon} = v \left[\Lambda_{\epsilon} + 1/2 \alpha_{\epsilon} \left(\frac{\partial v}{\partial X} \right)^2 \right] \quad (7)$$

$$\tilde{E} = \frac{\partial^2 T}{\partial \epsilon^2} = v \left[\Lambda_{\epsilon\epsilon} + 1/2 \alpha_{\epsilon\epsilon} \left(\frac{\partial v}{\partial X} \right)^2 \right]$$

will be needed for subsequent wave analysis. Normally $E > 0$ but the second order modulus \tilde{E} , may be positive or negative.

3. WAVE ANALYSIS

The basic premise of this particular wave theory lies in modeling the wave as a propagating singular surface across which there exists a jump discontinuity in a particular variable. Dynamic loadings will commonly produce either second-order acceleration waves, having a discontinuity in the particle acceleration at the wave front, or first-order shock waves³ having a jump in the particle velocity at the wave front. Acceleration waves will be considered here.

As mentioned, a wave is modeled as a propagating singular surface of zero thickness moving with speed U . The jump of a quantity ϕ across this surface is defined by $[\phi] = \phi^- - \phi^+$ where ϕ^+ and ϕ^- are the limiting values of ϕ immediately ahead of and behind the wave, respectively. An acceleration wave is therefore defined as a wave across which the particle velocity, strain, and volume distribution are continuous but their spatial and temporal derivatives are not. Thus, this type of motion carries propagating discontinuities in the particle acceleration and various other gradients of the strain and volume distribution. The jump in the particle acceleration $[\ddot{x}]$ is called the wave's amplitude, and will be denoted by $a(t)$. Note that for compressive waves, $a(t) > 0$, while for expansive waves, $a(t) < 0$.

Following singular surface analysis procedures which have now become somewhat standardized, specific relations for the wave speed and amplitude behavior can be determined. Specifically, Nunziato and Walsh [30] showed that for distributed body theory, the wave speeds are given by the roots of a quartic equation thus

implying the existence of two types of waves with speeds given by

$$U_F^2 = 1/2 \left[C_1^2 + C_2^2 + \sqrt{(C_1^2 - C_2^2)^2 + 4\beta} \right] \tag{8}$$

$$U_S^2 = 1/2 \left[C_1^2 + C_2^2 - \sqrt{(C_1^2 - C_2^2)^2 + 4\beta} \right]$$

where

$$C_1^2 = \frac{(vT)_\epsilon^+}{\rho_o v_o}, \quad C_2^2 = \frac{(h_{v_x})^+}{\rho_o k}, \quad \beta = \left(\frac{v^+}{v_o} \right) \frac{(h_\epsilon)^+ (T_{v_x})^+}{\rho_o^2 k} \tag{9}$$

with subscripts ϵ, v and X meaning partial differentiation with respect to the indicated variable, and $()^+$ meaning immediately ahead of the wave. The speed U_F denotes the "fast" wave speed which is associated predominantly with the elasticity of the granules, and will disappear if the granules are incompressible. The quantity U_S is the "slow" wave speed which is connected to the compressibility of the material due to consolidation, and will vanish if there are no voids ($v = 1$).

With regard to the wave amplitude behavior, Nunziato and Walsh [30] have found that the amplitude for one-dimensional wave propagation satisfies the following nonlinear Bernoulli equation

$$\frac{da}{dX} = \kappa(X) a^2 - \mu(X) a \tag{10}$$

where $\mu(X)$ and $\kappa(X)$ are material coefficients given in general by rather lengthy expressions. The coefficient $\mu(X)$ is related to dispersive effects, while $\kappa(X)$ reflects both the elastic response of the granules and dispersive effects. Depending on the nature of κ and μ , the theory can predict growth or decay of wave amplitude. Using the specific constitutive form given by Eq. (6), for the case of a "fast" wave propagating into material at rest in its reference condition, the coefficients become

$$\mu(X) = \frac{1}{2U_F^2} \left[\frac{U_F^2}{v_o} + \frac{(\alpha)_{\epsilon_o}}{2\gamma_o} \left(\frac{\partial^2 v}{\partial X^2} \right)_o \right] \left(\frac{\partial v}{\partial X} \right)_o \tag{11}$$

$$\kappa(X) = \frac{-1}{2\gamma_o U_F^4} \left[(\Lambda)_{\epsilon\epsilon_o} + 1/2 (\alpha)_{\epsilon\epsilon_o} \left(\frac{\partial v}{\partial X} \right)_o^2 \right] = \frac{-\tilde{E}_o}{2v\gamma_o U_F^4}$$

where the fast wave speed is given by

$$U_F = \sqrt{E_o / v_o \gamma_o} \tag{12}$$

with E_o and \tilde{E}_o being the reference values of the first and second order moduli.

In order to have real wave speeds, $E_o \geq 0$ and therefore Eq. (7) implies that

$$(\Lambda)_{\epsilon_o} + 1/2 (\alpha)_{\epsilon_o} \left(\frac{\partial v}{\partial X} \right)_o^2 \geq 0 \tag{13}$$

which can be regarded as an equation restricting certain constitutive and microstructural parameters.

4. VOLUME DISTRIBUTION FUNCTIONS

In order to apply the distributed body theory and develop a wave propagation analysis, it is necessary to have explicit constitutive forms, see for example Eq. (6), and the initial volume distribution $v_o(X)$ must also be specified. Any proposed volume distribution function should reflect the density variations and other microstructural features within the material. It is difficult to construct such a function which characterizes these variations precisely and yet has the smoothness requirements to be compatible with the theory. We will follow the approach that $v_o(X)$ should be a continuous function in order to perform certain required differentiations and integrations and that it yield the correct average density.

As discussed previously, in constructing a wave propagation analysis, Nunziato, et al. developed a specific volume distribution function [32]. Their work was for a granular material, PBX-9404, an explosive powder/binder system. They proposed a *periodic structure* of the form

$$v_o(X) = v_a + (1 - v_a) \cos \frac{2\pi X}{l} \quad (14)$$

where v_a and l are material constants.

The quantity v_a would be given by the overall average density of the material divided by the granule density and is thus related to the average value of the volume distribution. The second material constant l is referred to as a characteristic length associated with this periodic structure. Clearly l specifies the length of the repeating units of the microstructure. For granular materials, l would be related, but not necessarily equal, to the average grain size. In regard to this characteristic length, the work of Shahinpoor [33] is appropriate to consider. Shahinpoor did experiments of randomly packed spherical granules on a flat surface. His work demonstrated the concept of distinct packing geometries referred to as "Voronoi cells." It is evident that for some packing geometries, if a periodic structure is assumed, the characteristic length l would be equal to the Voronoi cell size, and thus could be several grain diameters.

Since the mechanical response of most geological materials like sand or gravel is affected by in situ conditions such as overburden, the microstructure will be globally nonhomogeneous, i.e., be depth dependent. With this in mind, another volume distribution function which can predict such a structure may be written as

$$v_o(X) = 1 - (1 - v_b) e^{-BX} \quad (15)$$

where v_b and B are material constants. Clearly for this case, the material becomes more dense with depth X into the medium. The constant v_b is the volume distribution at the free surface $X = 0$, and the constant B determines the rate of consolidation with depth. It should be pointed out that this exponential form does not contain any periodic structure; hence, it should produce monotonic results for the wave propagation characteristics.

A final volume distribution function which is proposed involves the combination of the periodic form (14) and the exponential form (15). The combined form employs simply the product of these two relations, i.e.,

$$v_o(X) = \left[v_a + (1 - v_a) \cos \frac{2\pi X}{l} \right] \left[1 - (1 - v_b) e^{-BX} \right] \quad (16)$$

and again v_a , v_b , l and B are material constants. It is evident that this form will thus produce a combined periodic-exponential depth dependent microstructure. The three volume distribution functions are given by Eqs. (14), (15) and (16) and are shown in Fig. 1.

4. WAVE MOTION RESULTS

Based upon the wave motion theory, a computer code was developed to handle any of the three volume distribution functions given in Eqs. (14), (15) and (16). The constitutive form employs Eq. (6), with the specific values for the two material functions α and Λ and their needed derivatives. With regard to the wave speed calculations, since the variation of speed within individual grains is normally not measurable, the developed code calculates the average wave speed. This is done through an integration process over spatial distance employing a numerical Gauss quadrature scheme. In order to calculate the amplitude behavior, the

non-linear differential equation (10) was numerically integrated using a fourth-order Runge-Kutta procedure.

Specific wave motion results for each of the three proposed volume distribution functions will now be presented. Results include wave speed and amplitude attenuation. Depending upon which volume distribution function is used in the modeling, a wide variety of predicted output can result by varying particular constitutive, microstructural, and other input parameters. The constitutive parameters in the theory are α_ϵ , $\alpha_{\epsilon\epsilon}$, Λ_ϵ and $\Lambda_{\epsilon\epsilon}$, while the microstructural parameters are v , v_X , v_{XX} , v_a , v_b , l , and B , and the input parameter would be the initial wave amplitude a_0 . In principle, the constitutive parameters would be a function of the microstructural parameters as demonstrated in Eq. (6). However, explicit relationships for these parameters have not yet been determined. Therefore, only constant values will be used for these various parameters.

For the periodic distribution model, the microstructural parameters are the average porosity v_a and the characteristic length l . Specific constitutive parameters which seem to give reasonable results for geomechanics materials are $\alpha_\epsilon = -450$ lb, $\alpha_{\epsilon\epsilon} = 109$ lb, $\Lambda_\epsilon = 3 \times 105$ lb/in² and $\Lambda_{\epsilon\epsilon} = -108$ lb/in.

Figure 2 illustrates the effect of porosity on the wave speed versus propagation depth. Three different values of v_a are shown using a characteristic length of $l = 0.1$ in. As expected, the average wave speed decreases with increasing porosity. Figure 3 shows the effect of the characteristic length on the wave speed, and it is seen that the wave speed will increase with l . This result is apparently related to the fact that, with an increase in l , the wave will see fewer microstructural changes per unit length of travel and will thus suffer fewer scatterings. For the periodic microstructural model, the average wave speed will oscillate during the first few grains and will then be essentially constant thereafter.

Amplitude behavior is illustrated in Fig. 4 for various cases of microstructure and initial input acceleration amplitude. Figure 4a shows the amplitude behavior for three different initial amplitudes, $a_0 = 5 \times 10^3$, 1×10^4 , and 5×10^4 in/s². Clearly, the expected result can be seen in that higher initial amplitudes decay faster than the lower amplitude waves. Comparing Figs. 4a and 4b indicates the effect of porosity on the amplitude attenuation. It is observed that the attenuation rate is dependent upon v_a and as v_a decreases (i.e., increasing porosity) the rate of attenuation increases. This result is also consistent with the variation in wave speed with v_a shown in Fig. 2. Comparing Figs. 4b and 4c demonstrates the effect of l on amplitude attenuation. These figures indicate that larger values of l result in less attenuation, which is consistent with the previous observation regarding the variation of wave speed with l .

For the exponential volume distribution model the constitutive parameters were chosen as $\alpha_\epsilon = -8 \times 106$ lb, $\alpha_{\epsilon\epsilon} = 4.8 \times 10^8$ lb, $\Lambda_\epsilon = 3 \times 10^5$ lb/in² and $\Lambda_{\epsilon\epsilon} = -1.0$ lb/in². This model contains the microstructural parameters of the free surface porosity v_b and the depth rate of consolidation B . As before, the input parameter is the initial amplitude a_0 . Figures 5 and 6 show typical results concerning the effects of these parameters on the wave propagation variables. Figure 5 shows the effect of v_b on the average wave speed. For this case, the wave speed increases with depth due to the overall decrease in porosity with depth. Figure 6 shows the effect of v_b and the initial amplitude on wave attenuation. These results give trends similar to the previous observations for the periodic distribution function; that is, higher initial amplitude waves attenuate faster and the attenuation rate increases with porosity.

For the combined periodic-exponential distribution model, the chosen constitutive parameters that were used are $\alpha_\epsilon = 73 \times 10^5$ lb, $\alpha_{\epsilon\epsilon} = 5 \times 10^8$ lb, $\Lambda_\epsilon = 3 \times 10^5$ lb/in² and $\Lambda_{\epsilon\epsilon} = -750$ lb/in². This model contains all four microstructural parameters v_a , v_b , l , and B . These, along with the initial amplitude a_0 , provides considerable parameter variations. Only a portion of the possible parametric variations will be presented, and these are shown in Figs. 7 and 8. Figure 7 shows the effect of v_b on the average wave speed illustrating again a slower propagational speed for more porous media. Figure 8 shows the effect of the initial amplitude and porosity on wave attenuation. These results indicate the same trends as observed for the preceding cases, namely an increase in attenuation with initial acceleration and porosity.

5. SUMMARY AND CONCLUSIONS

This paper has presented a wave propagation study based upon a distributed body model of geological media. A one-dimensional theory has been developed for explosive transient loadings using singular surface wave theory. General formulas for the wave speed and amplitude attenuation were taken from the previous work of Nunziato et al [30-32]. Specific forms for the volume distribution were constructed to model geological materials, and these were incorporated into the general wave theory. A general computer code was written to calculate specific results from the model for a variety of constitutive and microstructural model

parameters. Three specific forms of the volume distribution function included a periodic model giving a repeatable microstructure with distance, an exponential form with a depth dependent effect corresponding to *in situ* over-burden, and a combined periodic-exponential form yielding both repeatable and depth dependent microstructure.

In regard to wave speed, since the local speed through each granule is difficult to observe, the average wave speed was computed by the code. It should be pointed out that the actual wave speed will vary in an oscillatory manner for volume distributions which have a periodic nature. It is observed that for the periodic and periodic-exponential distribution cases, the average wave speed will oscillate through the first couple of periodic lengths (barely discernable from Figs. 2, 3, and 7) and then will gradually approach an asymptotic value. As expected, results indicate that porosity generally decreases the wave speed. However, it is more interesting to note that other microstructural parameters also have a major effect. For example, results for the periodic volume distribution indicate that the periodic length l , plays the role of decreasing the wave speed as l gets smaller.

Although the theory is capable of predicting both growth or decay of wave amplitude, for the cases considered here the wave amplitude was found to decrease with propagational distance. The attenuation rate was found to be higher in more porous media, and initially higher amplitude waves decayed faster than waves with a lower initial amplitude.

The work described here deals solely with deterministic analyses. Probabilistic studies [34] have been conducted within the framework of the distributed body theory. Such work investigated the effects of allowing the characteristic length l , and the average porosity v_a , for the periodic model, to be random variables, i.e. to have an average value and a standard deviation. Output probabilistic results were given for the expected value and for plus or minus one standard deviation bounds.

The theoretical results of this work appear to generally match both qualitatively and quantitatively data on wave propagation in soils. Unfortunately, experimental data on wave propagation through structured geological media with precisely known microstructure was not available to the authors. Consequently, comparisons with data could not be made at the present time. Current work is under way at the University of Rhode Island to collect such data, and future comparisons will be made.

→ **ACKNOWLEDGMENT** This research was supported by grants from the U.S. Army under contracts DACA39-85-C-0023 and DAAL03-86-K-0125.

REFERENCES

1. K. Iida, "Velocity of Elastic Waves in a Granular Substance," *Bull. Earthquake Res. Inst.* 17, 783-808 (1939).
2. T. Takahashi and Y. Sato, "On the Theory of Elastic Waves in Granular Substance," *Bull. Earthquake Res. Inst.* 27, 11-16 (1949).
3. D.S. Hughes and J.H. Cross, "Elastic Wave Velocities in Rocks at High Pressures and Temperatures," *Geophys.* XVI-4, 577-593 (1951).
4. D.S. Hughes and J.L. Kelly, "Variation of Elastic Wave Velocity with Saturation in Sandstone," *Geophys.* 17, 739-752 (1952).
5. F. Gassman, "Elastic Waves Through a Packing of Spheres," *Geophys.* 16, 673-685 (1951).
6. H. Brandt, "A Study of the Speed of Sound of Porous Granular Media," *J. of Appl. Mech.* 22, 479-486 (1955).
7. J. Duffy and R.D. Mindlin, "Stress-Strain Relations and Vibration of a Granular Medium," *J. of Appl. Mech.*, 585-593 (1957).
8. J.A. Hudson, "The Scattering of Elastic Waves by Granular Media," *Q. J. of Mech. and Appl. Math.* 21, 487-502 (1968).
9. E.H. Fletcher, "Random Walk Model of Ideal Granular Mass," *ASCE J. Soil Mech. Found. Div.* (American Society of Civil Engineers) 98#SM10, Proceedings Paper 8444, 1379-1392 (1971).

10. L.S. Fu, "A New Micro-Mechanical Theory for Randomly Inhomogeneous Media," *Wave Propagation in Homogeneous Media and Ultrasonic Non-Destructive Evaluation* (AMD) 62, Ed.: G.C. Johnson, American Society of Mechanical Engineers (1984).
11. P.L. Chambre, "Speed of Plane Wave in a Gross Mixture," *J. Acoust. Soc. Am.* 26, 329-331 (1984).
12. V.K. Varadan, V.V. Varadan and Y. Ma, "Propagation and Scattering of Elastic Waves in Discrete Random Media," *Proc. 20th Annual Meet. Soc. of Eng. Sci.* (University of Delaware) 310 (1983).
13. S.N. Endley and H. Peyrot, "Load Distribution in Granular Media," *ASCE J. Eng. Mech. Div.*, 99-111 (1977).
14. P.A. Cundall and D.L. Strack, "A Discrete Numerical Model for Granular Assemblies," *Geotechnique* 29, 47-65 (1979).
15. J.W. Brown, D.W. Murnell and J.H. Stout, "Propagation of Explosive Shock Through Rubble Screens," (Miscellaneous Paper SL-80-7) U.S. Army Engineer Waterways Experiment Station, Vicksburg, MS.
16. L.W. Morland, "Elastic Anisotropy of Regularly Jointed Media," *Rock Mech.* 8, 35-48 (1976).
17. J.M. Hill and M.E. Harr, "Elastic and Particulate Media," *ASCE J. Eng. Mech. Div.* 108, 596-604.
18. H.E. Read and K.C. Valanis, "An Endochronic Constitutive Model for General Hysteretic Response of Solids," Final Report Research Project 810, Electric Power Research Institute, Palo Alto, CA (1979).
19. H.C. Lin and H.C. Wu, "Strain Rate Effect in the Endochronic Theory of Viscoplasticity," *J. Appl. Mech.* 43 92-96.
20. Z.P. Bazant, R.J. Krizek and C.L. Sheih, "Hysteretic Endochronic Theory for Sand," *ASCE J. Eng. Mech. Div.* 109, 1073-1095 (1983).
21. S.L. Passman, "Mixture of Granular Materials," *Int. J. Eng. Sci.* 15, 117-283 (1977).
22. M.M. Carroll and A.C. Holt, "Static and Dynamic Pore-Collapse Relations for Ductile Porous Materials," *J. Appl. Phys.* 43 759-761, 1626-1636 (1972).
23. A. Drescher and G. De Josselin De Jong, "Photoelastic Verification of a Mechanical Model for the Flow of a Granular Material," *J. Mech. Phy. Solids* 20, 337-351 (1972).
24. A. Drescher, "Application of Photoelasticity to the Investigation of Constitutive Laws for Granular Materials," *Proc. IUTAM-Symp. Optical Methods in Solid Mechanics*, Poltiers, France (1979).
25. A.J. Durelli and D. Wu, "Use of Coefficients of Influence to Solve Some Inverse Problems in Plane Elasticity," *J. Appl. Mech.* 50, 288-296 (1983).
26. H.P. Rossmannith and A. Shukla, "Photoelastic Investigation of Dynamic Load Transfer in Granular Media," *Acta Mech.* 42, 211-225 (1982).
27. A. Shukla and C. Damania, "Experimental Investigation of Wave Velocity and Dynamic Contact Stress in an Assembly of Disks," *Experi. Mech.* 27, 268-281 (1987).

28. S. Nemat-Nasser and M.M. Mehrabadi, "Micromechanically Based Rate Constitutive Descriptions for Granular Materials," *Mechanics of Engineering Materials*, Eds: C.S. Desai and R.H. Gallagher, Wiley (1984).
29. M.A. Goodman and S.C. Cowin, "A Continuum Theory for Granular Materials," *Arch. Rat. Mech. Anal.* **44**, 249-266 (1972).
30. J. Nunziato and E. Walsh, "On the Influence of Void Compaction and Material Non-uniformity on the Propagation of One-Dimensional Acceleration Waves in Granular Materials," *Arch. Rat. Mech. Anal.* **64**, 299-316 (1977).
31. J. Nunziato and S. Cowin, "A Nonlinear Theory of Elastic Materials with Voids," *Arch. Rat. Mech. Anal.* **72**, 175-201 (1979).
32. J. Nunziato, J.E. Kennedy and E. Walsh, "The Behavior of One-Dimensional Acceleration Waves in an Inhomogeneous Granular Solid," *Int. J. Eng. Sci.* **16**, 647-648 (1978).
33. M. Shahinpoor, "Frequency Distribution of Voids in Randomly Packed Monogranular Layers," *Mechanics of Granular Materials: New Models and Constitutive Relations*, Eds: J.T. Jenkins and M. Satake, Elsevier (1983).
34. M.H. Sadd, M. Hossain and B. Rohani, "A Study of Explosive Wave Propagation in Granular Materials with Microstructure," Final Report, SL-86-35, U.S. Army Engineer Waterways Experiment Station (1986).

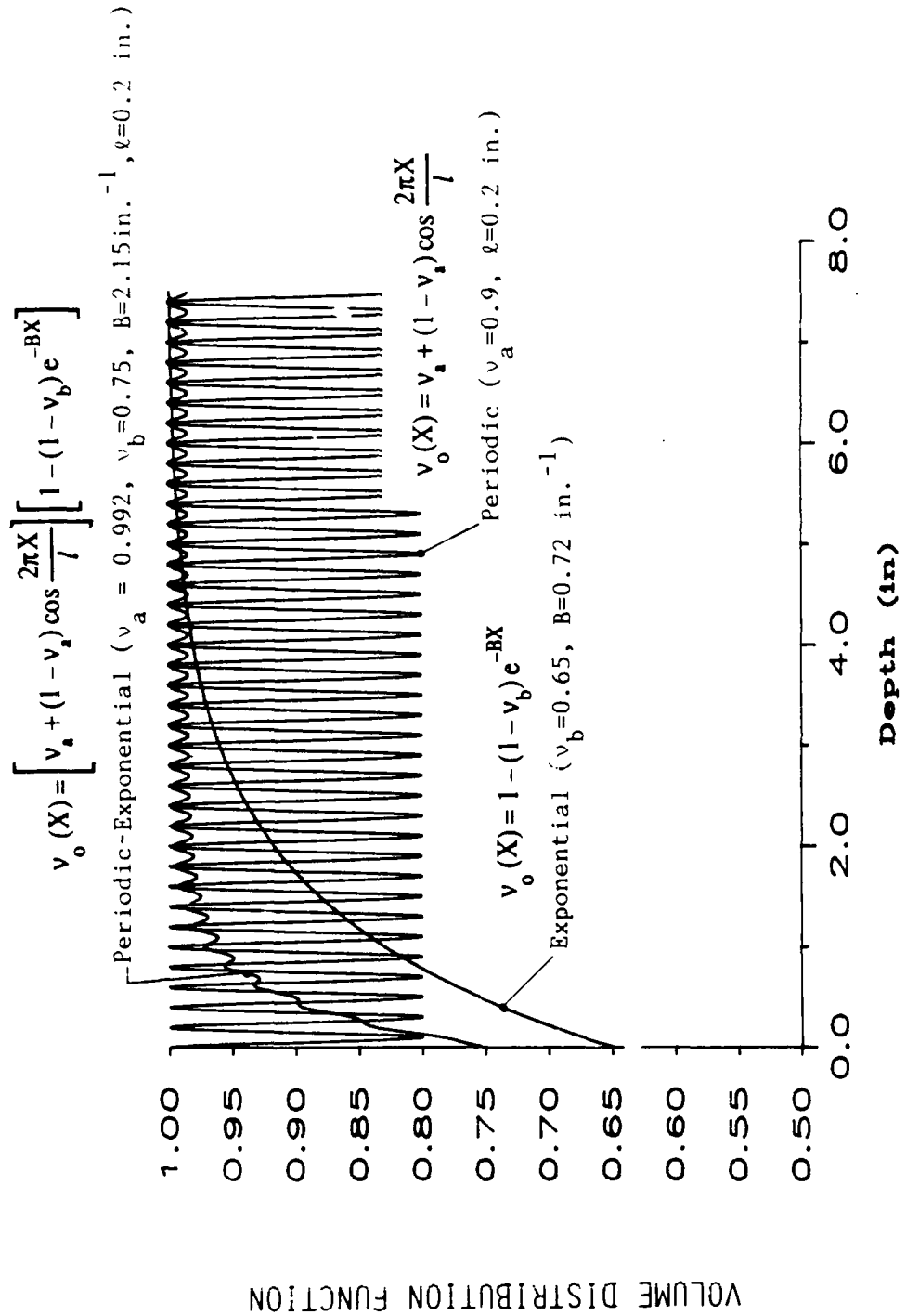


Figure 1. Volume Distribution Functions

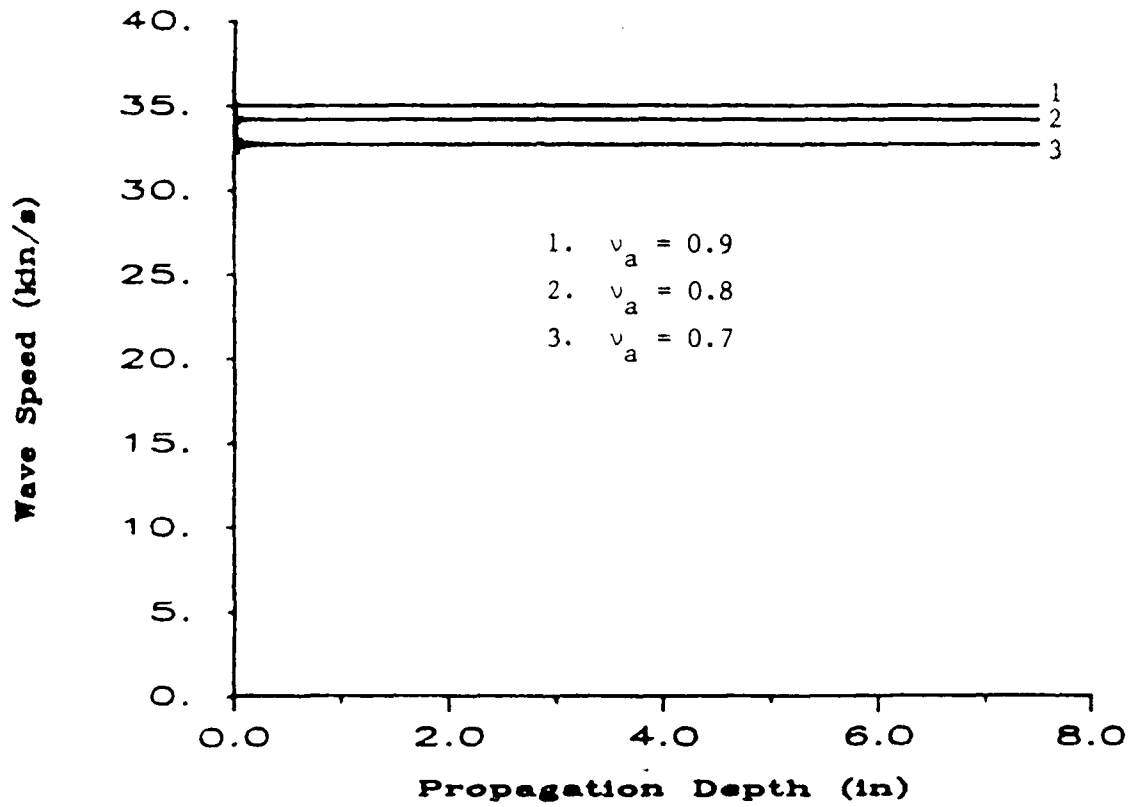


Figure 2. Wave Speed Versus Depth for a Periodic Volume Distribution with $\ell = 0.1$ in.

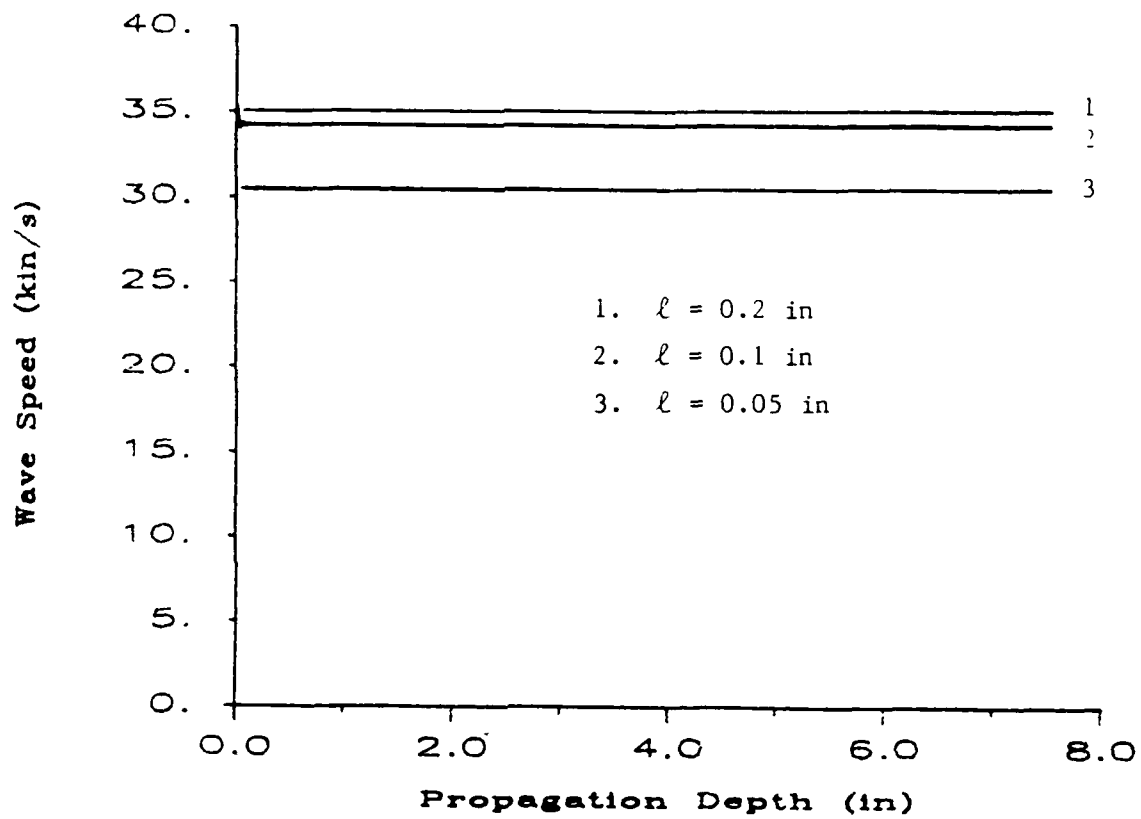
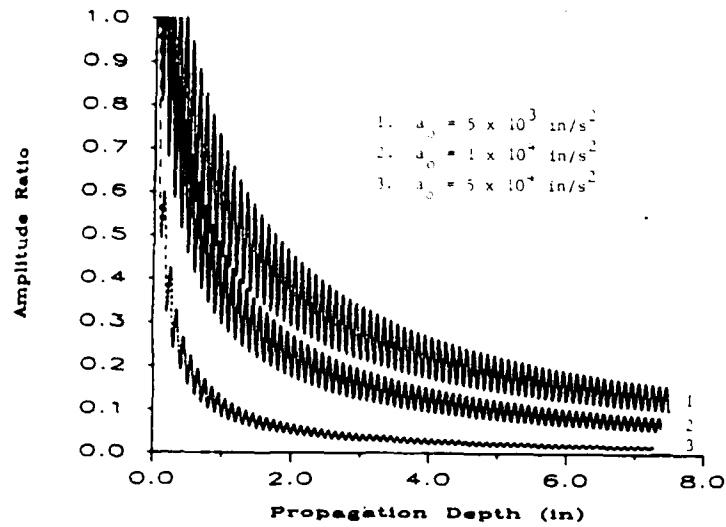
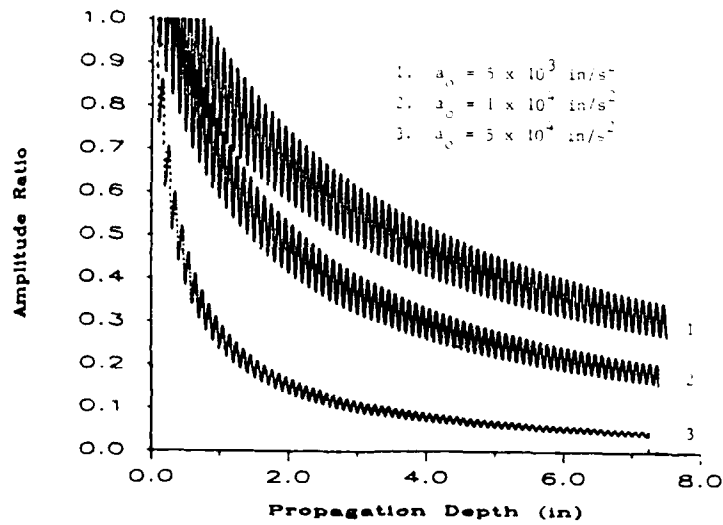


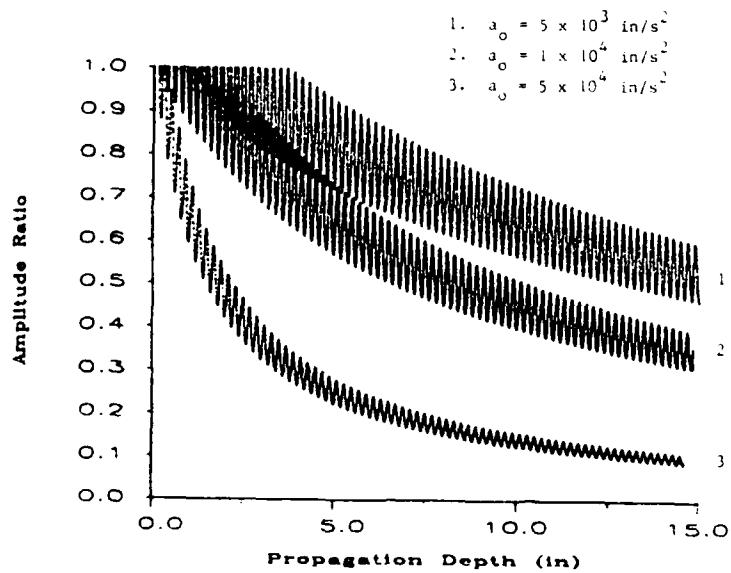
Figure 3. Wave Speed Versus Depth for a Periodic Volume Distribution with $v_a = 0.8$.



(a) $l = 0.1 \text{ in}$ and $v_a = 0.7$



(b) $l = 0.1 \text{ in}$ and $v_a = 0.8$



(c) $l = 0.2 \text{ in}$ and $v_a = 0.8$

Figure 4. Amplitude Behavior for a Periodic Volume Distribution
 A13

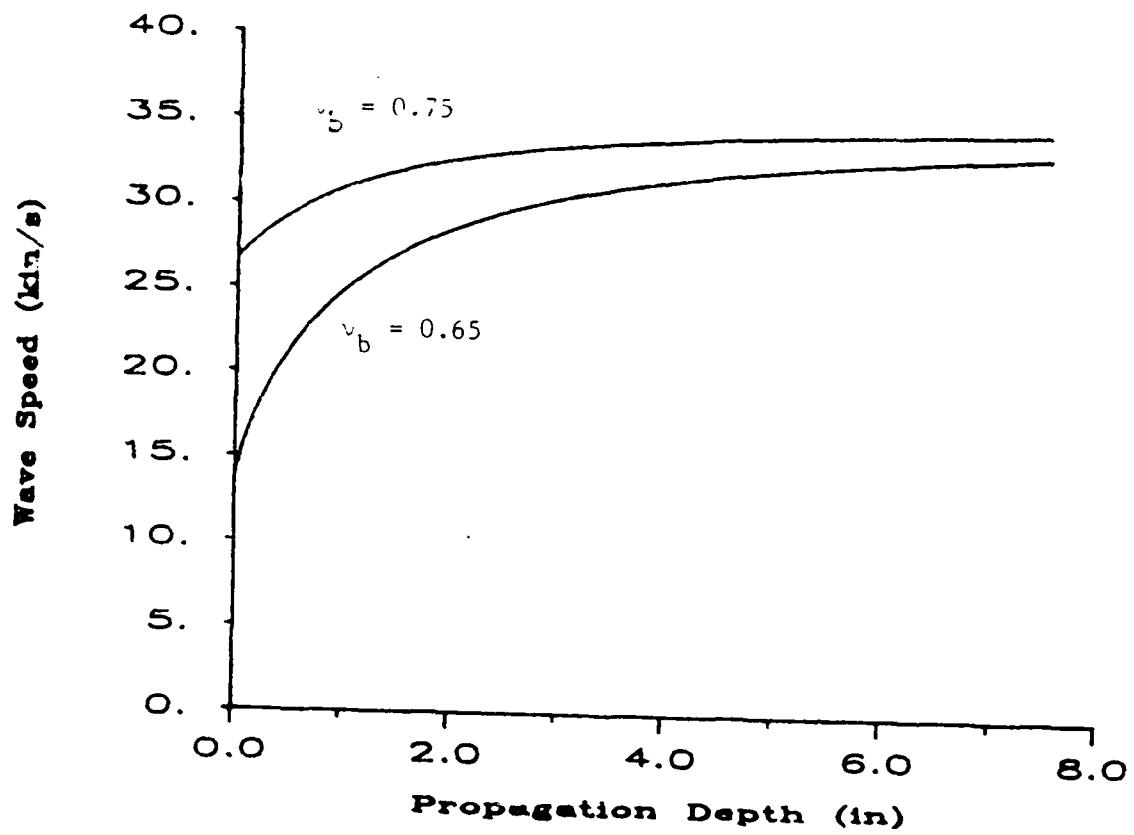
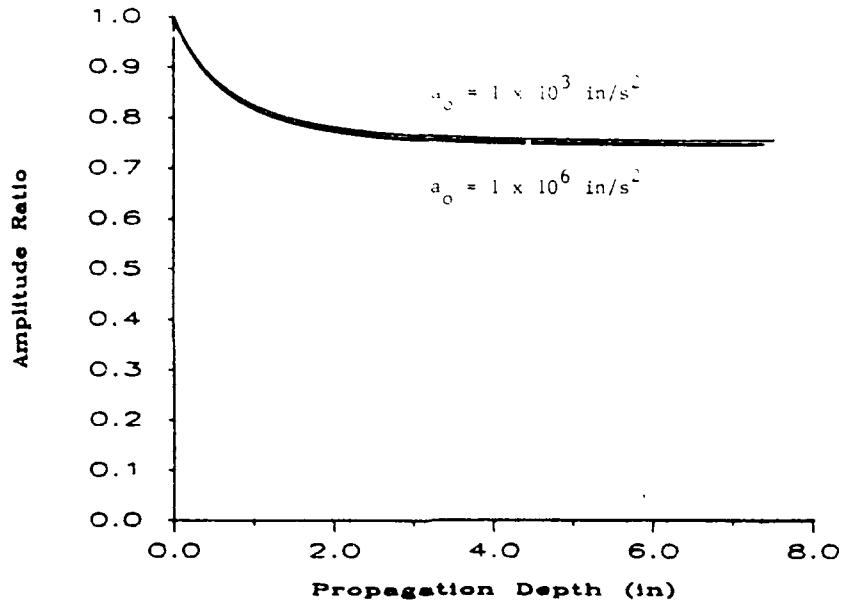
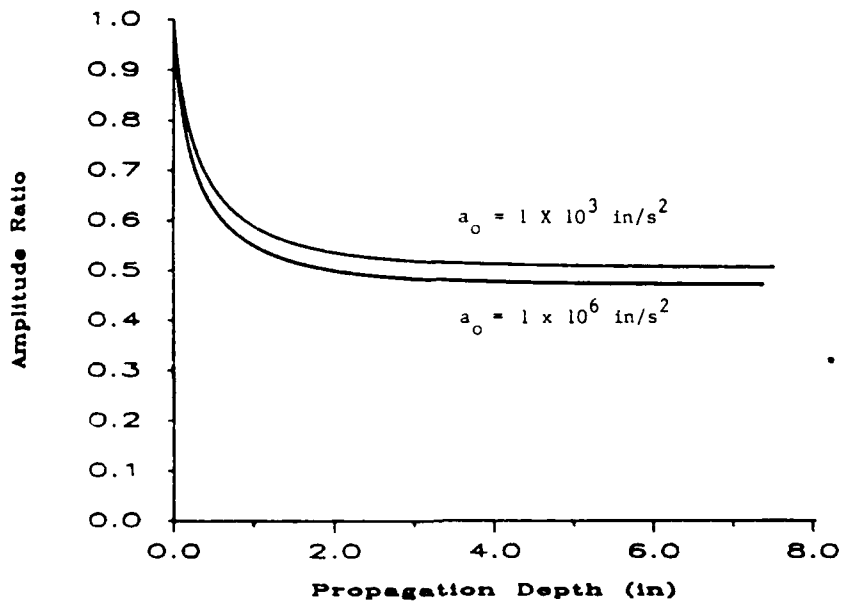


Figure 5. Wave Speed Versus Depth for an Exponential Volume Distribution with $B = 0.72 \text{ in}^{-1}$.



(a) $v_b = 0.75$ and $B = 0.72 \text{ in}^{-1}$.



(b) $v_b = 0.65$ and $B = 0.72 \text{ in}^{-1}$.

Figure 6. Amplitude Behavior for an Exponential Volume Distribution

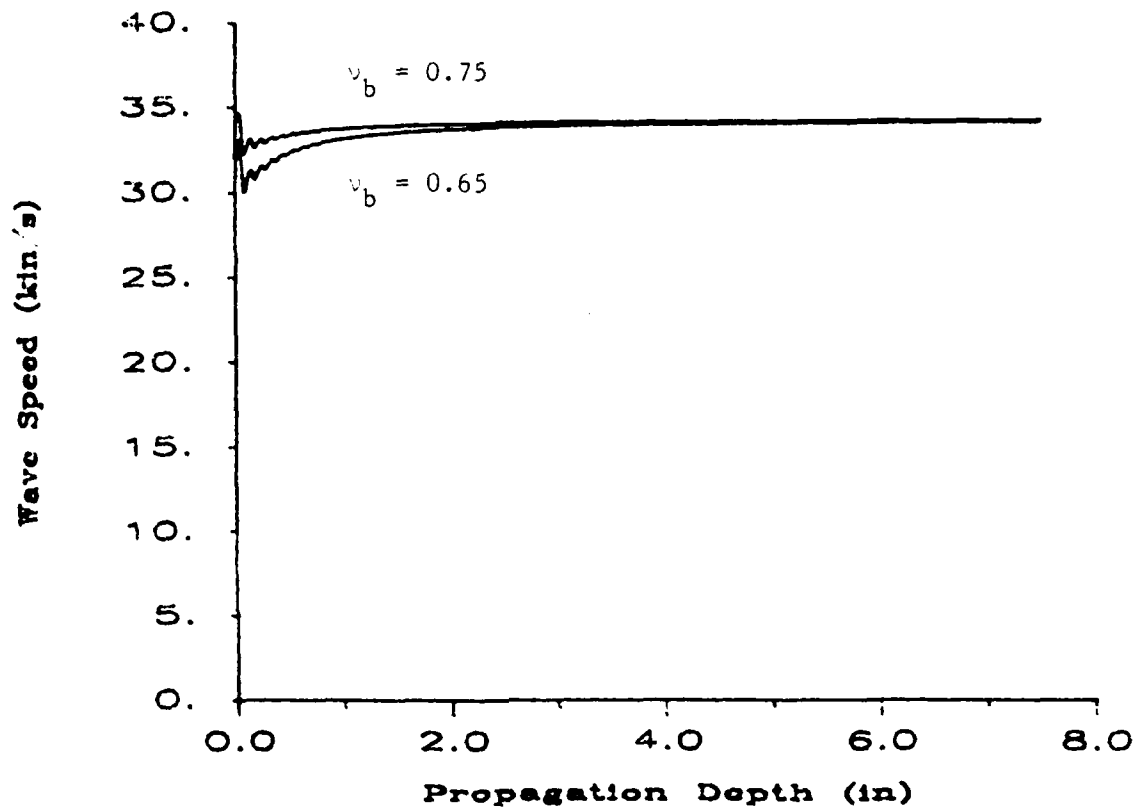
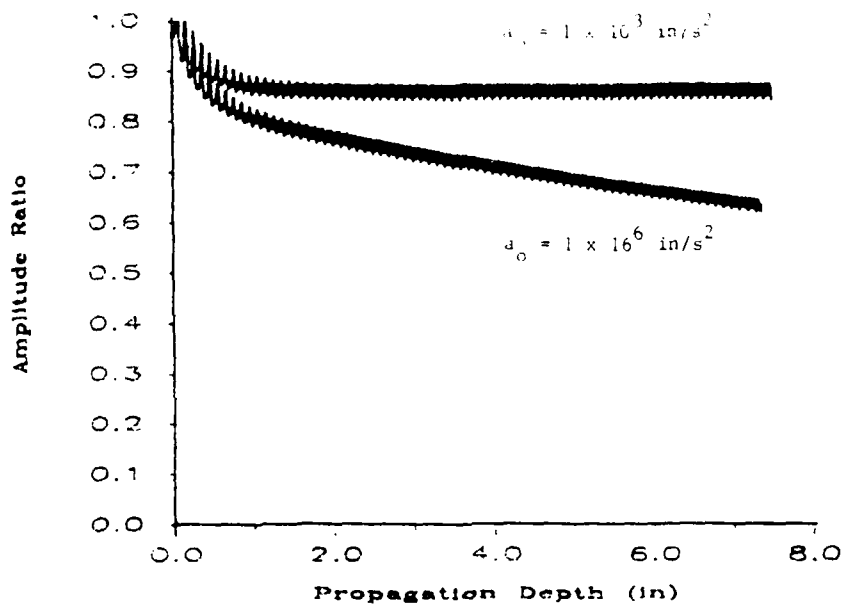
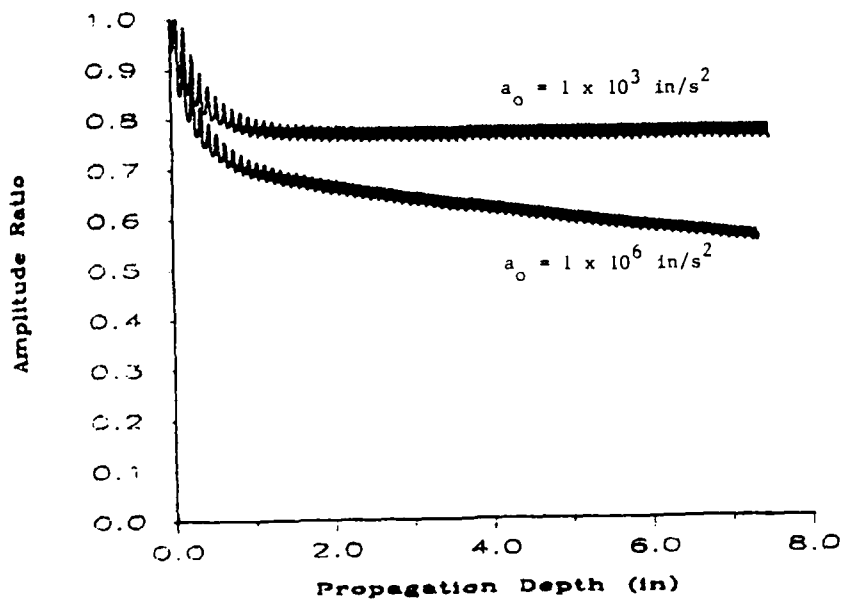


Figure 7. Wave Speed Versus Depth for a Periodic-Exponential Volume Distribution with $v_a = 0.992$, $B = 2.16 \text{ in}^{-1}$ and $\ell = 0.1 \text{ in}$.



(a) $v_b = 0.75$



(b) $v_b = 0.65$

Figure 8. Amplitude Behavior for a Periodic-Exponential Volume Distribution with $v_a = 0.992$, $\ell = 0.1 \text{ in}$ and $B = 2.16 \text{ in}^{-1}$.

Paper B

*Proceedings of the 4th International Conference on
Computational Methods and Experimental Measurements
Capri, Italy, May 1989*

Computational and Experimental Modeling of Wave Propagation in Granular Materials

M. H. Sadd, A. Shukla and H. Mei

*Department of Mechanical Engineering & Applied Mechanics
University of Rhode Island, Kingston, RI, 02881, U.S.A.*

ABSTRACT

A computational and experimental study has been conducted on the propagation of mechanical waves in granular materials. The computational study employed the use of the *distinct element method* whereby the motion of each granule in the material is modeled by rigid-body dynamics assuming each particle interaction has a particular stiffness and damping. The experimental investigation has used the method of *dynamic photoelasticity* to collect photographic data which provide information on the wave speeds, inter-granular contact loadings, and wave spreading characteristics. The experimental results provide special dynamic material constants necessary for the computational modeling, and they also provide data for comparison purposes. Results from both the computational and experimental studies indicate that *local microstructure* plays an important role in the wave propagation through such materials.

INTRODUCTION

A granular medium can be characterized as a collection of distinct particles which can displace independently from one another and interact only through contact mechanisms. Because of this discrete character, the mechanical behavior of such materials under static and dynamic loading conditions is very difficult to model. It is now generally accepted that the local microstructure or fabric, i.e. the local geometrical arrangement of particles, plays a dominant role in the transmission of mechanical loadings through these materials. Porosity, which provides only an average estimate of microstructure, is by itself not sufficient to accurately predict the behavior of granular materials. Our aim here is to understand the dynamic behavior of this type of material when it is subjected to explosive loadings of short duration which produce propagating stress waves. The discrete medium will act as a structured wave guide, providing selective paths for the waves to propagate. Amplitude attenuation will then depend strongly upon the selected path of

propagation, and thus the wave propagation is linked to the medium microstructure.

A large volume of reported research on the mechanical behavior of granular materials exists in the literature. Constitutive models have employed for example: elastic/plastic contact theories [1-3], fabric tensors [4], distributed body models [5,6], endochronic theories [7], pore collapse mechanisms [8], and probabilistic approaches [9,10]. In addition, a numerical scheme developed by Cundall and Strack [11], called the distinct element method has also been used to simulate granular media by modeling the behavior of large assemblies of circular disks. In this method, the contact forces and displacements of an assembly of disks are determined through a series of calculations tracing the movements of each of the individual disks. The method is based on the use of an explicit numerical scheme in which the interaction of the granules is modeled using rigid-body dynamics assuming each particle interaction has a particular stiffness and damping. Several successful applications of this method have been reported [12,13], and based upon these, this method has been developed and applied to the wave propagation problems to be reported here.

For applications to wave propagation, the movements of each of the disks is a result of the propagation through the medium of disturbances originating at the loading points. Consequently, the wave speed and amplitude attenuation will be a function of the physical properties of the discrete medium, i.e. the microstructure. Through the use of base line experimental data from dynamic photomechanics studies on a simple straight chain of disks, the required dynamic stiffness and damping parameters were determined. These values were then used to predict the wave motion in other more complex geometries.

DISTINCT ELEMENT MODELING

The distinct element approach uses Newtonian rigid-body mechanics to model the translational and rotational motion of each disk in a model assembly. In the numerical routine, time steps are taken over which velocities and accelerations are assumed to be constant. In addition, it is also assumed that during this time step, disturbances cannot propagate from any disk further than its immediate neighbors. This then makes the method explicit, and therefore at all times the resultant forces on any disk are determined solely by its interactions with the disks it is in contact.

Consider the case of two disks in contact as shown in Figure 1. The position, velocity, acceleration, angular velocity, angular acceleration, radius, and mass of disk 1 are labeled as: r_1 , v_1 , a_1 , ω_1 , α_1 , R_1 , and m_1 , with like notation for disk 2. The unit normal vector n and unit tangential vector t are defined as shown.

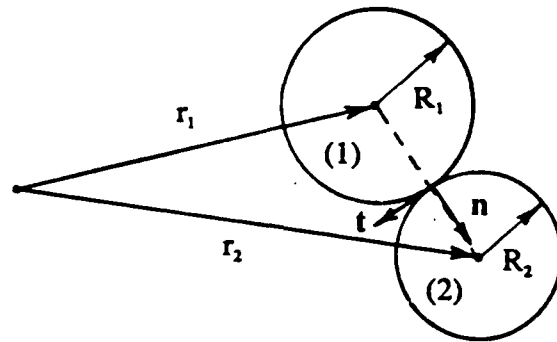


Figure 1. Schematic of Disk Interaction

The normal component of relative contact velocity between the two disks is given by

$$v_n = (\mathbf{v}_1 - \mathbf{v}_2) \cdot \mathbf{n} \quad (1)$$

while the tangential relative velocity is

$$v_t = (\mathbf{v}_1 - \mathbf{v}_2) \cdot \mathbf{t} - (\omega_1 R_1 + \omega_2 R_2) . \quad (2)$$

Using a finite difference scheme with constant properties over the time interval, the relative velocities may be integrated with respect to time to yield the incremental relative normal and tangential displacements, i.e.

$$\Delta x_n = v_n \Delta t = [(\mathbf{v}_1 - \mathbf{v}_2) \cdot \mathbf{n}] \Delta t \quad (3)$$

$$\Delta x_t = v_t \Delta t = [(\mathbf{v}_1 - \mathbf{v}_2) \cdot \mathbf{t} - (\omega_1 R_1 + \omega_2 R_2)] \Delta t .$$

In a similar way, the absolute velocity may be computed from the acceleration using the relation

$$\Delta \mathbf{v} = \mathbf{a} \Delta t . \quad (4)$$

These relative displacement increments are to be used with a particular contact force-displacement law in order to calculate the forces on each disk in the assembly. Through allowable deformations, the disks in contact are permitted to overlap with one another such that the distance between their centers will become less than $(R_1 + R_2)$. While the general technique could include a complex nonlinear contact law, the present study incorporates a simple linear relation of the form

$$\Delta F_n = K_n \Delta x_n \quad (5)$$

$$\Delta F_t = K_t \Delta x_t ,$$

where K_n and K_t are the normal and tangential contact stiffnesses. At each time step, the force increments ΔF_n and ΔF_t are added to the sum of the total forces F_n and F_t on each disk from previous time steps, i.e.

$$(F_n)_N = (F_n)_{N-1} + \Delta F_n \quad (6)$$

$$(F_t)_N = (F_t)_{N-1} + \Delta F_t ,$$

where the indices N and $N-1$ refer to times t_N and t_{N-1} , and $\Delta t = t_N - t_{N-1}$. A Coulomb-type friction law is incorporated to deal with the tangential loading. This law is defined by

$$(F_t)_{\max} = \mu F_n + c , \quad (7)$$

where μ is the coefficient of friction and c is the cohesion between the two disks. If the absolute value of $(F_t)_N$ found from equation (6)₂ is larger than $(F_t)_{\max}$, then $(F_t)_N$ is set equal to $(F_t)_{\max}$.

The motion of each disk is calculated using Newton's second law of motion. Since the behavior of real granular media involves energy dissipation, forms of damping should be incorporated into the model. Two forms of such damping are therefore introduced. A *local damping* proportional to the relative disk velocities, and a *global damping* proportional to the absolute disk velocities will be included in the force balance laws. Applying Newton's law to disk 1, therefore yields

$$F_1 - C_n v_{n1} n - C_t v_{t1} t - C_g v_1 = m_1 a_1 \quad (8)$$

$$M_1 - C_n v_{n1} R_1 - C_g \omega_1 = I_1 \alpha_1 ,$$

where F and M are the resultant force and moment on the disk, C_n and C_t are the local damping coefficients for the normal and tangential directions, C_g is the global damping coefficient, and I_1 is the moment of inertia of the disk. Equations (8) can thus be solved for the accelerations a_1 and α_1 over each time increment. With the accelerations known, the velocities follow from application of equation (4) and the relative displacements can then be computed from equation (3). This leads to new values of the forces through (5) for the next time increment, and the cycle is repeated again for each disk. In this manner, large assemblies of disks can be analyzed in a reasonable amount of computer time. Values of the stiffness and damping parameters appropriate for a given material are difficult to measure. For the static case, the stiffness properties may be computed from Hertz theory or from other elasticity analyses. However, for the dynamic case involving loadings of short duration, estimates of the model parameters are extremely difficult to make. It is here that experimental dynamic photoelasticity can be used.

EXPERIMENTAL TECHNIQUE

The optical technique of dynamic photoelasticity along with high speed photography is very well suited to study wave propagation in different assemblies of granular media. Details on the wave speed, inter-granular contact forces, and wave spreading phenomena may all be determined through this experimental method. The granular medium was simulated by assemblies of one inch diameter discs which were fabricated from a brittle polyester material, *Homalite 100*. The dynamic loading was achieved by exploding a small charge of PETN in a specially designed charge holder directly on top of one of the grains. Experimental granular assemblies were placed in the optical bench of a *high speed multiple spark gap camera*. The details of this camera are given in [14]. This high speed photographic system operates as a series of high intensity, extremely short duration pulses of light and provides 20 photoelastic images at discrete times during the dynamic event. Framing rates of up to 10^6 frames per second are attainable using this photographic system. Typical photographs obtained during the experiments are shown in Figures 2 and 3. These photographs show the *isochromatic fringes* at different times as the stress wave passes through the granular assemblies. Figure 2 illustrates the propagation of a stress wave down a single straight chain of disks, while Figure 3 shows the dynamic fringe patterns associated with waves moving through three different two-dimensional assemblies.

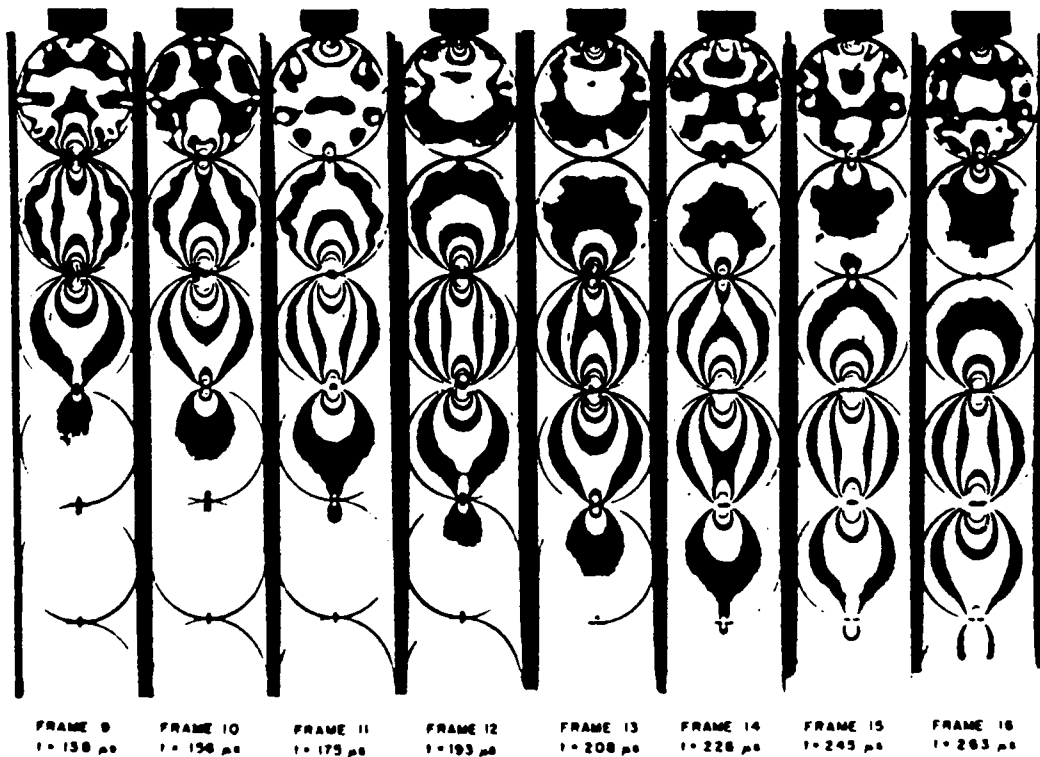
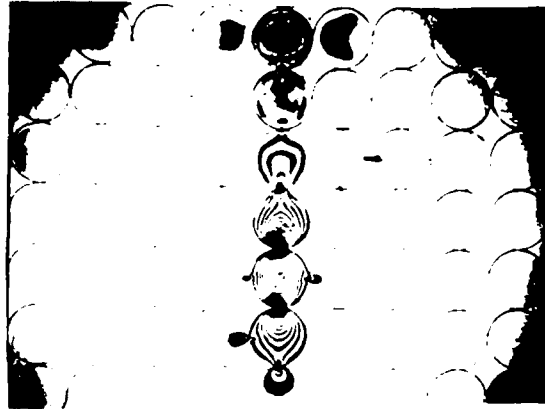
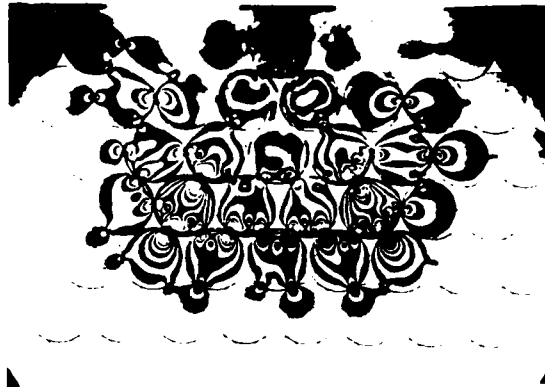


Figure 2. Photoelastic Fringe Patterns of the Single Disk Chain for a Sequence of Times



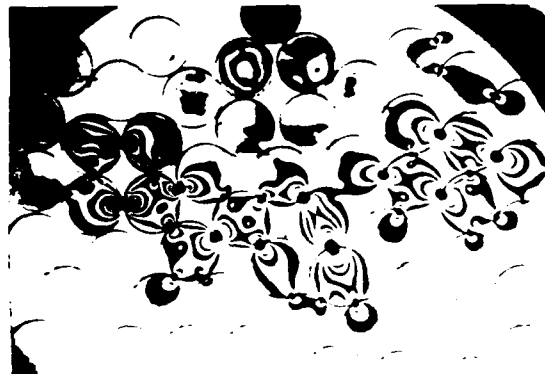
FRAME 19, $t = 184.5 \mu s$

(a) Body-Centered Cubic Geometry



FRAME 12, $t = 125 \mu s$

(b) Hexagonal Close Packing



FRAME 18, $t = 159.5 \mu s$

(c) Random Packing

Figure 3. Photoelastic Fringe Patterns

The isochromatic fringes obtained during the experiments are lines of constant maximum shear stress. These fringes are related to the stress field by the *stress optic law*

$$\sigma_1 - \sigma_2 = Nf_o/h , \quad (9)$$

where, σ_1 and σ_2 are the principal stresses, N is the fringe order, f_o is the material fringe value, and h is the thickness of the model.

Shukla and Nigam [15] have shown that equation (9) when combined with the Hertz contact stress equations can be used to analyze the stress field in the vicinity of the contacts shown in the Figures 2 and 3. This analysis yields both the normal and the tangential contact forces as a function of time. Some particular values of the peak contact forces obtained in these geometries are shown in Figures 4 and 5, and these are to be used in conjunction with the numerical study.

RESULTS AND CONCLUSIONS

In order to apply the distinct element method to various granular assemblies, values for the model parameters (stiffness and damping coefficients) must be determined. For the dynamic case, we expect that the contact stiffnesses K_n and K_t , will be difficult to calculate from simple static Hertz contact theory. In addition, values for the damping would also be difficult to calculate from say elastodynamic theory. Hence, the dynamic photoelastic experiments were used to provide this information. Experiments were performed on a *single straight chain* of disks (see Figure 2), and these experiments were considered to be our *calibration tests*. Appropriate values for these stiffness and damping coefficients were thus determined to match the data from the calibration experiments. These values were then retained in the model to predict the wave motion in other more complicated geometries. For the cases to be reported here the contact stiffnesses were taken as $K_n = K_t = 6.4 \times 10^6$ N/m, and the local normal damping coefficient was $C_{in} = 32$ N·s/m. Global damping was not included, and tangential contact loading was set to zero. The input loading was chosen to be a triangular profile of 60 μ s duration, and the time step was taken as $\Delta t = 2\mu$ s.

Results from the distinct element modeling are shown in Figures 4 and 5 for four different assemblies, i.e. the single straight chain, body-centered cubic, hexagonal close packing, and a random packing. Numerical predictions of the maximum inter-granular contact loadings (normalized with respect to the input loading) are shown at various contacts in the assemblies. For comparison, the corresponding experimental values are also given in parentheses. As mentioned, the straight chain experiment was actually used to determine the model parameters. For the body centered cubic geometry shown in Figure 4, experiments indicate that for input excitation directed along a column chain, the resulting wave motion will occur only along that chain.

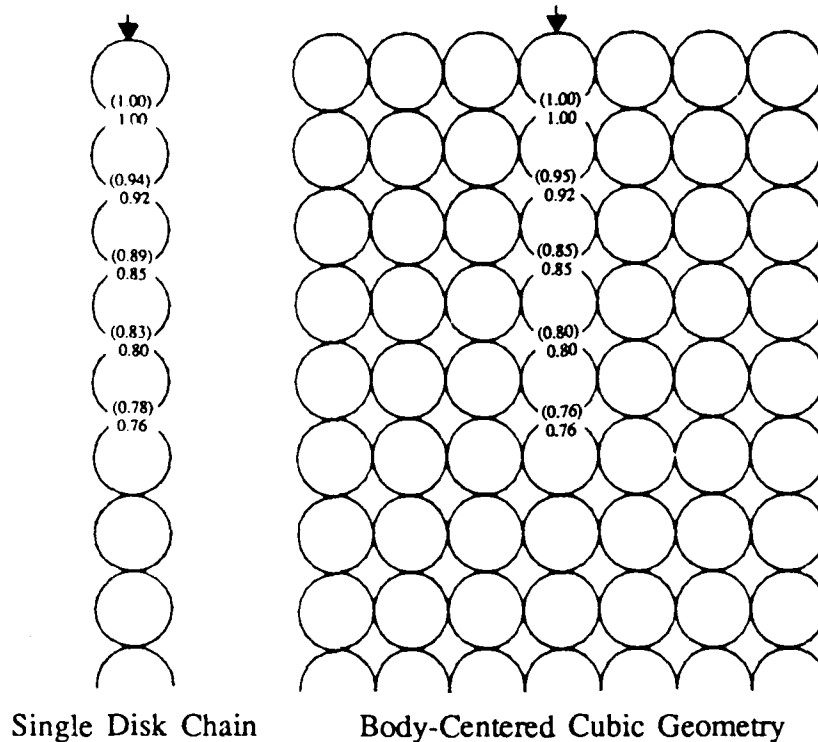


Figure 4. Distinct Element Predictions and Comparisons

This was also predicted numerically as seen from Figure 4. On the other hand, the hexagonal close packing geometry allows wave motion in many different chains and paths (this can be seen from the experiments shown in Figure 3). Some of the numerical predictions are compared with experiments for this geometry for two principal chains as shown in Figure 5. The random model material offers the most complex wave transmission phenomena. This model contains some grains with noticeable tangential inter-granular contact loadings. However, as seen in Figure 5, our frictionless numerical simulation provides contact values which are generally comparable to the experimental data.

Results of this study illustrate the dependence of microstructure on the wave propagation. In order to describe local microstructure or fabric, it is convenient to define the term *branch vectors* which are drawn from the mass centers of adjacent disks. The angle between neighboring branch vectors may be denoted as a *branch angle*. It is therefore clear from Figures 4 and 5 that the inter-granular contact force, which is a measure of the wave amplitude, behaves quite differently when the wave propagates through media with large changes in the branch vector distribution. Further numerical and experimental studies are underway in an attempt to model additional dynamic phenomena in granular media.

ACKNOWLEDGEMENT

This research was supported by the Army Research Office under contract number DAAL03-86-K-0125.

REFERENCES

- [1] Deresiewicz, H. "Mechanics of Granular Matter", *Advances in Applied Mechanics*, Vol. V, Academic Press, New York, 1958.
- [2] Walton, K. "The Effective Elastic Moduli of a Random Packing of Spheres", *J. Mech. Phys. Solids*, Vol. 35, pp 213-226, 1987.
- [3] Petrakis, E. and Dobry, R. "A Self Consistent Estimate of the Elastic Constant. of a Random Array of Equal Spheres with Application to Granular Soil Under Isotropic Conditions", Report CE-86-04, Rensselaer Polytechnic Institute, Troy, NY, 1986.
- [4] Nemat-Nasser, S. and Mehrabadi, M.M., "Stress and Fabric in Granular Masses", *Mechanics of Granular Materials: New Models and Constitutive Relations*, pp 1-8, Elsevier, New York, 1983.
- [5] Goodman, M.A. and Cowin, S.C., "A Continuum Theory for Granular Materials", *Arch. Rat. Mech. Anal.*, Vol. 44, pp 249-266, 1972.
- [6] Sadd, M.H. and Hossain, M., "Wave Propagation in Distributed Bodies with Applications to Dynamic Soil Behavior", to appear in *Journal of Wave-Material Interaction*, December, 1988.
- [7] Bazant, Z.P., Krizek, R.J., and Shieh, C.L., "Hysteretic Endochronic Theory for Sand", *J. Eng. Mech.*, Vol. 109, pp 1073-1095, 1983.
- [8] Carroll, M.M. and Holt, A.C., "Static and Dynamic Pore-Collapse Relations for Ductile Porous Materials", *J. Appl. Phys.*, Vol. 43, pp 1626-1636, 1972.
- [9] Endley, S.N. and Peyrot, A.H., "Load Distribution in Granular Media", *J. Eng. Mech. Division of ASCE*, Vol. 103, pp 99-111, 1977.
- [10] Fu, L.S., "A New Micro-Mechanical Theory for Randomly Inhomogeneous Media", *Wave Propagation in Homogeneous Media and Ultrasonic Non-Destructive Evaluation*, Applied Mechanics Division-Vol. 62, American Society of Mechanical Engineers, 1984.
- [11] Cundall, P. and Strack, D.L., "A Discrete Numerical Model for Granular Assemblies", *Geotechnique*, Vol. 29, pp 47-65, 1979.
- [12] Thornton, C. and Barnes, D.J., "Computer Simulated Deformation of Compact Granular Assemblies", *Acta Mech.*, Vol. 64, pp 45-61, 1986.
- [13] Bathurst, R.J. and Rothenburg, L., "Micromechanical Aspects of Isotropic Granular Assemblies with Linear Contact Interactions", *J. Appl. Mech.*, Vol. 55, pp 17-23, 1988.
- [14] Riley, W.F. and Dally, J.W., "Recording Dynamic Fringe Patterns with a Cranz-Schardin Camera", *Exp. Mech.*, Vol. 9, pp 27-33, 1969.
- [15] Shukla, A. and Nigam, H., "A Numerical-Experimental Analysis of the Contact Stress Problem", *J. Strain Anal.*, Vol. 20, pp 241-245, 1985.

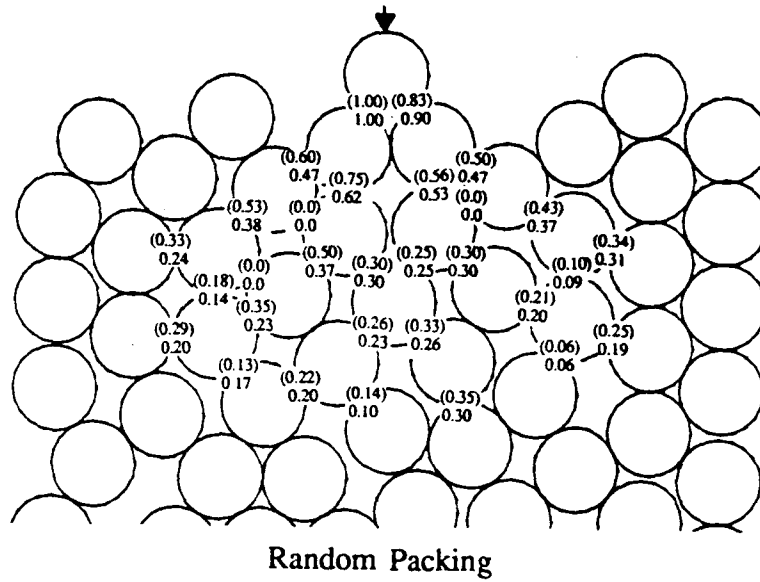
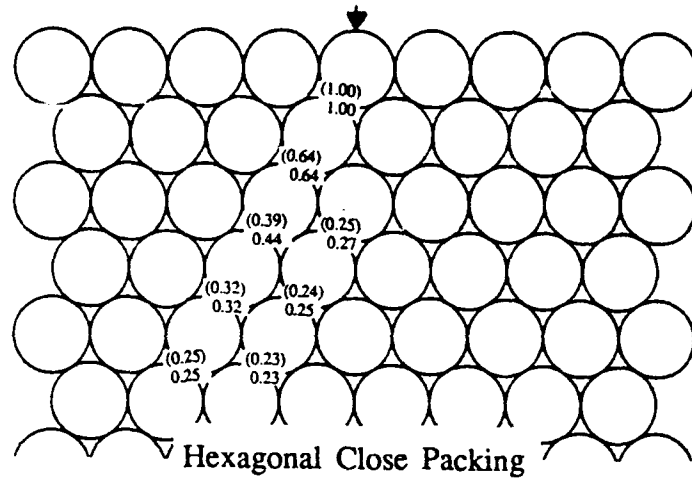


Figure 5. Distinct Element Predictions and Comparison

Paper C

Micromechanics and Inhomogeneity - The Toshio Mura Anniversary Volume
ed. G.J. Weng, M. Taya and H. Abe, Springer-Verlag, New York, 1989.

The Effect of Voids and Inclusions on Wave Propagation in Granular Materials

by

M. H. Sadd, A. Shukla, H. Mei and C. Y. Zhu
Department of Mechanical Engineering & Applied Mechanics
University of Rhode Island, Kingston, RI, 02881, U.S.A.

Abstract

Theoretical and experimental studies have been conducted on the dynamic response of granular materials containing local discontinuities of voids and inhomogeneous inclusions. The granular medium was simulated by a specific assembly of circular disks which were subjected to explosive loadings of short duration. Voids were created by removing particular disks from the assembly, while inclusions were constructed by replacing certain disks with ones of a higher impedance material. The computational simulation was accomplished through the use of the distinct element method in which the intergranular contact forces and displacements of the assembly disks are determined through a series of calculations tracing the movements of each of the individual disks. The experimental study employed the use of photoelasticity in conjunction with high speed photography to collect photographic data of the propagation of waves in transparent assemblies of model granular media. Comparisons were made between the computational results and the experimental data for the local intergranular contact forces around each void or inclusion. Both voids and inclusions produce local wave scattering through various reflection mechanisms, and the results seem to indicate that the inclusions produced higher local wave attenuation.

1. Introduction

Granular media can be described as a collection of distinct particles which can displace independently from one another and which interact only through contact mechanisms. This type of media transmits loadings through discrete paths, and therefore the mechanical behavior of such materials under static and dynamic loading conditions is very complex and difficult to model. It is now generally accepted that the *local microstructure or fabric*, i.e. the local geometrical arrangement of particles, plays a dominant role in the transmission of mechanical loadings through these materials. The material *porosity* provides only an average estimate of microstructure, and by itself it is not sufficient to accurately predict the behavior of granular materials. Our general aim here is to understand the dynamic behavior of this type of material when it is subjected to

explosive loadings of short duration which produce propagating stress waves. The discrete medium will act as a structured wave guide, providing selective paths for the waves to propagate. Amplitude attenuation will then depend strongly upon the selected path of propagation, and thus the wave propagation is strongly linked to the medium microstructure.

A considerable amount of research on the mechanical behavior of granular materials has been reported in the literature. Constitutive models have employed for example: *elastic/plastic contact theories* (Deresiewicz, 1959, Walton, 1987, and Petrakis and Dobry, 1986), *fabric tensors* (Nemat-Nasser, 1983), *distributed body models* (Goodman and Cowin, 1972), *endochronic theories* (Bazant, 1983), *pore collapse mechanisms* (Carroll and Holt, 1972), and *probabilistic approaches* (Endley and Peyrot, 1977, and Fu, 1977). The concept of modeling granular media as an array of elastic disks or spheres lead to the initial attempts at predicting wave propagation phenomena. Early wave propagation studies include Iida (1939), Takahashi and Sato (1949), Hughes and Cross (1951), Hughes and Kelly (1952), Gassman (1951), Brandt (1955), and Duffy and Mindlin (1957). This initial work investigated the propagation velocity as a function of confining pressure, particle size and geometrical packing. This particular modeling concept lead to work in determining the elastic constants of particular granular assemblies, see for example, Hendron (1963), Petrakis and Dobry (1986), and Walton (1987). In addition, wave propagation studies for granular and porous media by Nunziato et.al. (1978) and Sadd and Hossain (1989) have employed the distributed body theory. Experimental studies of this problem employing the method of *dynamic photoelasticity* have been reported by Shukla et.al. (1985,1987,1988). In this method, high speed photography was used to collect photographic data of wave propagation in transparent model materials composed of assemblies of birefringent disks.

A numerical scheme developed by Cundall and Strack (1979), called the *distinct element method* has also been used to simulate granular media by modeling the behavior of large assemblies of circular disks. In this method, the contact forces and displacements of an assembly of disks are determined through a series of calculations tracing the movements of each of the individual disks. The method is based on the use of an explicit numerical scheme in which the interaction of the granules is modeled using rigid-body dynamics assuming each particle interaction has a particular stiffness and damping. For applications to wave propagation, the movements of each of the disks is a result of the propagation through the medium of disturbances originating at the loading points. Consequently, the wave speed and amplitude attenuation (intergranular contact force) will be a function of the physical properties of the discrete medium, i.e. the microstructure. Several successful applications of this method have been reported (Thorton and Barnes, 1986, Bathurst and Rothenburg, 1988, and Sadd et.al., 1989), and based upon these, this method has been developed and applied to the wave propagation problems to be reported here.

The present study focuses on a specific aspect of wave propagation in granular materials, namely the effects of *voids* and *inclusions*. It is well known that actual granular media contains both voids and heterogeneous inclusions. These quantities further complicate an already complex microstructural material. Most past studies on wave propagation in these materials have been limited to looking at aggregate assemblies with uniform packing geometries. Our focus here is to investigate the local effects produced by voids and inclusions in regular arrays of circular disks, and of primary concern, is the wave scattering in the vicinity of the microstructural defect. The wave propagation

phenomena is to be studied through the determination of the intergranular contact force distribution in the neighborhood of a particular void or inclusion. This problem has been studied using the computational method of distinct elements, and using the experimental technique of dynamic photoelasticity.

2. Distinct Element Method

The distinct element method is a simplified modeling concept which uses Newtonian rigid-body mechanics to model the translational and rotational motion of each disk in a model assembly. The technique establishes a discretized time stepping numerical routine, in which granule velocities and accelerations are assumed to be constant over each time interval. It is also assumed that during each time step, disturbances cannot propagate from any disk further than its immediate neighbors. Under these assumptions, the method becomes explicit, and therefore at any time increment the resultant forces on any disk are determined solely by its interactions with the disks it is in contact.

In order to describe the method, consider the case of two disks in contact as shown in Figure 1. The position, velocity, acceleration, angular velocity, angular acceleration, radius, and mass of disk 1 are labeled as: r_1 , v_1 , a_1 , ω_1 , α_1 , R_1 , and m_1 , with like notation for disk 2. The unit normal vector n and unit tangential vector t are defined as shown.

The normal component of relative contact velocity between the two disks is given by

$$v_n = (v_1 - v_2) \cdot n \quad (2.1)$$

while the tangential relative velocity is

$$v_t = (v_1 - v_2) \cdot t - (\omega_1 R_1 + \omega_2 R_2) \quad (2.2)$$

Using a finite difference scheme with constant properties over the time interval, the relative velocities may be integrated with respect to time to yield the incremental relative normal and tangential displacements, i.e.

$$\begin{aligned} \Delta x_n &= v_n \Delta t = [(v_1 - v_2) \cdot n] \Delta t \\ \Delta x_t &= v_t \Delta t = [(v_1 - v_2) \cdot t - (\omega_1 R_1 + \omega_2 R_2)] \Delta t \end{aligned} \quad (2.3)$$

In a similar way, the absolute velocity may be computed from the acceleration using the relation

$$\Delta v = a \Delta t \quad (2.4)$$

These relative displacement increments are to be used with a particular contact force-displacement law in order to calculate the forces on each disk in the assembly. Through allowable deformations, the disks in contact are permitted to overlap with one another such that the distance between their centers will become less than $(R_1 + R_2)$. While the general technique could include a complex nonlinear contact law, the present study incorporates a simple linear relation of the form

$$\begin{aligned}\Delta F_n &= K_n \Delta x_n \\ \Delta F_t &= K_t \Delta x_t ,\end{aligned}\quad (2.5)$$

where K_n and K_t are the normal and tangential contact stiffnesses. At each time step, the force increments ΔF_n and ΔF_t are added to the sum of the total forces F_n and F_t on each disk from previous time steps, i.e.

$$\begin{aligned}(F_n)_N &= (F_n)_{N-1} + \Delta F_n \\ (F_t)_N &= (F_t)_{N-1} + \Delta F_t ,\end{aligned}\quad (2.6)$$

where the indices N and $N-1$ refer to times t_N and t_{N-1} , and $\Delta t = t_N - t_{N-1}$. A Coulomb-type friction law is incorporated to deal with the tangential loading. This law is defined by

$$(F)_{\max} = \mu F_n + c ,\quad (2.7)$$

where μ is the coefficient of friction and c is the cohesion between the two disks. If the absolute value of $(F)_N$ found from equation (2.6)₂ is larger than $(F)_{\max}$, then $(F)_N$ is set equal to $(F)_{\max}$.

Using Newton's second law of motion, the acceleration of each disk at each time interval can be determined. Now since the behavior of real granular media involves energy dissipation, the modeling introduces damping mechanisms. Two forms of such damping are therefore introduced. A *local damping* proportional to the relative disk velocities, and a *global damping* proportional to the absolute disk velocities will be included in the force balance laws. Applying Newton's law to disk 1, therefore yields

$$\begin{aligned}F_1 - C_{ln} v_{n1} \mathbf{n} - C_{lt} v_{t1} \mathbf{t} - C_g v_1 &= m_1 a_1 \\ M_1 - C_{lr} v_{r1} R_1 - C_g \omega_1 &= I_1 \alpha_1 ,\end{aligned}\quad (2.8)$$

where F and M are the resultant force and moment on the disk, C_{ln} and C_{lt} are the local damping coefficients for the normal and tangential directions, C_g is the global damping coefficient, and I_1 is the moment of inertia of the disk. Equations (2.8) can thus be solved for the accelerations a_1 and α_1 over each time increment. With the accelerations known, the velocities follow from application of equation (2.4) and the relative displacements can then be computed from equation (2.3). This leads to new values of the forces through (2.5) for the next time increment, and the cycle is repeated again for each disk. In this manner, large assemblies of disks can be analyzed in a reasonable amount of computer time. Values of the stiffness and damping parameters appropriate for a given material are difficult to measure. For the static case, the stiffness properties may be computed from Hertz theory or from other elasticity analyses. However, for the dynamic case involving loadings of short duration, estimates of the model parameters are difficult to make. In order to determine estimates of these model parameters, experimental results from dynamic photoelasticity were employed. Data from simple calibration tests on a single chain of disks were used to determine values for the contact stiffness and damping for the disk assemblies under study. For the stiffness parameter, the dynamic stiffness was written as

$$K_n = \alpha K_n^{(s)},\quad (2.9)$$

where $K_n^{(s)}$ is the static contact stiffness from Hertz theory given by

$$K_n^{(s)} = \frac{\pi h E_1 E_2}{2(E_1 + E_2)} \quad (2.10)$$

and α is a *dynamic stiffness coefficient* which is to be determined by the experiments, h is the disk thickness, and E_1 and E_2 are the elastic moduli of the two disks in contact. The α coefficient may be thought of as an adjustment parameter, less than unity, which accounts for the fact that the entire disk will not deform during the dynamic event.

3. Photomechanics Studies

A series of dynamic photoelastic experiments were conducted to provide experimental information on the effect of voids and inclusions on the wave propagation phenomena. For the experimental study, the granular medium was simulated with assemblies of polymeric birefringent disks of *Homalite 100*, 25.4mm in diameter and 6.25mm thick. In all the experiments reported here, the disks were assembled in an hexagonal close packing geometry as shown in Figure 2. Voids in the assembly were created by removing disks from different locations, while inclusions were created by replacing particular disks with ones of a different material (steel). Dynamic loading was achieved by detonating a small charge of PETN in a specially designed charge holder, which was mounted at the top-centerline of the model assemblies. The experimental models were placed in the optical bench of a high speed photographic system. This high speed photographic system operated as a series of high intensity, extremely short duration pulses of light and provided 20 photoelastic images at discrete times during the dynamic event. Framing rates of up to 10^6 frames per second are achievable, and this allows studies of wave propagation to be made, see Riley and Dally (1969).

A typical sequence of four images from each experiment are shown in Figures 2 through 6. The photographic data shows the isochromatic fringe patterns at different times as the stress wave propagates through the model assemblies. The wave propagation history can thus be clearly seen from a sequence of such photographs. Figure 2 illustrates the wave patterns for the assembly with no voids or inclusions. Figures 3 and 4 show the wave motion for the cases of single and multiple voids, while Figures 5 and 6 illustrate the cases with inclusions of higher density and stiffness. Inspection of the photographs reveals that the wave length λ , of the loading pulse is much larger than the disc diameter D ; in fact $\lambda \approx 4D$. Furthermore, in most cases the fringe pattern around the contact points are symmetric on either side of the contact points and are similar to the fringes obtained under static compression. Both these features indicated that around the contact zone, quasi static loading was present during the wave propagation event. Thus Hertz theory can be used to estimate the stress field in the vicinity of the contacts.

The isochromatic fringes photographed during the experiments are lines of constant maximum shear stress, and are related to the stress field by the *stress optic law*

$$\sigma_1 - \sigma_2 = N f_o / h \quad (3.1)$$

where σ_1 and σ_2 are the principal stresses, N is the fringe order, f_o is the material fringe value, and h is the model thickness. Using relation (3.1) along with the Hertz contact stress equations, Shukla and Nigam (1985) have developed a scheme to compute the quasi-

static stress field in the vicinity of the contacts between each grain. These contact stresses may then be integrated along the contact length to determine the normal and tangential contact forces transmitted between the disks at various times during the dynamic process. Thus the intergranular contact loading, which is related to the wave amplitude, can be experimentally computed. These experimental results can then be compared with the theory, and they can also be used to determine necessary material model parameters (e.g. the contact stiffness and damping) in order to use the distinct element method.

4. Results and Comparisons

Specific results of the distinct element modeling along with comparisons to the experimental data will now be given for particular granular assemblies containing voids and inclusions. The basic assembly geometry is a hexagonal close packing arrangement shown in Figure 7. The theoretical model used an input loading of triangular time dependence with a $60\mu\text{s}$ duration to model the explosive loading from the experiments. The local stiffness and damping parameters K_n , K_t , C_{in} , and C_{it} needed in the distinct element model were determined from experimental tests conducted on straight single chains of disks. These calibration experiments provided specific values for the wave speed and amplitude attenuation for a very simple geometry. The model parameters were thus chosen to produce the best match to the calibration data, and these values were then retained in the model to be used for calculations of more complicated geometry. The contact stiffnesses for Homalite-to-Homalite contacts were taken as $K_n = K_t = 6.4 \times 10^6 \text{ N/m}$ ($\alpha = 0.27$), and the local normal damping coefficient was $C_{in} = 32 \text{ Ns/m}$. Global damping was not included, and tangential contact loading was set to zero. The time stepping increment was taken to be $2\mu\text{s}$ for all cases studied, and this was felt to be appropriate to calculate the essential features of the dynamic event.

Results from the distinct element technique are shown in Figure 7 for the basic granular media with no voids or inclusions. Numerical predictions of the maximum intergranular contact loadings (normalized with respect to the input loading) are shown at various contacts in the assembly. The corresponding experimental values are also given in parentheses. The contact loading values are symmetric about the assemblies' vertical centerline, and the results indicate the rapid attenuation which occurs along various chains or paths in the assembly. Comparison of theoretical with experimental contact loadings indicate that they differ by an average amount of 25%. Experimental determination of the wave speed was accomplished from the known position of the fringe patterns in the photographs. These results indicated that the leading wave front in the Homalite assemblies, propagates at approximately 995 m/s, which is about 50% of the P-wave speed in the virgin disk material. Wave speed predictions from the distinct element model matched well (within 10%) to these measured values.

Figures 8 and 9 illustrate the case of a granular media with voids present. Figure 8 contains a single void, while Figure 9 contains a series of voids down the vertical centerline of the assembly. The presence of a void produces significant local wave scattering and attenuation, especially along the main vertical chain down the centerline of the assembly. Local inter-granular contact forces become elevated near the void; however, at contacts remote from the void, the loading values are similar in magnitude (with the exception of points on the vertical centerline) to those in Figure 7. Computational and experimental contact loads compare to within an average difference of 15% for the

assemblies with voids.

The cases of granular media with inclusions of different material are shown in Figures 10 and 11. This situation is attempting to model the local effects of heterogeneity in a granular medium. Figure 10 illustrates the case of a single inclusion, and Figure 11 contains the case of several inclusions down the vertical centerline of the assembly. As mentioned the inclusion is simply a disk of a different material, and in this case the inclusion material was steel, which in comparison to the granular material (Homalite 100) has a much higher stiffness and density. The contact stiffness between the Homalite and steel disks was calculated using relations (2.9) and (2.10) retaining the same value of α . The local damping parameter C_{in} , was kept the same for this case, since there was only a small number of inclusions present.

There will be an impedance mismatch at the contacts of the Homalite and steel, and thus there will be a sizeable difference between the reflection and transmission phenomena at these contacts in comparison to those of the rest of the medium. For example, at point C in Figure 10, the wave is attempting to propagate from a relatively soft material into a stiff material. Consequently, a sizeable reflection occurs at this contact producing an upward traveling wave and a large contact force. Very little wave motion is transmitted into the inclusion, and thus the inclusion acts to block the wave motion along the vertical disk chain. For the inclusion cases, the average difference between theoretical predictions and experimental data was 20-30%.

5. Conclusions

The methods of distinct elements and dynamic photomechanics have been used to study the effects of voids and heterogeneous inclusions on the wave propagation in granular materials. The granular medium was simulated by a specific assembly of circular disks arranged in an hexagonal close packing geometry. The voids were created by removing particular disks, while inclusions were constructed by replacing particular disks with ones of a higher modulus material. Comparisons were made between the computational results and the experimental data for the local intergranular contact forces around each void or inclusion. Although comparisons produced some differences as high as 30%, it is felt that since the experimental data itself contains scatter of approximately 10%, the computational scheme does provide reasonable predictions. Improvements of the modeling procedures could be accomplished by incorporating a more sophisticated dynamic contact law.

Comparing the results, it is apparent that both the voids and inclusions cause local wave scattering. In comparison to the case with no voids or inclusions, elevated contact forces occur near the discontinuity, and along particular paths dictated by the local microstructure, rapid wave amplitude attenuation occurs. A void produces wave scattering through free-surface reflection from the empty volume, whereas the inclusion causes sizeable reflections from the material of higher impedance. Comparing the path AB in Figures 8 and 10, it appears that the inclusion produces higher attenuation than the void. Current work continues on these studies, and investigations are underway on wave propagation in granular materials with additional and more complex microstructural features.

Acknowledgement

This research was supported by the Army Research Office through contract number DAAL03-86-K-0125.

References

- Bathurst, R.J. and Rothenburg, L., 1988, "Micromechanical Aspects of Isotropic Granular Assemblies with Linear Contact Interactions", *J. Appl. Mech.*, Vol. 55, pp 17-23.
- Bazant, Z.P., Krizek, R.J., and Shieh, C.L., 1983, "Hysteretic Endochronic Theory for Sand", *J. Eng. Mech.*, Vol. 109, pp 1073-1095.
- Brandt, H., 1955, "A Study of the Speed of Sound of Porous Granular Media", *J. Appl. Mech.*, Vol. 22, pp 479-486.
- Carroll, M.M. and Holt, A.C., 1972, "Static and Dynamic Pore-Collapse Relations for Ductile Porous Materials", *J. Appl. Phys.*, Vol. 43, pp 1626-1636.
- Cundall, P. and Strack, D.L., 1979, "A Discrete Numerical Model for Granular Assemblies", *Geotechnique*, Vol. 29, pp 47-65.
- Deresiewicz, H., 1958, "Mechanics of Granular Matter", *Advances in Applied Mechanics*, Vol. V, Academic Press.
- Duffy, J. and Mindlin, R.D., 1957, "Stress-Strain Relations and Vibration of a Granular Medium", *J. Appl. Mech.*, Vol. 24, pp 585-593.
- Endley, S.N. and Peyrot, A.H., 1977, "Load Distribution in Granular Media", *J. Eng. Mech. Division of ASCE*, Vol. 103, pp 99-111.
- Fu, L.S., 1984, "A New Micro-Mechanical Theory for Randomly Inhomogeneous Media", *Wave Propagation in Homogeneous Media and Ultrasonic Non-Destructive Evaluation*, Applied Mechanics Division-Vol. 62, American Society of Mechanical Engineers.
- Gassman, F., 1951, "Elastic Waves Through a Packing of Spheres", *Geophysics*, Vol. 16, pp 673-685.
- Goodman, M.A. and Cowin, S.C., 1972, "A Continuum Theory for Granular Materials", *Arch. Rat. Mech. Anal.*, Vol. 44, pp 249-266.
- Hendron, A.J., 1963, "The Behavior of Sand in One-Dimensional Compression", Ph.D. Thesis, University of Illinois.
- Hughes, D.S. and Cross, J.H., 1951, "Elastic Wave Velocities in Rocks at High Pressures and Temperatures", *Geophysics*, Vol. 16, pp 577-593.
- Hughes, D.S. and Kelly, J.L., 1952, "Variation of Elastic Wave Velocity with Saturation in Sandstone", *Geophysics*, Vol. 17, pp 739-752.
- Iida, K., 1939, "The Velocity of Elastic Waves in Sand", *Bull. Earthquake Research Inst. Japan*, Vol. 17, pp 783-808.
- Nemat-Nasser, S. and Mehrabadi, M.M., 1983, "Stress and Fabric in Granular Masses", *Mechanics of Granular Materials: New Models and Constitutive Relations*, pp 1-8, Elsevier.
- Nunziato, J.W., Kennedy, J.E. and Walsh, E., 1978, "The Behavior of One-Dimensional Acceleration Waves in an Inhomogeneous Granular Solid", *Int. J. Engng. Sci.*, Vol. 16, pp 637-648.

- Petrakis, E. and Dobry, R., 1986, "A Self Consistent Estimate of the Elastic Constants of a Random Array of Equal Spheres with Application to Granular Soil Under Isotropic Conditions", Report CE-86-04, Rensselaer Polytechnic Institute, Troy, NY.
- Riley, W.F. and Dally, J.W., 1969, "Recording Dynamic Fringe Patterns with a Cranz-Schardin Camera", *Exp. Mech.*, Vol. 9, pp 27-33.
- Sadd, M.H., Shukla, A. and Mei, H., 1989, "Computational and Experimental Modeling of Wave Propagation in Granular Materials", *Proc. 4th Intl. Conf. Computational Methods and Experimental Measurements*, Capri, Italy, May, 1989.
- Sadd, M.H. and Hossain, M., 1989, "Wave Propagation in Distributed Bodies with Applications to Dynamic Soil Behavior", to appear in *Journal of Wave-Material Interaction*.
- Shukla, A. and Nigam, H., 1985, "A Numerical-Experimental Analysis of the Contact Stress Problem", *J. Strain Anal.*, Vol. 20, pp 241-245.
- Shukla, A. and Damania, C., 1987, "Experimental Investigation of Wave Velocity and Dynamic Contact Stresses in an Assembly of Discs", *Exp. Mechanics*, Vol. 27, pp 268-281.
- Shukla, A., Zhu, C.Y. and Sadd, M.H., 1988, "Angular Dependence of Dynamic Load Transfer Due to Explosive Loading in Granular Aggregate Chains", *J. Strain Analysis*, Vol. 23, pp 121-127.
- Takahashi, T. and Sato, Y., 1949, "On the Theory of Elastic Waves in Granular Substance", *Bull. Earthquake Research Inst. Japan*, Vol. 27, pp 11-16.
- Thornton, C. and Barnes, D.J., 1986, "Computer Simulated Deformation of Compact Granular Assemblies", *Acta Mech.*, Vol. 64, pp 45-61.
- Walton, K., 1987, "The Effective Elastic Moduli of a Random Packing of Spheres", *J. Mech. Phys. Solids*, Vol. 35, pp 213-226.

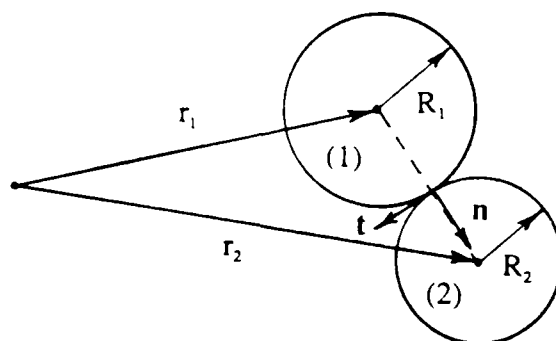
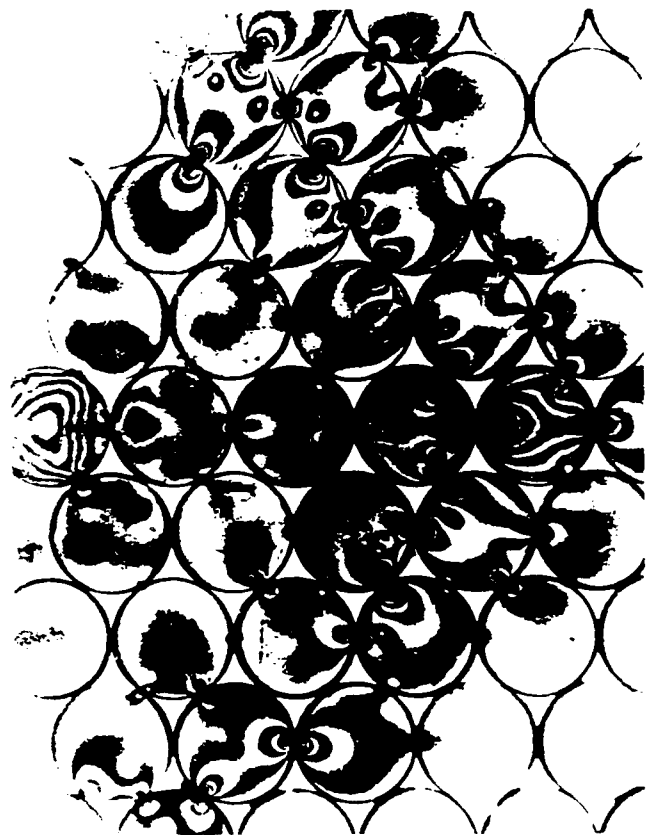


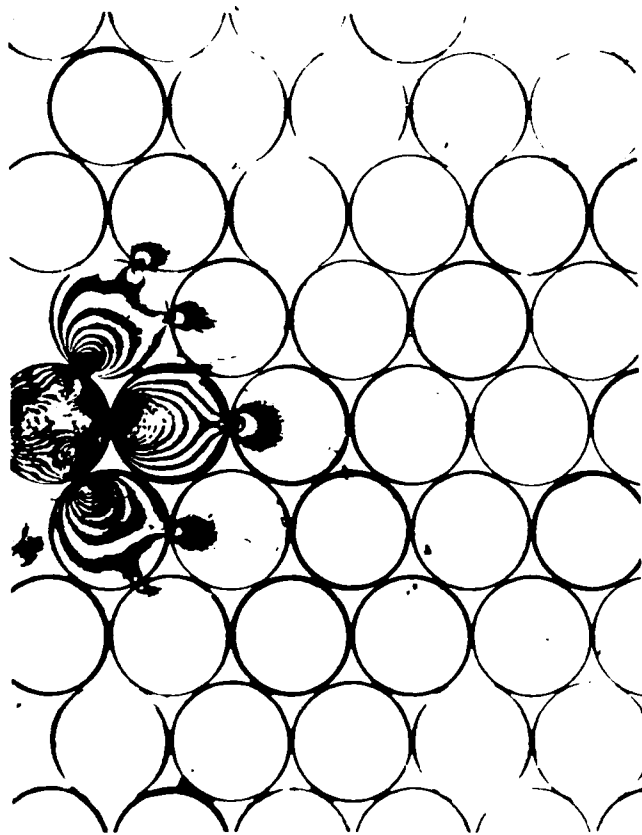
Figure 1. Schematic of Disk Interaction



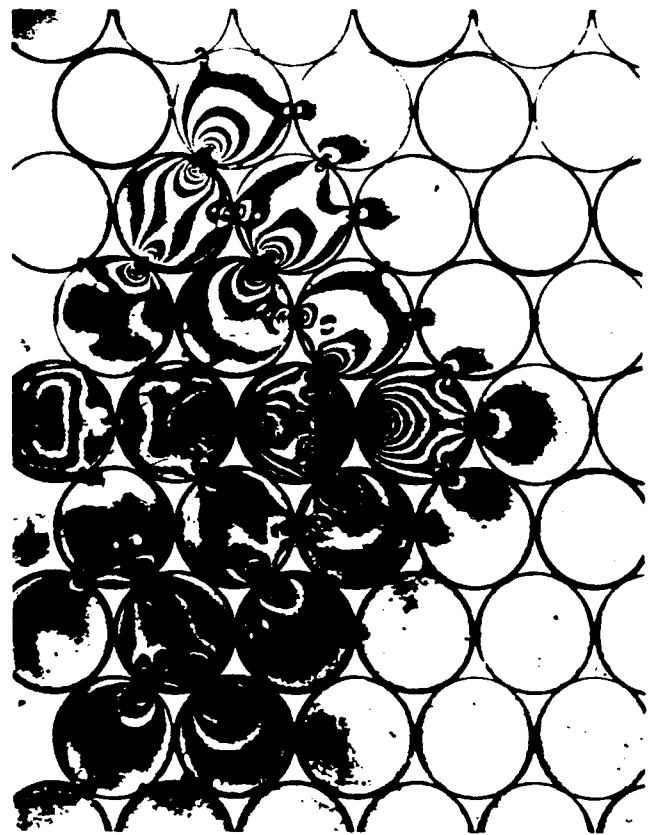
FRAME 11 TIME 124 (μ s)



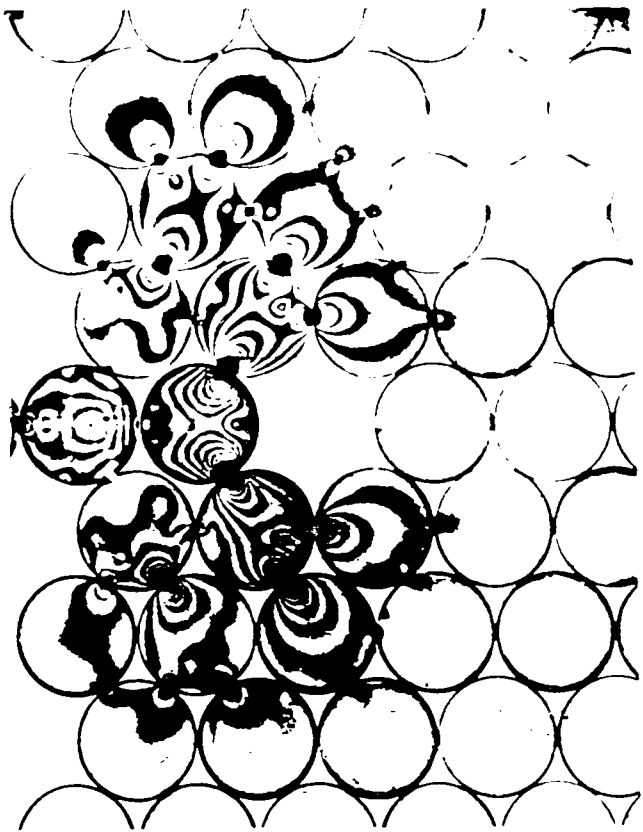
FRAME 17 TIME 157 (μ s)



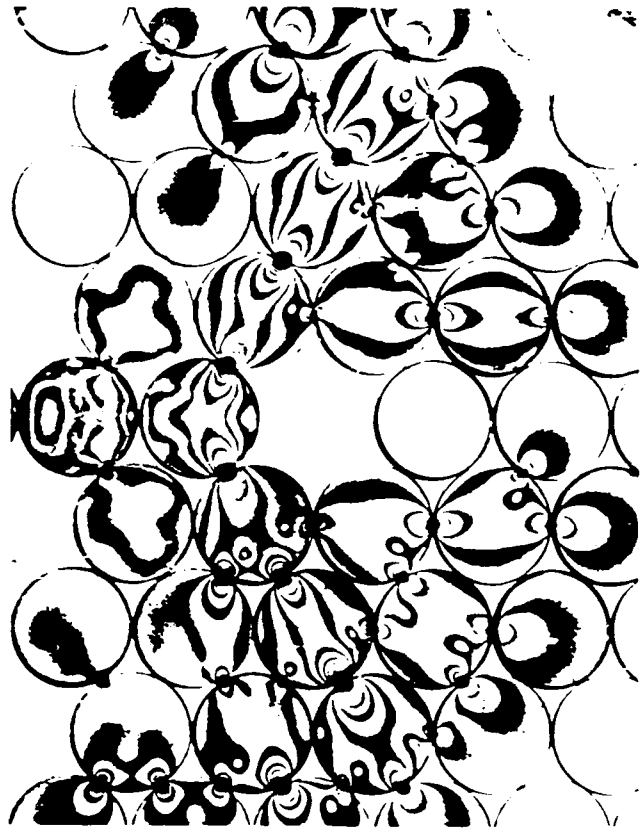
FRAME 5 TIME 79 (μ s)



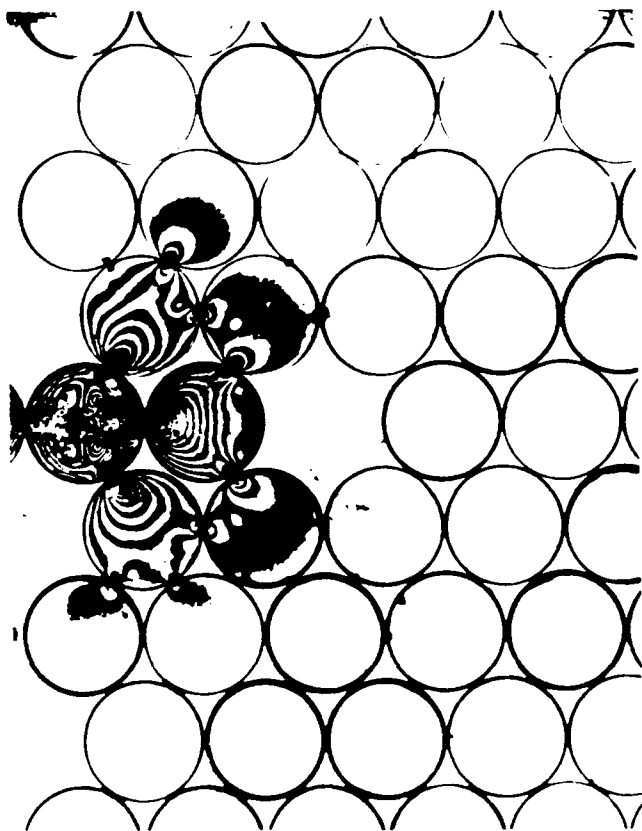
FRAME 13 TIME 120 (μ s)



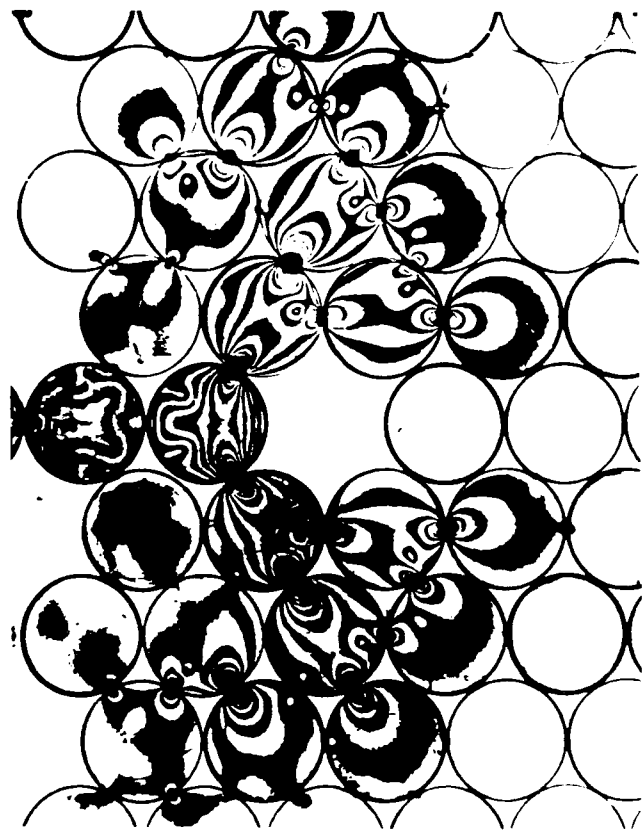
FRAME 11 TIME 118 (μ s)



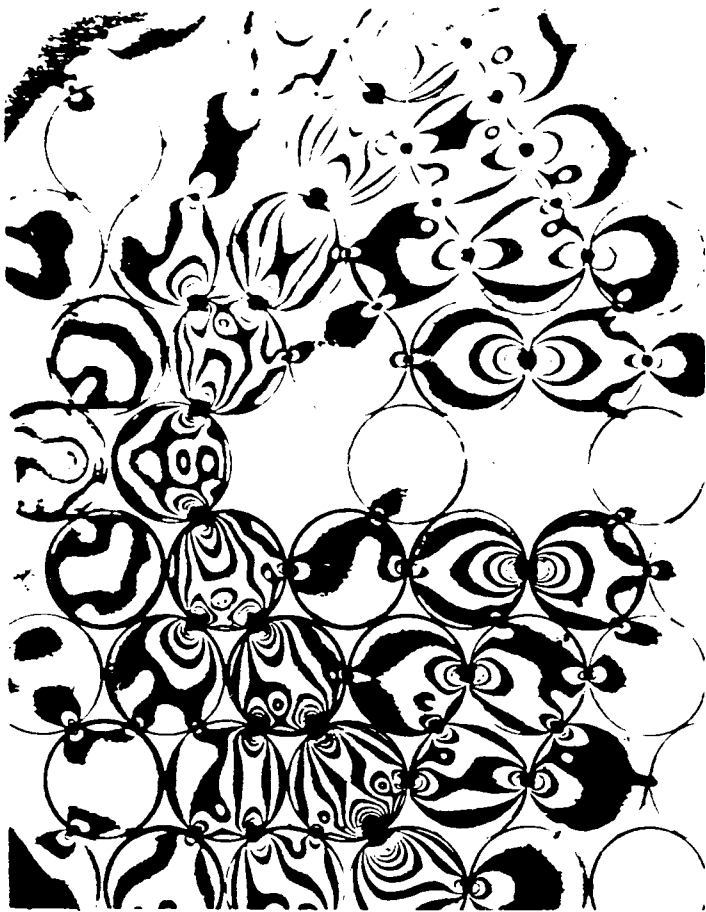
FRAME 19 TIME 166 (μ s)



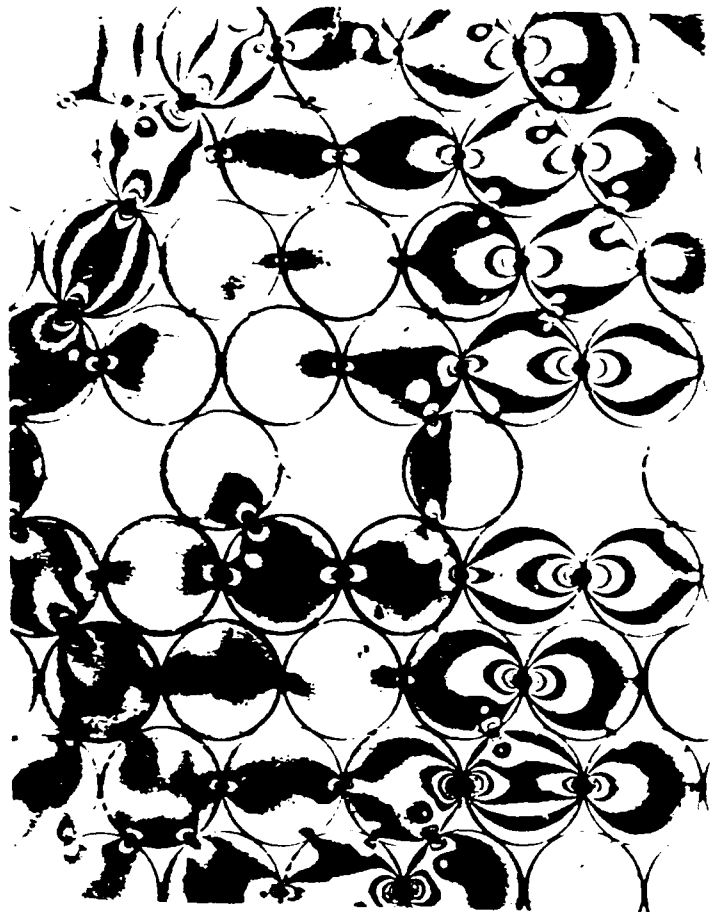
FRAME 5 TIME 83 (μ s)



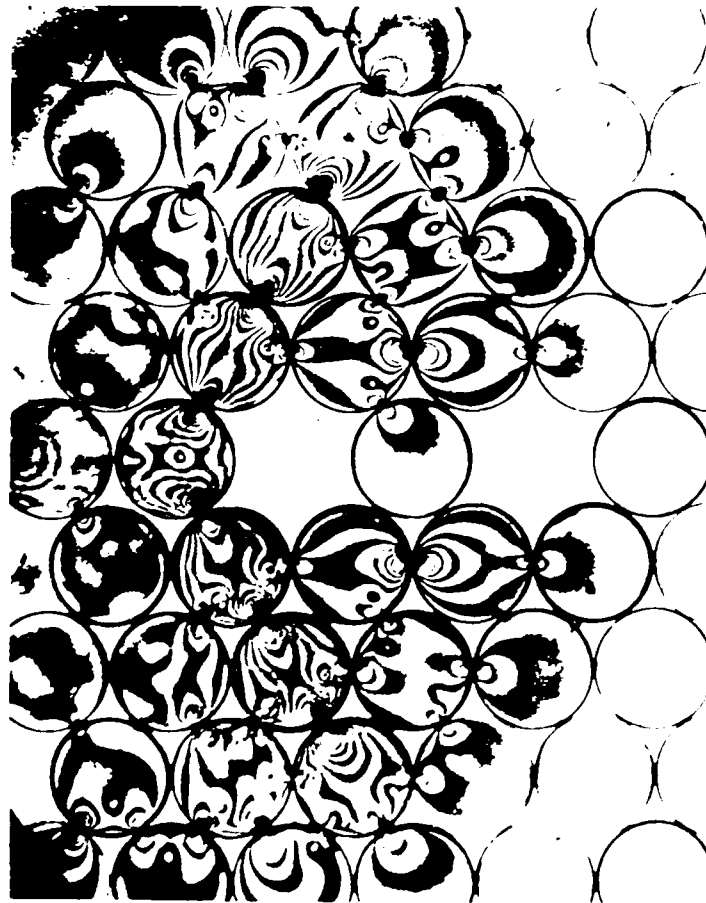
FRAME 15 TIME 142 (μ s)



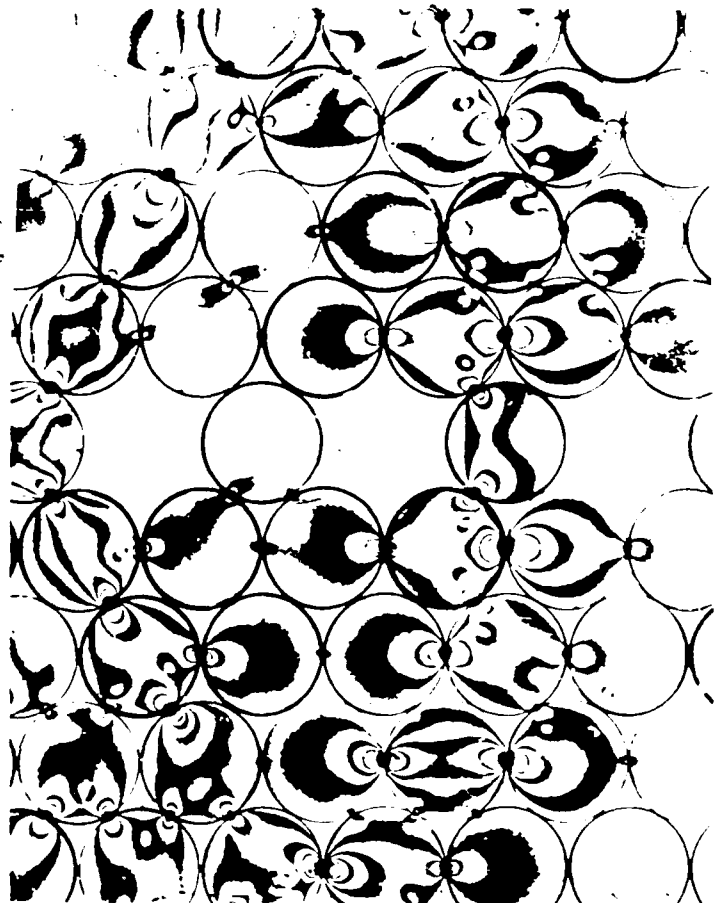
FRAME 10 TIME 179 (μ s)



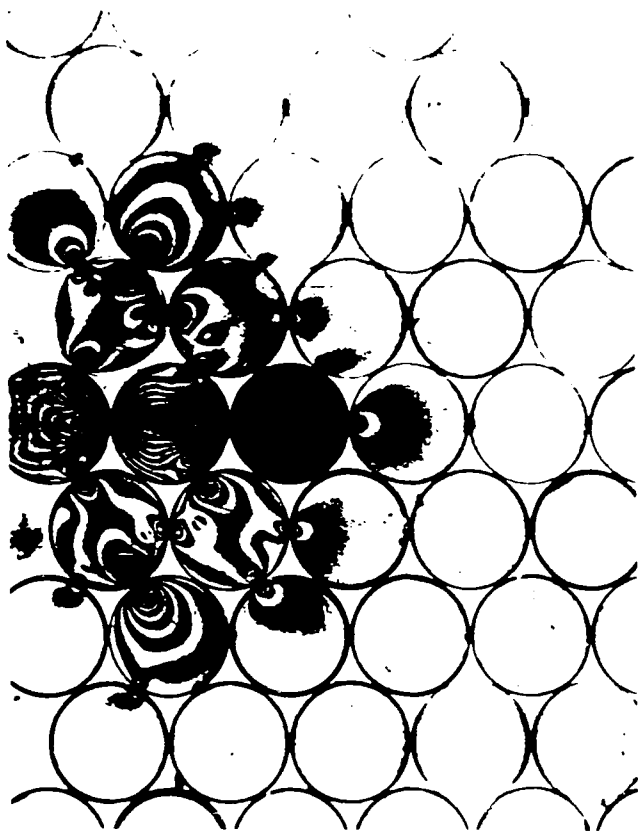
FRAME 11 TIME 209 (μ s)



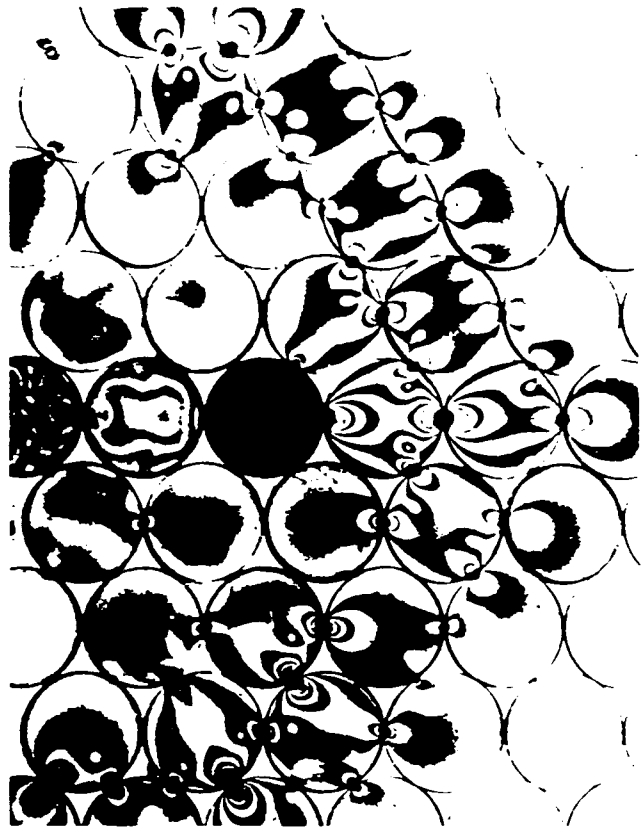
FRAME 5 TIME 151 (μ s)



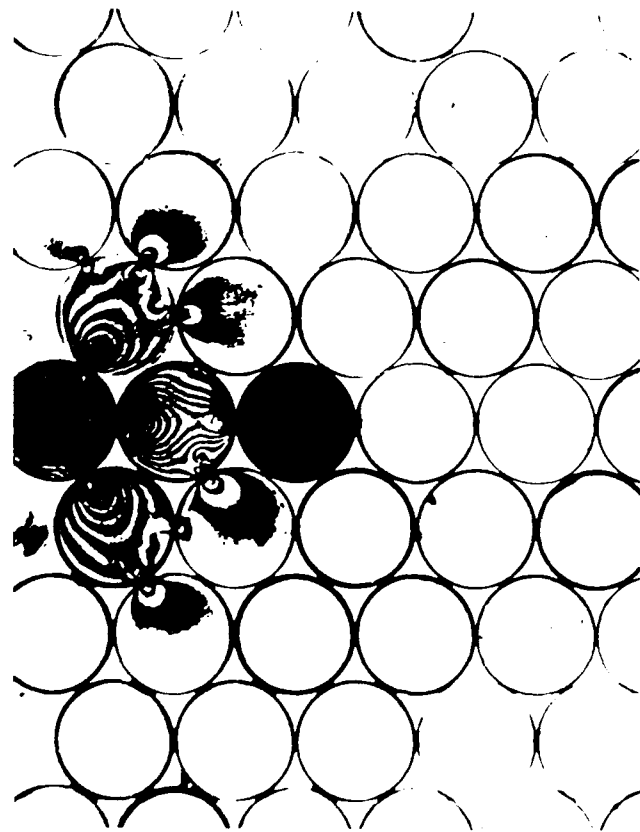
FRAME 12 TIME 210 (μ s)



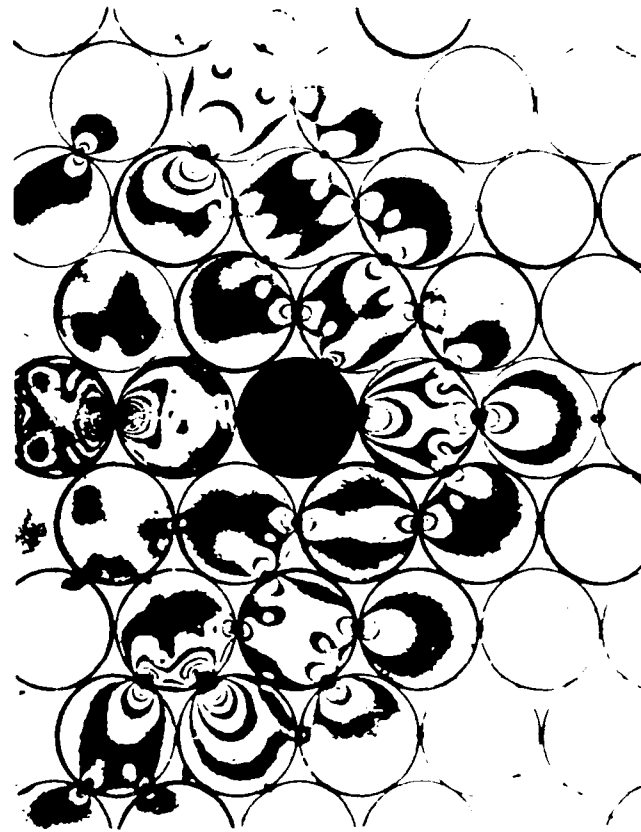
FRAME 9 TIME 105 (μ s)



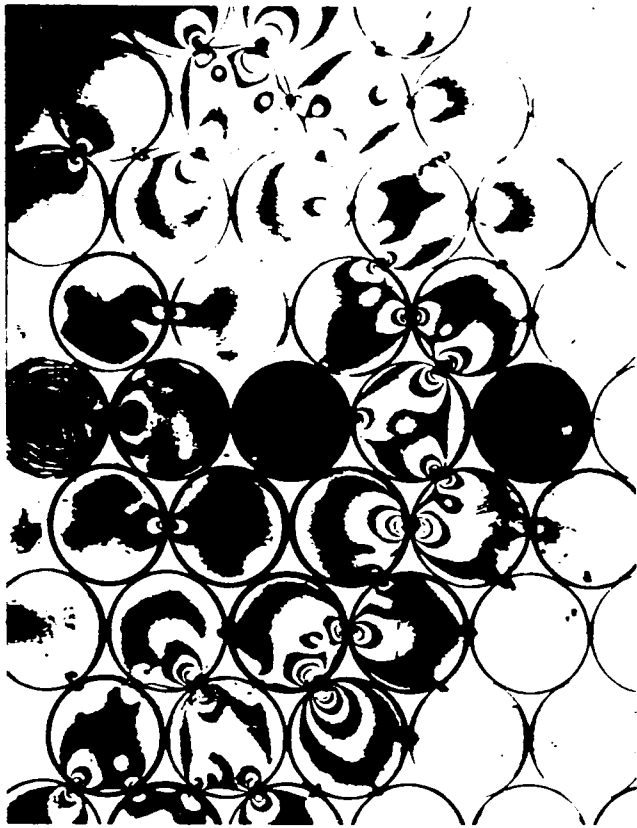
FRAME 19 TIME 164 (μ s)



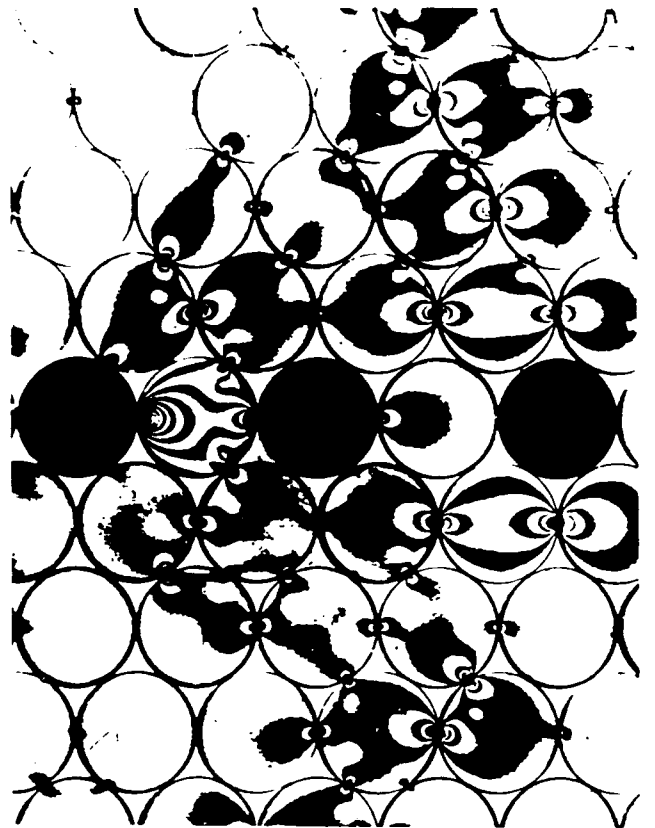
FRAME 5 TIME 82 (μ s)



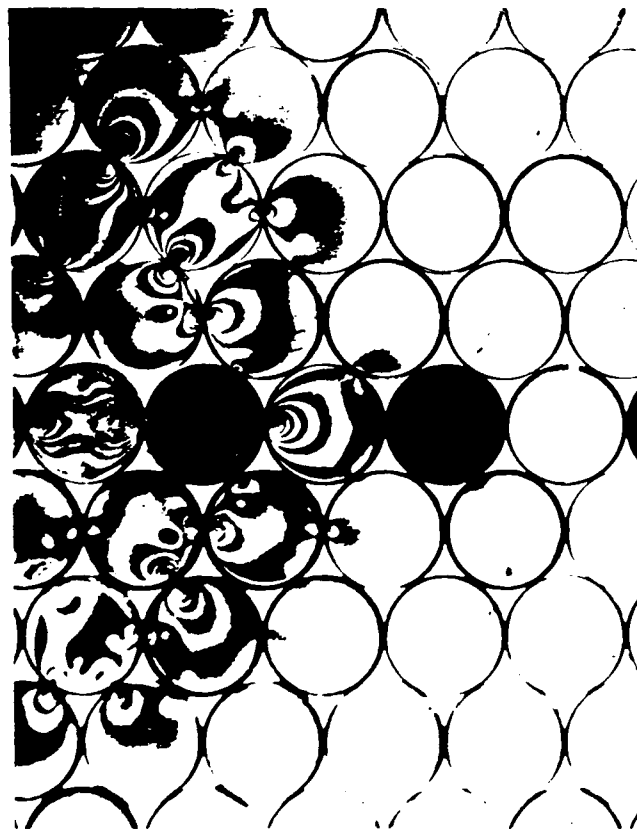
FRAME 15 TIME 141 (μ s)



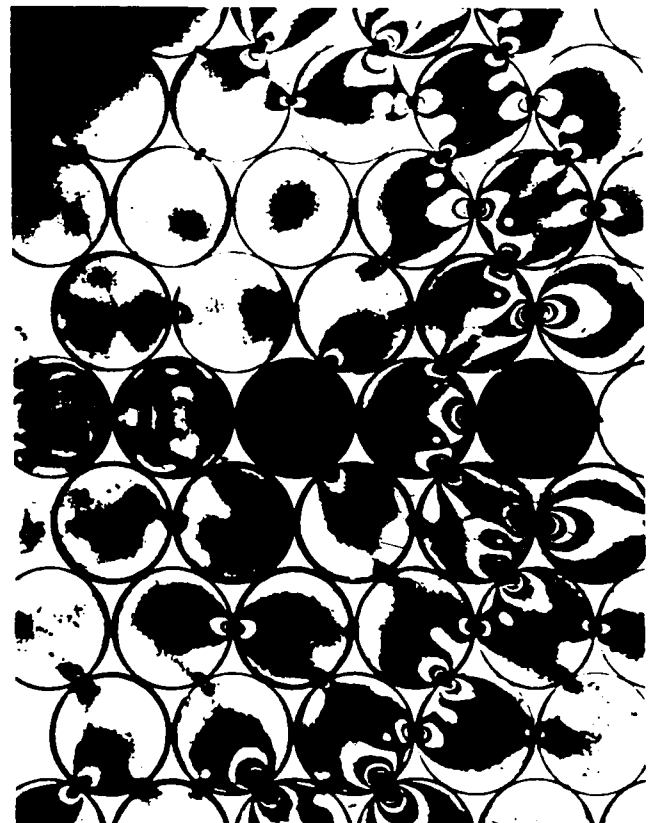
FRAME 6 TIME 158 (μ s)



FRAME 19 TIME 233 (μ s)



FRAME 1 TIME 131 (μ s)



FRAME 11 TIME 188 (μ s)

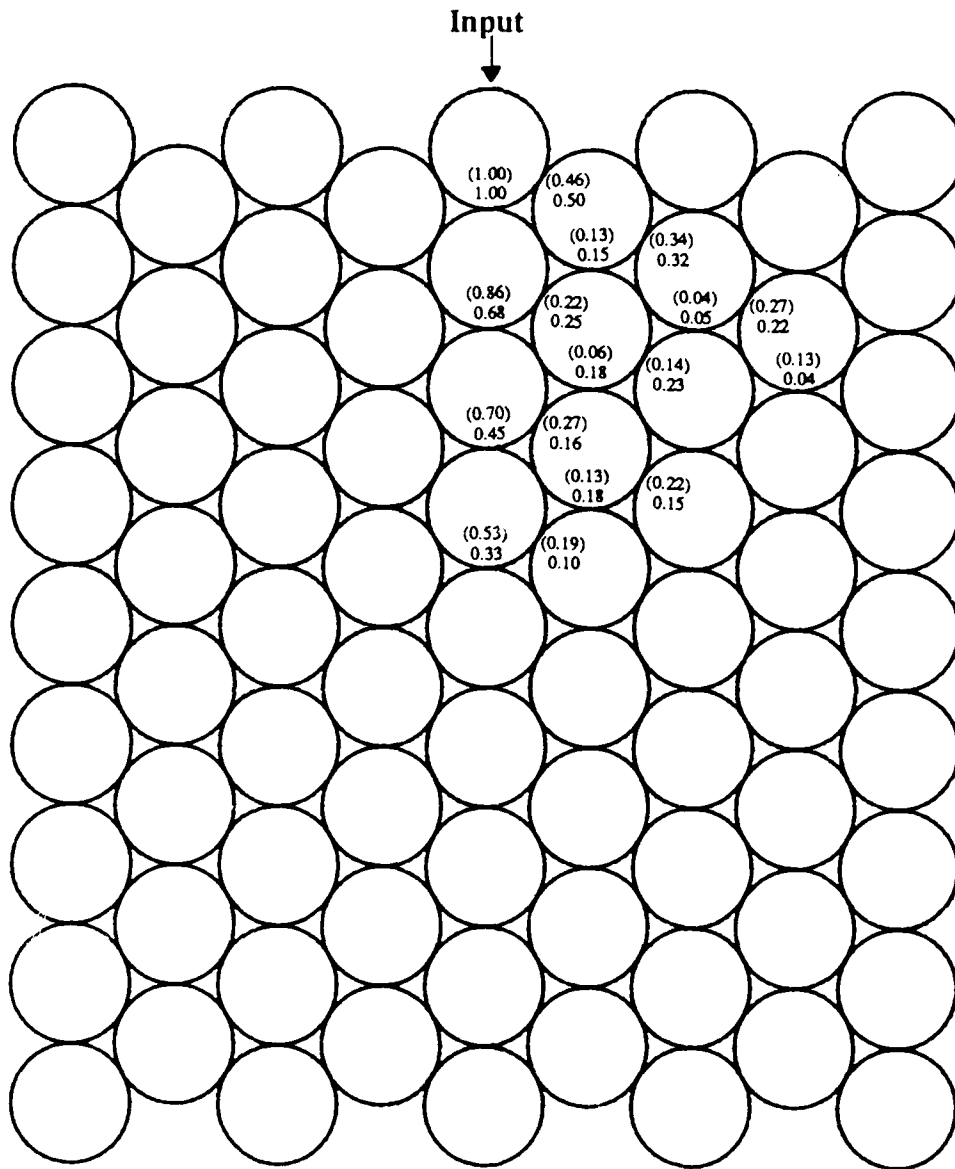


Figure 7. Normalized Maximum Contact Loading Comparisons: No Voids or Inclusions.

Experimental Data in Parentheses

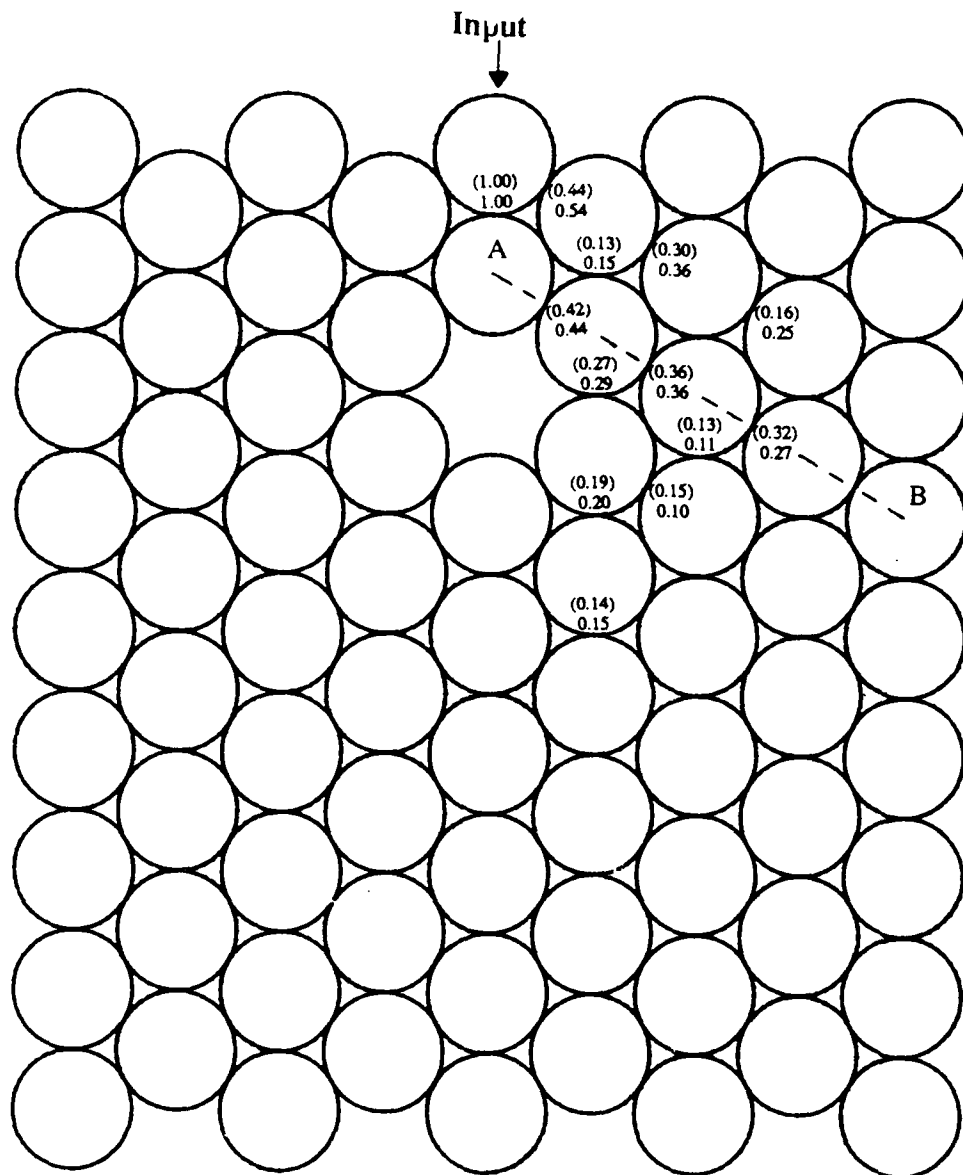


Figure 8. Normalized Maximum Contact Loading Comparisons: Single Void.
 Experimental Data in Parentheses

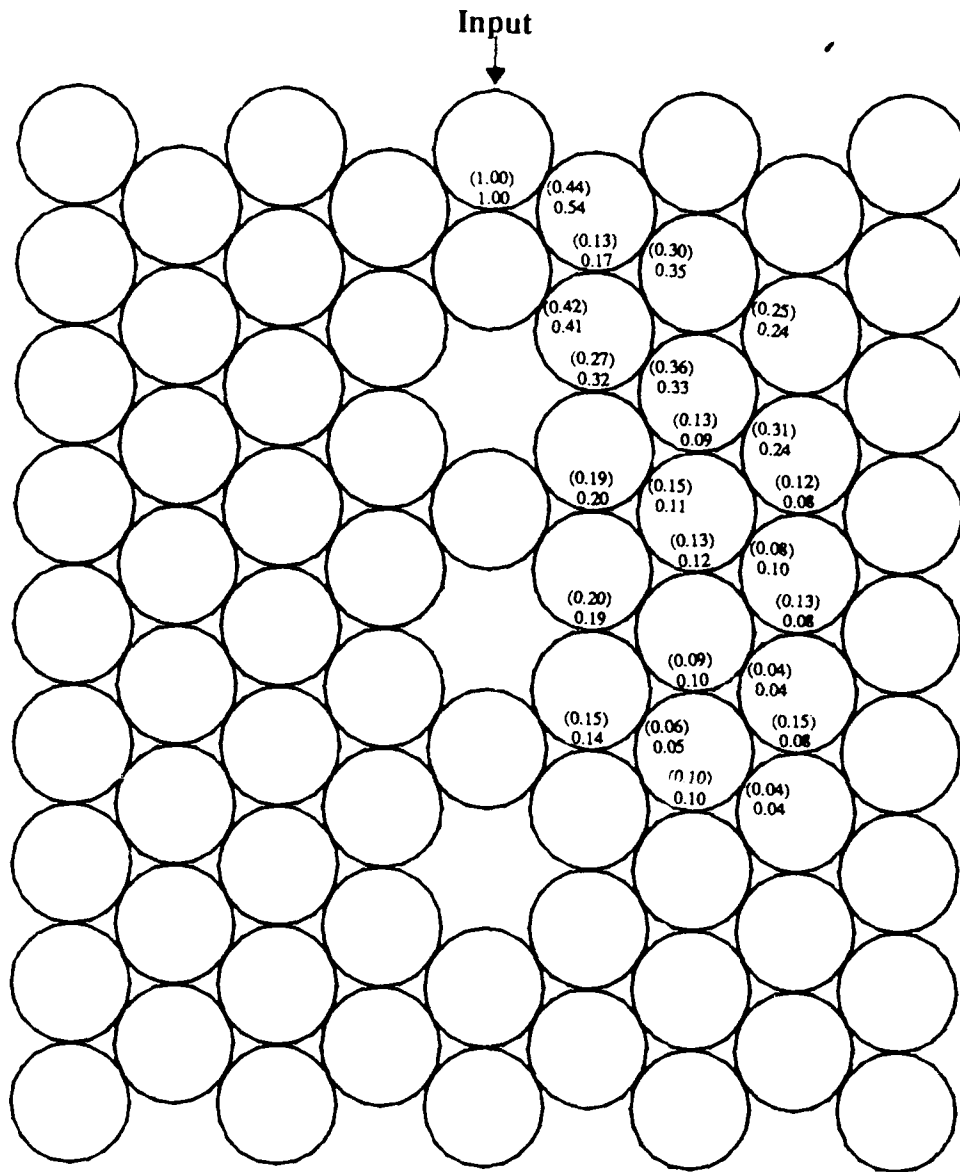


Figure 9. Normalized Maximum Contact Loading Comparisons: Series of Voids.

Experimental Data in Parentheses

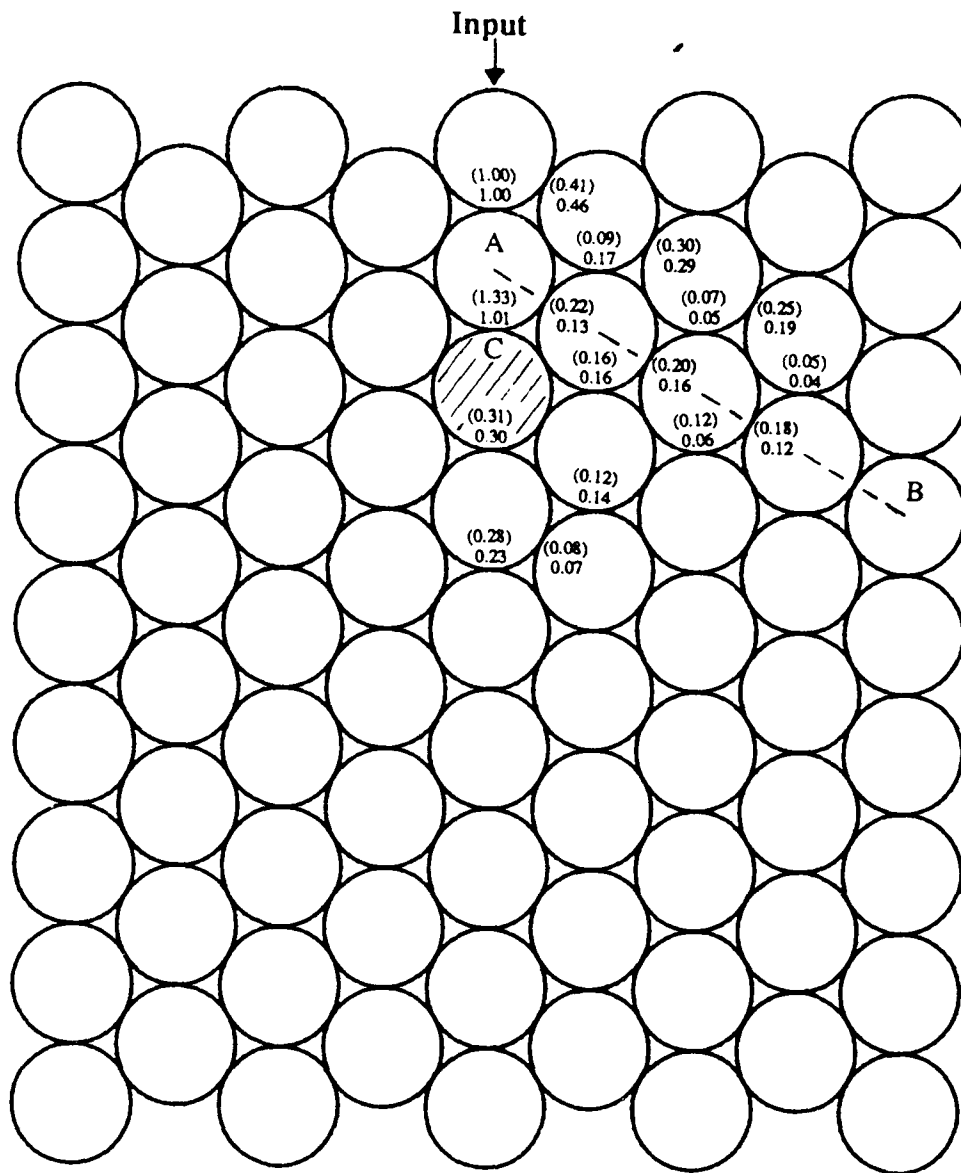


Figure 10. Normalized Maximum Contact Loading Comparisons: Single Inclusion.

Experimental Data in Parentheses

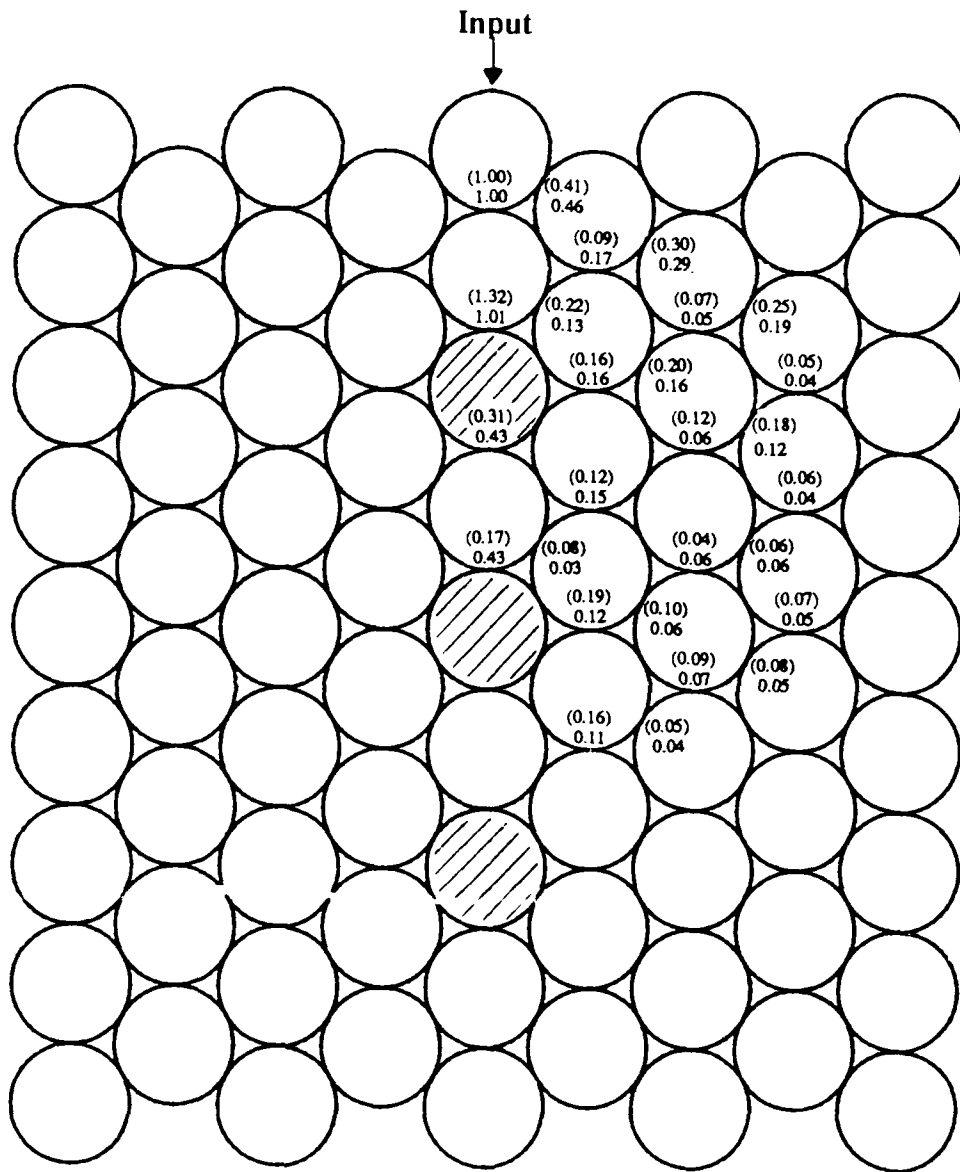


Figure 11. Normalized Maximum Contact Loading Comparisons: Series of Inclusions.

Experimental Data in Parentheses

Paper D

International Symposium of Wave Propagation in Granular Media
ASME Winter Annual Meeting, 1989.

Use of Load Transfer Coefficients to Predict Dynamic Loads in Granular Assemblies

by

C. Y. Zhu, A. Shukla and M. H. Sadd

*Dynamic Photomechanics Laboratory
Department of Mechanical Engineering & Applied Mechanics
University of Rhode Island, Kingston, RI, 02881*

ABSTRACT

An experimental-numerical hybrid technique has been developed to predict the intergranular contact load transfer in granular media subjected to explosive loading. The granular media was simulated by assemblies of circular discs in contact. The peak contact load transfer coefficients, i.e. the ratio of the maximum output contact load to the input contact load as a function of the contact angle, of a given particle were obtained through controlled experimental studies. These coefficients along with the principle of superposition were then used to predict the peak contact loads in several deterministic as well as random assemblies of discs. Although the numerical scheme was rather simple, the predicted results compared favorably with the experimental data for several different assemblies.

NOMENCLATURE

C	Peak contact load transfer coefficient
D	Diameter of a disc
f_c	Material fringe value
h	Thickness of a disc
N	Fringe order
P _i	Input peak contact load
P _o	Output peak contact load
θ_i	Contact angle
λ	Wave length
σ_1, σ_2	Principal stresses

INTRODUCTION

Knowledge of wave propagation in granular materials is of importance in many branches of engineering. These include powder metallurgy, transducer design, earthquake engineering, soil mechanics etc. Granular powders are of great importance to the forming of many solid materials. These materials for one reason or another can not be extruded, rolled or drawn, molded and fired, grown as crystals or cast from a melt, and so are frequently

sintered by either static or dynamic compression of powders. Such sintering processes are characterized by load transfer and flow of particles in a granular media. In addition, granular materials are excellent shock wave attenuators and as such have applications as diverse as transport packing materials and shock isolation materials for explosive chambers. A granular medium is composed of a large number of distinct particles as well as some voids. The particles can displace independently from one another. The voids may be filled with gas, as in a sample of dry sand, or they may be filled with liquids, as in a sample of wet sand. The discrete character of the granular media results in a quite complex behavior under conditions of dynamic loading.

The study of granular media from a microstructure point of view started many years ago with research modelling granular media as aggregate assemblies of discs or spheres. Early work by Iida [1], Takahashi and Sato [2], Hughes and Cross [3], Gassman [4] and Brandt [5] employed a normal granular contact force concept, while Duffy and Mindlin [6] included tangential forces as well. This initial work investigated wave propagation velocity as a function of confining pressure, particle size and aggregate geometry. Important new work has been done by Oda [7], Nemat-Nasser and Mehrabadi [8], et al. in the development of so-called fabric tensor theories for granular materials. The development of distributed body theory by Goodman and Cowin [9] has also proved useful in modelling such materials. Computational work in modeling large aggregate assemblies of particles has been carried out by using the distinct element method of Cundall and Strack [10], see also Sadd et al. [11].

With regard to experimental techniques, the method of photoelasticity provides whole field data during an experiment and makes it possible to determine the contact load between neighboring granular particles. Dantu [12] and Wakabayashi [13], Drescher and de Josselin de Jong [14], and Durelli and Wu [15] have employed photoelasticity to study the granular media behavior under static loading. Shukla et al. [16] [17] [18] have used photoelasticity combined with high speed photography to investigate the wave propagation phenomena due to explosive loading of an assembly of discs. Experimental methods provide sufficient information to determine wave speeds, dynamic contact loads, etc. in different kinds of granular packings under various loading conditions.

An experimental-numerical hybrid technique for analyzing the dynamic load transfer in a granular medium is discussed in this paper. In the experiments, dynamic loading was achieved by detonating a small charge of PETN in a specially designed charge holder, which was mounted at the top of the experimental model. High speed photography and dynamic photoelasticity were used to experimentally determine the peak contact loads between all the particles. The granular medium was simulated by assemblies of circular discs in various packing geometries as shown in Fig. 1. The microstructure of the granular medium can be characterized by branch vectors drawn from the mass centers of adjacent discs as shown in Fig. 2. The angle θ , as shown in Fig. 2, is drawn between any two neighboring branch vectors and is denoted as the contact angle. Initially a series of calibration experiments of controlled microstructure were conducted in which the contact angles between the granules were systematically varied. The data obtained from each experiment was analyzed to get a load transfer coefficient, i.e. a ratio of the maximum output contact load to the input contact load for a given disc. This load transfer coefficient was obtained for several contact angles and number of contacts per disc. With various load transfer coefficients determined, a numerical scheme was developed using the experimental data and based on the principle of superposition. Predictions were made of the intergranular contact loadings for several model assemblies with different microstructure as shown in Fig. 1. Numerical predictions were compared with experimental data for these models. Although the numerical scheme is very simple, the predicted results compared fairly well with the photoelastic experimental data.

DETERMINATION OF THE TRANSFER COEFFICIENTS

Granular media transmit mechanical loadings primarily through contact mechanisms between adjacent particles. This phenomenon is quite a complex process and strongly depends on the contact angle between the particles. For simplicity the granular materials were simulated by assemblies of one inch diameter, 1/4 inch thick discs of Homalite 100. The maximum number of the contact points for a disc in this study is 6 as shown in the hexagonal packing in Fig. 3a. It was shown in our previous work [19] that a mechanical signal can transfer through a contact point only when the contact angle is less than 90° . With respect to the input loading point of a particle, only three contact points namely 1, 2 and 3 as shown in Fig. 3a will have contact angles less than 90° . So if the mechanical signal enters a disc through a contact point, only three contact points will be able to transmit the response. In this study, all the particle interactions in the granular assembly were represented by a general four contact point model as shown in Fig. 3b. For the case of $\theta_1 \geq 90^\circ$ and $\theta_3 \geq 90^\circ$ only two contact points may transfer dynamic signals, as shown in Fig. 3c, whereas for the case of $\theta_1 < 90^\circ$ and $\theta_3 \geq 90^\circ$, dynamic signals can be transmitted through three contact points as shown in Fig. 3d.

In order to get the peak contact load transfer coefficients, experiments were conducted on the three groups of models, that is, the two, three and four contact point models shown in Fig 3b, 3c and 3d. In experiments of the two contact point model, contact angles θ_1 and θ_3 were kept at 90° . Only contact angle θ_2 was systematically varied from 0° to 90° . In experiments of the three contact point model, contact angle θ_3 was kept at 90° , and both contact angles θ_1 and θ_2 were systematically varied. In experiments of the four contact point model, all three contact angles θ_1 , θ_2 and θ_3 were systematically varied. The experimental models were placed in the optical bench of a high speed multiple spark gap camera. The camera was triggered at some prescribed

delay time after igniting the explosive. The high speed photographic system operated as a series of high intensity extremely short duration pulses of light and provided 20 isochromatic fringe images at discrete times during the dynamic event.

A careful inspection of the photographs obtained from the experiments revealed that the wave length, λ , of the loading pulse was much larger than the disc diameter D , in fact $\lambda=4D$. Furthermore, in most cases the fringe patterns around the contact points are symmetric on either side of the contact points and similar to the fringes obtained under static compression. Both these features indicate that around the contact zone, quasi-static loading was present during the wave propagation event. Thus Hertz contact stress theory can be used to estimate the stress field in the vicinity of the contact.

The isochromatic fringes photographed during the experiments are lines of constant maximum shear stress, and are related to the stress field by the stress optic law

$$\sigma_1 - \sigma_2 = Nf_o / h \quad (1)$$

where σ_1 and σ_2 are the principal stresses, N is the fringe order, f_o is the material fringe value, and h is the model thickness

In equation (1), σ_1 and σ_2 are substituted from Hertz contact stress field equations, involving unknowns of contact length b and friction factor β . This equation was solved using an overdeterministic method developed by Shukla and Nigam [20] to accurately determine the contact length and friction factor from the full field photoelastic fringe patterns. These obtained values were substituted in the Hertz stress field equations and the contact stresses were numerically integrated along the contact length to obtain the normal and tangential contact loads.

The peak contact load transfer coefficient C_j at contact point j is a function of the contact angles θ_1 , θ_2 and θ_3 , and is defined as the ratio of the output peak contact load P_o to the input peak contact load P_i , i.e.

$$C_j = C_j(\theta_1, \theta_2, \theta_3) = P_o / P_i \quad j=1, 2, 3 \quad (2)$$

For a two contact point model, as shown in Fig. 3c, C_1 and C_3 are identically equal to zero since contact angles θ_1 and θ_3 are 90° , while for three contact point model, as shown in Fig. 3d, C_3 is identically zero.

The transfer coefficients C_j thus obtained from the three groups of experiments were plotted as a function of the contact angles θ_1 , θ_2 and θ_3 , as shown in Figs. 4 to 6. In Fig. 4, curve 1 represents the ratio of P_o/P_i vs. contact angle θ_2 when both the contact angles θ_1 and θ_3 are equal to 90° . Since both P_{o1} and P_{o3} are zero, it actually represents the transfer coefficient C_2 of the two contact point model. The remaining curves in Fig. 4 represent the transfer coefficients C_2 vs. contact angle θ_2 of the three contact point model when contact angle θ_3 is 90° and θ_1 is also a constant but less than 90° (it is equal to 30° , 45° , 60° and 75° respectively). Fig. 5 shows the transfer coefficients C_3 vs. contact angle θ_3 for the four contact point model when the contact angles $\theta_1, \theta_2 = 0^\circ$ with various values of θ_1 , while Fig. 6 shows the transfer coefficient C_2 vs. contact angle θ_1 for the same four contact point model. The transfer coefficient C_1 for the four contact point model can be obtained easily using Figs. 4 and 6 and the property that $C_1(\theta_1, \theta_2, 90^\circ) = C_2(\theta_2, \theta_1, 90^\circ)$ and $C_1(\theta_1, 0^\circ, \theta_3) = C_3(\theta_3, 0^\circ, \theta_1)$.

NUMERICAL METHOD

The experimentally determined peak contact load transfer coefficients were used to construct a numerical scheme capable of predicting dynamic load transfer in granular aggregate assemblies

ferences. Several assumptions were used in this numerical method. First, only normal contact loading was considered in this study. The tangential contact loads were assumed to be zero. Next the speed of propagation of the mechanical signal is assumed to be constant, a fact which has been observed from the experiments. The load transfer coefficients are taken to be independent of the loading amplitude. Finally, simple superposition of loading, as shown in Fig. 7, is used when more than one input contact load occurs on a given disc.

Figs. 4 to 6 combined with a Lagrangian interpolation method have been used to obtain all the necessary transfer coefficients to predict the peak contact loads in granular media. As an example consider the transfer coefficients for a four contact point model ($\theta_1=60^\circ$, $\theta_2=0^\circ$ and $\theta_3=65^\circ$) as shown in Fig. 3b. Since θ_1 and θ_3 are equal to the two contact angles of curve 4 in Fig. 5, the transfer coefficient C_1 can be obtained directly and is equal to 0.273. In contrast, the transfer coefficient C_2 can not be obtained directly by using Fig. 5. However it can be obtained by using the curves in Fig. 5 combined with the Lagrangian interpolation method and the symmetrical property $C_1(60^\circ, 0^\circ, 65^\circ) = C_1(65^\circ, 0^\circ, 60^\circ)$. Using the values $C_1(60^\circ, 0^\circ, 60^\circ) = 0.28$, $C_1(70^\circ, 0^\circ, 60^\circ) = 0.294$, $C_1(80^\circ, 0^\circ, 60^\circ) = 0.32$ and our Lagrangian interpolation method, we get $C_1(60^\circ, 0^\circ, 65^\circ) = C_1(65^\circ, 0^\circ, 60^\circ) = 0.286$. The transfer coefficients C_2 can be obtained directly from curve 3 in Fig. 6, $C_2 = C_2(60^\circ, 0^\circ, 65^\circ) = 0.775$.

After the three transfer coefficients have been obtained, the relevant output peak contact loads for the four contact point model can be computed easily. According to the definition of the peak contact load transfer coefficient, the three output peak contact loads P_{21} , P_{22} and P_{23} at contact points 1, 2 and 3 are calculated as follows,

$$\begin{aligned} P_{21} &= C_1 P_1 \\ P_{22} &= C_2 P_1 \\ P_{23} &= C_3 P_1 \end{aligned} \quad (3)$$

RESULTS AND DISCUSSION

The experimental-numerical hybrid method was used to predict peak contact loads at every contact point in various models of granular media. Four different microstructural packings illustrated in Fig. 1 were used in this study. Experimental fringe patterns obtained for each of the microstructures are shown in Figs. 8 to 11. The comparison of the numerical and experimental results are shown in Figs. 12 to 15.

Fig. 8 shows a sequence of eight photographs obtained as the wave travels in a single chain granular medium for the geometry of Fig. 1a. In this geometry each particle has two contact points, hence only one transfer coefficient is needed to model this geometry. This transfer coefficient is obtained from Fig. 4, $C_2 = C_2(90^\circ, 0^\circ, 90^\circ) = 0.97$. The peak contact loads at each contact point can be determined as follows,

$$\begin{aligned} P_2 &= C_1 P_1 \\ P_3 &= C_2 P_2 = C_2^2 P_1 \\ &\vdots \\ P_n &= C^{n-1} P_1 \end{aligned} \quad (4)$$

The comparison of numerical and experimental peak contact loads in the single chain is shown in Fig. 12. The average peak contact load error for this model is computed to be 5%. The results are in very good agreement because most of the assumptions made in our numerical model are satisfied.

Fig. 9 shows a sequence of four photographs obtained as the

wave travels in a hexagonal closed packing (HCP) granular medium for the geometry of Fig. 1b. In this geometry each particle has six contact points. The major load in this assembly is transferred by two primary chains, 1 and 2, shown in Fig. 1b. Experimental data showed that the tangential contact loads were very close to zero for the primary chains, hence they behaved similar to the single chain assemblies. In the HCP model there are only two independent contact angles, $\theta_1 = \theta_3 = 60^\circ$ and $\theta_2 = 0^\circ$, with respect to the input load. Thus only two transfer coefficients were needed for the HCP model. From Figs. 5 and 6, we obtain the two transfer coefficients, $C_1(60^\circ, 0^\circ, 60^\circ) = C_1(60^\circ, 0^\circ, 60^\circ) = 0.28$, $C_2(60^\circ, 0^\circ, 60^\circ) = 0.75$. These coefficients were used to determine the peak contact loads throughout the assembly. The comparison of numerical and experimental results of the peak contact loads for the HCP model is shown in Fig. 13. The average error of the peak contact loads for this model is 13%, with the average error along the center line of the primary chain being only 6%.

Fig. 10 shows a sequence of four photographs obtained as the wave travels in the geometry of Fig. 1c, which will be referred to as a half hexagonal closed packing (HHCP) granular medium. In this geometry a particle has either four or five contact points. It is observed that most of the energy was transferred through a vertical column consisting of the HHCP cells under the explosive and several horizontal chains as shown in Figs. 10 and 14. The peak contact loads were obtained by the same method discussed previously. The comparison of numerical and experimental peak contact loads is shown in Fig. 14. It was found that the average error for this model is 12%. However the average error along the center line of the horizontal chains is only 7.5%.

Fig. 11 shows a sequence of four photographs as the wave travels in a random packing granular medium for the geometry of Fig. 1d. In this geometry particles have contact points ranging from two to six. The fringes in Fig. 11 reveal a complex nature of load transfer phenomenon. The energy transfer showed no preferential direction in this model. In the former three models, the tangential contact loads, especially along the main path of the energy transfer, were quite small. However in this random model, at the contacts near the explosive point, the fringes appeared unsymmetrical with respect to the contact points. So it appears that sizable tangential loadings existed in this case. Away from the explosive point, the fringes showed the tendency to become symmetric with respect to the contact points. Again from Figs. 4 to 6 all the transfer coefficients necessary for the determination of the peak contact loads in the random packing granular medium were obtained. The comparison of numerical and experimental peak contact loads is shown in Fig. 15. The tangential contact loads tend to increase the average error in the peak contact loads. This error was computed to be 19.0% for this model.

SUMMARY

A hybrid experimental-numerical technique has been developed to predict dynamic contact loadings due to explosive loading in different assemblies of circular discs. For a known geometrical arrangement of the discs the technique can predict contact loads at any point in the assembly for a given input loading. The method utilizes experimentally generated load transfer coefficients along with simple linear superposition in space. The results from this scheme are compared with those obtained experimentally using the method of dynamic photoelasticity. In general, the results are in good agreement for regular packings of the discs. However for a random packing the agreement is marginal, and this is primarily due to the fact that the numerical scheme currently does not take into account tangential contact loads which were quite large in random arrangement. Further, the superposition method does not account for any angular

dependence of wave length of the loading pulse. It was shown in our previous work [19] that the duration of contact loads is dependent on the contact angles. Thus to obtain better predictions, superpositions must be used both in space as well as time.

ACKNOWLEDGEMENTS

The authors would like to acknowledge the support of the Army Research Office under the contract No.DAAL03-86-K-0125.

REFERENCES

- [1] Iida, K., "The Velocity of Elastic Waves in Sand," Bull. Earthquake Research Inst., Japan, Vol.17, 1939.
- [2] Takahashi, T. and Sato, Y., "On the Theory of Elastic Waves in Granular Substance," Bull. Earthquake Research Inst. Japan, Vol.27, 1949.
- [3] Hughes, D. S. and Cross, J. H., "Elastic Wave Velocities in Rocks at High Pressures and Temperature," Geophysics, Vol.17, 1952.
- [4] Gassman, F., "Elastic Waves Through a Packing of Spheres," Geophysics, Vol.16, 1951.
- [5] Brandt, H., "A Study of The Speed in Sound of Porous Granular Media," J. Appl. Mech., Vol.22, 1955.
- [6] Duffy, J. and Mindlin, R. D., "Stress-Strain Relation and Vibration of a Granular Medium," J. Appl. Mech., Vol.24, 1957.
- [7] Oda, M., "Significance of Fabric in Granular Mechanics," in Proc. U.S.-Japan Seminar on Continuum Mechanical and Statistical Approaches in The Mechanics of Granular Materials, ed. Cowin, S. C. and Statake, M., Gakujutsu Bunken Fukyukai, pp.7-26, 1978.
- [8] Nemat-Nasser, S. and Mehrabadi, M. M., "Stress and Fabric in Granular Masses," in Mechanics of Granular Materials: New Models and Constitutive Relations, ed. Jenkins, J. T. and Statake, M., Elsevier Sci. Pub., pp.1-8, 1983.
- [9] Goodman, M. A. and Cowin, S. C., "A Continuum Theory for Granular Materials," Arch. Rat. Mech. Anal., Vol.44, 1972.
- [10] Cundall, P. and Strack, D. L., "A Discrete Model for Granular Assemblies," Geotechnique, Vol.29, 1979.
- [11] Sadd, M. H., Shukla, A. and Mei, H., "Computational and Experimental Modeling of Wave Propagation in Granular Materials," Proc. 4th International Conference on Computational Methods and Experimental Measurements, Capri, Italy, May, 1989.
- [12] Dantu, P., "Contribution a l'etude Mecanique et Geometrique des Milieux Pulverulents," Proc. 4th Int. Conf. Soil Mech. Fdn. Engng, Landon, pp.144, 1957.
- [13] Wakabayashi, T., "Photoelastic Method for Determination of Powdered Mass," Proc. 7th Jap. Nat. Congr. Appl. Mech., pp.153-192, 1957.
- [14] Drescher, A. and De Josselin De Jong, G., "Photoelastic Verification of a Mechanical Model for the Flow of a Granular Material," J. Mech. Phys. Solids, Vol.20, 1972.
- [15] Durelli, J. and Wu, D., "Use of Coefficients of Influence to Solve Some Inverse Problems in Plane Elasticity," J. Appl. Mech., Vol.50, 1983.
- [16] Shukla, A. and Damania, C., "Experimental Investigation of Wave Velocity and Dynamic Contact Stress in an Assembly of Discs," J. Exp. Mech., Vol.27, 1987.
- [17] Shukla, A. and Rossmannith, H. P., "Dynamic Photoelastic Investigation of Wave Propagation and Energy Transfer Across Contacts," J. of Strain Analysis, Vol.21, 1986.
- [18] Shukla, A., and Zhu, C. Y., "Influence of the Microstructure of Granular Media on Wave Propagation and Dynamic Load Transfer," J. of Wave-Material Interaction, Vol.3, 1988.
- [19] Shukla, A., Zhu, C. Y. and Sadd, M. H., "Angular Dependence of Dynamic Load Transfer Due to Explosive Loading in Granular Aggregate Chains," J. of Strain Analysis Vol.23, 1987.
- [20] Shukla, A. and Nigam, H., "A Numerical-Experimental Analysis of the Contact Stress Problem," J. of Strain Analysis, Vol.20, 1985.

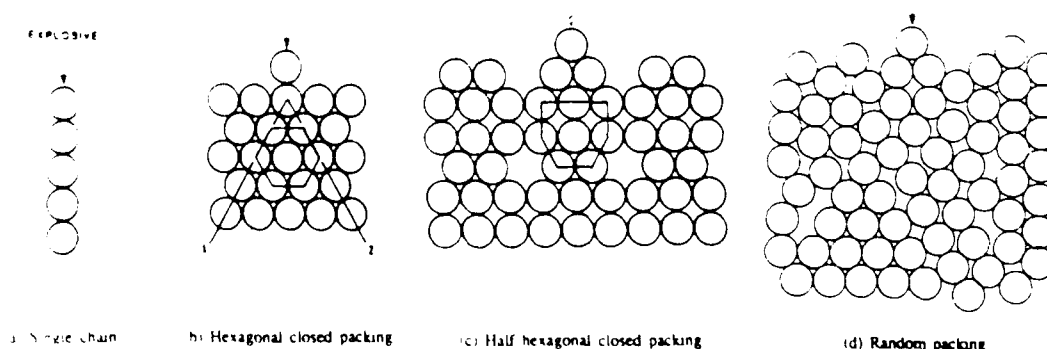


Figure 1 Microstructural arrangements used in different experiments

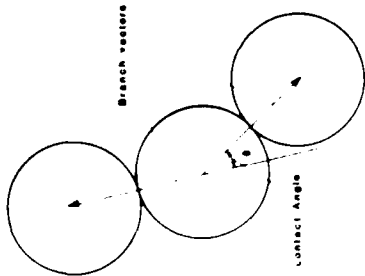


Figure 2 Branch vectors and contact angle, θ

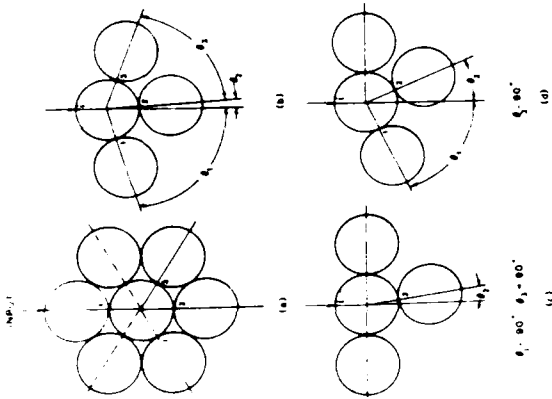


Figure 3 General four contact point models

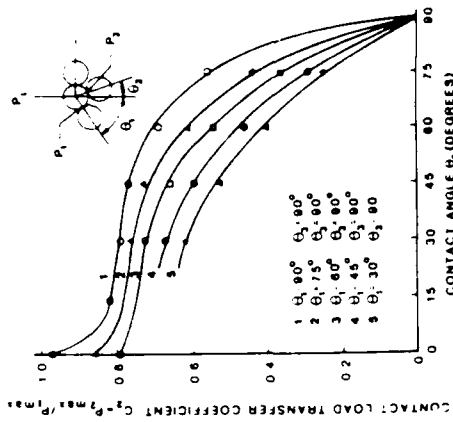


Figure 4 Contact load transfer coefficient, C_2

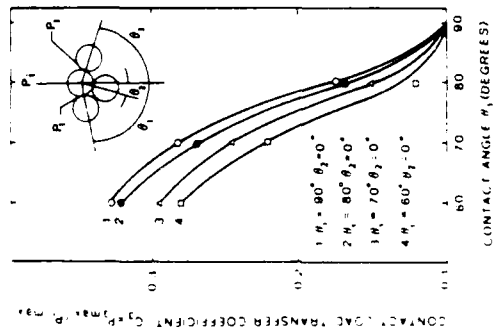


Figure 5 Contact load transfer coefficient, C_2

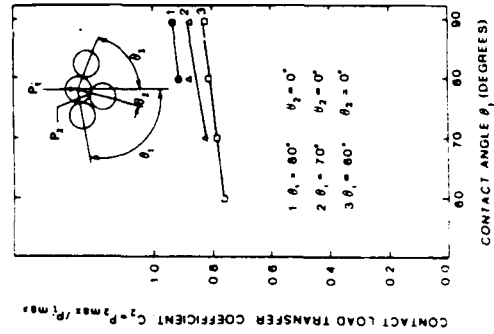


Figure 6 Contact load transfer coefficient, C_2

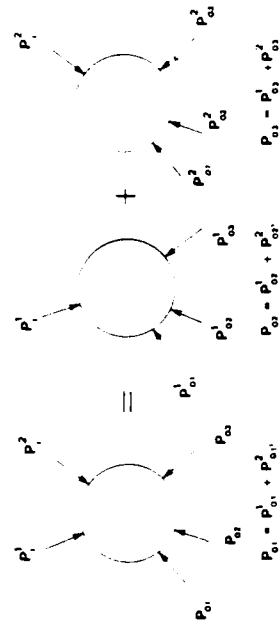


Figure 7 Superposition model for two input loadings

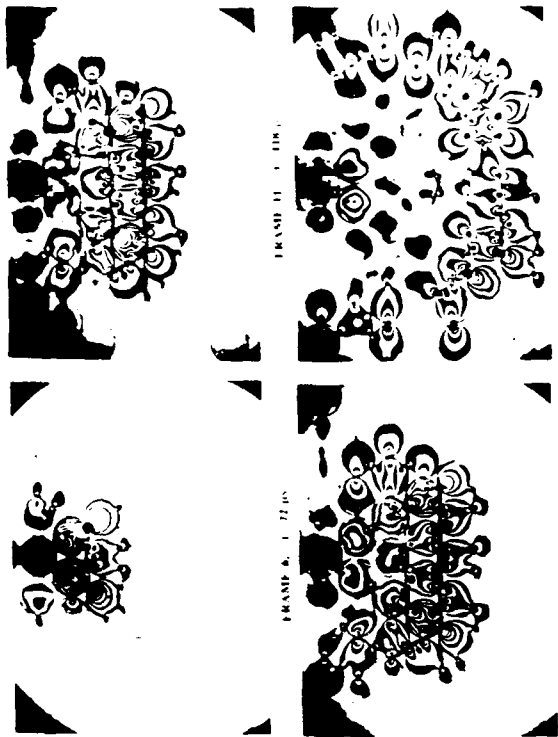


Figure 4
Isosymmetric groups obtained in a HCP arrangement (geometry II)

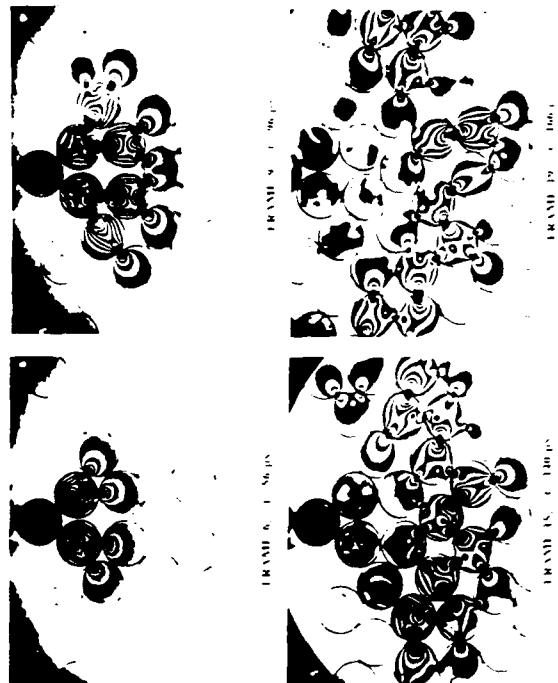


Figure 5
Isosymmetric groups obtained in a HCP arrangement (geometry III)

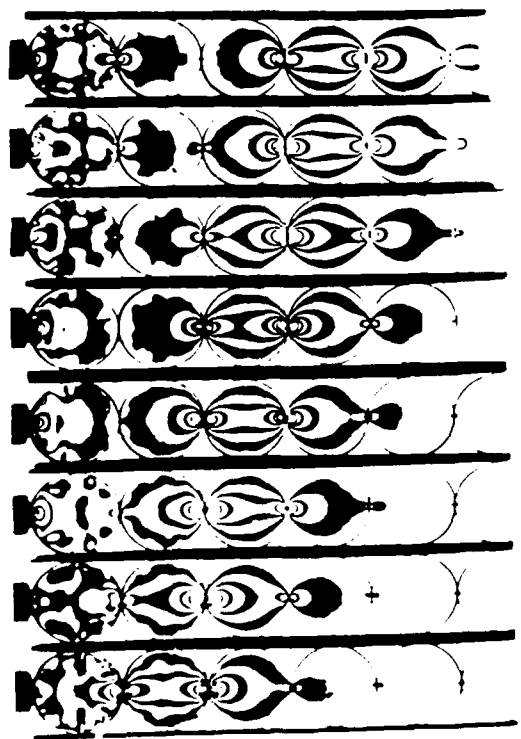


Figure 6
Isosymmetric groups obtained in a HCP arrangement (geometry I)

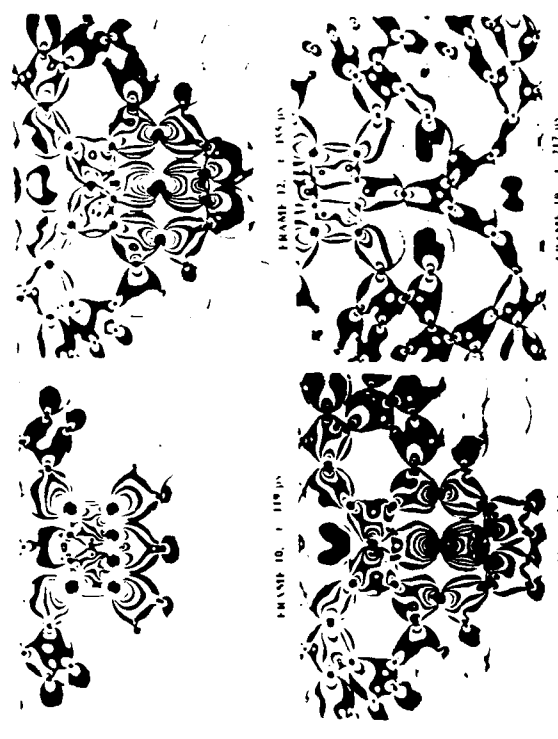


Figure 7
Isosymmetric groups obtained in a HCP arrangement (geometry II)

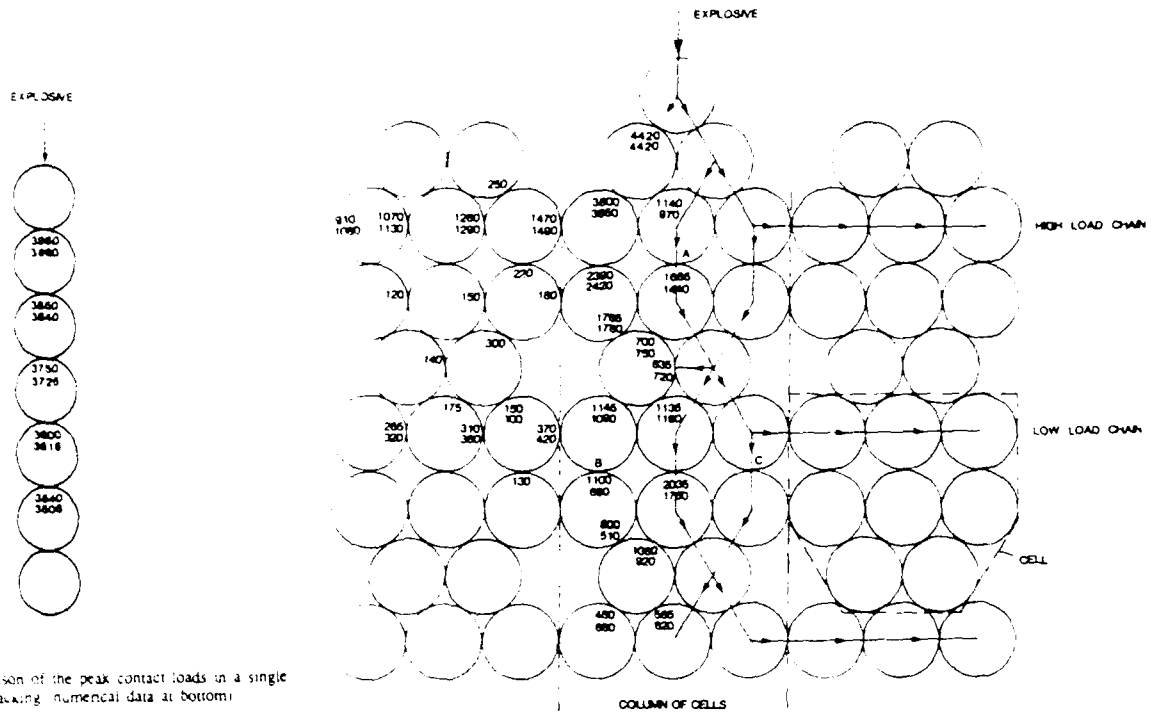


Figure 12 Comparison of the peak contact loads in a single chain packing (numerical data at bottom)

Figure 14 Comparison of the peak contact loads in a HHCP arrangement (numerical data at bottom)

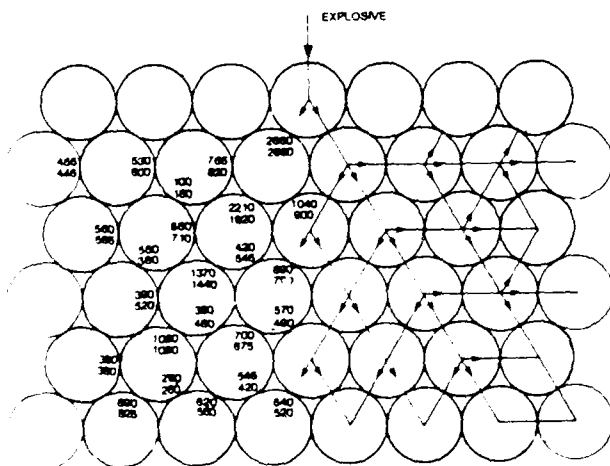


Figure 13 Comparison of the peak contact loads in a HCP arrangement (numerical data at bottom)

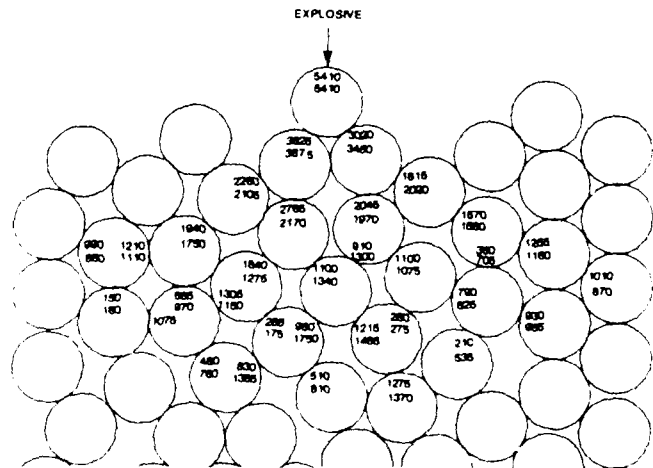


Figure 15 Comparison of the peak contact loads in a random packing arrangement (numerical data at bottom)

Paper E

INFLUENCE OF THE MICROSTRUCTURE OF GRANULAR MEDIA ON WAVE PROPAGATION AND DYNAMIC LOAD TRANSFER

A. SHUKLA AND C. Y. ZHU
Dynamic Photomechanics Laboratory
Department of Mechanical Engineering & Applied Mechanics
University of Rhode Island
Kingston, RI 02881

ABSTRACT

Dynamic load transfer in granular material occurs essentially through contact mechanisms between each grain. This phenomenon is quite a complex process and depends inherently on the microstructural packing arrangement of the media. An experimental investigation is conducted to study wave propagation in systematic aggregates of disc assemblies. Attention is focused on load transfer path, wave velocities, wave attenuation and the stresses which are generated at the contacts due to the passage of stress waves. The optical technique of photoelasticity along with high speed photography is utilized to get the whole field stress distribution in the granular media which is subjected to explosive loading. The granular media is simulated by circular discs made of photoelastic materials. Several systematic arrangements of these discs are used in different experiments. The results show that the load transfer phenomenon depends strongly on the microstructure of the media. Experiments are performed with initially unstressed media as well as media with prestress.

1. INTRODUCTION

It is commonly observed that the microstructural packing or the fabric of the granular media strongly affects its mechanical behavior. Considerable effort has been spent both experimentally and theoretically to look at the influence of microstructure on deformation and strength of granular media. Oda [1, 2] was among the first to observe the microstructure or fabric of sand in unloaded and deformed specimens. These specimens were tested in the triaxial and direct shear apparatus by using thin sections and a polarized microscope. Borowicka and Arthur [3, 4] observed and measured the microstructural change of sand loading by means of either microscopy or radiography. Konishi [5] conducted biaxial compression and simple shear tests on two dimensional granular media, fabricated from epoxy resin cylinders, and examined the microstructure change and the state of stress in the granules using photoelasticity. All this experimental work and that of several others [6, 7] suggest that the concept of the fabric of the granular media can be very useful in understanding their mechanical properties. Based on these experimental findings, several theoretical [8, 9] models have developed constitutive equations for the granular media taking into account the microstructural characteristics. However, most of this work has been done for static loading conditions. Recently, Shukla and Damania [10] have conducted dynamic experiments using photoelasticity to study wave propagation in granular media. Their experiments show that the dynamic load transfer depends on the angle made by the normals at the contact points of two adjacent granules.

The purpose of this study is to evaluate the effect of different microstructure or fabric of granular media on the wave propagation phenomenon. A total of five different regular microstructural arrangements as shown in Fig. 1 are considered for the experiments. The choice of these microstructural arrangements is based on the work of Shahinpoor [11] who has demonstrated that the randomly oriented granules follow certain distinct packing geometries referred to as Voronoi cells. High speed photography was used to record dynamic isochromatic fringes in the birefringent granules as a function of time due to the passage of stress waves. Dynamic contact stresses at each contact point and average wave velocities were calculated from the

experimental data. The effect of microstructure on these quantities was evaluated. An experiment was also conducted to look at the effect of prestress on the wave propagation phenomenon in the body centered cubic geometry.

2. EXPERIMENTAL PROCEDURE

The geometries of the models used in this study are shown in Fig. 1. Five different microstructural packings or cells based on the work of Shahinpoor [11] were investigated. The granular media was simulated with one inch diameter 1/4 inch thick Homalite 100 discs. Homalite 100 is a brittle polyester material which becomes temporarily birefringent under the application of load. Dynamic loading was achieved by detonating a small charge of PETN in a specially designed charge holder, which was mounted either at the top or at the center of the model assemblies as also shown in Fig. 1. The experimental models were placed in the optical bench of a high speed multiple spark gap camera. The camera was triggered at some prescribed delay time after igniting the explosive. This high speed photographic system operated as a series of high intensity, extremely short duration pulses of light and provided 20 photoelastic images at discrete times during the dynamic event. A typical sequence of four images from each experiment are shown in Figs. 2-7.

3. ANALYSIS PROCEDURE

A careful inspection of the photographs obtained from the experiments revealed that the wave length λ of the loading pulse was much larger than the disc diameter D ($\lambda = 4D$). Furthermore, the fringe pattern around the contact points were symmetric on either side of the contact points and were similar to the fringes obtained under static diametral compression. Both these features indicated that around the contact zone, quasi static loading was present during the wave propagation event. Thus Hertz equations were used to obtain the contact stresses, strains and loads.

From the Hertz contact stress theory, the stress field equations around the contact region of two bodies, as shown in Fig. 8, are represented as

$$\sigma_{zz} = -\frac{b}{\pi\Delta} [z(b\phi_1 - x\phi_2) + \beta z^2 \phi_2] \quad (1)$$

$$\begin{aligned} \sigma_{xx} = & -\frac{b}{\pi\Delta} \left\{ z \left(\frac{b^2 + 2z^2 + 2x^2}{b} \phi_1 - \frac{2\pi}{b} - 3x\phi_2 \right) + \right. \\ & \left. + \beta [(2x^2 - 2b^2 - 3z^2) \phi_2 + \frac{2\pi x}{b} + 2(b^2 - x^2 - z^2) \frac{x}{b} \phi_1] \right\} \quad (2) \end{aligned}$$

$$\sigma_{zx} = -\frac{b}{\pi\Delta} \left\{ z^2 \phi_2 + \beta [(b^2 + 2x^2 + 2z^2) \frac{z}{b} \phi_1 - 2\pi \frac{z}{b} - 3xz \phi_2] \right\} \quad (3)$$

where ϕ_1 and ϕ_2 are

$$\phi_1 = \frac{\pi(M+N)}{MN\sqrt{2MN + 2x^2 + 2z^2 + 2b^2}}$$

$$\phi_2 = \frac{\pi(M-N)}{MN\sqrt{2MN + 2x^2 + 2z^2 + 2b^2}}$$

$$M = \sqrt{(b+x)^2 + z^2}, \quad N = \sqrt{(b-x)^2 + z^2} \quad \text{and}$$

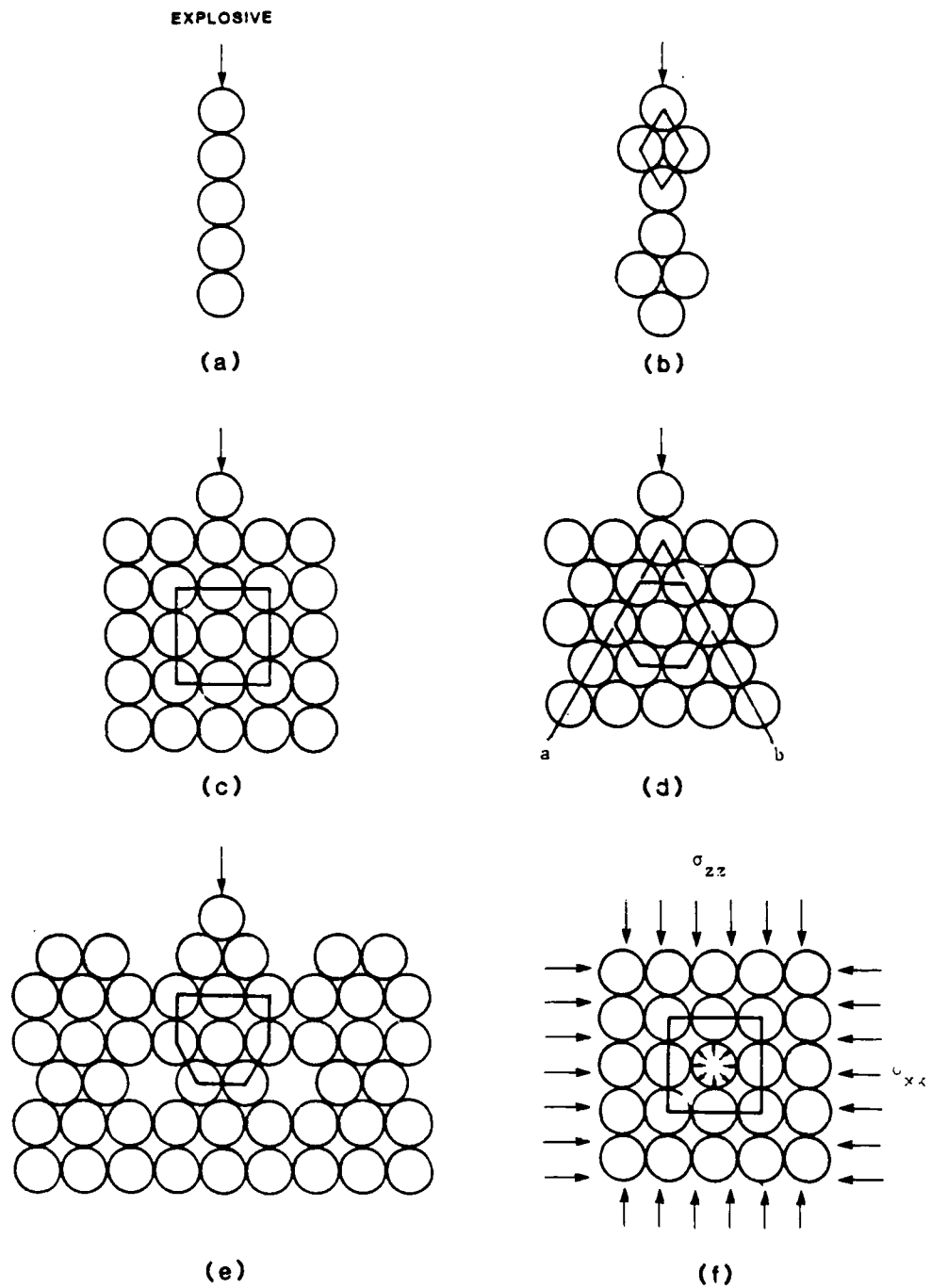


Figure 1. Microstructural arrangements used in different experiments.

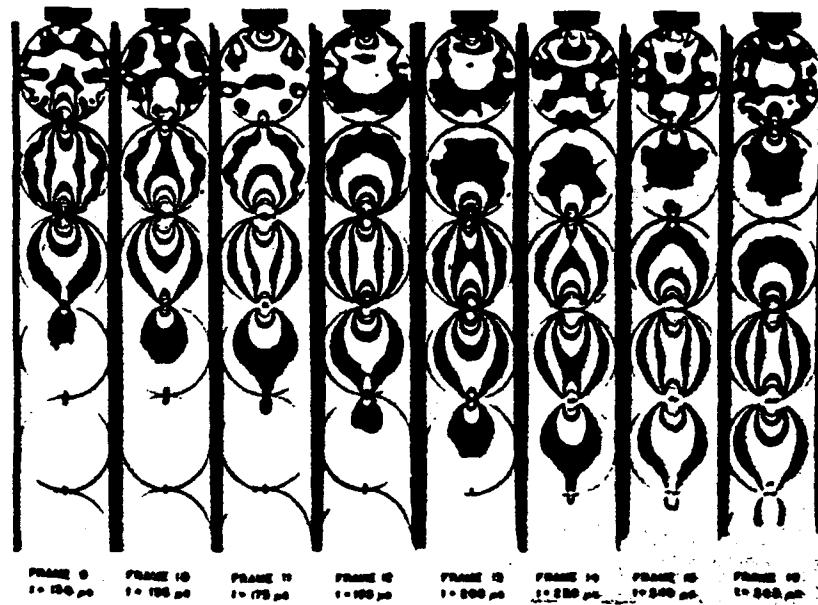


Figure 2. Isochromatic fringes obtained in a single chain arrangement, geometry 1a.

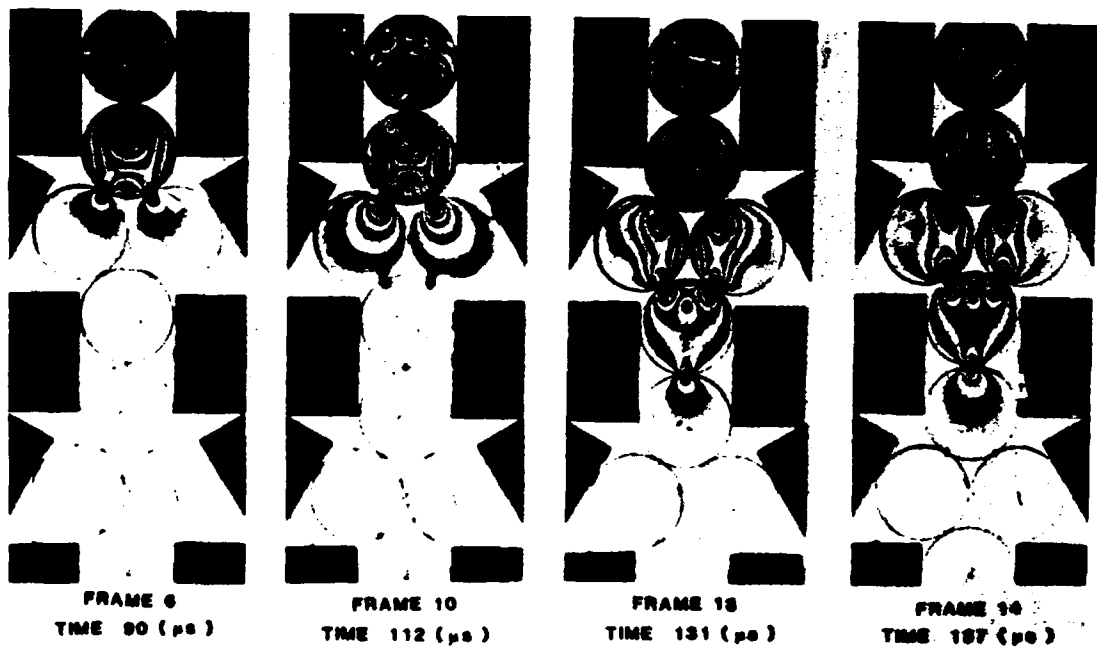


Figure 3. Isochromatic fringes obtained in geometry 1b.

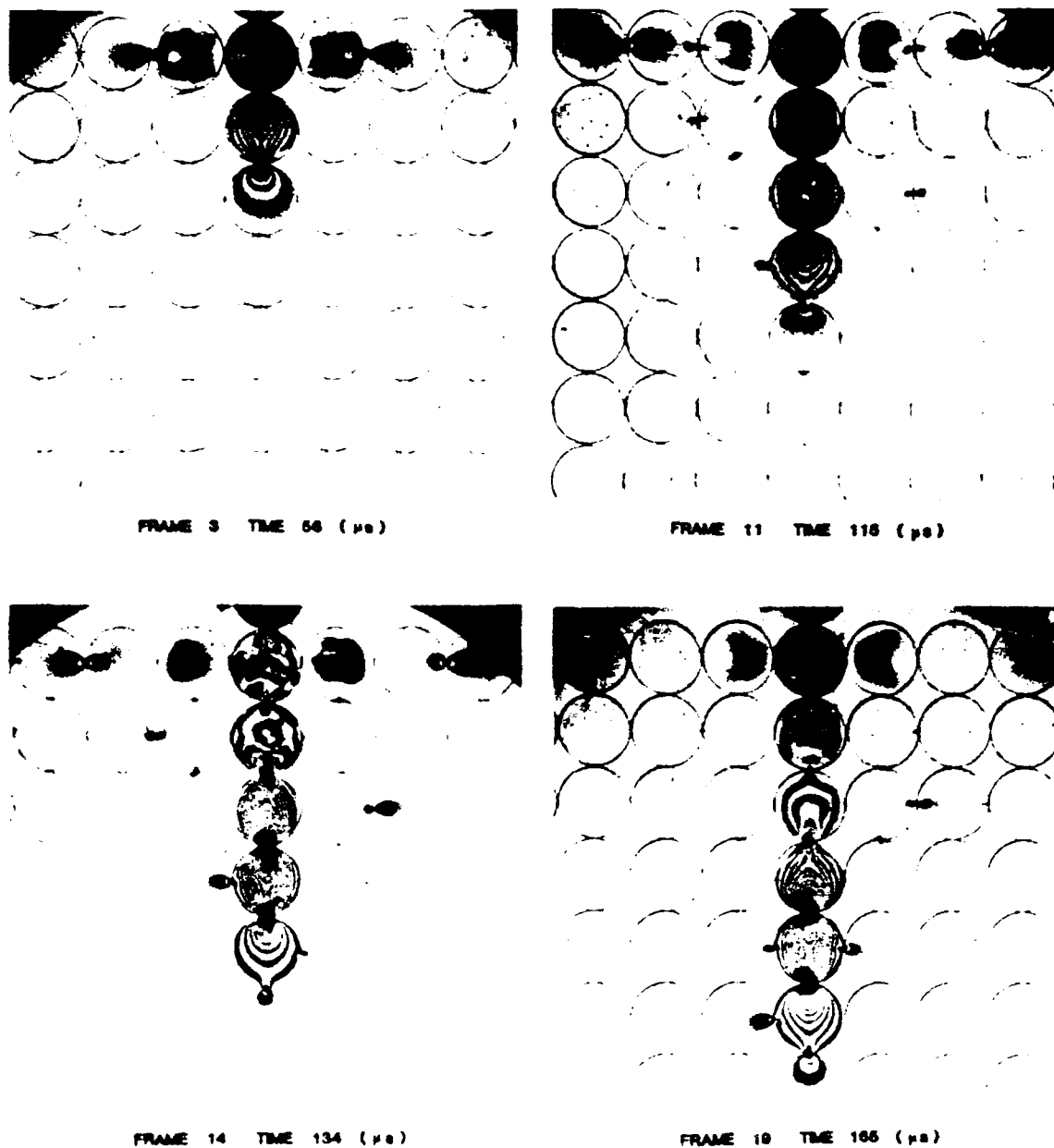


Figure 4. Isochromatic fringes obtained in a BCC arrangement, geometry 1c.

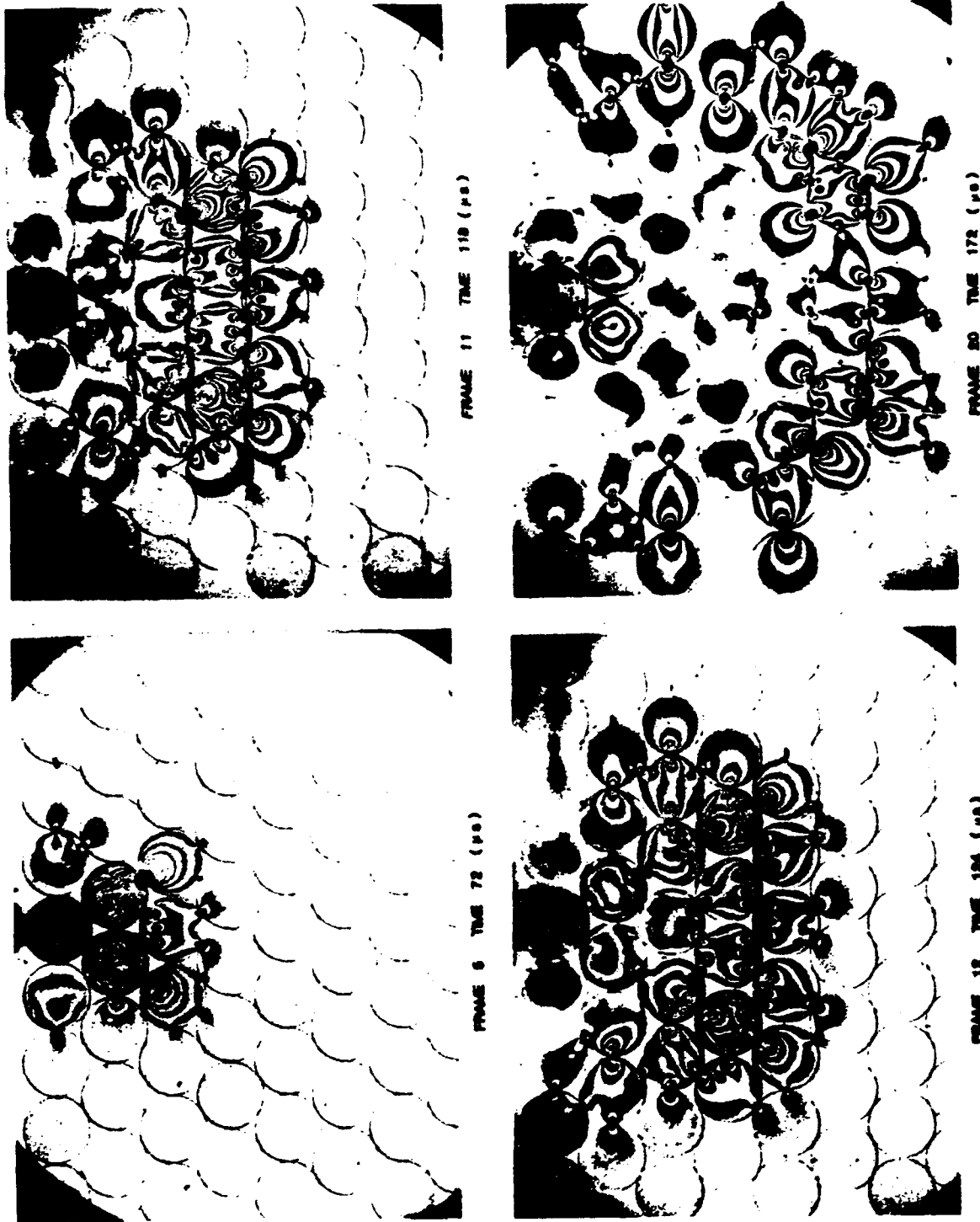


Figure 5. Isochromatic fringes obtained in a HCP arrangement, geometry 1c.

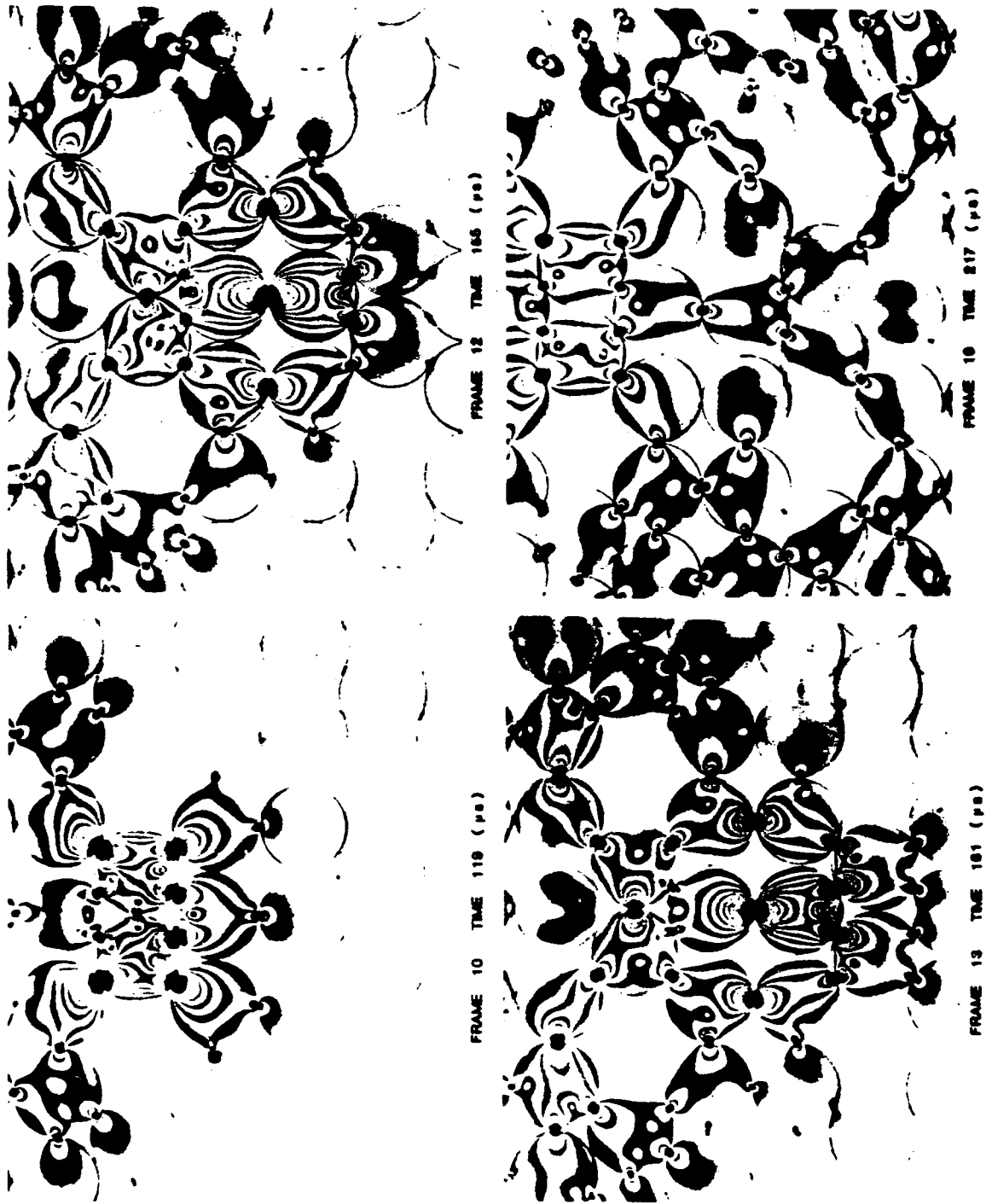


Figure 6. Isochromatic fringes obtained in geometry 1c.

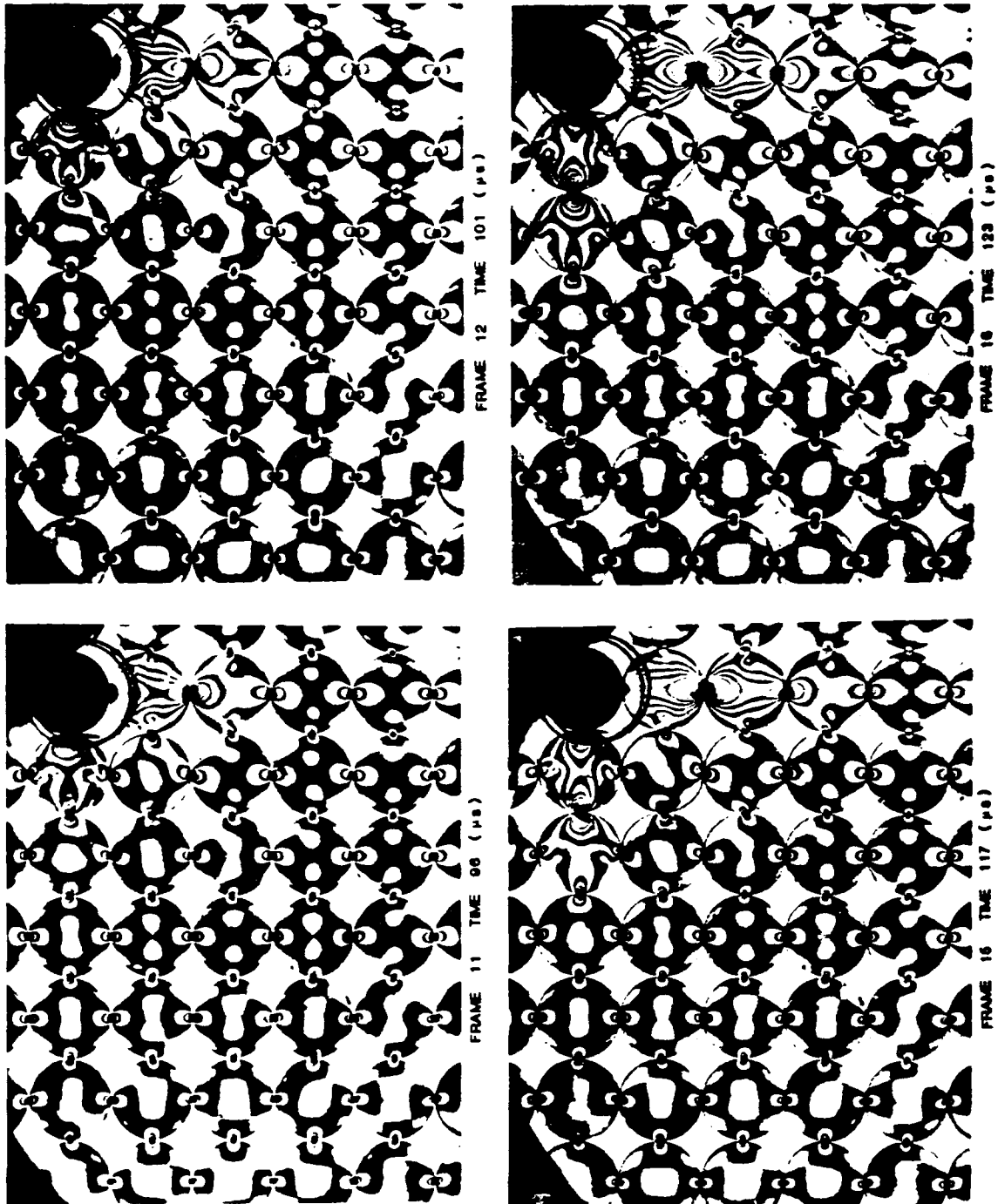


Figure 7. Isochromatic fringes obtained in a prestressed model, geometry II.

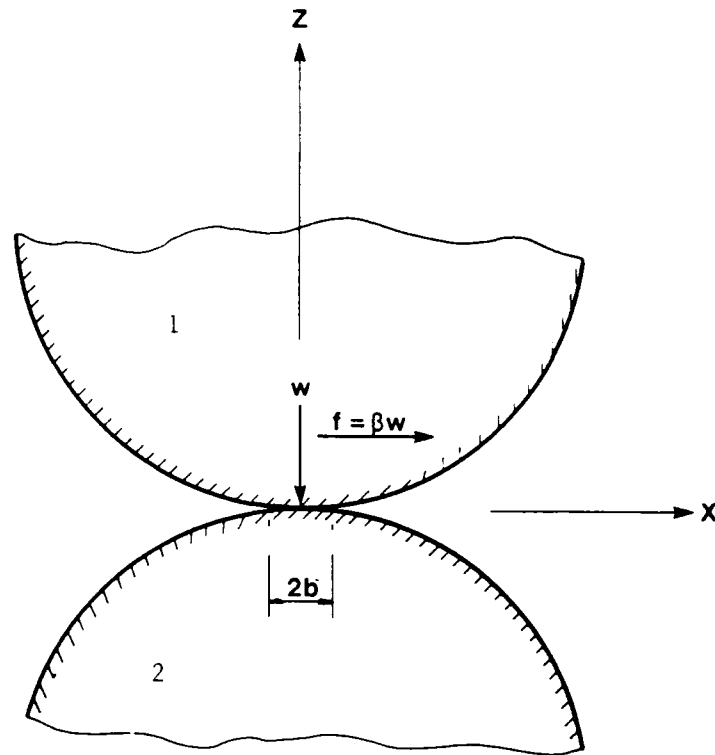


Figure 8. Coordinate system for two discs in contact.

$$\Delta = \frac{1}{A+B} \left(\frac{1-\nu_1^2}{E_1} + \frac{1-\nu_2^2}{E_2} \right)$$

$$A = \frac{1}{4} \left(\frac{1}{R_1} + \frac{1}{R_2} + \frac{1}{R_1'} + \frac{1}{R_2'} \right) +$$

$$+ \frac{1}{4} \sqrt{\left[\left(\frac{1}{R_1} - \frac{1}{R_1'} \right) + \left(\frac{1}{R_2} - \frac{1}{R_2'} \right) \right]^2 - 4 \left(\frac{1}{R_1} - \frac{1}{R_1'} \right) \left(\frac{1}{R_2} - \frac{1}{R_2'} \right) \sin^2 \alpha}$$

$$.B = \frac{1}{4} \left(\frac{1}{R_1} + \frac{1}{R_2} + \frac{1}{R_1'} + \frac{1}{R_2'} \right) -$$

$$- \frac{1}{4} \sqrt{\left[\left(\frac{1}{R_1} - \frac{1}{R_1'} \right) + \left(\frac{1}{R_2} - \frac{1}{R_2'} \right) \right]^2 - 4 \left(\frac{1}{R_1} - \frac{1}{R_1'} \right) \left(\frac{1}{R_2} - \frac{1}{R_2'} \right) \sin^2 \alpha}$$

Subscripts 1 and 2 refer to the bodies making the contact as shown in Fig. 8. R_1, R_1', R_2 and R_2' are the

principal radii of curvature at the point of contact and α is the angle between the corresponding planes of the principal curvatures. E is the modulus of elasticity and ν is Poisson's ratio.

The stress field equations are coupled with the stress optic law

$$\sigma_1 - \sigma_2 = \frac{Nf}{h} \quad (4)$$

where σ_1, σ_2 are the principal stresses, N is the fringe order, f_σ is the material fringe value, and h is the model thickness.

In order to accurately determine the contact length and friction factor from the full field photoelastic data, Eq. (4) is solved using an overdeterministic method developed by Shukla and Nigam [12]. These values were substituted in the Hertz stress field Eqs. (1 - 3) and the contact stresses were numerically integrated along the contact length to obtain the contact loads.

4. RESULTS AND DISCUSSION

The dynamic isochromatic photographs obtained from all the experiments showed the full field development of the load transfer process in the bulk of the granular media. These photographs clearly reveal the effect of microstructure on the load transfer process and provided the data necessary to obtain the wave velocity in every direction and also the normal and tangential load at every contact point.

Fig. 2 shows a sequence of four photographs obtained during wave propagation in a single chain of discs (geometry 1a). The wavelength of the pulse is seen to be around four discs diameters. Also the fringes are normal to the contact and there are no fringes due to the side supports of the loading frame. This clearly illustrates that there is no energy transfer occurring at the side supports and that all the energy is channelled down the chain. From the photographs the wave front position was plotted as a function of time. The gradient of this graph gave the instantaneous wave velocity. It was observed that the wave velocity drops from 1240 m/s to 1000 m/s in the initial four inches of travel. After this the wave travels with a constant velocity of 1000 m/s. The reason for the initial high velocity may be that the first few discs are compressed stronger against each other and the ratio of the incremental strains to incremental stresses might be very large. This will lead to larger effective modulus and thus higher velocity.

The contact loads obtained from photoelastic fringes were plotted for different contacts as a function of time as shown in Fig. 9. At a given contact the load increased from zero to a peak value and then gradually decreased to zero. A typical duration of the pulse at the contact was 110 μ s. The wavelength of the pulse was calculated by taking the product of average wave speed and the pulse duration at the contact. The wavelength thus obtained was 120 mm (i. e., around four disc diameters). This value compared well with the visual observation from the photographs. Due to internal losses within the granule, energy spent in closing the contact and some frictional and reflection effects, the peak contact loads dropped as the distance from the explosive loading increased. Using the values of peak loads, it was found that there was a 20% decrease in load as the wave travelled 5 disc diameters starting from the second disc. This is much higher when compared with the drop in peak load for a uniform bar which is 2% for the same distance of travel.

Fig. 3 shows a sequence of four photographs obtained due to wave propagation in geometry 1b. This geometry has a coordination number of three, i.e., each grain is in contact with three other grains. The wavelength of the loading pulse is about 5 disc diameters. Again, no fringes appear at the contacts with the supporting loading frame indicating that all the energy is channelled along the cell structure. The average wave velocity in the vertical direction was found to be 800 m/s. This is about 20 percent lower than the average velocity in the single chain disc assembly. This decrease in the average velocity is largely due to the fact that the wave velocity is largest in the direction normal to the contact points. When contact points between two adjacent granules deviate from 180° this velocity drops. Thus the wave velocity in this assembly is higher when the transfer occurs from a granule which is vertically on top of the other, whereas the velocity drops when the granules are at an angle to each other.

Besides the wave velocity, the photoelastic fringes were also analyzed to get the contact loads as a function of time as shown in Fig. 10. The peak contact load at the contact point 1 was found to be 1300N. As the wave entered the following two contacting granules the peak load dropped by 40% at contact points 2 and 3. The loading wave then enters the next granule through contact points 4 and 5. Since these points are not normal to points 2 and 3 the peak loads further drop by 35 percent. The contact load at point 4 builds up

as energy which is channelled in through two contact points has only one exit point. The peak load at point 6 was found to be 700N. Thus in going from point 1 to 6, a vertical distance equal to 2.73 times the diameter of the disc, there is an attenuation of about 46 percent in the peak load. This is considerably larger than the drop seen in the single chain assembly and clearly indicates the effect of microstructure on the wave propagation phenomenon.

The wave propagation phenomenon in a Body Centered Cubic (BCC) arrangement, geometry 1c, is shown in the four frames of Fig. 4. The wave propagated only in a single chain in this arrangement. No energy was transferred to other chains in the assembly. Comparison of Fig. 4 and Fig. 2 shows that the wave propagation phenomenon is identical for the single chain and the BCC packing, when the explosive loading is on the top of a disc in the assembly.

The photoelastic fringes for the hexagonal closed-packing arrangement, geometry 1d, are shown in Fig. 5. The wave propagation in this experiment does occur in two dimensions. The load transfer in this experiment can be categorized by two distinct chains: the primary chains (such as chains a and b as shown in Fig. 1d) which emanate from the disc on which the explosive loading takes place and the secondary chains which emanate due to contact of other discs with the discs in the primary chain.

The normal and tangential loads were computed from the photoelastic data at each point as a function of time. It was observed that the tangential loads were very close to zero for the primary chains. Thus, the contacts of the primary chains were frictionless, indicating that they behaved similar to the single chain assemblies but with inclined orientation with respect to the explosive loading. The contact loads versus time for different contacts were plotted for the primary chains as shown in Fig. 11. The drop in the peak loads from one contact to another was large as compared to single chain or BCC packing experiments, since energy transfer occurs to the secondary chains as the wave propagates in the primary chain. The wave attenuation for 5 disc diameters of travel in the primary chain was 70% as compared to 20% for the single chain and the BCC packing. Also, the average velocity in the vertical direction was 950 m/s which was about the same as in a single chain experiment.

The peak normal contact load at different contact points and the load transfer paths are shown in Fig. 12. The peak loads in the triangular region enclosed by the main chains are considerably higher than the contact loads outside this area. This indicates that the region of intense loading due to explosion is in the envelope enclosed by the two primary chains.

From the BCC and HCP experiments, it was observed that the load transfer path and the magnitude of load transfer from one contact to another was related to the angle made by the normals to the contacting discs at the contact point. If the input loading is normal and the angle made by the normals between the two discs as shown in Fig. 13 is acute ($\alpha_{ij} < (\pi/2)$), no load transfer would occur; however, if the angle made by the normals is obtuse ($\alpha_{ij} > (\pi/2)$), mechanical signals would propagate through the contact. To further illustrate this point consider the load transfer into and from disc A in the HCP geometry. The normal contact loads at every contact point made by disc A with the neighbouring discs are shown in Fig. 14. Wave energy entering at point 1 shows maximum transfer across point 2 which is directly ahead of point 1. Although contact points 3 and 4 make the same angles with the main chain, the contact loads are higher at point 4 than point 3 due to the superposition of loads from the other discs. No load transfer occurs across points 5 and 6 as $\alpha_{ij} < (\pi/2)$ for these contact points. A detailed study of the angular dependence of load transfer in a granular media has been conducted by the authors and is presented elsewhere [13].

Fig. 6 shows a sequence of four photographs as the wave travels in geometry 1e. This geometry has coordination numbers of both 4 and 5. The isochromatic fringes show a complex nature of load transfer phenomenon. The peak normal contact loads at different contact points are shown in the left part of Fig. 15, while the main load transfer paths are shown in the right. In the vertical direction the bulk of the energy is channelled through a column consisting of the primary cell structure. In the horizontal direction there are two chains of load transfer. The first horizontal chain making contact with the primary cell carries most of the load and is shown in Fig. 15 as the high load chain. The first horizontal chain making contact with the second cell carries a lesser amount of load and is shown in Fig. 15 as the low load chain. It appears that this sequence is repeated as one goes down the column of the cells. The photograph from this experiment also shows that the energy entered each cell within the column through four contact points, i_1 to i_4 as shown in Fig. 15 and exits mostly through six contact points 0_1 to 0_6 . During wave propagation in this geometry, position of the maximum vertical contact load alternated from one cell to the other in the column between the point along the centerline (point A) and points on the side of the centerline (points B and C). When the

maximum vertical contact load was at the point along the center line, high load transfer occurred through the horizontal chain in the adjacent cells. However, when the maximum vertical contact load was on the side of the centerline a lesser load was transferred through the horizontal chains in the adjacent cells. The average wave velocity along the vertical direction in this geometry was 850 m/s whereas the horizontal chains showed a velocity of 1000 m/s. It should be pointed out here that when the input load to a disc had a large tangential component, some energy transfer did occur across to discs which were at right angles.

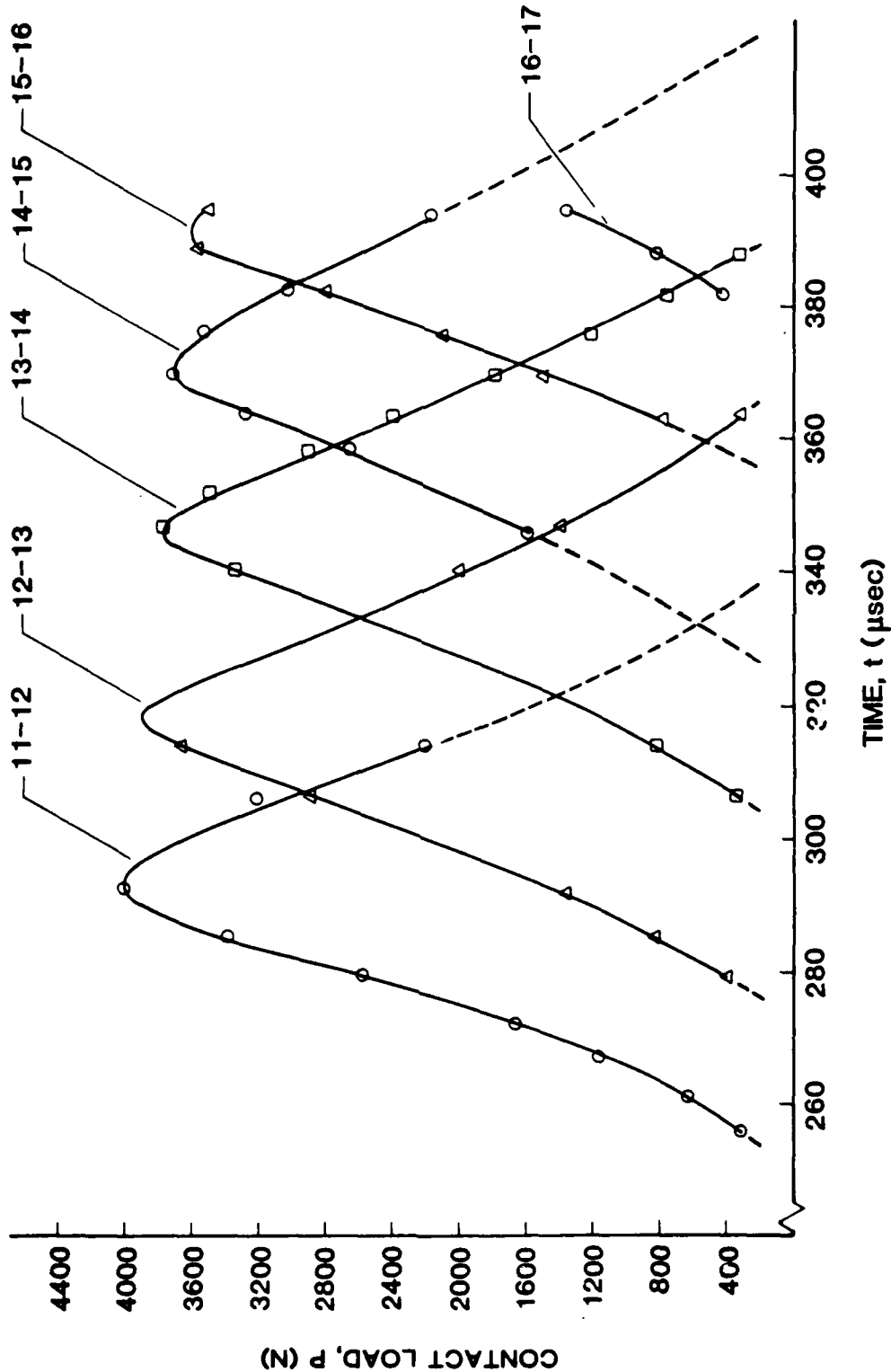


Figure 9. Contact loads as a function of time for geometry 1a.

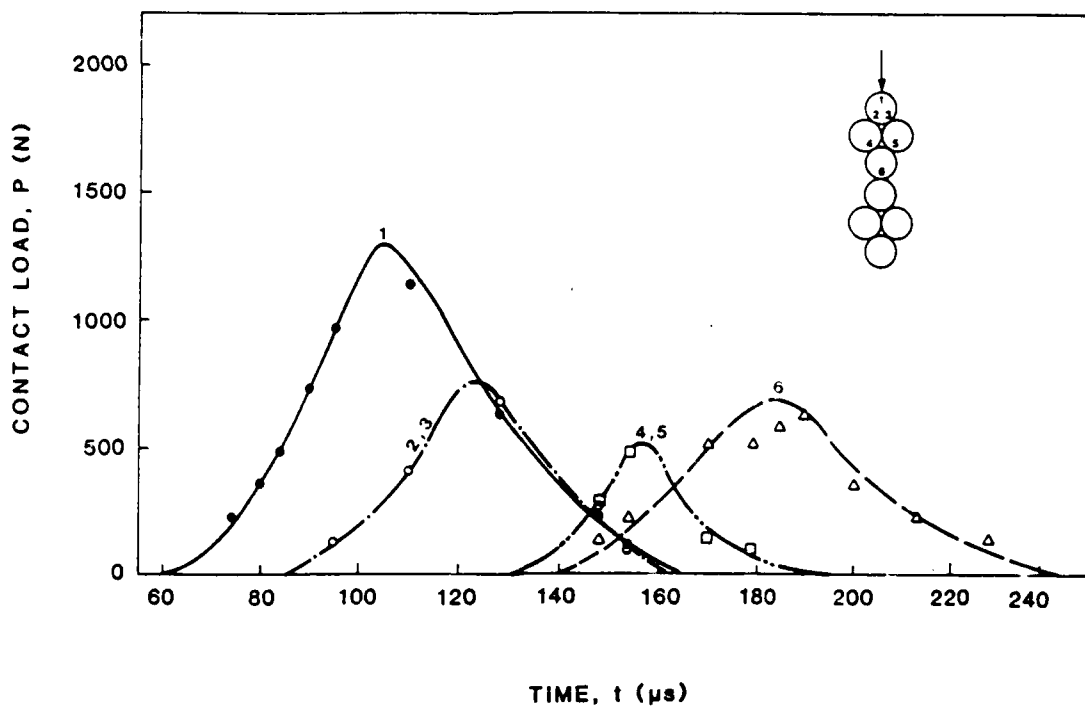


Figure 10. Variation of contact loads with time for geometry 1b.

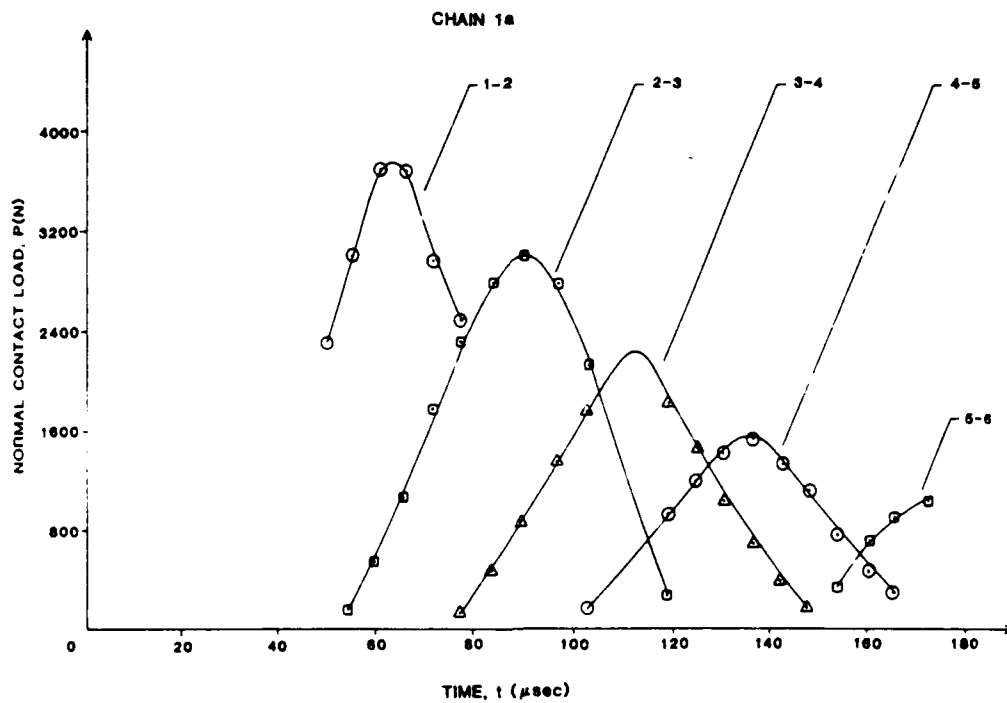


Figure 11. Variation of contact loads in primary chain with time for HCP arrangement, geometry 1d.

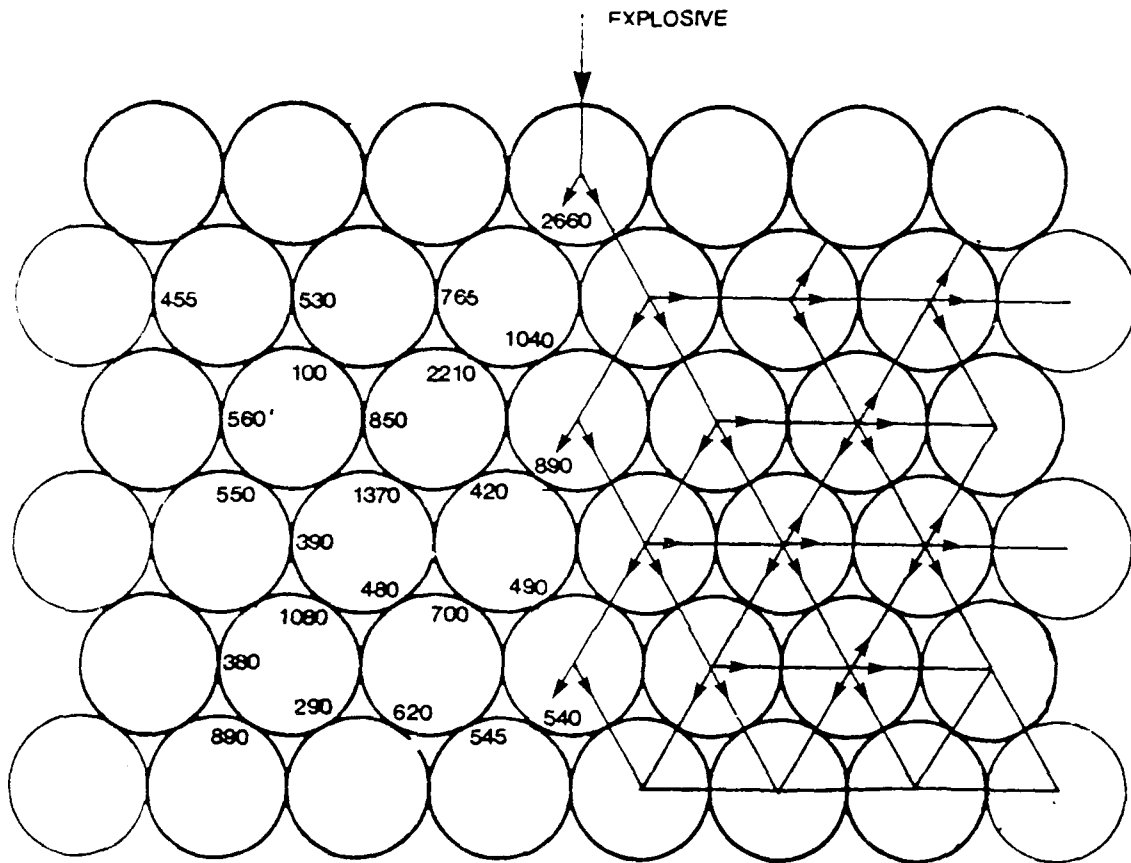


Figure 12. Peak normal contact loads at different contact points and the load transfer paths in the HCP geometry.

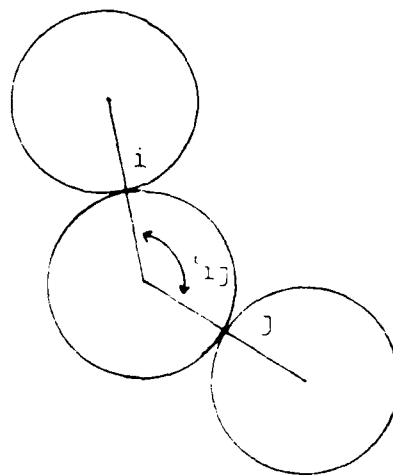


Figure 13. Contact angle made by normals drawn from the center of granules to the contact point.

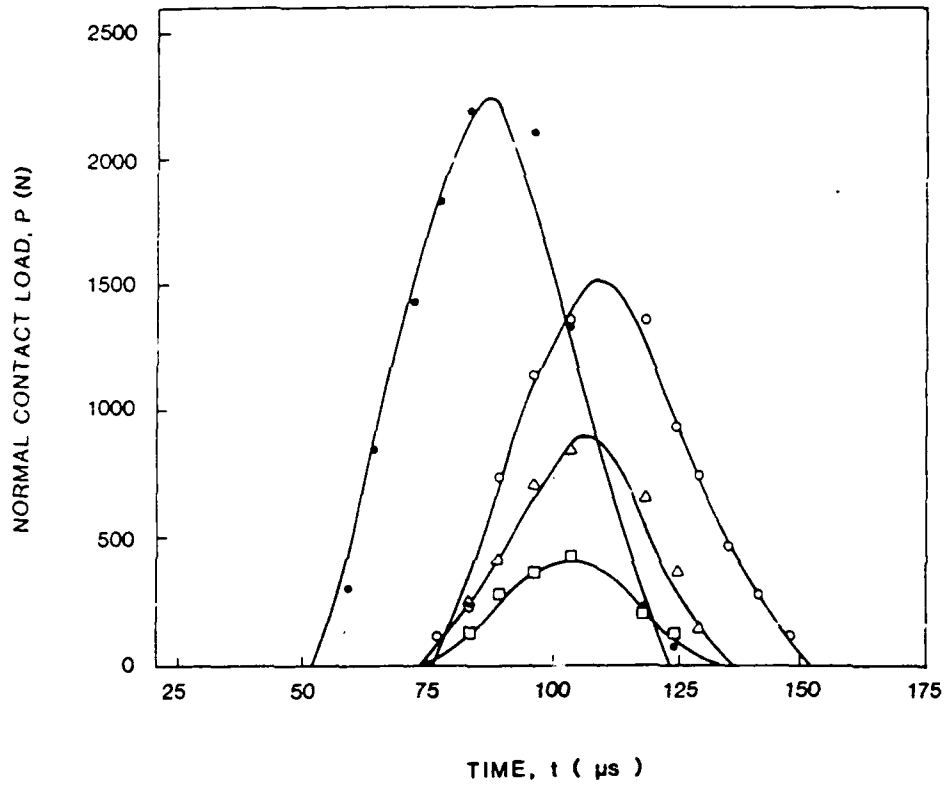


Figure 14. Contact load transfer profiles for various contacts on disc A.

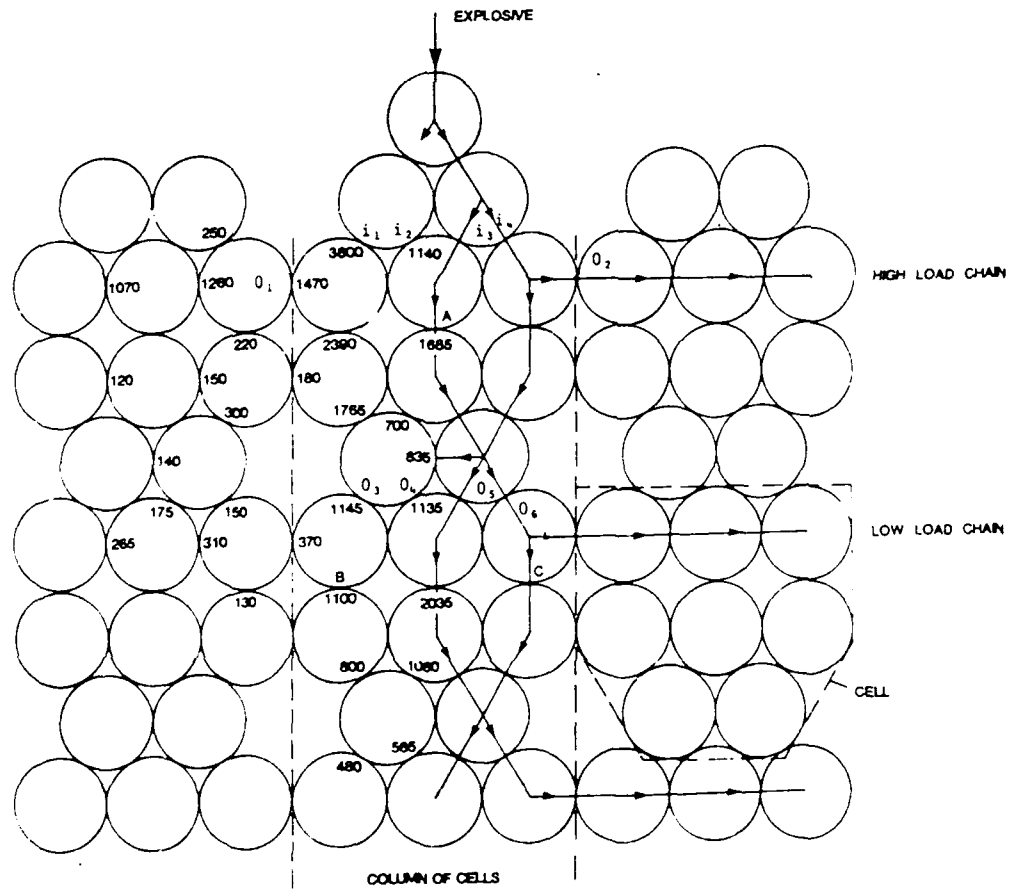


Figure 15. Peak normal contact loads at different contact points and load transfer paths in geometry 1c.

Finally, an experiment was conducted to study wave propagation in a BCC geometry with a prestress on it. The reason for conducting this experiment was to verify the results of Fig. 4. It was felt that maybe wave propagation in Fig. 4 was seen only in the vertical direction due to gravitational loading. Thus a biaxial prestress of 250N was applied to the BCC arrangement of discs using a specially designed loading fixture as shown in Fig. 16. The dynamic explosive loading was applied in the center. A series of four photographs obtained from this experiment are shown in Fig. 7. They verify that wave propagation only occurs along the two normal chains with no energy transfer across contacts which are at right angles. The only difference in this experiment was that the velocity was about 25% higher in comparison to the experiment without any prestress.

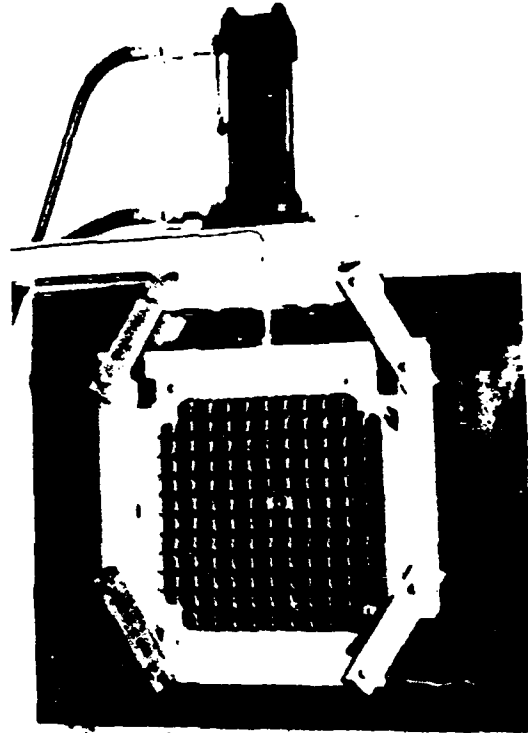


Figure 16. Biaxial loading frame.

5. SUMMARY

Dynamic photoelasticity was employed to study the effect of microstructure on wave propagation and dynamic load transfer in a granular media. The granular media was modeled as one and two dimensional arrays of circular discs fabricated from photoelastic material Homolite-100. The experimental data were analyzed to determine the wave velocities, identify characteristic dynamic load transfer paths and quantitatively calculate the dynamic contact forces at each contact point.

ACKNOWLEDGEMENTS

The authors would like to acknowledge the support of the Army Research Office under grant no. DAAL03-86-K-0125.

REFERENCES

1. M. Oda, "Initial fabrics and their relations to mechanical properties of granular materials," *Solid and Foundations* 12(1), (1972).
2. M. Oda, "Deformation mechanism of sand in triaxial compression tests," *Solid and Foundations* 12(4) (1972).
3. J.H. Borowicka, "Rearrangement of grains by shear tests with sand," *Proc. 8th ICSMFE* 1(1), (1973).
4. J.R.F. Arthur and T. Dunstan, "Radiograph measurements of particular packing," *Nature* 223 (1969).
5. J. Konish, "A microscopic study on granular materials during shearing process," *J. Fac. Engg. Shinshu Univ.*, 34 (1973).
6. J.R.F. Arthur and A.B. Phillips, "Homogeneous and layered sand in triaxial compression," *Geotechnique* 25 (1975).
7. A. Mahnood and J. K. Mitchell, "Fabric-property relationships in fine granular materials," *Clay and Clay Minerals* 22 (1974).
8. S.C. Cowin, "Microstructure continuum models for granular materials," *Proc. U.S. Japan Seminar on Continuum Mech. & Stats. Approaches in the Mechanics of Granular Materials*, (1978).
9. S.C. Cowin, "Continuum mechanical & statistical approaches in the mechanics of granular materials," *J. Rheology* 23-2 (1979).
10. A. Shukla and C. Damania, "Experimental investigation of wave velocity and dynamic contact stress in an assembly of discs," *J. Expt. Mech.* 27-3, 268-281 (1987).
11. M. Shahinpoor, *Frequency Distribution of Voids in Randomly Packed Monogranular Materials: New Methods and Constitutive Relations*, ed by J.T. Jenkins and M. Stake, Elsevier (1983).
12. A. Shukla and H. Nigam, "A numerical analysis of contact stress problem", *J. Strain Analysis* 20-4 (1986).
13. A. Shukla, C.Y. Zhu and M.H. Sadd, "Angular dependence of dynamic load transfer due to explosive loading in two dimensional granular aggregates", *J. Strain Analysis* to be published

ANGULAR DEPENDENCE OF DYNAMIC LOAD TRANSFER DUE TO EXPLOSIVE LOADING IN GRANULAR AGGREGATE CHAINS

A. SHUKLA *Department of Mechanical Engineering and Applied Mechanics, University of Rhode Island.*

C. Y. ZHU *Department of Mechanical Engineering and Applied Mechanics, University of Rhode Island.*

M. SADD *Department of Mechanical Engineering and Applied Mechanics, University of Rhode Island.*

An experimental investigation was conducted to study the dependence of packing geometry on the dynamic load transfer in two dimensional granular aggregate chains. The granular media was simulated by circular discs made of photoelastic material. The experimental method utilizes the combination of high speed photography and photoelasticity to visualize the dynamic load transfer phenomenon in two dimensional model chains subjected to explosive loading. The photographs thus obtained were analysed to get the normal and tangential loads at the contact points as a function of time. The results indicate that the load transfer is strongly dependent on the angle between the vectors drawn from the mass centres of the contacting granules.

1 INTRODUCTION

Granular media transmit mechanical loadings primarily through contact mechanisms between each grain. This phenomenon is quite a complex process and depends inherently on the microstructural packing arrangements of the media. Porosity alone is not a sufficient measure to characterize such a load transfer process. Recently, several theoretical and experimental investigations (1)(2)† have been conducted to relate microstructure to macroscopic behaviour. A general finding of some of this work is that local microstructure or fabric is significant and that particular fabric vectors and tensors can be used to develop theories to predict the mechanical behaviour of such materials. In particular, branch vectors between the mass centres of typical grains and normal vectors in the direction of the contact normals have been proposed (see Fig. 1). Specifically, Nemat-Nasser *et al.* (1) have suggested mechanical constitutive relations based upon writing the stress as a function of a second order fabric tensor, F_{ij} , where

$$F_{ij} = \frac{1}{M} \sum_{n=1}^M l_i^{(n)} l_j^{(n)} \quad (1)$$

with M being the number of n -contacts per unit volume. This study addresses this issue for the case of dynamic load transfer by investigating the effects of the angle between branch vectors on the wave propagation through granular aggregate assembly chains.

The term 'contact angle' is defined as the angle between any two branch vectors connecting the mass

centres of a pair of granules, as shown in Fig. 1. This angle plays an important part in determining the dynamic load transfer in such a medium. Examples of this fact have been shown in the work of Shukla and Damania (3) and are shown in Figs 2 and 3. These dynamic photoelastic figures illustrate how waves from an explosive charge, located at the top of each photograph, move through two different granular packing arrangements.

Studies of the load transfer in granular media have been previously conducted. Drescher and De Josselin De

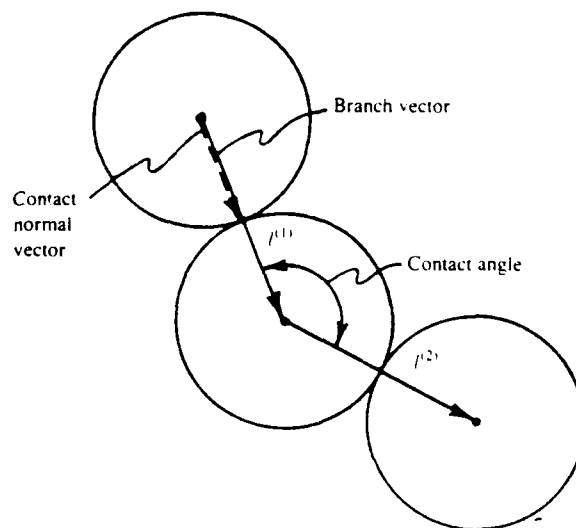


Fig. 1. Branch vectors connecting the mass centres of a pair of granules

The MS of this paper was received at the Institution on 10 April 1987 and accepted for publication on 18 January 1988
 † References are given in the Appendix

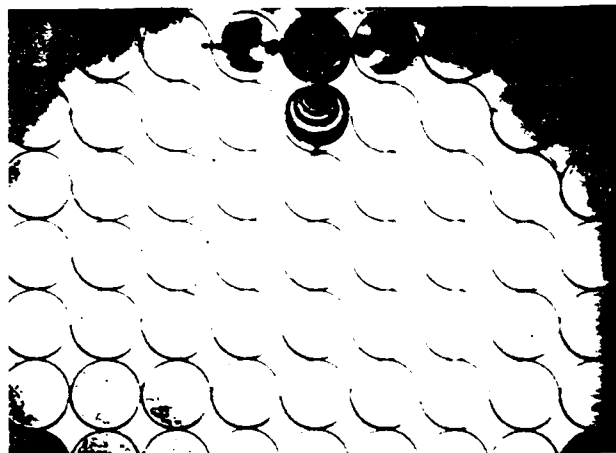
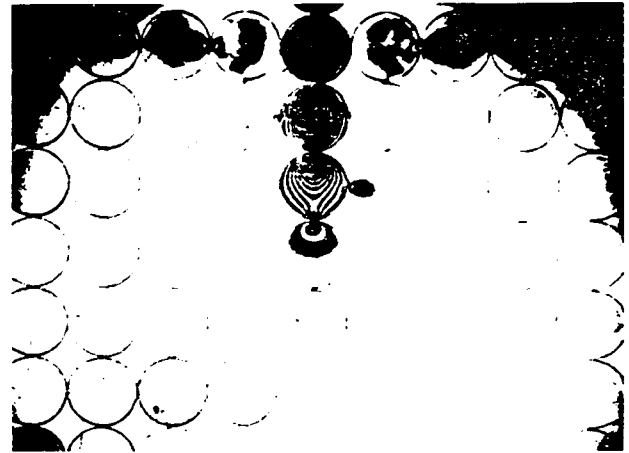
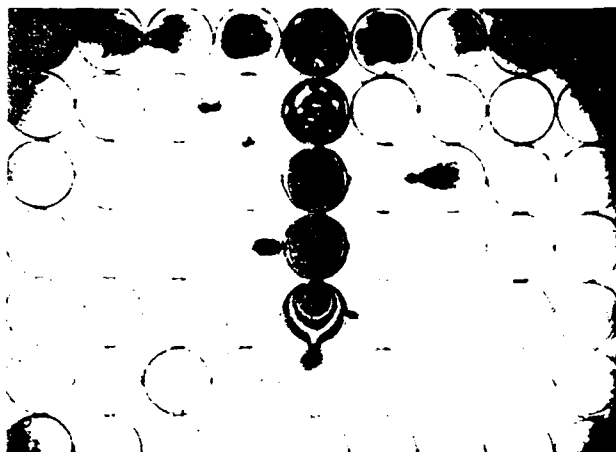
Frame 3. $t = 55.5 \mu\text{s}$ Frame 9. $t = 93.5 \mu\text{s}$ Frame 14. $t = 133 \mu\text{s}$ Frame 19. $t = 164.5 \mu\text{s}$

Fig. 2. Isochromatic fringes due to explosive loading in a body-centred cubic arrangement

Jong (4) have simulated granular media by using assemblies of circular discs, and then studied the static load transfer through the assembly by means of photo-mechanics. Rossmannith and Shukla (5) extended this idea to the dynamic case through the use of high speed photography. Additional dynamic work was also carried out by Shukla and Damania (3), and Shukla and Rossmannith (6). Most of this previous work focussed on wave propagation phenomenon in general without going into details of relating specific microstructure to the associated wave motion.

The purpose of this investigation was to study the relation between the dynamic load transfer and the contact angle in single disc chains of circular granules. This specific relation will prove to be useful in characterizing how local microstructure affects the wave propagation phenomena. Dynamic photoelasticity along with high speed photography are employed to collect time-dependent data on the rapidly moving wave motion. Simplified Hertz contact stress theory along with photo-mechanics has been used to determine the load transfer between pairs of granules. The wave motion of interest here is transient in nature being produced by explosive

loadings of short duration yielding a primary wave length of approximately four to five grain diameters.

2 EXPERIMENTAL PROCEDURE

The experimental model used in this study was comprised of disc chain assemblies of Homalite 100 discs as shown in Fig. 4. Homalite 100 is a birefringent brittle polyester material whose mechanical and optical properties are well characterized ($E = 4.8 \text{ GPa}$, $\nu = 0.35$, and $f_o = 21.9 \text{ kN/m}$). The discs were 1 in in diameter and 1/4 in thick. The angles θ_1 and θ_2 in the assembly were changed in a series of experiments. During the experiments the discs were dynamically loaded by firing a small charge of explosive PETN in a specially designed charge holder. The wave propagation phenomenon due to explosive loading in the granular media was studied using the technique of dynamic photoelasticity and high speed photography.

The models were placed in the optical bench of a high speed multiple spark gap camera. The camera was triggered at some prescribed delay time after igniting the explosive. This high speed photographic system operated

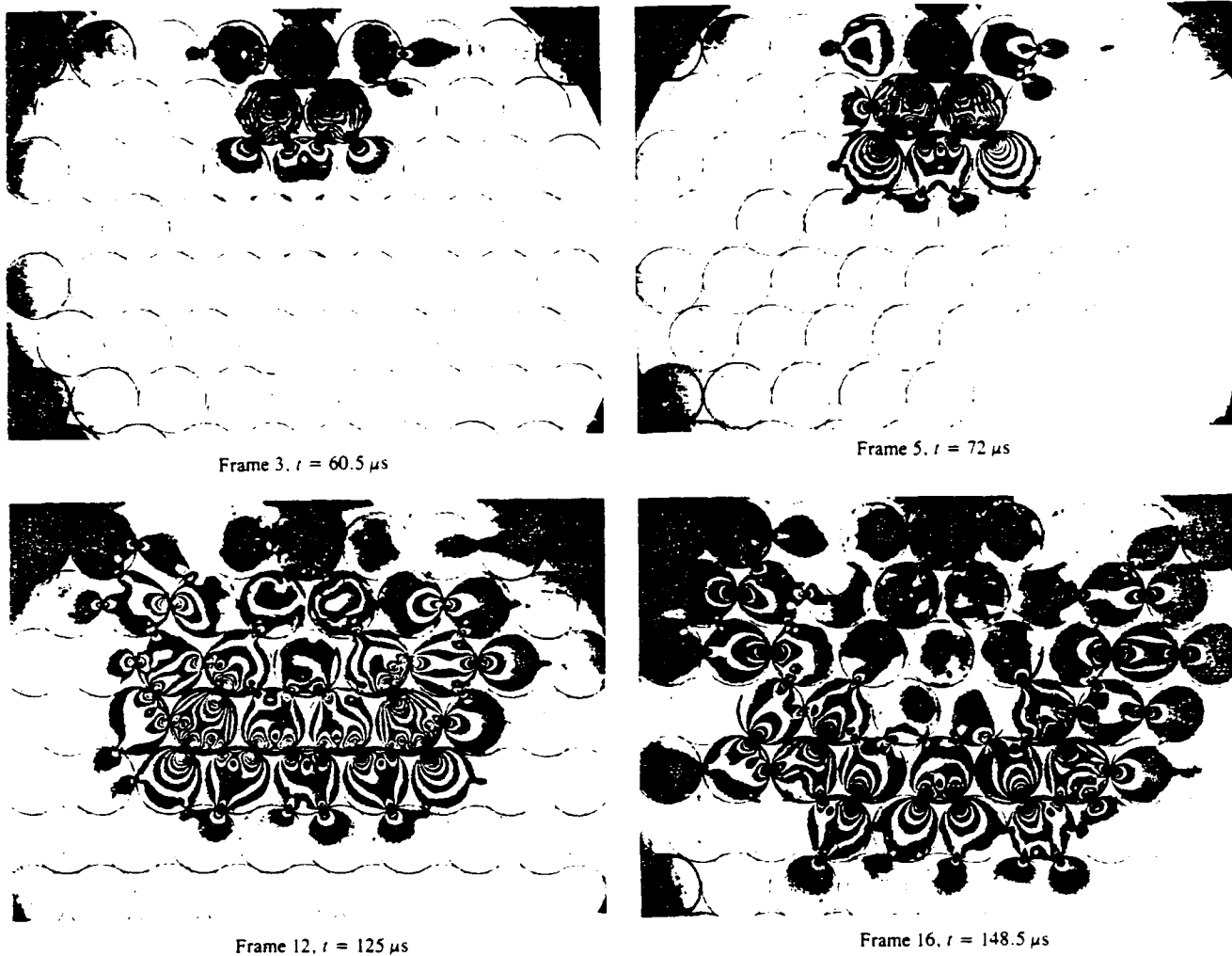


Fig. 3. Isochromatic fringes due to explosive loading in a hexagonal cubic arrangement

as a series of high intensity, extremely short duration pulses of light and provided 20 photoelastic images at discrete times during the dynamic event. A typical sequence of three images for two different orientations is shown in Figs 5 and 6. These photographs of the wave propagation process at different stages of development provided the data necessary to obtain the contact loads along different chains.

3 ANALYSIS PROCEDURE

A careful inspection of the photographs obtained from the experiments revealed that the wave length, λ , of the loading pulse was much larger than the disc diameter, D . The wave length was determined by measuring the length of the photoelastic fringe patterns of the loading pulse, and the data indicated that $\lambda \approx 4D$. Furthermore, the fringe patterns around the contact points were symmetric on either side of the contact points and were similar to the fringes obtained under static diametral compression as shown in Fig. 7. Both these features indicated that around the contact zone, quasi static loading was present during the wave propagation event. Thus

Hertz equations were used to obtain the contact stresses, strains, and loads.

From the Hertz contact stress theory (7), the stress field equations around the contact region of two discs, as shown in Fig. 8, are represented as

$$\begin{aligned}
 \sigma_{zz} &= -\frac{b}{\pi\Delta} \{z(b\phi_1 - x\phi_2) + \beta z^2\phi_2\} \\
 \sigma_{xx} &= -\frac{b}{\pi\Delta} \left[z \left(\frac{b^2 + 2z^2 + 2x^2}{b} \phi_1 - \frac{2\pi}{b} - 3x\phi_2 \right) \right. \\
 &\quad \left. + \beta \left\{ (2x^2 - 2b^2 - 3z^2)\phi_2 + \frac{2\pi x}{b} \right. \right. \\
 &\quad \left. \left. + 2(b^2 - x^2 - z^2) \frac{x}{b} \phi_1 \right\} \right] \\
 \sigma_{zx} &= -\frac{b}{\pi\Delta} \left[z^2\phi_2 + \beta \left\{ (b^2 + 2x^2 + 2z^2) \right. \right. \\
 &\quad \left. \left. \times \frac{z}{b} \phi_1 - 2\pi \frac{z}{b} - 3xz\phi_2 \right\} \right] \quad (2)
 \end{aligned}$$

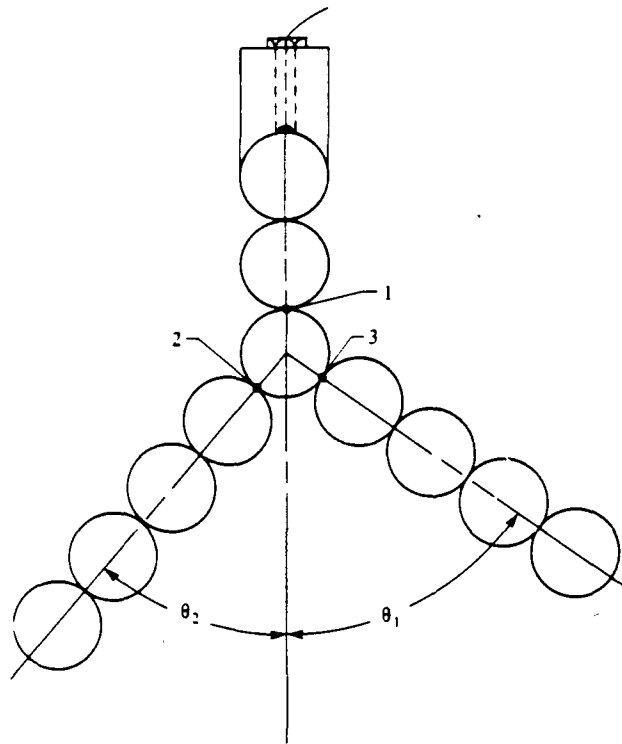


Fig. 4. Geometrical arrangement used in experiments

where ϕ_1, ϕ_2 are

$$\phi_1 = \frac{\pi(A + B)}{AB\sqrt{(2AB + 2x^2 + 2z^2 - 2b^2)}}$$

$$\phi_2 = \frac{\pi(A - B)}{AB\sqrt{(2AB + 2x^2 + 2z^2 - 2b^2)}}$$

$$A = \sqrt{\{(b + x)^2 + z^2\}};$$

$$B = \sqrt{\{(b - x)^2 + z^2\}}; \quad \Delta = 2R \frac{1 - \nu^2}{E} \quad (3)$$

with E = modulus of elasticity, ν = Poisson's ratio, β is a friction factor, and b is the half contact length.

The stress field equations are coupled with the stress optic law

$$\sigma_1 - \sigma_2 = \frac{Nf_\sigma}{h} \quad (4)$$

where σ_1, σ_2 are the principal stresses, N is the fringe order, f_σ is the material fringe value, and h is the model thickness.

In order to accurately determine the contact length and friction factor from the full field photoelastic data, equation (4) is solved using an overdeterministic method developed by Shukla and Nigam (8). These values were substituted in the Hertz stress field equations (2) and (3) and the contact stresses were numerically integrated along the contact length to obtain the contact loads.

4 RESULTS AND DISCUSSION

A series of five groups of experiments was conducted with the geometry shown in Fig. 4. These groups include



Fig. 5. Typical isochromatic fringes obtained in symmetric arrangement ($\theta_1 = \theta_2$)

a parametric study of the effects of the branch angles θ_1 and θ_2 on load transfer phenomenon. The branch angles included the values of 30, 45, 60, 75, and 90 degrees. The dynamic isochromatic photographs obtained for two of these experiments are shown in Figs 5 and 6. Using the stress field equations (2) and (3) along with (4), and the photoelastic fringes near the contact points, gives the intensity of the contact stresses. The fringes are sym-

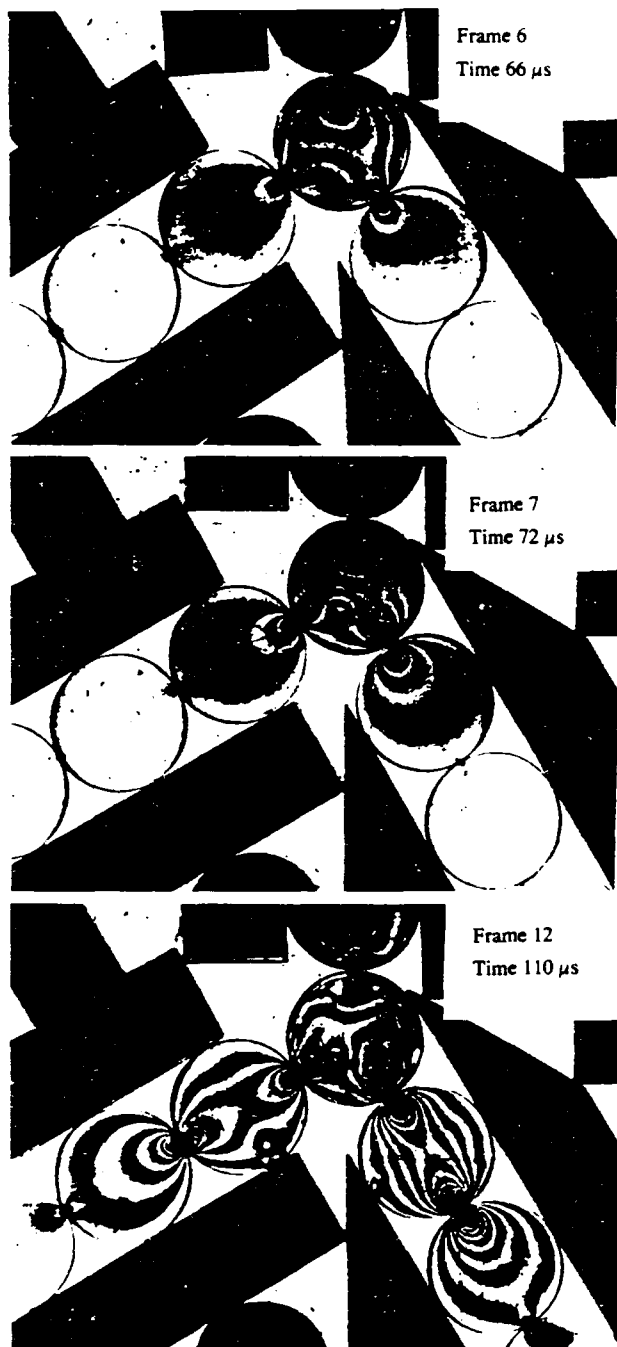


Fig. 6. Typical isochromatic fringes obtained in unsymmetric arrangement ($\theta_1 = \theta_2$)

metric in both chains, indicating predominantly normal loading. The absence of any fringe patterns at contact points along the side supports confirms that all energy is channelled along the disc chains and no loss of energy occurs to the side supports. The normal contact loads obtained from these photographs for a specific experiment are shown in Fig. 9 for case of $\theta_1 = 75$ degrees and $\theta_2 = 30$ degrees. The three contact loads at each of the three contact points are labelled P_1 , P_2 , and P_3 as shown. The load at each contact point increases as the wave interacts with it, builds up to a peak value, and then monotonically decays to zero. It can clearly be seen

that as the branch angle increases the dynamic peak load drops. However, the wavelength of the loading pulse increases with the branch angles. Figure 10 shows another typical case with $\theta_1 = 90$ degrees and $\theta_2 = 30$ degrees. For this case the load P_3 in the 90 degree branch was found to be zero.

Since the significant point in our study is not the actual loadings but rather the transfer characteristics, the ratio of transmitted to incident loads is to be used. This ratio has symmetry with respect to the branch angles θ_1 and θ_2 , i.e., P_2/P_1 as a function of θ_1 and θ_2 is the same as P_3/P_1 written as a function of θ_2 and θ_1 . Consequently only one ratio, P_2/P_1 , will be considered in detail. Figure 11 shows this load transfer ratio as a function of contact angles θ_1 and θ_2 . This figure illustrates the rapid attenuation of the load transfer with the branch angle, and it also shows the inter-relationships of θ_1 and θ_2 on the load transfer. For example, a higher value of θ_1 produces less load transfer attenuation for a given branch angle, θ_2 .

The effect of branch angles on the signal wave length is shown in Fig. 12. Here the duration of contact is plotted against the angle θ_2 . It is observed that a significant increase in this duration time occurs as the branch angle, θ_2 , is increased. This means that the granular assembly will act as a wave guide which will increase the wave length of the transmitted transient signal.

5 CONCLUSIONS

The experimental study conducted in this paper demonstrates the angular dependence of dynamic load transfer in two dimensional granular media. The results indicate the following.

- (1) Rapid attenuation of load transfer occurs as the branch angle increases from 0 to 90 degrees.
- (2) The attenuation of load transfer also depends on the inter-relationship between the two branch angles.
- (3) The wavelength of the loading pulse increases with the branch angle. Here again the inter-relationships between the branch angles has an influence on the duration of the contact load. The wavelength almost doubles as the contact angle increases from 15 to 75 degrees.

It should be pointed out that the current work represents only a first step in understanding the wave propagation process in a complex aggregate assembly. For example, in considering the wave motion in Fig. 3, many waves take very complex paths during their propagation histories. The simple two branch geometries considered in the current study can then be interpreted as only a beginning in the understanding of how the local micro-structure effects the transmission of waves in granular materials. Finally, theoretical-numerical work is also underway to calculate this dynamic load transfer phenomena, and this will be reported in the near future.

ACKNOWLEDGEMENTS

The authors would like to acknowledge the support of the Army Research Office under the contract no. DAAL03-86-K-0125.

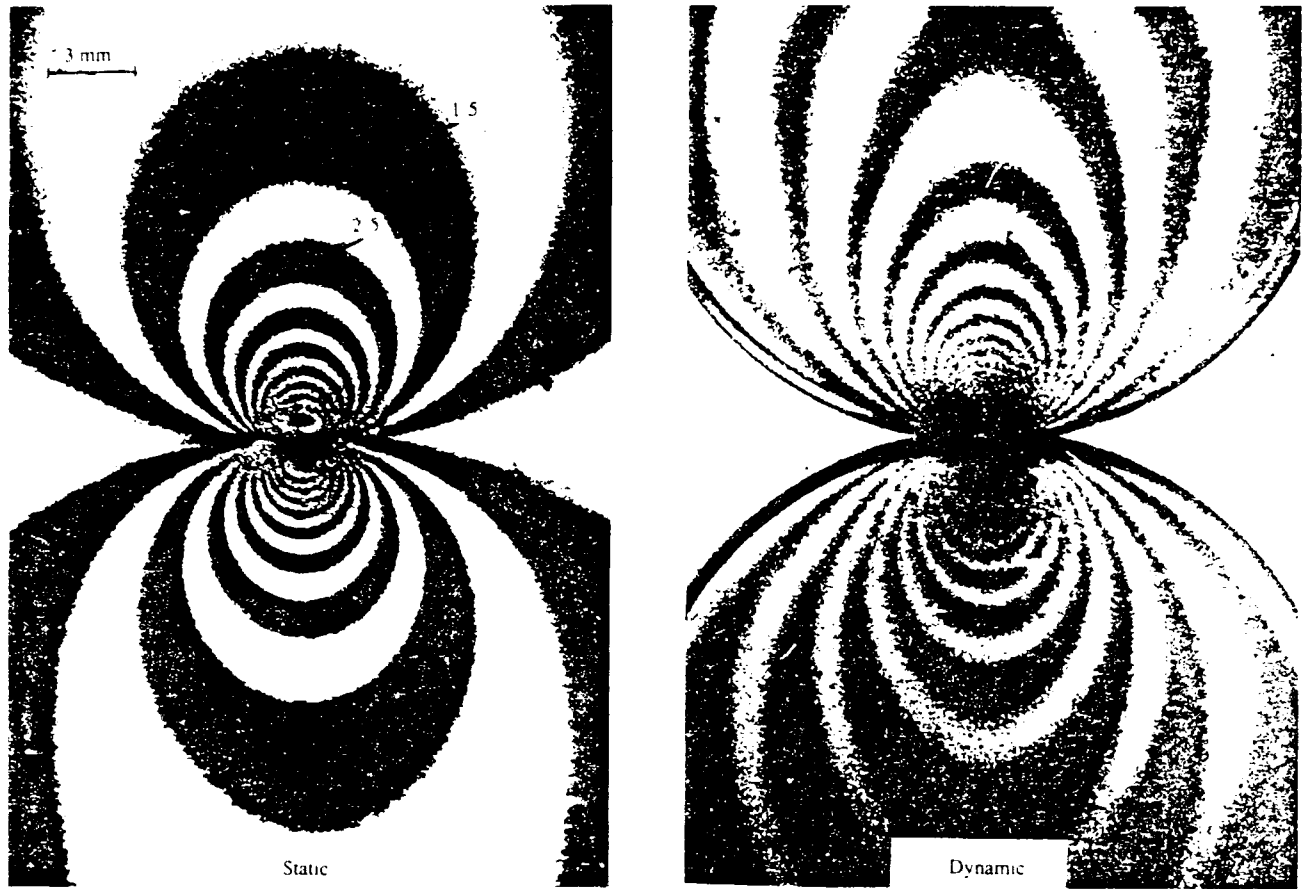


Fig. 7. Comparison of static and dynamic isochromatic fringes.

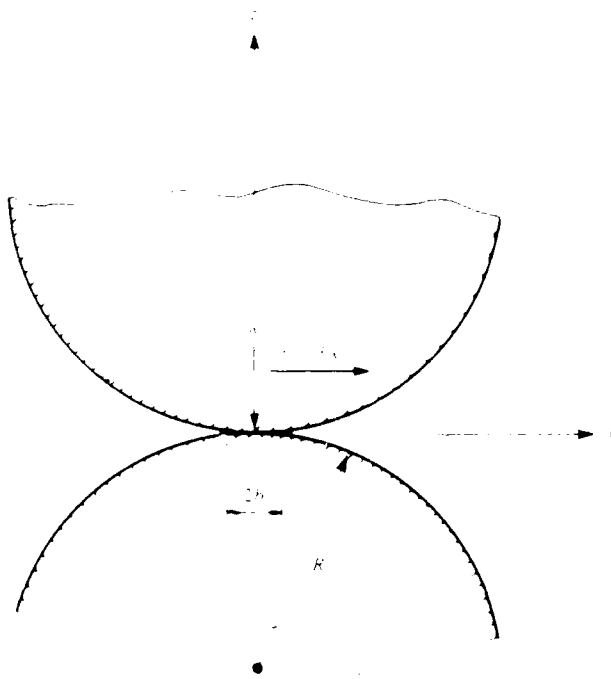


Fig. 8. Schematic diagram for two spheres in contact, w and u are the distributed normal and tangential loadings per unit length.

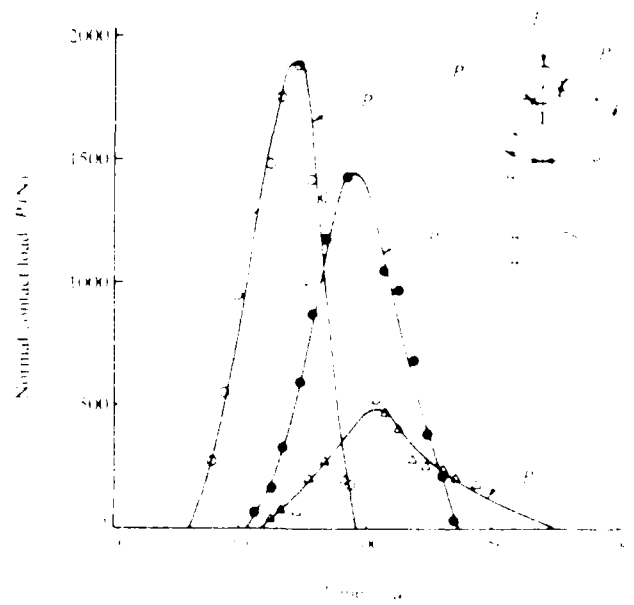


Fig. 9. Normal contact load as a function of time.

DYNAMIC LOAD TRANSFER IN TWO-DIMENSIONAL GRANULAR AGGREGATES

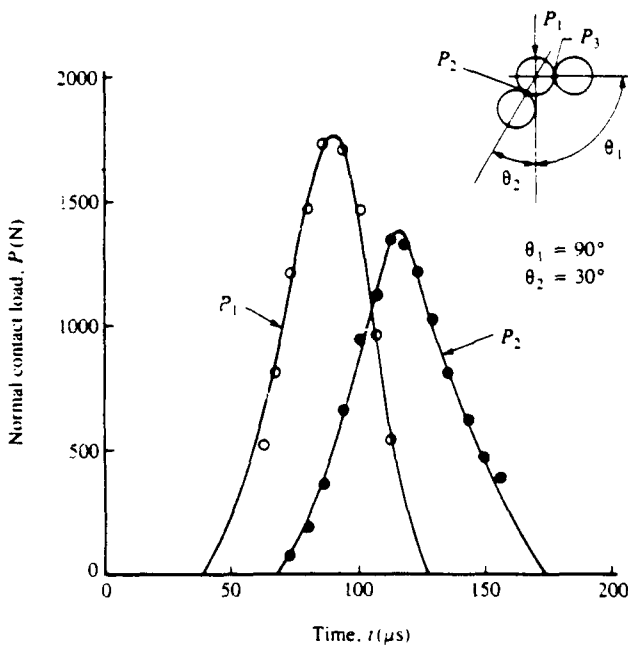


Fig. 10. Normal contact load as a function of time

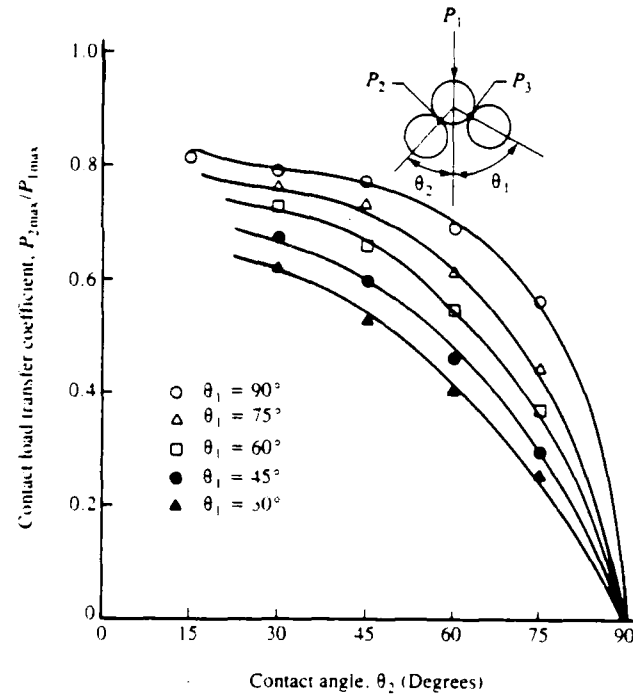


Fig. 11. Load transfer coefficient as a function of branch angle θ_2 for various values of θ_1

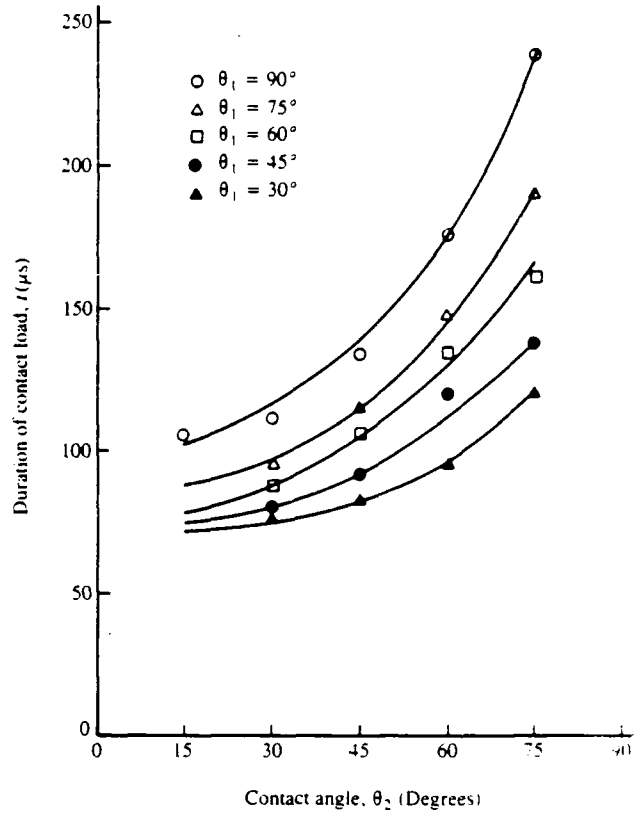


Fig. 12. Duration of contact load as a function of branch angle θ_2 for various values of θ_1

APPENDIX

REFERENCES

(1) NEMAT-NASSER, S. and MEHRABADI, M. M., 'Micro-mechanically based rate constitutive descriptions for granular materials', in *Mechanics of Engineering Materials*, 1984 (Edited by C. S. Resai and R. H. Gallagher, (John Wiley, New York).

(2) ODA, M., KONISHI, J., and NEMAT-NASSER, S., 'Some experimentally based fundamental results on the mechanical behavior of granular materials', *Geotechnique*, 1980, **30**, 479-495.
 (3) SHUKLA, A. and DAMANIA, C., 'Experimental investigation of wave velocity and dynamic contact stresses in an assembly of discs', *Expl Mech.*, 1987, **27**, 268-281.
 (4) DRESCHER, A. and DE JOSSELIN DE JONG, G., 'Photoelastic verification of a mechanical model for the flow of a granular material', *J. Mech. Phys Solids*, 1972, **20**, 337-351.
 (5) ROSSMANITH, H. P. and SHUKLA, A., 'Photoelastic investigation of dynamic load transfer in granular media', *Acta Mech.*, 1982, **42**, 211-225.
 (6) SHUKLA, A. and ROSSMANITH, H. P., 'Dynamic photoelastic study of wave propagation and energy transfer across contacts', *J. Strain Analysis*, 1986, **21**, 213-218.
 (7) BORESI, A. P., SIDEBOTTOM, O. M., SEELY, F. B., and SMITH, J. O., *Advanced Mechanics of Materials*, 1978 (John Wiley, New York).
 (8) SHUKLA, A. and NIGAM, H., 'A numerical experimental analysis of the contact stress problem', *J. Strain Analysis*, 1985, **20**, 241-245.

Paper G

WAVE PROPAGATION IN POROUS MEDIA AS A FUNCTION OF FLUID SATURATION

BY

A. Shukla and V. Prakash

Dynamic Photomechanics Laboratory

Department of Mechanical Engineering and Applied Mechanics

University of Rhode Island, Kingston, RI 02881

ABSTRACT

An experimental investigation is conducted using dynamic photoelasticity and high speed photography to study the wave propagation due to blast loading in porous media as a function of fluid saturation. The porous media has been modelled as continuous solid containing particular arrays of holes or voids. The study has focused mainly on the effect of the porous structure on transient pulse propagation as well as the effect of the moisture in the pores on wave propagation. A series of experiments have been conducted using a sheet of Homalite 100 with different geometry of the periodic array of holes. A small amount of explosive is used to generate the stress wave. Dynamic photoelastic photographs are taken with the high speed camera as the wave propagates across the holes. These data are analyzed to obtain the wave velocity as well as the stress wave attenuation in the porous media.

INTRODUCTION

The problem of interaction of elastic waves with discontinuities or boundaries of complex shapes arises in situations where waves propagate through a medium having cavities, inclusions or cracks. Due to material inelasticity and inhomogeneity, the wave propagation in a discontinuous medium is much more involved than homogenous elastic wave propagation and it shows directional as well as frequency dependence. This phenomenon becomes significant for step loading pulses where the wavelength are of the order of the size of the discontinuities. Such problems denoted as scattering and diffraction problems have long standing interest in acoustics and electromagnetic wave theory.

Composite materials such as concrete, ceramics, etc. are characterized by the number of pores, voids or fluid filled cavities. The influence of these pores on the deformation and the failure of these materials has not been interpreted uniquely. Since areas of stress concentration may arise in the vicinity of these pores, it is believed that the pores may play a role in influencing the crack and wave propagation in these materials. Moreover, porous materials are used extensively for shock isolation as they are capable of absorbing large quantities of energy during impact loading. Hence the behavior of these materials under impulsive loading has been of substantial interest to engineers.

Wave propagation in a discontinuous media has also been of interest to the soil and rock mechanics community. The propagation of elastic waves in the earth's crust is most intimately related to the properties of soil and rock. The elastic properties of these substances are greatly affected by the amount of water contained in them, packing density, porosity, the size of the particles that form the substances, and the binding material which they contain. Current interest in geomechanics is focussed on the transient phenomena occurring in earthquakes, wave loading and consolidation. Moreover the increasing needs for urban and resource development demand faster, safer and more efficient procedures for underground excavations of rock. Most methods of rapid excavation in hard rock use some form of dynamic loading, such as explosive or water jet. This type of loading produces stress waves which induce crack initiation and propagation.

The initial attempts to study rock media and soil structure as arrays of elastic particles (eg. spheres and discs) were made by Iida (1,2), Takashashi and Sato (3), Gasmann (4) and Brandt (5). They investigated the propagation velocity as a function of confining pressure, particle size and aggregate geometry. The effect of water content in the pores on elastic velocity has been studied by several investigators. Oliphant (6) and Owen (7) found that slight additions of water caused a sharp drop in velocity with a slow decrease as the saturation approached 100 percent. Hughes and Jones (8) measured the dilation wave velocity of samples of very low porosity, less than 1%. Using the same apparatus and methods, Hughes and Cross (9) measured the velocity in Soienhofer Limestone (porosity 4%) and Caplen Dome Sandstone (porosity 5%) for dry and saturated samples.

A considerable amount of research is also under way in determining the internal structure of porous and granular media by various sounding techniques. For example, acoustic emission methods have been presented by Hardy (10), while Allison and Lama (11) have discussed a low amplitude vibration technique to predict rock structure.

Current research in wave propagation in such media has involved, for example, statistical theories by Varadan et al (12) or mixture theories by Junger (13). Analytical approaches are often limited as they cannot fully account for the material inhomogeneity, isotropy and defects. Most of the previous work focused on wave propagation phenomena in general without going into the details of relating specific microstructure to the associated wave motion.

This paper reports on an experimental study of wave propagation due to explosive loading in a porous medium. The porous medium was modelled as an array of holes machined in a continuous sheet of a brittle polyester material Homalite 100. The study looked at the wave propagation phenomenon from a microscopic point of view by going into the details of the geometric nature of the porous structure. The geometry of the pores was changed by varying the size of the holes, changing the pitch or the spacing between the holes and changing the geometric arrangement of the holes. In all the experiments the stress waves were produced by explosive loadings of short duration. Dynamic photoelasticity and high speed photography were employed to collect the time dependent data as the wave front moved rapidly through the porous structure.

EXPERIMENTAL PROCEDURE

To investigate the behavior of stress-waves in the periodically flawed half-plane, also referred to as the porous medium, a series of dynamic photoelastic experiments was conducted. The photoelastic models were fabricated from a large sheet of Homalite-100 having dimensions of 254mm x 305mm x 6.4mm. Homalite-100 is a birefringent brittle polyester material whose mechanical and optical properties are well characterized. The stress-strain behavior of this material is similar to that of rock. An array of holes having a pitch p and diameter d was machined to simulate the porous media.

Figure 1 shows the geometry of the porous model. Dynamic loading to produce the incident wave was achieved by detonating 80mg of lead azide directly on top of the model.

Two different arrangements of the holes were used as shown in Fig.2. The arrangement of holes in the first and second type of configurations are referred to as geometry A and B respectively. For geometry A three different pitches of 6.25mm, 12.7mm and 25.4mm were used. The diameter of the holes was increased in steps to achieve different porosities. Porosity is defined as:

$$\% \text{ porosity} = \frac{\pi [d/2]^2}{p^2} * 100$$

where d is the diameter and p is the pitch of the holes.

Due to the constraints in machinability of Homalite 100 and to avoid obscurity of the fringe pattern in the photographs, the porosity was limited to a maximum of 70%. Tables 1 and 2 list the pitch, the diameter of the holes and the corresponding porosity which were used with geometry A experiments.

For geometry B, two different pitches of 12.7mm and 25.4mm were used. Again, different diameter holes were used for each of these pitches to achieve different porosities. Table 3 shows the pitch, the diameters of the holes, and the corresponding porosity which were used with this geometry.

In the saturated porous media experiments, water was used as the saturation fluid. It was contained within the pores by sandwiching both sides of the photoelastic models by means of thin plexiglass sheets [14]. The sides of these sandwiched models were made leak proof by pressing them with pressure binders. Care was taken to minimize the number of air bubbles so as to achieve a high degree of saturation [15,16].

The wave propagation phenomenon due to explosive loading was studied using the technique of dynamic photoelasticity and high speed photography. The models were placed in the optical bench of the high speed multiple spark gap camera. The camera was triggered at a prescribed delay time after igniting the explosive. The high speed photographic system operates as a series of extremely short duration pulses of high intensity light and provides 20 photoelastic images at discrete time intervals during the dynamic event. These photographs of the wave propagation process at different stages of development provided the necessary data to obtain the velocity and attenuation of the

leading front of the longitudinal wave.

ANALYSIS

The sequence of 20 photographs obtained from the high speed camera were analyzed to obtain the compressional wave velocity and the stress wave attenuation in both the unsaturated and the saturated porous media. The compressional wave velocity was obtained by plotting the instantaneous position of the wavefront with respect to time. The gradient of this line gave the average compressional wave velocity. Figure 3 shows a typical position versus time plot. The portion of the curve between X and Y represents the region during which the stress wave was in the porous zone. The portion of the curve before point X and after point Y represent the regions before the stress wave entered the porous zone and after it emerged from it respectively.

The fringe patterns were further analyzed to determine the propagation and attenuation characteristics of the porous media. To obtain the attenuation characteristics, a plot of the maximum normalized fringe order around the hole versus the hole number (along the line $\Theta=0$) was obtained. The normalization was done with respect to the maximum fringe order on the first hole directly below the explosive charge. To separate the effects of material and geometric attenuation, an expression of the form

$$N_{\max} = \frac{N_0 e^{-ky}}{\sqrt{y}}$$

for the maximum fringe order was sought, where y is the distance from the loading source and k , the coefficient of material attenuation. The term $y^{-1/2}$ accounts for the geometric attenuation in two dimensional space (plate). The attenuation coefficient and the constant N_0 were obtained by plotting $N_{\max} y^{1/2}$ vs. y on a semilog scale. In order to compare the saturated and unsaturated porous media with the unflawed material the attenuation curves for all three were plotted together.

RESULTS AND DISCUSSION

The first series of experiments was conducted with geometry A and involved five models with pitch equal to 12.7mm. The diameter of the holes was increased in steps to achieve porosity ranging from zero to seventy percent. With the detonation of the explosive, longitudinal and shear waves were produced which travelled with velocities of 2140 m/s and 1220 m/s respectively in the plate. As the longitudinal wave passes over the first row of the array of holes the stresses around them start to build up. Since the diameter of the holes is much less than the radius of curvature of the approaching wave front the fringes tend to align themselves in a direction which is normal to the approaching wavefront as shown in Fig 4. As the wavefront impinges upon the hole boundary scattering and diffraction takes place and reflected longitudinal waves and shear waves are produced. The reflected waves interact with the propagating wave altering the semicircular nature of the wavefront. With the larger diameter holes, the ratio λ/d (where λ is the wavelength of the pulse and d the diameter of the holes) decreases resulting in an increased level of scattering and diffraction.

Figure 5 shows a typical set of photographs obtained during the wave propagation experiments. These dynamic isochromatic fringes show the development of the wavefront as the wave propagates through the porous medium. With continued reflection from each row of holes and the superposition of the reflected waves, the curvature of the leading dilatational wavefront keeps on decreasing as the wave moves further into the porous zone. This phenomenon increases for higher porosities. Figure 6 shows the location and the shape of the wavefront for a given porosity.

The dynamic photoelastic photographs were analyzed to get the leading wave velocity. Figure 7 shows the variation in wave velocity as a function of porosity. The dilatational wave velocity, measured in a direction directly below the charge (along the line $\theta=0$), is less than the dilatational wave velocity in an unflawed half-plane. The wave velocity decreases by almost 18% as the porosity is increased from 0 to 20%. As the porosity is increased further, the drop in velocity is small until the 50% porosity mark is passed, after which wave velocity decreases sharply and drops down to almost 60% of its value for the unflawed half-plane.

The dilatational wave velocity also shows directional dependence and tends to decrease as the angle θ is increased. Figure 8 shows that the velocity at any angle

theta depends upon the diameter of the holes in the porous zone. For small diameter holes, little change in velocity can be seen as the angle theta is increased from 0-30%. But as the diameter of the holes is increased, the wave velocity drops noticeably and this drop increases as the angle theta is increased. Around Θ equal to 30° , there is a drop in velocity of 6% for the 9.6mm diameter holes, 10% for the 10.9 mm diameter hole and 16% for the 11.7mm holes. This dependence of the wave velocity in the porous zone on the angle theta is due to the fact that the wave sees a different kind of microstructure for different values of theta. This decrease in velocity also accounts for the decrease in the curvature of the wavefront mentioned earlier.

Effect of Pitch

A series of experiments was conducted to study the effect of pitch, or the spacing between the holes on the wave propagation phenomenon. Figure 9 shows typical photographs of the stress wave propagation in the porous medium for three different values of pitch. As the pitch is increased, the ratio of the number of holes to that of the wavelength of the stress wave decreases, resulting in reduced diffraction and scattering of the stress wave. The influence on the stress around the holes due to neighboring holes is also reduced.

Figure 10 shows the normalized wave velocity vertically below the explosive charge as a function of porosity for holes at three different pitches. For all three pitches, the wave velocity decreases as the porosity of the medium is increased. However, for a given porosity, the wave velocity increases as the pitch is increased. This behavior in stress wave velocity is also observed in other directions ($\Theta \neq 0$).

Effect of Geometry

To study the effect of microstructure or the arrangement of the pores on wave propagation characteristics, the arrangement of the holes in the porous media was changed from geometry A (cubic arrangement) to geometry B (hexagonal arrangement). Figure 11 shows typical isochromatic fringes obtained during wave propagation in geometry B. These fringes show more scattering and diffraction than obtained with geometry A. Figure 12 shows the wave velocity as a function of porosity vertically below the explosive charge

for geometry B. The velocity in geometry B decreases with porosity like it does in geometry A. The velocity increases as the pitch goes up for a given porosity. Although the velocity vertically below this explosive charge shows a similar trend in both geometries, the absolute value of velocity in geometry B is much lower than in geometry A. This comparison is shown in Fig. 13.

For geometry B, the stress wave velocity also shows directional dependence but here, unlike geometry A, the velocity increases as the angle is increased from 0-30°.

Figure 14 shows the normalized wave velocity as a function of angle Θ for a given pitch and varying porosities in geometry B. The velocity increases with Θ and, for Θ equal to 30°, this velocity almost approaches the velocity for geometry A at $\Theta=0^\circ$. A similar trend, but in the opposite direction, can be seen for geometry A where the stress wave velocity decreased with angle Θ and for $\Theta=30^\circ$ approached the wave velocity in geometry B at $\Theta=0^\circ$. This behavior can be explained by looking closely at the microstructure the wave sees as the angle Θ is increased in both geometries. Figure 15 shows a schematic of the microstructure the wave sees at an angle of 45° in geometries A and B. It is interesting to note that, at 45°, the pore arrangement in geometry B appears like geometry A at 0° and vice-versa. Changing the angle further from 45° to 90° causes the microstructure to go back to the one observed for $\Theta=0^\circ$.

Effect of Moisture in the Pores

A series of experiments was conducted with geometry A to study the effect of moisture in the pores on the wave propagation phenomenon. Figure 16 shows typical isochromatic fringes obtained when the stress wave propagates in porous media. These photographs were analyzed to study both the wave velocity as well as the stress wave attenuation. Figure 17 shows the normalized wave velocity as a function of the porosity for three different pitch arrangements. The trend in velocity is very similar to the one obtained for unsaturated media. However the velocities in the saturated media are much lower than those for unsaturated media as shown in Fig. 18. For small porosities ($\eta \leq 20\%$) the amount of moisture per unit volume is very small and therefore there is no difference in velocities. As the porosity is increased beyond 20% the velocity shows a much more rapid drop in a saturated media than an unsaturated one. This can be

explained to some extent by the fact that the composite density for the porous media with water is higher than that of a porous media with air in the holes. These results are in agreement with those obtained by others [1,2,7,9] for saturated soils.

Attenuation of the Stress Waves

The compressive wave front attenuates rapidly as the stress wave propagates through the porous media. As in the case of the stress wave velocity, the attenuation of the stress wave depends strongly on the microstructure of the porous media. Larger the size of the holes, the higher is the porosity and greater is the attenuation of the stress wave. Moreover, the wave shows a higher attenuation as the pitch or the spacing between the holes is reduced. The geometry or the configuration of the holes also effects the attenuation characteristics and there is higher attenuation for Geometry "B" than for Geometry "A". This is to be expected since the stress wave undergoes much more scattering and diffraction when it propagates through the porous media with Geometry "B" than it does in Geometry "A".

Figure 19 shows the isochromatic fringe pattern showing the circumferential fringe distribution around the periphery of the holes for two different hole diameters. To obtain the attenuation characteristics, a plot of the maximum normalized fringe order vs. the hole number (along the line $\theta=0$) was obtained. Figure 20 shows the plot of the attenuation curves for both the unsaturated and saturated porous media for Geometry "A" and pitch = 12.7mm. The attenuation curves are drawn for porosity of 11% and 20%. Figure 21 shows the attenuation curves for the case of unsaturated porous media with Geometry "B" and porosity equal to 20% and 46%, respectively. For the sake of comparison, the geometric attenuation in an unflawed halfplane is also drawn on the same plots.

To characterize the attenuation of the stress wave in the porous media and to separate the geometric damping from the material damping, $N_{max}y^{-1/2}$ was plotted as a function of y on a semilog scale as shown in Figs 23 & 24. These plots were analyzed to calculate the attenuation coefficients which are shown in Table 4. These values give us an idea of the attenuation characteristics of the porous material. Higher values of "K" indicate higher attenuation of the stress wave in that material.

CLOSURE

Dynamic photoelasticity along with high speed photography were used to study wave propagation in porous media. Plate specimens were fabricated from Homalite-100 and an array of holes, having a specific geometry, were machined in them to simulate the porous media. The specimens were loaded explosively on one edge and the resulting isochromatic fringe patterns were analyzed to obtain the compressional wave velocity and the stress wave attenuation in the porous material.

The stress wave speed dropped with increasing porosity. For a given porosity, the wave speed is lower for smaller pitch in both the geometries. The wave-velocity also showed strong dependence on the microstructure of the porous media. Geometry B showed a larger drop in velocity than Geometry A for the same porosities. Due to the point loading and the geometry of the porous models, the stress wave exhibits directional dependence as it sees a different kind of microstructure as a function of the angle theta.

The stress wave shows appreciable attenuation in the porous media. The attenuation observed was separated into its geometric and material components. The coefficients for the material attenuation were calculated for different porous medias and are summarized in Table 4. From the table it can be seen that the attenuation constants are higher for the case of porous media with a higher porosity and they decrease for the porous media with a larger pitch but having the same porosity. Moreover the attenuation constants are higher for the configuration of the holes in geometry B than in geometry A.

The wave propagation characteristics also depend on whether the porous medium is nearly saturated or unsaturated. Nearly saturated porous media show a larger drop in wave velocity than the unsaturated media. Moreover the stress wave attenuation is much higher in a nearly saturated medium than an unsaturated one.

ACKNOWLEDGEMENT - The authors would like to acknowledge the support of the Army Research Office under grant No. DAA L03-86-K-0125.

REFERENCES

1. Iida, K., "Velocity of Elastic Waves in Sand," Bulletin Earthquake Research Institute, Japan, Vol. 17, 1939, pp. 783-807.

2. Iida, K., "Velocity of Elastic Waves in Sand," Bulletin Earthquake Research Institute, Japan, Vol.27, 1949, pp. 11-16.
3. Takahashi, T. Sato, Y., "On the Theory of Elastic Waves in Granular Substance." Bulletin Research Institute, Japan, Vol. 27, 1949, pp. 11-16.
4. Gassman, F., "Elastic Waves through a Packing of Spheres." Geophysics, Vol. 16, 1951, pp. 673-685.
5. Brandt, H., "A Study of the speed of sound in Porous Granular Media." Journal of Applied Mechanics, Vol. 22, 1955, pp. 479-486
6. Oliphant, E., "Comparison of Field and Laboratory Measurements of Seismic Velocities in Sedimentary Rocks." Bulletin G.S.A., 61, 1950, pp. 759-788.
7. Owen, J.E., "Effect of Moisture upon Velocity of Elastic Waves in Amherst Sandstone." Bulletin of A.A.P.G. 19, 1935, pp. 9-18.
8. Hughes, O.S., and Jones, H.J., "Variation of the Elastic Moduli of Igneous Rocks with pressure and Temperature." Bulletin of G.S.A., 61, 150, pp. 843-856.
9. Hughes, O.S. and Cross, J.H., "Elastic Wave Velocities at High Pressures and Temperatures." Geophysics, 16, 1951, pp. 577-593.
10. Hardy, H.R., "Emergence of Acoustics Emission Micro-Seismic Activity as a Tool in Geomechanics." Proceedings of First Conference on Acoustic Emission Microseismic Activity on Geologic Materials, University Park, PA., USA, 1975.
11. Allison, H. and Lama, R.D., "Low Frequency Sounding Technique for Predicting Progressive Failure of Rock." Rock Mechanics, Vol. 12, 1979, pp.79-97.
12. Varadan, V.K., Varadan, V.V. and Ma, Y., "Propagation and Scattering of Elastic Waves in Discrete Random Media." Proc. of 20th Annual Meeting of SES, Univ. of Delaware, 1983.
13. Junger, M.C., "Dilatational Waves in an Elastic Solid Containing Lined, Gas Filled, Spherical Cavities." Journal of Acoustic, al Society of America, Vol. 69, 1981, pp. 1573-76.
14. Streeter, V.L. and Wylie, E.B., Hydraulic Transients, McGraw Hill, N.Y., 1967.
15. Richant, F.E., Hall, J.R. and Woods, R.D., Vibrations of Soils and Foundations, Prentice Hall, 1970, pp. 129-136.
16. Allen, N.F., Richard, R.E. and Woods, R.D., "Fluid Wave Propagation in Saturated and Nearly Saturated Sands", J. of Geotechnical Engineering, ASCE. Vol. 106, No. GT3, pp. 235-254, 1980 .

List of Figures

- Fig. 1. Geometry of the photoelastic model.
- Fig. 2. Geometry of the periodic array of the holes.
- Fig. 3. Position of the half order fringe as a function of time.
- Fig. 4. Interaction of stress waves with holes.
- Fig. 5. Isochromatic fringes showing wave propagation in a porous media.
- Fig. 6. Instantaneous position and shape of the leading half order fringe.
- Fig. 7. Normalized wave velocity for different porosities.
- Fig. 8. Influence of theta on normalized wave velocities.
- Fig. 9. Fringe pattern showing stress wave interaction with holes for three pitches.
- Fig. 10. Normalized wave velocity as a function of porosity for three different pitches.
- Fig. 11. Isochromatic fringe patterns for wave propagation in a porous media having geometry B.
- Fig. 12. Influence of porosity on normalized wave velocity for geometry B.
- Fig. 13. Comparison of the wave velocity in geometries A and B at different porosities.
- Fig. 14. Dependence of normalized wave velocity on angle Θ in geometry B.
- Fig. 15. Two configurations of holes correspond to two microstructures.
- Fig. 16. Fringe pattern showing wave propagation in a saturated porous media.
- Fig. 17. Changes of normalized wave velocity with porosity for saturated media.
- Fig. 18. Changes of normalized wave velocity with porosity for saturated and unsaturated porous media.
- Fig. 19. Photograph showing isochromatic fringes around the periphery of the holes.
- Fig. 20. Change in normalized fringe order as the wave travels through saturated and

unsaturated porous media of geometry A.

Fig. 21. Change in normalized fringe order as the wave travels through unsaturated porous media of geometry B.

Fig. 22. Semi-log plot to evaluate attenuation coefficient in geometry A.

Fig. 23. Semi-log plot to evaluate attenuation coefficient in geometry B.

TABLE 1

GEOMETRY A (UNSATURATED)

No.	PITCH (mm)	DIA. (mm)	POROSITY
1	6.4	3.2	20%
2	6.4	4.8	44%
3	6.4	5.6	60%
4	12.7	6.8	70%
5	12.7	3.2	05%
6	12.7	6.3	20%
7	12.7	9.5	46%
8	12.7	11.1	60%
9	12.7	11.9	70%
10	25.4	9.5	11%
11	25.4	12.7	20%
12	25.4	19.8	48%
13	25.4	23.8	70%

TABLE 2

GEOMETRY A (SATURATED)

S. No.	PITCH (mm)	DIA. (mm)	POROSITY
1	6.3	3.2	20%
2	6.3	4.8	44%
3	6.3	5.6	60%
4	6.3	6.0	70%
5	12.7	6.8	22%
6	12.7	9.5	46%
7	12.7	10.5	54%
8	12.7	11.9	70%
9	25.4	9.5	11%
10	25.4	12.7	20%
11	25.4	19.8	48%
12	25.4	23.8	70%

TABLE 3

GEOMETRY B (UNSATURATED)

No.	PITCH (mm)	DIA. (mm)	POROSITY
1	12.7	6.3	20%
2	12.7	9.5	46%
3	12.7	11.1	60%
4	12.7	11.9	70%
5	25.4	9.5	11%
6	25.4	12.7	20%
7	25.4	19.8	48%
8	25.4	23.8	70%

TABLE 4

GEOMETRY	PITCH (mm)	SATURATED OR UNSATURATED	POROSITY	ATTENUATION COEFFICIENT K (mm ⁻¹)
A	25.4	UNSATURATED	11%	0.007
A	25.4	UNSATURATED	20%	0.014
A	25.4	SATURATED	11%	0.028
A	25.4	SATURATED	20%	0.038
A	12.7	UNSATURATED	11%	0.070
A	12.7	UNSATURATED	20%	0.107
A	12.7	SATURATED	11%	0.088
A	12.7	SATURATED	20%	0.134
B	25.4	UNSATURATED	11%	0.022
B	25.4	UNSATURATED	20%	0.040
B	12.7	UNSATURATED	20%	0.078
B	12.7	UNSATURATED	46%	0.130

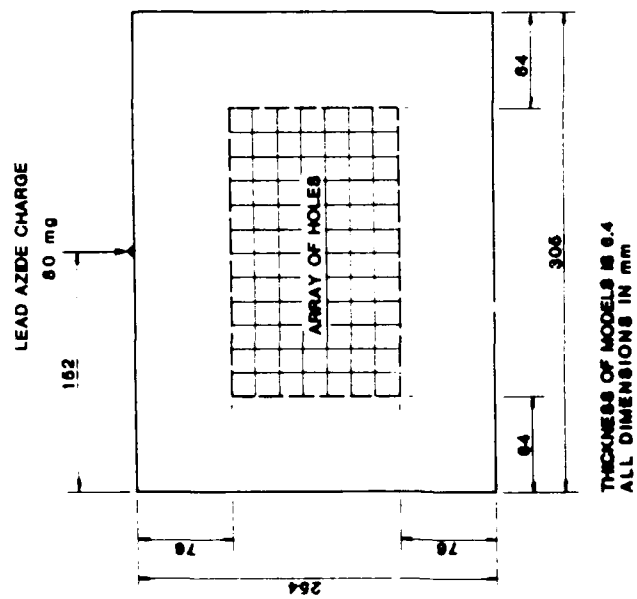


Fig. 1. Geometry of the photoelastic model.

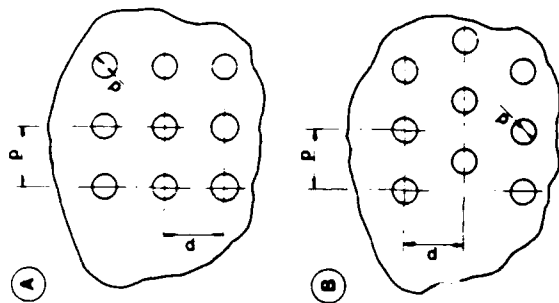


Fig. 2. Geometry of the periodic array of the holes.

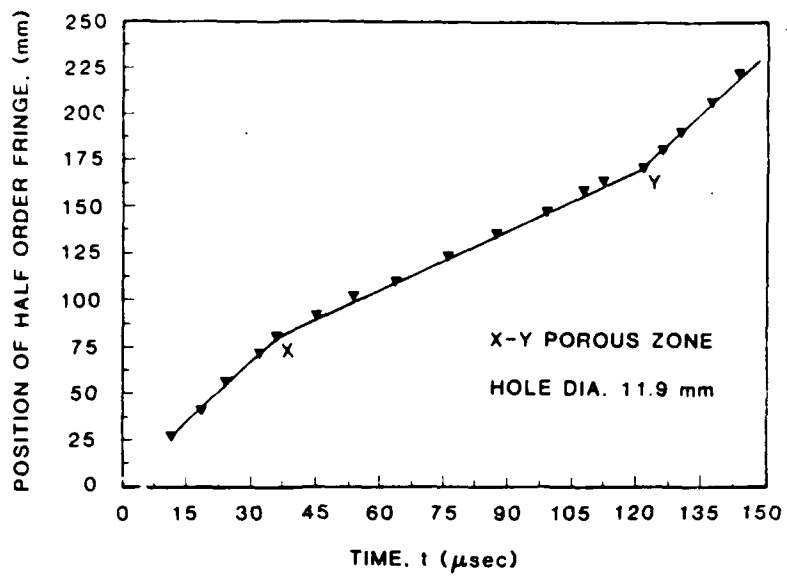


Fig. 3. Position of the half order fringe as a function of time.

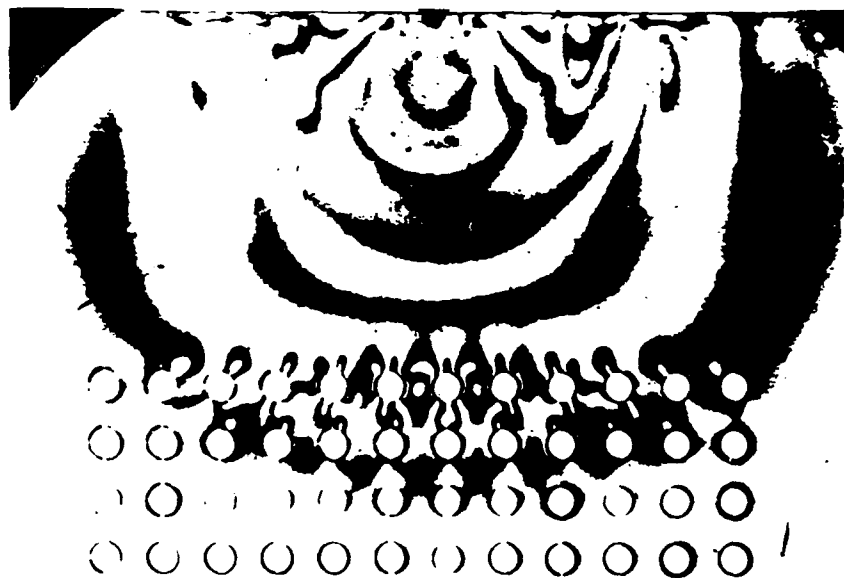
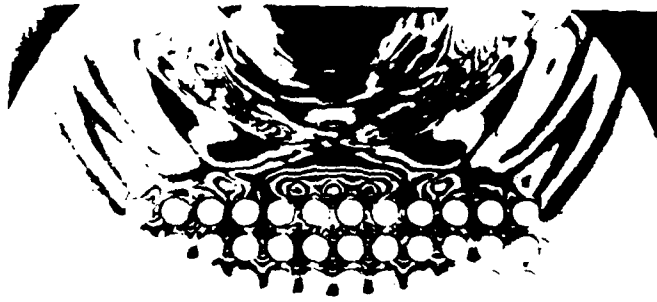
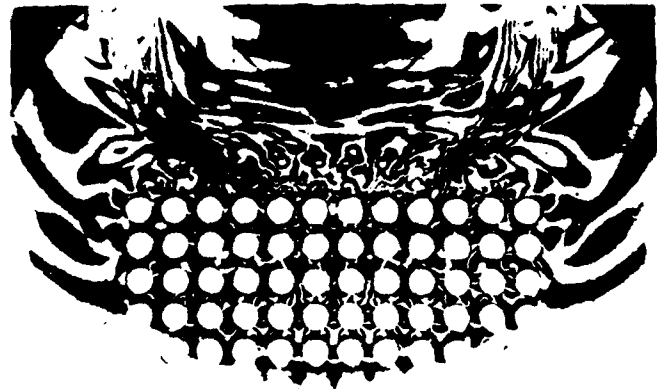


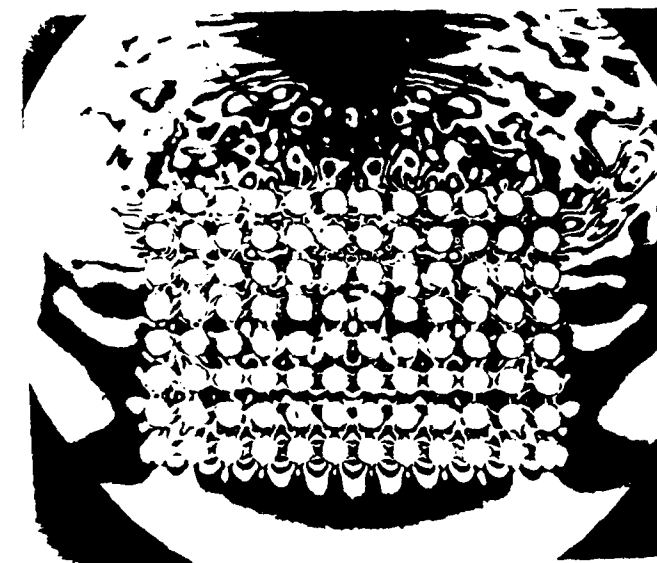
Fig. 4. Interaction of stress waves with holes.



FRAME 7 , $t = 52.0\mu\text{s}$



FRAME 10 , $t = 69.5\mu\text{s}$



FRAME 15 , $t = 106.0\mu\text{s}$

Fig. 5. Isochromatic fringes showing wave propagation in a porous media.

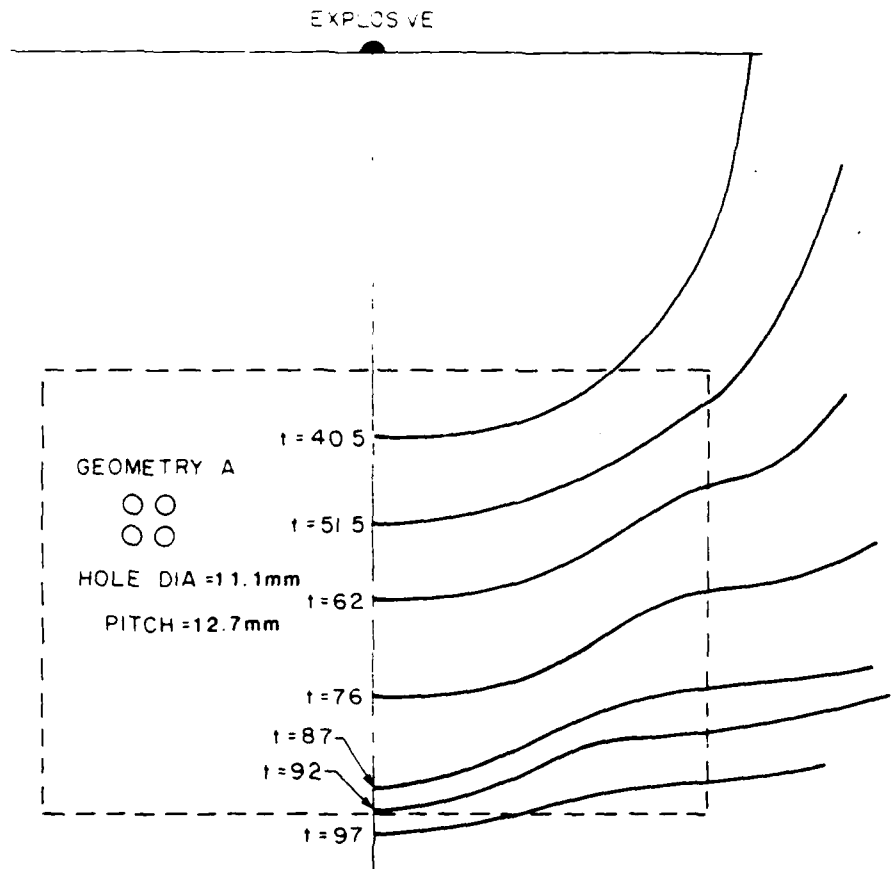


Fig. 6. Instantaneous position and shape of the leading half order fringe.

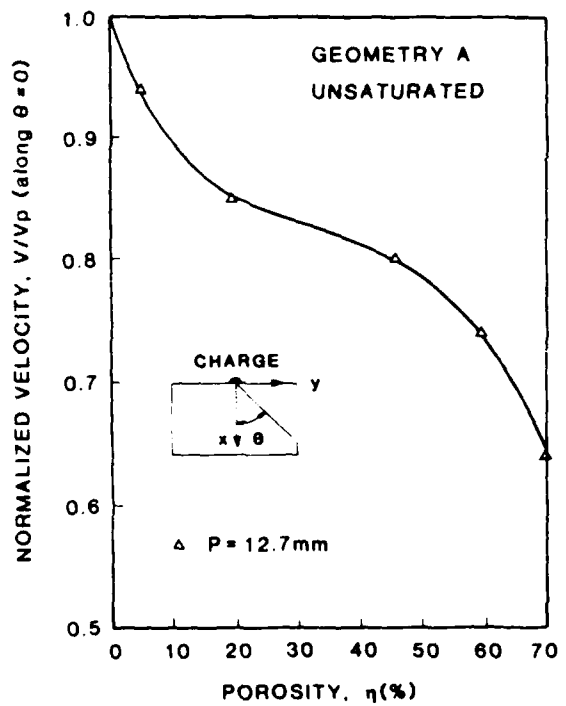


Fig. 7. Normalized wave velocity for different porosities.

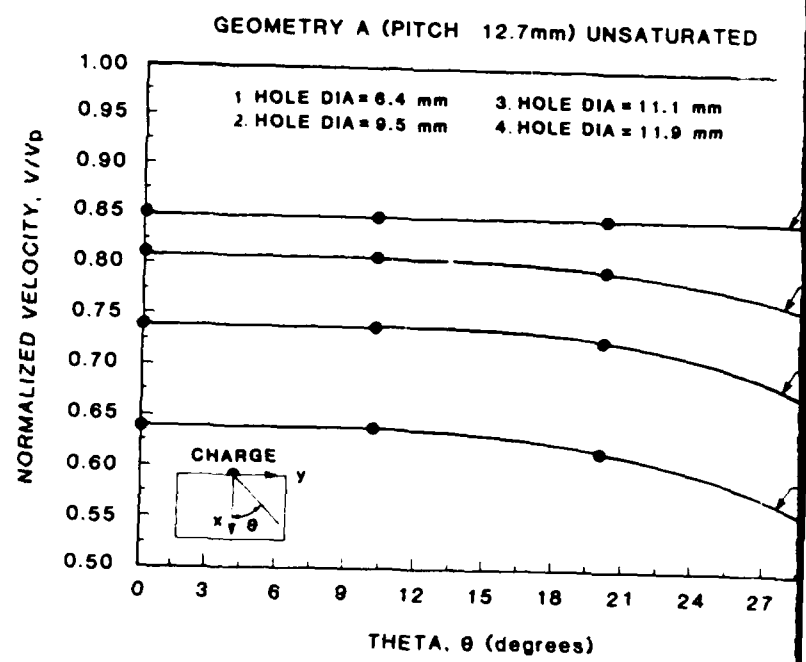
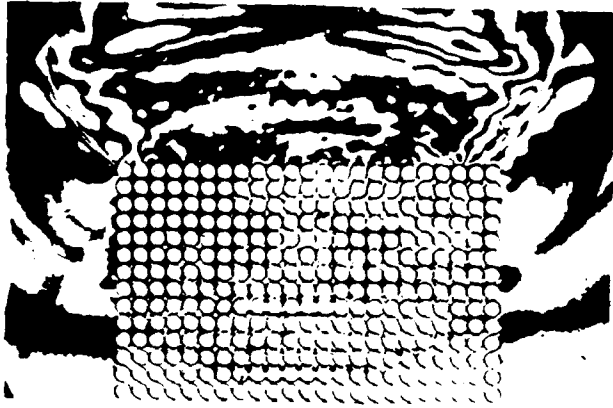
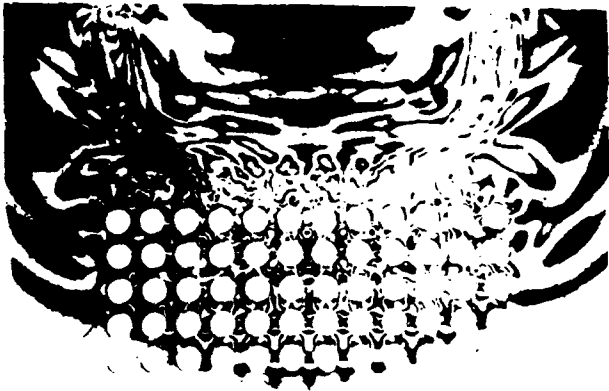


Fig. 8. Influence of theta on normalized wave velocities.



PITCH = 6.4 mm



PITCH = 12.7 mm



PITCH = 25.4 mm

Fig. 9. Fringe pattern showing stress wave interaction with holes for three pitches.

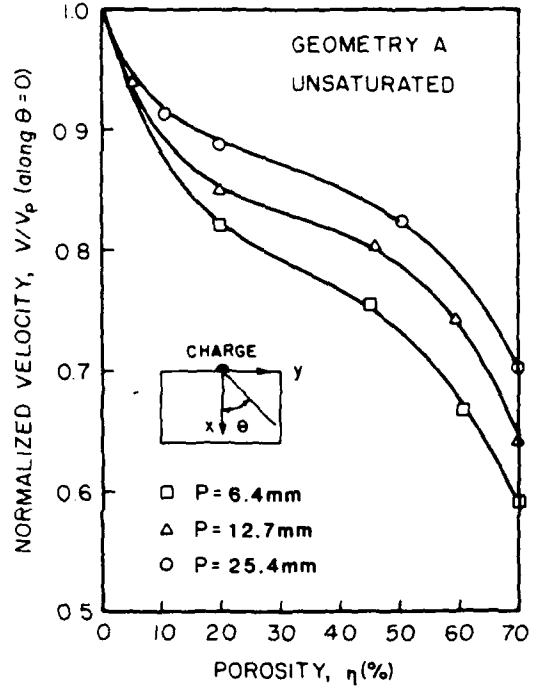


Fig. 10. Normalized wave velocity as a function of porosity for three different pitches.

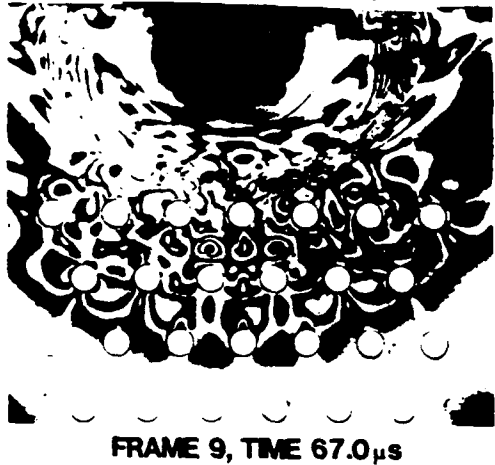
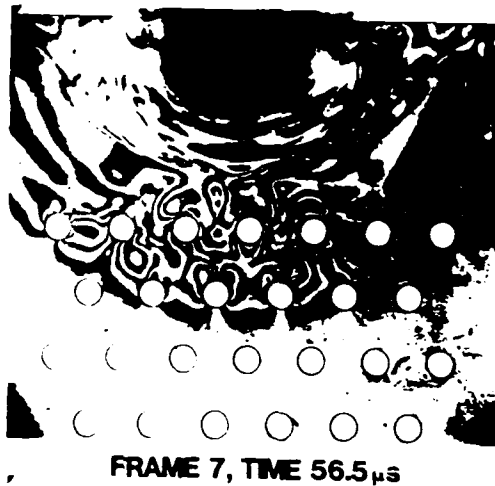


Fig. 11. Isochromatic fringe patterns for wave propagation in a porous media having geometry B.

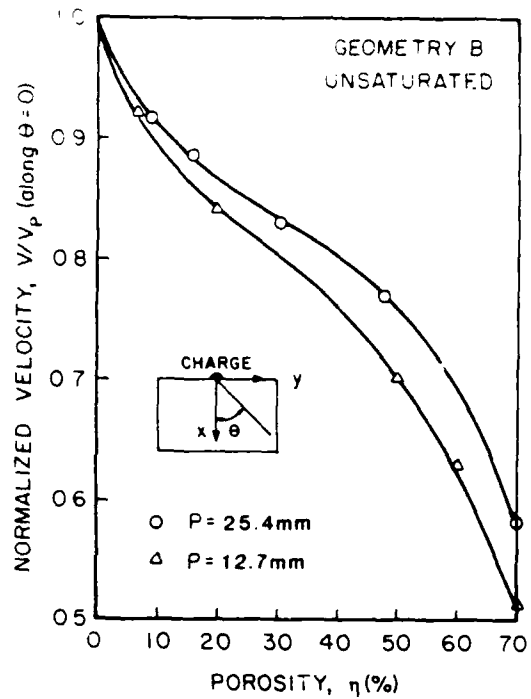


Fig. 12. Influence of porosity on normal wave velocity for geometry B.

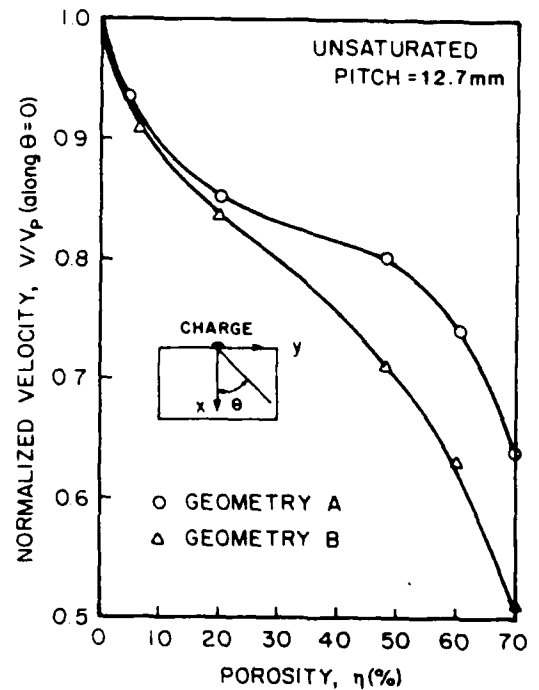


Fig. 13. Comparison of the wave velocity in geometries A and B at different porosities.

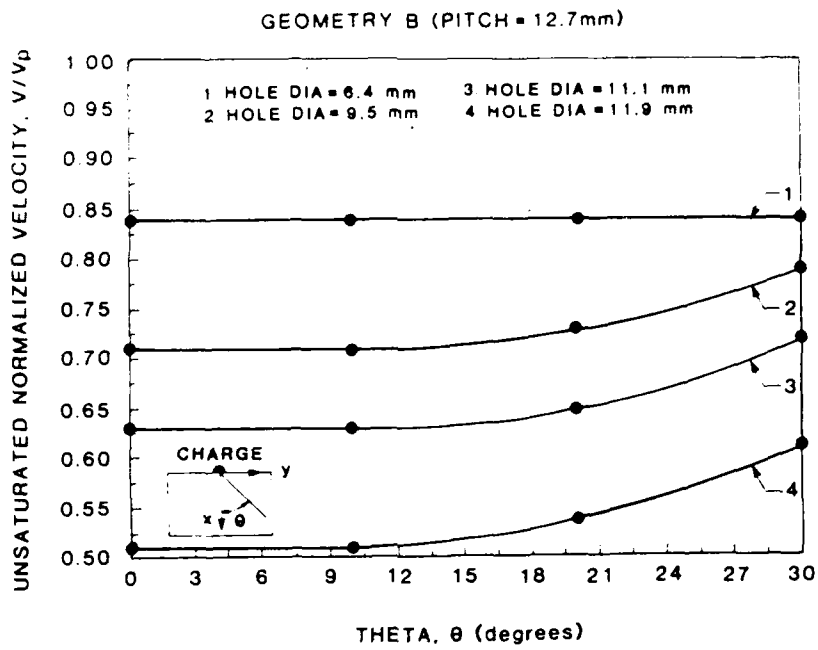


Fig. 14. Dependence of normalized wave velocity on angle θ in geometry B.

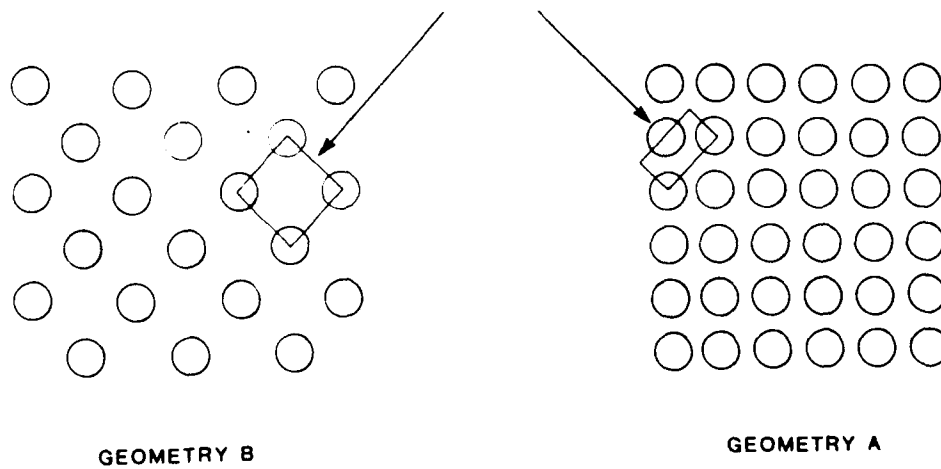
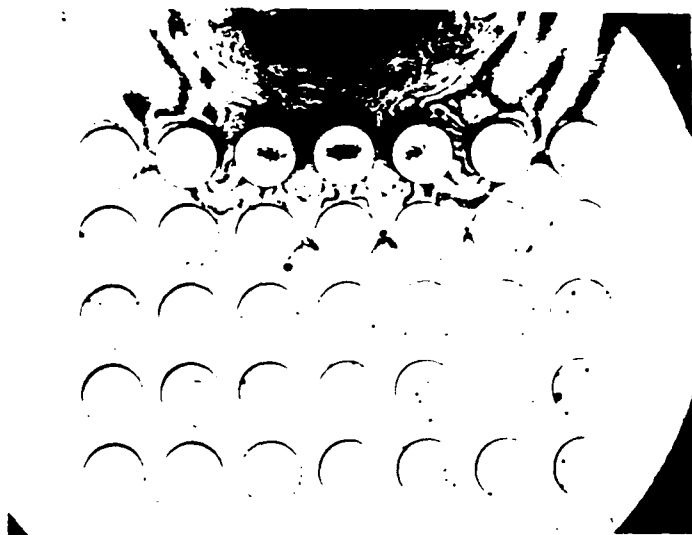
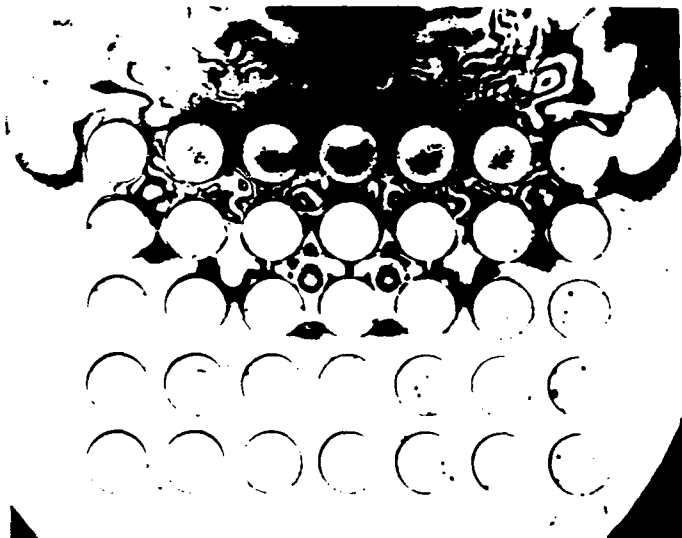


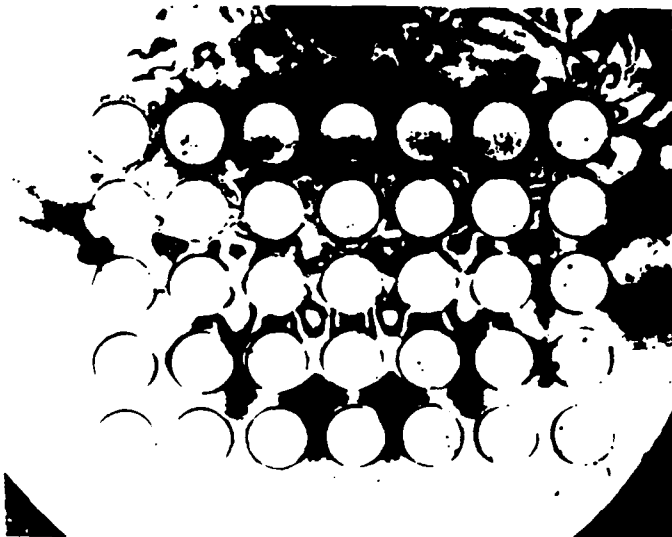
Fig. 15. Two configurations of holes correspond to two microstructures.



FRAME 7, TIME 49.5 μ s



FRAME 10, TIME 63.0 μ s



FRAME 14, TIME 91.5 μ s

Fig. 16. Fringe pattern showing wave propagation in a saturated porous media.

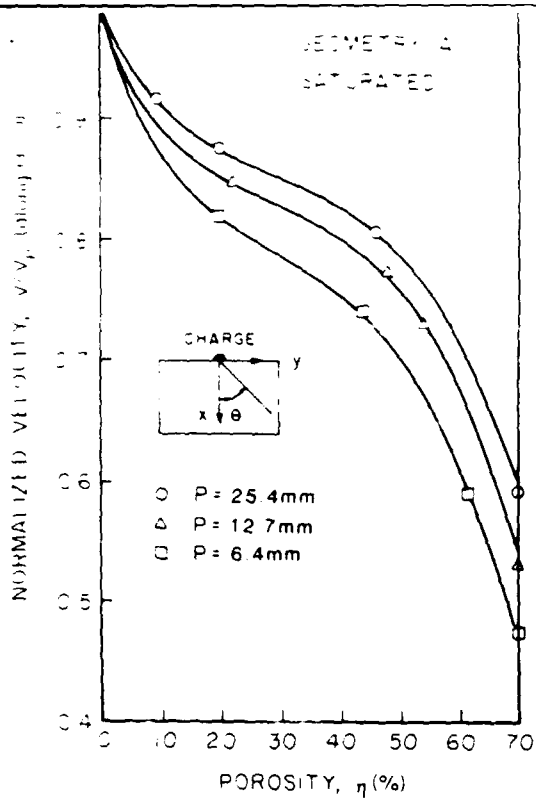


Fig. 17. Changes of normalized wave velocity with porosity for saturated media.

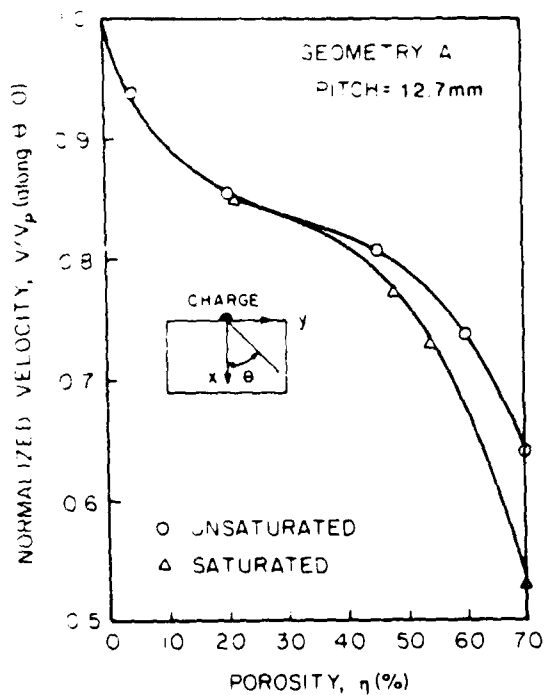


Fig. 18. Changes of normalized wave velocity with porosity for saturated and unsaturated porous media.

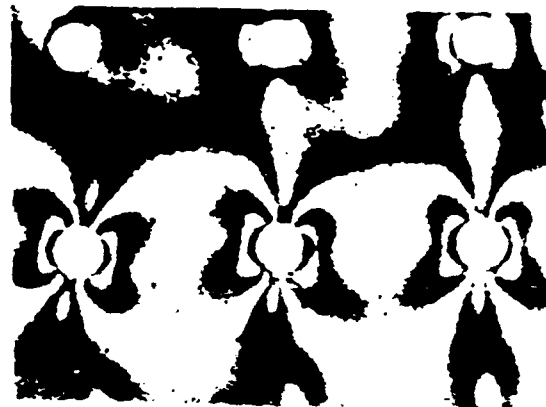


Fig. 19. Photograph showing isochromatic fringes around the periphery of the holes.

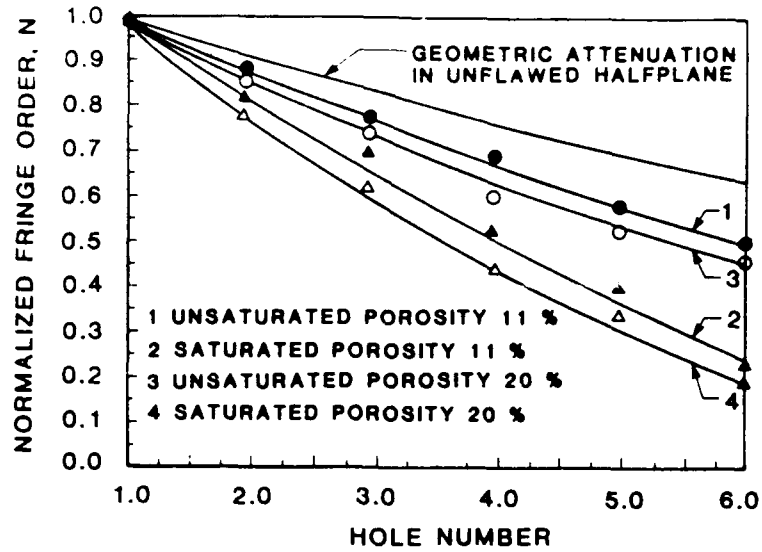


Fig. 20. Change in normalized fringe order as the wave travels through saturated and unsaturated porous media of geometry A.

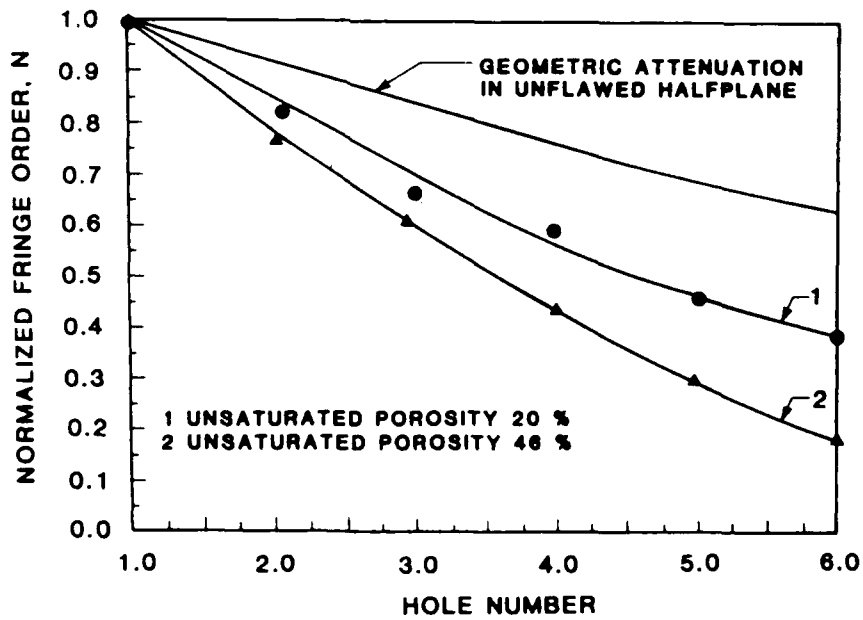


Fig. 21. Change in normalized fringe order as the wave travels through unsaturated porous media of geometry B.

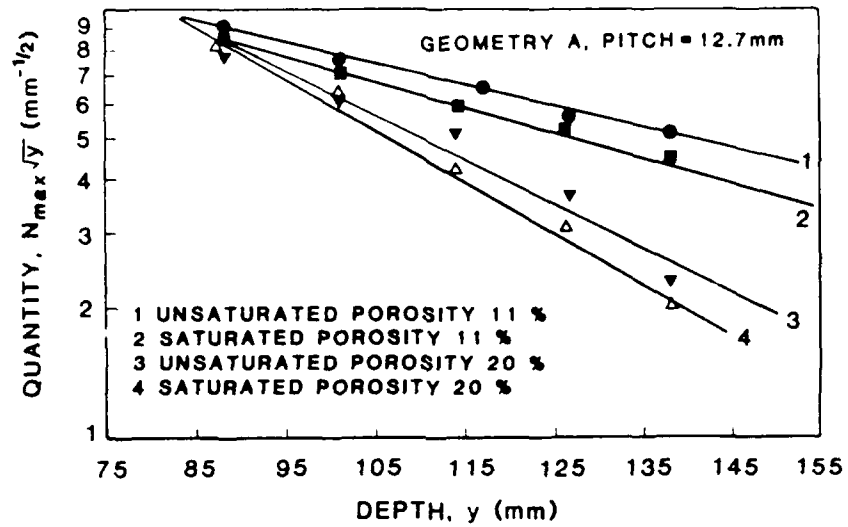


Fig. 22. Semi-log plot to evaluate attenuation coefficient in geometry A.

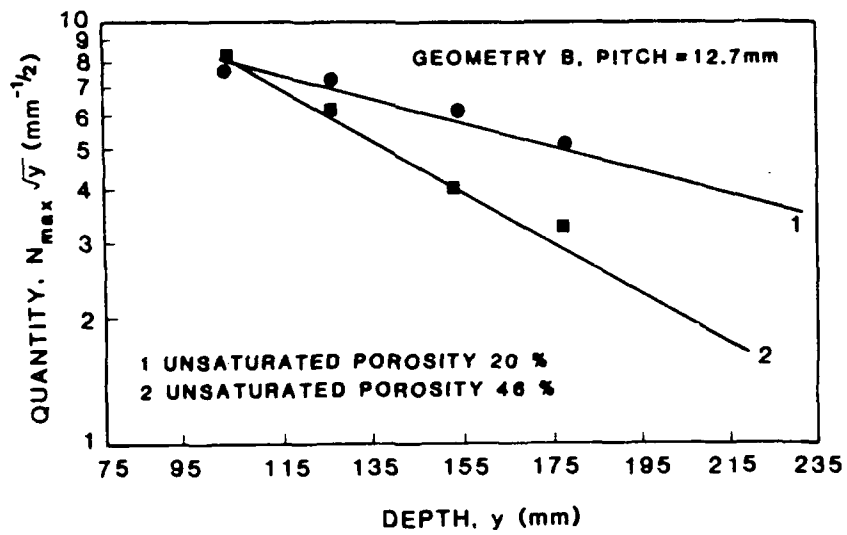


Fig. 23. Semi-log plot to evaluate attenuation coefficient in geometry B.

DYNAMIC PHOTOELASTIC INVESTIGATION OF WAVE PROPAGATION AND ENERGY TRANSFER ACROSS CONTACTS

A. SHUKLA *Department of Mechanical Engineering and Applied Mechanics, University of Rhode Island, Kingston, USA*

H. P. ROSSMANITH *Institute of Mechanics, Technical University, Vienna, Austria*

This paper deals with the dynamic contact of an explosively excited disc with another disc or a half-plane. Dynamic photoelastic recordings show the development of the time-dependent contact area and the formation of the highly complex diffraction pattern.

1 INTRODUCTION

The dynamic contact between elastic bodies and the transfer of momentum and energy across the contact area is fundamental to studies of dynamic load transfer in granular or particulate media. When a body made up of a large number of cohesionless particles is impacted upon with a punch or an explosive, transient dynamic load transfer paths develop which differ from those established during static loading. This difference occurs because, in dynamic loading, inertia effects play an important role. Most of the research to date in contact mechanics pertains either to static studies or when dynamic impact is considered; first order discretized lump mass models are employed. The dynamics and mechanics of physical impact between solid bodies up to the late 1960s is covered in references (1)–(4)†. Generally in these studies the impacting body is considered rigid and stress wave effects in the indenter are not taken into account. Also, in collision problems, the bodies are treated as particles and, again, wave propagation processes occurring within the body are not taken into account. Recently studies by Comninou *et al.* (5)(6) have focussed on the transmission of wave motion between two solids. In these theoretical studies plane waves are considered passing from one half plane to another. Several initial conditions are looked at, including an initial gap and also friction at the interface. A recent experimental study of dynamic load transfer in a granular media was done by Rossmannith and Shukla (7) where load transfer paths in both systematic and random aggregates of disc assemblies were recorded using dynamic photoelasticity.

This paper addresses the problem of formation of dynamic contacts between two solids. The experimental technique of dynamic photoelasticity is utilized to visualize the formation of contact and wave scattering between the bodies.

2 EXPERIMENTAL PROCEDURE

The experimental method utilized in this study was dynamic photoelasticity along with high speed photography. Dynamic photoelasticity provides global field data during the dynamic contact, such as the change of the state of stress in the vicinity of the contact region and in the bulk of the contacting solids, as a function of time and space.

In order to understand the physics of dynamic contact between two elastic solids a series of four controlled experiments was performed, where an explosively loaded disc was in contact with another disc or a half-plane and the explosive excitation was located either at the centre of the disc or at the rim. Figure 1 shows the photoelastic model and explosive arrangement and Table 1 lists the characteristics of the dynamic loading.

The circular discs of radius $R = 76.2$ mm and the half-plane were fabricated from a 6.35 mm thick sheet of Homalite 100 which is a commercially available clear transparent polyester. This photoelastic material becomes temporarily birefringent when subjected to a state of stress and gives rise to optical interference fringes when viewed in a circular polariscope. These fringes are known as isochromatics and represent lines along which the difference of the principal normal stresses is constant (8)(9).

Dynamic loading was achieved by means of small charges of 150 mg PETN (experiments Nos 1 and 2) or of 100 mg lead azide (PbN_6) (experiments Nos 3 and 4). The explosive excitation source is located at the centre, A, of the disc in experiments Nos 1 and 2 and at the top, B, in experiments Nos 3 and 4. In the experiments with a

Table 1. List of experiments of dynamic contact

Experiment number	Configuration	Location of charge	Charge
No. 1	Disc/half-plane	Centre	150 mg PETN
No. 2	Disc/disc	Centre	150 mg PETN
No. 3	Disc/disc	Top	100 mg PbN_6
No. 4	Disc/half-plane	Top	100 mg PbN_6

The MS. of this paper was received at the Institution on 9 September 1985 and accepted for publication on 13 May 1986

† References are given in the Appendix

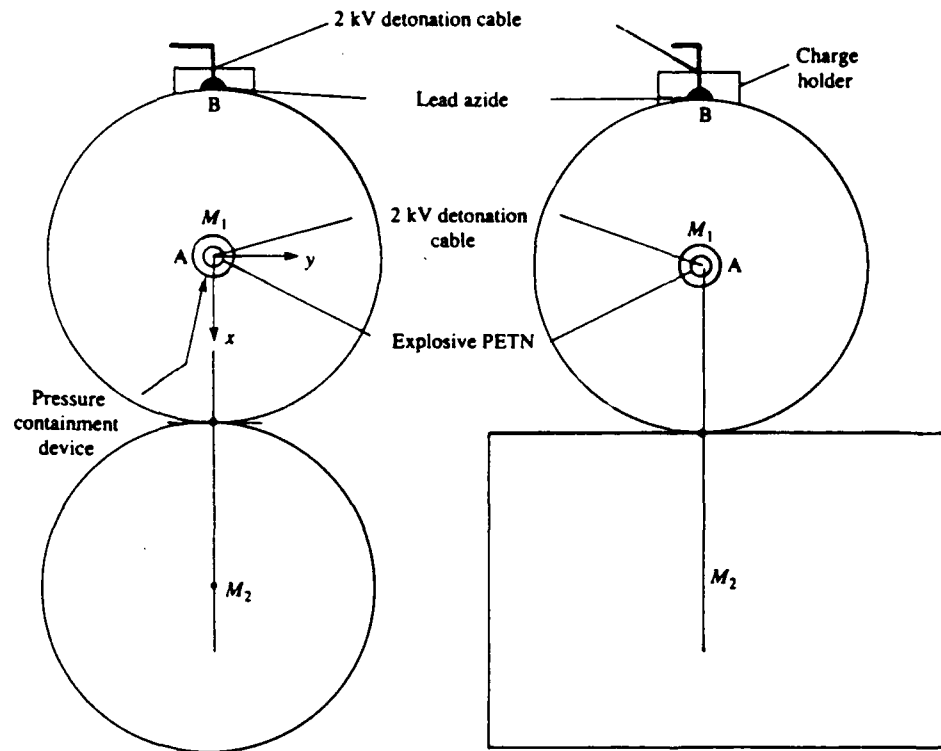


Fig. 1. Photoelastic model and dynamic loading arrangement

centre charge, a specially developed pressure containment device was utilized to prevent the field of view from being obscured by the rapidly expanding cloud of combustion gas products.

For photoelastic fringe pattern recording, a multiple spark gap camera of the Cranz-Schardin type was used. The system and its use in dynamic photoelasticity have been documented frequently in the literature, see, e.g., (9). The experimental outcome is a record of a time-controlled sequence of 20 images of the spatial configuration of the dynamic process at discrete times. Thus, a sequence of 20 ultra-short flash photographs are obtained that show individual stages of the evolution of the wave interaction process. In these wave propagation experiments the camera was operated at 200 000 frames per second and provided an observation period of 100 μ s with an additional initial delay of 25 μ s.

3 THEORETICAL CONSIDERATIONS

3.1 Size of dynamic contact area

Consider two discs of radii R_i ($i = 1, 2$) touching at a point $P_c(R_1, 0)$ as shown in Fig. 1. Let the centres of the discs be fixed at $M_1(0, 0)$ and $M_2(R_1 + R_2, 0)$. Upon detonation of a cylindrical explosive charge at the centre of disc No. 1 a circular crested detonation pulse radiates from M_1 . The displacements, u_r, u_z , and the stresses, $\sigma_{rr}, \sigma_{\theta\theta}$ vary according to Bessel functions. For 'large' values of r , the asymptotic expansions yield a plane wave approach. 'Large values' of r are attained within 4 to 5 zeroes of the Bessel function, and in the experiments this distance r corresponds to a few plate thicknesses b ($r \approx 8b$). Furthermore, any explosively induced pulse disturbance can be considered the result of the superposition of a set of harmonic waves.

The data reduction procedures for circular cylindrical

pressure waves as developed in (11) render relations between the strains, $\epsilon_r, \epsilon_\theta$, and stresses, σ_r, σ_θ , and the isochromatic fringe order distribution, N . In 2D dynamic photoelastic wave propagation experiments an r^{-1} attenuation as associated with an expanding spherical wave is commonly observed which is in marked contrast to the $r^{-1/2}$ attenuation of the amplitude for cylindrical waves as predicted by theory (12)(13). For wave positions far from the detonation centre a linear relationship between radial stress, σ_r , and radial particle velocity, v_r , (14), $\sigma_r = \rho c_1 v_r$, may be assumed to hold throughout the pulse. This 'far-field' approximation corresponds to a local replacement of the detonation wave by a plane wave with r^{-1} attenuation and is supported by experimental findings.

For contact investigations, the radial expansion of the edge of the explosively excited disc is of interest. Free radial expansion can occur along the circumference except in the region of contact. In Fig. 1, as disc No. 1 expands, the contact area increases in time. The dynamic contact problem is further complicated due to pulse diffraction at the edge of contact and transmission across the contact due to time dependent boundary conditions. The situation is illustrated in Fig. 2, where two different stages of contact area development during the passage of a half sine pulse are shown. In Fig. 2 the distance $A'A''$ of the intersection points of the two circles with radii $R_1 + u_r$ and R_2 is an upper limit for the extension of contact. For two discs the distance $A'A''$ is given by

$$A'A'' = 2a(t) = 2R_1 \sqrt{\left\{ \left(1 + \frac{u_r}{R_1} \right) - \epsilon^2 \right\}} \quad (1)$$

$$\epsilon = \left(\frac{R_1}{R_2} + \frac{u_r^2}{2R_1 R_2} + \frac{u_r}{R_2} + 1 \right) \left(1 + \frac{R_1}{R_2} \right)^{-1} \quad (2)$$

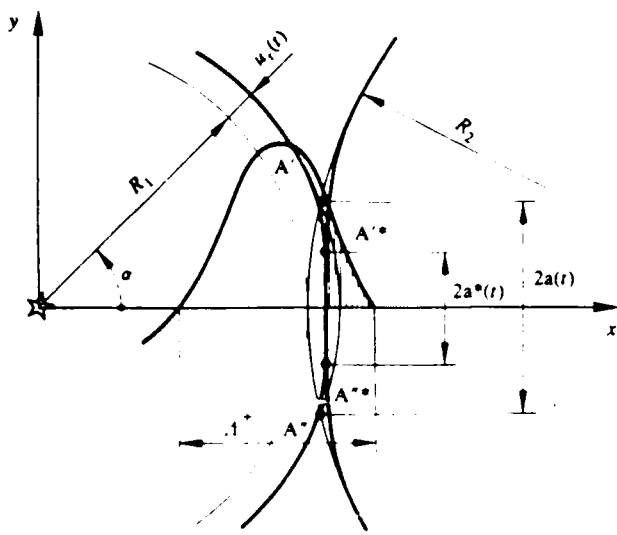


Fig. 2. Dynamic contact of two discs showing contact area development

which reduces to $\epsilon = 1$ for the disc - half plane experiments. Results for Homalite 100 with $c_1 = 2120$ m. sec. a half sine pulse length of $\Lambda_2 = 12.5$ mm and, of peak fringe order $N_{max} = 30$ for the disc-disc arrangement ($R_1 = R_2 = R = 76.2$ mm) and the half plane-disc arrangement ($R_1 = 76.2$ mm, $R_2 = \infty$), yield contact times of $12 \mu s$ and maximum upper bound for the contact area of $a/R \leq 0.007$ (disc-half plane) and $a/R \leq 0.005$ (disc-disc).

Time change of size of contact area depends primarily on the slope of the incident wave. Once contact is established for an elemental section of the circumference, energy is transferred to the receptor disc and the ratios of particle speeds of the respective waves involved in reflection and transmission across the contact area are the same as the ratios between the wave amplitudes. A typical wave front construction for the dynamic contact

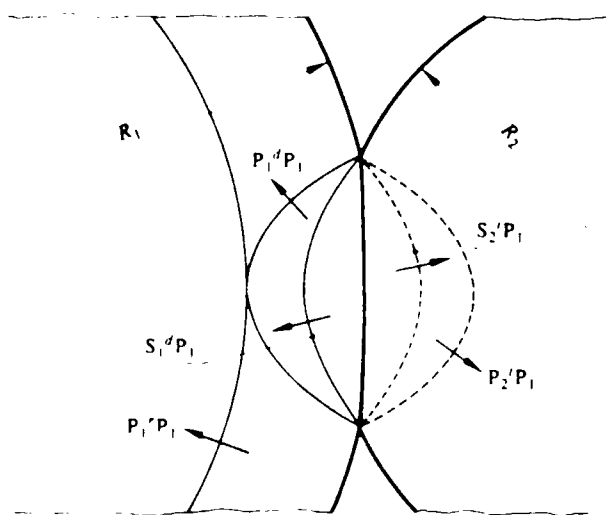


Fig. 3. Diffraction and reflection of an incident elastic P wave during formation of elastic contact ——— reflected waves, - - - - transmitted waves

is shown in Fig. 3. Time-dependent wave diffraction about the moving contact edge during increasing and receding contact (contact cycles) poses a challenging theoretical problem. An exact quantitative analytical treatment of this problem is not feasible to date. Numerical work for simulation of dynamic contact behavior is in progress.

4 EXPERIMENTAL RESULTS AND DISCUSSION

The results of the dynamic photoelastic experiments will be discussed here. For convenience the experiments with centre charge and the top charge will be discussed separately.

4.1 Dynamic contact experiments with centre charge

The first experiment refers to the disc-half plane geometry. An explosive charge of 150 mg of PETN was detonated at the centre of the disc. A sequence of three photographs obtained during the experiment are shown in Fig. 4. Upon detonation of the explosive charge a

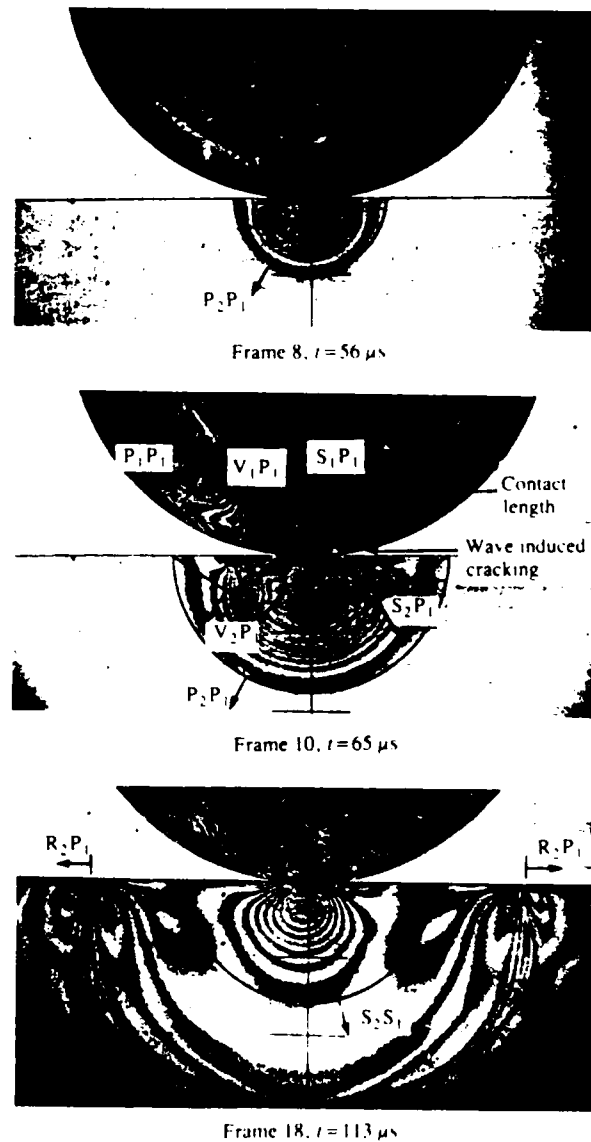


Fig. 4. Centre charge induced dynamic contact showing P wave interaction

cylindrical longitudinal (compressive) wave, P_1 , emerges and radiates from the centre of the disc. Due to cracking and breakdown of the borehole the rotational symmetry is disturbed and this gives rise to a P wave along with a random shear wave which quickly outdistances the emerging cracks. Hence, P and S waves are emitted from the detonation site and interact with the contact zone.

The first photograph, frame No. 8, taken at $t = 56 \mu\text{s}$ after detonation, shows the dynamic situation at a time shortly after initial contact is established. The expanding compressive incident P_1 wave has been reflected along the free sections of the boundary to yield a tensile P_1P_1 wave. Part of the energy and momentum of the wave has been transferred across the contact. The exact location of the front of diffracted transmitted P_2P_1 wave is difficult to locate (12); however, it is a common practice to identify the wave front with a line drawn just ahead of the $N = 1.2$ fringe. Although the contact area is obscured by a pseudocoustic, an estimate of the contact length was made. At time $t = 56 \mu\text{s}$ the contact length was approximately 15 mm.

In frame No. 10 of Fig. 4, taken at $t = 65 \mu\text{s}$, the reflected and transmitted longitudinal and shear pulses have separated and the resulting fringe pattern in the half plane is similar to the pattern that would be generated upon detonation of a concentrated charge at the centre of the contact zone. With increasing time after contact the fringe pattern in the half plane unfolds into a longitudinal wave P_2P_1 , a shear wave S_2P_1 , a von-Schmidt or head wave, V_2P_1 , and a Rayleigh surface-wave, R_2P_1 . The corresponding waves in the disc are labeled P_1P_1 , S_1P_1 , V_1P_1 , and R_1P_1 . Rayleigh-wave-induced cracking in the disc at a position adjacent to the end of the contact zone was observed in this experiment.

Progressive dynamic contact formation due to shear wave interaction with the contact is shown in the third photograph of Fig. 4, frame No. 18 taken at $t = 113 \mu\text{sec}$. The front of the S_2S_1 wave is located 43 mm below the half plane boundary and this matches well with the theoretical predictions. The R_2P_1 Rayleigh waves have completely separated from the other bulk waves and propagate with speed $c_R = 110 \text{ m/sec}$ along the free boundary. The increased number of fringes at the contact zone is indicative of increased contact stresses.

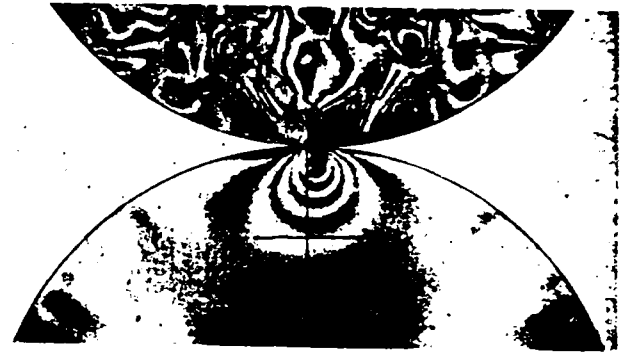


Frame 7, $t = 84 \mu\text{s}$

Fig. 5 Top charge induced dynamic contact showing P wave interaction



Frame 12, $t = 127 \mu\text{s}$



Frame 15, $t = 155 \mu\text{s}$



Frame 16, $t = 175 \mu\text{s}$

Fig. 6. Top charge induced dynamic contact showing S wave interaction

In a second experiment a disc assembly was used with the same centre charge. The results were qualitatively similar to the ones obtained in experiment No. 1.

4.2 Dynamic contact experiments with top charge

The third experiment was done with a disc-disc assembly. A charge of 100 mg of lead azide was exploded on the top edge of the first disc. This explosion generates P and S waves which propagate in the body of the disc and Rayleigh surface waves that travel along the circumference of the disc.

The P wave which travels with a velocity of $c_1 = 2120 \text{ m/sec}$ is the first wave to interact with the contact. This interaction is shown in Fig. 5.

Frame No. 7, taken at $t = 84 \mu\text{s}$ after detonation, shows the establishment of contact where part of the wave energy is already transferred across the contact. The contact area is proportional to the size of the pseudocoustic that forms at the contact zone (15). The contact

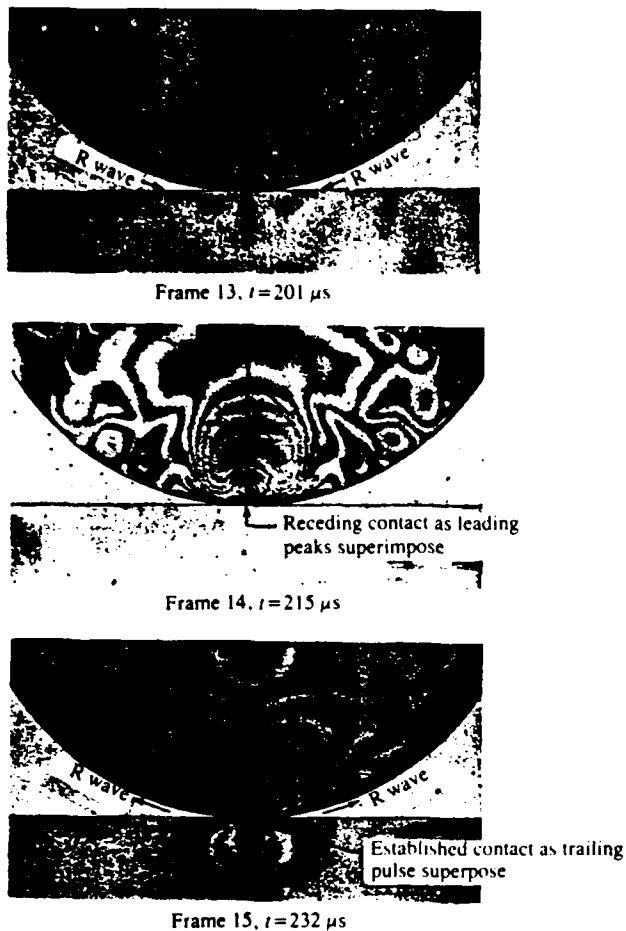


Fig. 7. Top charge induced dynamic contact showing R wave interaction

length in this frame is estimated to be approximately 1.5 mm. Diffraction and transmission of the incident P wave generates P and S waves in both discs and also gives rise to R waves that travel along the outer boundaries of the discs.

The sequence of photographic recordings, Fig. 6, shows the interaction of the incident S wave with the contact. Frame No. 12, taken at $t = 127 \mu\text{s}$, depicts the early stage of S wave diffraction about, and S wave transmission across, the contact surface. Due to the shearing nature of the wave the fringe pattern in the vicinity of the contact region is unsymmetrical. Moreover, the experimental recordings reveal that this fringe pattern oscillates about the normal to the contact plane. This effect can be seen in later frames. In frame No. 15 at $t = 155 \mu\text{s}$ the smallest visible fringe below the contact in the receptor disc is of order $N = 6$ as opposed to a maximum visible fringe order of $N = 3$ in frame No. 12. This increase is indicative of severe contact stresses. This is also evident from the increase of the size of the pseudocautics at the edges of the contact area. In frame No. 15 the contact length is about 2 mm. Frame No. 16 at $t = 175 \mu\text{s}$ shows the propagation of the $S_2 S_1$ wave and the $R_2 S_1$ Rayleigh wave generated by shear wave interaction. The Rayleigh wave interaction with the contact could not be studied in this experiment as the time duration of the experiment was not long enough.

The second experiment was performed with the disc - half plane assembly. The timings were adjusted so that R wave interaction with the contact could be observed. The interaction of the P and S wave with the contact were similar to the previous experiment. The R wave interaction is shown in the sequence of photographs in Fig. 7. Frame No. 13, taken at $t = 210 \mu\text{s}$, shows the R waves as they approach the contact region. Since the leading part of the R wave exerts circumferential tension, the contact area will recede due to radial contraction. This is shown in frame No. 14, taken at $t = 215 \mu\text{s}$, where the leading peaks of the R waves overlap and the contact has been lost. In frame No. 15, taken at $t = 232 \mu\text{s}$, the compressive trailing parts of the R waves superimpose and contact is re-established. Part of the energy of the R waves is transferred into the half plane, as can be seen from the fringe development in frame No. 15.

5 CONCLUSIONS

Dynamic photoelastic investigation of the interaction of elastic stress waves with contacts in solids provides full-field information of diffraction, reflection, and transmission processes as a function of time. Qualitative evaluation of dynamic isochromatic fringe patterns reveals that the individual wave types interact with the contact region in a distinctive way.

Incident P waves give rise to relatively strong transmitted and reflected P, S, and R waves. The intensity of the reflected R waves is high enough to initiate cracking on either side of the contact zone in the donor disc. This occurs due to the joint action of large tensile stresses at the surface in the leading part of the R wave and high friction in the contact area.

During S wave interaction with the contact comparatively little energy and momentum is transferred across the contact area. The interface shearing stress and shear deformations reverse sign during S wave interaction.

Very little energy and momentum are transferred into the receptor solid during the R wave interactions because of receding contact during the passage and superposition of the leading R pulse. Although contact is re-established during the passage of the trailing compressive R pulse, the normal component of displacement is very small and, consequently, little energy is transferred across the contact.

Further work on the quantitative evaluation of experimental fringe pattern recordings on the basis of the approximate wave analysis developed in the paper is in progress. Attention is focused on quantities of interest, such as distribution of contact stresses as a function of time and space, and amount of energy and momentum transferred across the contact area. The experimentally recorded patterns will serve as input for numerical simulation of dynamic contact behaviour. A hybrid experimental-numerical analysis of contact stress fringe pattern for a quasi static problem where the wave length is larger than the particle size has already been developed (16).

ACKNOWLEDGEMENT

The authors would like to acknowledge the support of NSF under Grant No. CEE 8314233 and Army Research Office under Grant No. DAAL03-86-K-0125.

APPENDIX

REFERENCES

- (1) HERTZ, M., 'Über die Berührung fester elastischer Körper', *Journal für die reine und angewandte Mathematik*, 1982, **92**, 156-171.
- (2) GLADWELL, G. M. L., *Contact problems in the classical theory of elasticity*, 1980 (Sijthoff and Noordhoff, The Netherlands).
- (3) GOLDSMITH, W., *Impact*, 1960 (Edward Arnold, London).
- (4) KINSLOW, R. (Editor), *High-velocity impact phenomena*, 1970 (Academic Press, New York).
- (5) COMNINOU, M., BARBER, J. R. and DUNDURS, J., 'Disturbance at a frictional interface caused by a plane elastic pulse', *J. appl. Mech.*, 1982, **49**, 361-365.
- (6) BARBER, J. R., COMNINOU, M. and DUNDURS, J., 'Contact transmission of wave motion between two solids with an initial gap', *Int. J. Solids Structures*, 1982, **18**, 775-781.
- (7) ROSSMANITH, H. P. and SHUKLA, A., 'Photoelastic investigation of dynamic load transfer in granular media', *Acta Mech.* 1982, **42**, 211-225.
- (8) DALLY, J. W., *Experimental stress analysis*, 2nd Edition, 1978 (McGraw-Hill, New York).
- (9) DALLY, J. W., 'Classical and advanced methods of photoelasticity', *The photoelastic effect and its applications*, 1973 (Ottignies, Belgium); 1975 (Springer, New York).
- (10) GRAFF, K. F., *Wave motion in elastic solids*, 1975 (Clarendon Press, Oxford).
- (11) DALLY, J. W., 'Data analysis in dynamic photoelasticity', *Expl. Mech.*, 1967, **7**, 332-338.
- (12) ROSSMANITH, H. P. and KNASMILLNER, R. E., 'The wave front problem in dynamic photoelasticity', *Acta Mech.*, 1986, in press.
- (13) ROSSMANITH, H. P. and KNASMILLNER, R. E., 'On the attenuation of detonation stress waves in a plate', Technical University, Vienna, Report ASF 3864, 1984.
- (14) RINEHART, J. S., 'Stress transients in solids', *Hyperdynamics*, 1975 (Santa Fe, New Mexico).
- (15) THEOCARIS, P. S. and STASSINAKIS, C. A., 'The elastic contact of two disks by the method of caustics', *Expl. Mech.*, 1978, **18**, 409-415.
- (16) SHUKLA, A. and NIGAM, H., 'A numerical-experimental analysis of contact stress problems', *J. Strain Analysis*, 1985, **20**, 241-245.

Paper I

Dynamic Load Transfer due to Explosive Loading in Virgin and Damaged Granular Rock Media

by

V. Prakash and A. Shukla
Department of Mechanical Engineering and Applied Mechanics
The University of Rhode Island
Kingston, RI 02881

Abstract

An experimental investigation is conducted to study dynamic load transfer in granular rock media. The granular media is modelled as a one-dimensional chain of disks fabricated from four different types of white Vermont marble. The study mainly focusses on the effect of the microstructure on transient pulse propagation. The transient pulse is generated by exploding a small charge of lead azide on top of the disk assembly. During wave propagation dynamic contact strains are recorded using strain gages. This information is used to calculate wave velocity and attenuation as a function of the cumulative damage in the disk assembly.

Introduction

The response of particulate materials to impulsive loading, has been of substantial interest to both engineers and researchers. The stress wave propagation in such a media, due to explosive loading, depends primarily upon the load transfer process by which the mechanical signals are transmitted. This phenomenon is related to the properties, geometry as well as the microstructural arrangement of the particles in the media. As the stress wave passes through the system rearrangement of the particles takes place. Further, depending upon the amplitude of the stress wave, damage can occur in the particles. Thus the transmitted stress-wave carries along with it the information regarding the microstructural re-arrangements of the grains. The wave propagation characteristics of the resulting media is different as compared to that of the virgin material. Moreover, it has been observed that for real earth materials like sand and rock, this load transfer phenomenon is also a function of the state and the history of the applied load.

The concept of modelling granular media as an array of elastic particles led to the initial attempts at predicting wave propagation through such media. Early work by Iida [1,2], Hughes and Cross [3], Hughes and Kelly [4], Gassman and Brandt [5] employed a normal granular contact force concept. An excellent review by Deresiewicz [6] summarizes both the static and dynamic studies prior to 1958. Experimental studies of the load transfer in granular media have been previously conducted by Drescher and DeJosselin [7] who simulated granular media by using assemblies of circular disks. They studied the static load transfer through the assembly of the disks using photomechanics.

Rossmannith and Shukla [8] extended this idea to the dynamic case with the help of high speed photography. Additional dynamic work was also carried out by Shukla and Damania [9] and Shukla and Zhu [10].

The present paper focuses attention on the wave propagation and load transfer in a single one dimensional chain of disk assembly. The disks were fabricated from four different grades of white Vermont marble each having a different microstructure. The stress wave is generated by exploding a small amount of Lead Azide on top of the disk assembly. The dependence of the stress wave velocity on the microstructure of various grades of marble rocks is studied. Attempt has also been made to investigate and quantify the damage that occurs in these one dimensional aggregate of disks under repeated stress wave loading. Tensile splitting tests are performed to estimate the residual strength of the damaged disks. Photomicrographs are taken at various stages of the shock wave loading process. Moreover, the stress-wave velocity as well as wave attenuation characteristics are obtained as a function of the accumulated damage in the grains.

The results indicate that a correlation exists between the grain size and the stress-wave velocity. It is seen that the average stress-wave velocity is higher for rock disks with larger grain size. Rapid attenuation in the stress wave peak load occurs in the first few disks and then attains a steady rate of decay. The residual tensile strength of the disks first decreases with the applied load and then approaches a limiting value before eventually fracturing. The stress-wave velocity rises considerably and reaches a terminal velocity upon repeated shock wave loading. The photomicrographs taken at various stages of the shock wave loadings indicate that large scale crumbling and pitting takes place near the contact zone. This leads to microcracking and eventual failure of the disks.

Experimental Procedure and Analysis

A series of experiments are conducted using a single chain assembly of disks as shown in Fig. 1. These disks were fabricated from four different cores of Vermont marble having different microstructures as shown in Fig. 2. The disks were 1.25 inches (31.75mm) in diameter and 0.5 inches (12.7mm) in thickness. The assembly of the disks was explosively loaded using 15mg of Lead Azide in a specially designed steel charge holder. The resulting dynamic load transfer phenomenon in the disks was studied using electrical resistance strain gages. In the experiments the wave length of the explosive loading pulse was sufficiently large as compared to the disk diameters, thus resulting in a quasi-static type of loading around the contact zone. Hertz contact theory along with the experimentally obtained strains were used to obtain the contact stresses, strains and the dynamic loads.

From the Hertz contact stress theory, the stress field equations around the contact region of two bodies, as shown in Fig. 3, are represented as:

$$\sigma_{zz} = \frac{-b}{\pi\Delta} \{z(b\phi_1 - x\phi_2) + \beta z^2 \phi_2\} \quad (1)$$

$$\sigma_{xx} = \frac{-b}{\pi\Delta} \left\{ z \left(\frac{b^2 + 2z^2 + 2x^2}{b} \phi_1 - \frac{2\pi}{b} \cdot 3xz\phi_2 \right) + \beta \left((2x^2 - 2b^2 - 3z^2) \phi_2 + \frac{2\pi x}{b} + 2(b^2 - x^2 - z^2) \frac{x}{b} \phi_1 \right) \right\} \quad (2)$$

$$\sigma_{zx} = \frac{-b}{\pi\Delta} \left\{ z^2 \phi_2 + \beta \left[(b^2 + 2x^2 + 2z^2) \frac{z\phi_1}{b} - \frac{2\pi z}{b} \cdot 3xz\phi_2 \right] \right\} \quad (3)$$

where ϕ_1 and ϕ_2 are

$$\phi_1 = \frac{\pi (M+N)}{MN \sqrt{2MN+2x^2+2z^2-2b^2}}$$

$$\phi_2 = \frac{\pi (M-N)}{MN \sqrt{2MN+2x^2+2z^2-2b^2}}$$

$$M = \sqrt{(b+x)^2+z^2} \quad , \quad N = \sqrt{(b-x)^2+z^2} \quad \text{and}$$

$$\Delta = \frac{1}{(A+B)} \left(\frac{1-\nu_1^2}{E_1} + \frac{1-\nu_2^2}{E_2} \right)$$

$$A = 1/4 \left(\frac{1}{R_1} + \frac{1}{R_2} + \frac{1}{R_1'} + \frac{1}{R_2'} \right) +$$

$$\frac{1/4 \sqrt{\left[\left(\frac{1}{R_1} - \frac{1}{R_1'} + \frac{1}{R_2} - \frac{1}{R_2'} \right) \right]^2 - 4 \left(\frac{1}{R_1} - \frac{1}{R_1'} \right) \left(\frac{1}{R_2} - \frac{1}{R_2'} \right) \sin^2 \alpha}}{}$$

$$B = 1/4 \left(\frac{1}{R_1} + \frac{1}{R_2} + \frac{1}{R_1'} + \frac{1}{R_2'} \right) -$$

$$\frac{1/4 \sqrt{\left[\left(\frac{1}{R_1} - \frac{1}{R_1'} + \frac{1}{R_2} - \frac{1}{R_2'} \right) \right]^2 - 4 \left(\frac{1}{R_1} - \frac{1}{R_1'} \right) \left(\frac{1}{R_2} - \frac{1}{R_2'} \right) \sin^2 \alpha}}{}$$

Subscripts 1 and 2 refer to the two bodies making the contact as shown in Fig. 3. R_1 , R_1' , R_2 and R_2' are the principal radii of curvature at the point of contact and α is the angle between the corresponding planes of the principal curvatures. "E" is the modulus of elasticity and ν is the poisson's ratio.

Since the experiments were conducted for the single chain of disks, the contact stress field was defined by only one parameter and that is the contact length, $2b$. For the two-dimensional plane stress problem the contact strains are given by:

$$\epsilon_{zz} = \frac{1}{E} (\sigma_{zz} - \nu \sigma_{xx}) \quad (4)$$

Substituting for σ_{zz} and σ_{xx} from equation (1) and equation (2) and noting that $\beta=0$ (frictionless case for the single chain experiments) the contact strain is obtained as a function of the coordinates (x and z) and the contact length ($2b$). Since the strain gages are mounted normal to the contact point the coordinate " x " is equal to zero. The contact strain is plotted as a function of the normal distance from the contact for different values of ($2b$) as shown in Fig. 4. The location of the strain gage from the contact is known (i.e. " z " is known). Also, the strain at that location is known from the strain gage experiment. Thus by interpolation the contact strain and the contact length can be obtained.

Since the strain gages have a finite size it averages the strain over its grid area. This average strain is not equal to the strain at the grid geometric center. From the plot of the strain vs distance it can be seen that steep gradients in the strain exist near the contact point and the strain profiles peak around $z = 1.0$ mm. As the distance normal to the contact point increases the strain gradients reduce and the strain profiles become fairly

constant after $z = 6\text{mm}$. Thus it is important that the strain gages be placed beyond $z = 6\text{mm}$ so as to minimize the averaging error.

To estimate the error induced due to the averaging effect the percentage error is calculated by considering a strain gage with grid size ($L \times L$) positioned at a height " z " above the contact point. Now, the strain ϵ at the geometric center of the strain gage is calculated from equation 4. To evaluate the average strain the strain gage grid is divided into a matrix of 100×100 points and the strain at each point is evaluated. From this the average strain is computed. The results are presented in Fig 5, which shows the error due to averaging effect as a function of the gage grid length, L . The results are plotted for different heights, z above the contact points. The error is higher for strain gages closer to the contact points because of the steep strain gradients. Also the error increases as the strain gage size increases. For the size and the location of the strain gages used in this study the error is about 2%.

To investigate the relationship between the wave velocity and the size of the grains a one dimensional assembly of disks as described earlier was used. Strain gages were bonded on four separate disks in the chain at a height of 7mm above the contact point. The strain gages were suitably connected to the Nicolet Oscilloscope through bridge amplifiers. When the explosive was fired, the oscilloscope was triggered. Strain as a function of time was recorded. The transit time and the rise time of the gage are small (less than 1 %) as compared to the pulse duration. Also the frequency response of the bridge amplifiers was adequate for the experiments.

To study and quantify the damage induced in the media due to the propagation of the shock waves both the residual strength as well as the wave velocity was computed for the single chain of the disk assembly for repeated loadings. The residual tensile strength was measured by the tensile splitting tests. In these tests the disks fabricated from the cores of different grades of marble were laid vertically between the loading plates of the Instron machine in the compression mode. The load was slowly increased at a very slow-rate until the specimens failed by splitting across the vertical diameter. Assuming linear condition within the core the approximate tensile strength σ_t , was calculated using the equation:

$$\sigma = \frac{2P_{\max}}{\pi DT} \quad (5)$$

where P_{\max} - applied load at failure
D - Diameter of the core
T - Thickness of the specimen

To estimate the residual strength of the damaged rock disks 15 mg of Lead Azide was used to generate the shock wave through the assembly of disks. Tensile splitting test was performed on the first two disks taken out from the top of the assembly. Two new disks were placed on top of the disk assembly to replace the damaged disks. The chain assembly, this time was loaded twice, and again the top two disks were taken out and their residual tensile strength was obtained. This procedure was continued until the residual tensile strength was obtained for the disks which had been shocked six times.

To study the effect of compaction and the damage of the disks on the wave velocity strain gages were bonded on the first, second, fourth and the seventh disks in the chain

assembly. Again, 15mg of lead azide was used to generate the shock wave through the disk assembly. From the peaks of the strain profile the stress wave velocity was computed every time the disk assembly was loaded. This procedure was repeated six times, keeping the location of the strain gages the same, and each time average wave velocity and the stress wave attenuation was computed. This average wave velocity versus the number of times the assembly was loaded was plotted to obtain the variation of the wave velocity as a function of the load history.

RESULTS AND DISCUSSIONS

Wave Velocity in Virgin Rock Disk Assembly

A series of experiments were conducted with strain gages mounted 7mm from the contact point of the disks. Strain versus time plots at the location of the strain gages were recorded. A typical strain gage output profile is shown in Fig. 6. Position of the wave front versus time plots were drawn for marble "A", marble "C" and marble "D" disk assemblies. The average stress wave velocity was computed by drawing a least square fit line passing through the experimental points. The results indicate that the average wave velocity increases with the increasing grain size of the marble. The average grain size of marble "A" was 0.32mm and the stress wave velocity was 1210 m/sec. The grain size of marble "C" was higher and the corresponding stress-wave velocity obtained was 1425m/sec while marble "D" had the largest average grain size and a stress-wave velocity of 1525 m/sec. This trend is to be expected as the stress wave encounters a fewer number of grain boundaries or obstacles as it propagates through the granular rock material having a larger grain size.

To study the attenuation in the three different grades of marble mentioned above the normalized peak strain was plotted against the stress wave propagation distance. As seen from Fig. 7 all the three different grades of marble follow more or less the same pattern of attenuation, but the marble with the smaller grain size shows a higher attenuation. At a given contact the strain increased from zero to a peak value and then gradually decreased to zero. A typical duration of the pulse at the contact was 75 microseconds. The wavelength of the pulse was calculated by taking the product of the average wave speed and the pulse duration at the contact. The wave length obtained was 95 mm (around 4 disk diameter). Due to the internal losses within the disk, energy spent in closing the contact and some frictional and reflection effects, the peak contact loads dropped as the distance from the explosive loading was increased. Using the values of the normalized peak strains it is seen that a rapid attenuation in peak strain occurs as the wave propagates through the first contact. After this the decay in peak load is gradual with distance and attenuates to 25% of its peak value in the next nine disks.

The tensile splitting tests were performed on all the four different grades of virgin marble disks. Table "A" lists the tensile failure strength of the four disks. Results indicate that marble "C" had the highest tensile strength of 1440 N/m² while marble "D" had the lowest tensile strength of 930N/m². Marble "A" and marble "B" had almost similar tensile strengths of 1145N/m² and 1125N/m² respectively.

WAVE PROPAGATION IN DAMAGED ROCK DISKS

To quantify damage occurring in the rock disks, tensile splitting tests were carried

out to obtain the residual tensile strength. The tensile strength of the first two disks was only determined since most of the attenuation in stress waves occurs in these disks. Table B lists the residual tensile strength of the first two disks as a function of the number of times the assembly was loaded. It is observed that after the passage of the first shock wave the residual strength of the first disk falls down to almost 40% of its value in the virgin state. Additional drop of 10 percent in the tensile strength occurs when the second loading wave passes through the disk assembly. The residual strength remains fairly constant as the number of stress-wave loadings are increased further and eventually the disk fails by fracturing across the surface.

The tensile strength of the second disk in the assembly drops down by only 10% after the first two stress waves. This happens because the cumulative damage occurring in the second disk is small as compared to the first disk as the peak stress value attenuates to almost 60% by the time the stress wave propagates one disk diameter. As the number of shock wave loading is increased further the residual strength remains fairly constant until the fourth loading wave after which the tensile strength falls to 72% of the tensile strength value in the virgin state.

Next, the amount of explosive was gradually increased and its effect on the residual tensile strength studied. The results are shown in Table C. When 15 mg of lead Azide was used the tensile strength of the second disk falls down to 95% of its value in the virgin state after the passage of one shock wave. When the charge is increased to 20mg the tensile strength falls down to 90%. As the explosive charge is increased to 50mg the tensile strength drops considerably to 55%. In case of 20mg, 40mg and 50mg of lead Azide the first disk failed by fracturing across the surface. It is observed from all the experiments that the residual tensile strength of the disks approaches a limiting value of 650N/m^2 after which upon repeated loading the disk fractures.

The average wave velocity in the chain was calculated as a function of repeated explosive loading to study the effect of the cumulative damage on the wave velocity. Fig. 3 shows the plot of the average wave velocity as a function of the number of loading waves. The stress wave velocity is seen to increase considerably after the passage of first loading wave. The stress wave velocity increases to 1400m/sec from 1080m/sec which is the velocity obtained by loading the undamaged disk chain assembly. As the number of stress wave loadings is increased further the wave velocity undulates about the terminal velocity of 1450m/sec and eventually falls down considerably as the cumulative damage increases and fractures the disk. The increase in wave velocity with increased number of stress wave loading is a result of the compacting process by which the disks come closer to each other thus increasing the resultant stiffness of the disk chain assembly. This also results in closing of the preexisting voids and microcracks in the disks. The surface cracks impede the progress of the stress-wave as it has to travel around these cracks. Thus the compactive process reduces the transit time of propagation of stress waves resulting in an increase in velocity.

As the number of shock wave loadings is increased damage occurs around the contact zone due to high contact stresses and large scale crumbling and pitting is observed near the contact zone. Figure 9 shows the photomicrographs of the area near the contact zone of the disks after the passage of the first two stress waves. The stress wave velocity reaches a

terminal velocity at this stage. Upon repeated loading the microcracks grow and engulf the entire contact zone. These microcracks combine together to create open cracks on the disk surface as shown in photomicrograph in Fig. 10. This microcracking of the contact zone lowers the stiffness of the assembly and the cracks impede the propagation of the stress wave and hence lower the stress wave velocity.

CONCLUSIONS

Dynamic strain gage technique is employed to study wave propagation and dynamic load transfer in granular rock media. The granular rock media was modelled as a one dimensional array of circular disks fabricated from different grades of Vermont marbles having different microstructures. The dynamic data was analyzed to obtain average wave velocity, stress wave attenuation for both virgin as well as damaged rock media. The residual strength of the rock disks was estimated after the passage of the stress wave using tensile splitting tests. The damage in the disks was studied by taking optical micrographs of the disk surface. The results indicate that:

1. A correlation exists between the microstructure of the rock material and the stress wave velocity. Larger the grain size of the rock media higher is the stress-wave velocity.
2. Rapid attenuation in the peak contact loads, and thus the amplitude of the stress wave, takes place initially as the wave propagates through the granular rock media and then approaches a steady rate of decay. It is observed that the stress wave attenuation decreases as the average grain size of the marble increases.
3. The stress wave velocity increases sharply after the passage of the first shock wave. Upon repeated explosive loading the stress-wave velocity approaches a terminal velocity and eventually falls off as the disk fails by fracturing across the surface.
4. The residual tensile strength of the disk decreases as the number of shock waves are increased. Further, a limiting residual strength value exists which remains fairly constant upon repeated loading until the disk fractures.

Acknowledgements-

The authors would like to acknowledge the support of the Army Research Office under grant no. DAA L03-86-K-0125.

References

1. Iida, K., "Velocity of Elastic Wave in Sand", Bulletin Earthquake Research Institute, Volume 17, 1939, pp. 783-807.
2. Iida, K., "Velocity of Elastic Waves in a Granular Substance", Bulletin Earthquake Research Institute, Japan, Volume 27, 1949, pp. 11-16.
3. Hughes, D.S. and Gross, J.H., "Elastic Wave velocities at High Pressures and Temperatures", Geophysics, XVI, 1951, pp 577-593.
4. Hughes, D.S. and Kelley, J.L., "Variation of Elastic Wave Velocity with saturation in Sandstone", Geophysics, XVII, 1951, pp 739-752.
5. Grossman, F., "Elastic Waves through a packing of Spheres", Geophysics, XVI, 1951, pp 673-685.
6. Deresiewicz, H., "Mechanics of Granular Media", Advances in Applied Mechanics, V, Academic Press Inc., 1958.
7. Drescher, A. and DeJosselin de Jong G., "Photoelastic Verification of a Mechanical Model for Flow of Granular Material", J. Mech. and Physics of Solids, 20, pp 337-351, 1972.

8. Rossmannith, H.P. and Shukla, A., "Photoelastic Investigations of Dynamic Load Transfer in Granular Media", Acta Mechanica, 42, pp 211-225, 1982.
9. Shukla, A. and Damania, C., "Experimental Investigations of Wave velocity and dynamic contact stresses in an assembly of disks", Experimental mechanics, Vol 27-number 3, pp 268-281, 1987.
10. Shukla, A. and Zhu, C.Y., "Influence of the Microstructure of Granular media on Wave Propagation and Dynamic Load Transfer", J. of Wave Material Interaction, vol. 3, No. 3.

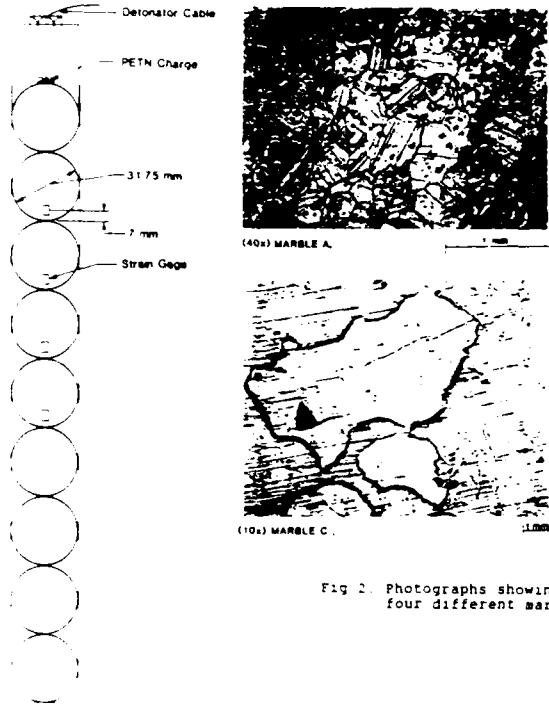


Fig 1. A single chain assembly of disks.

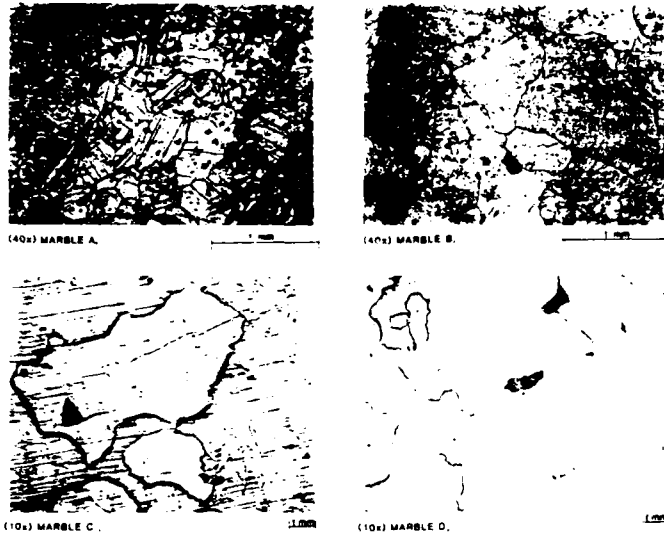


Fig 2. Photographs showing the microstructure of the four different marbles.

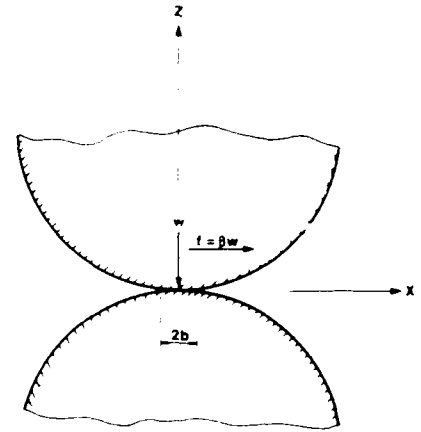


Fig 3. Schematic of the two bodies in contact.

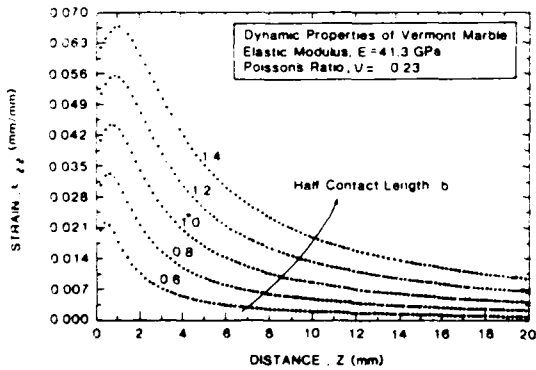


Fig 4. Contact strain as a function of the normal distance.

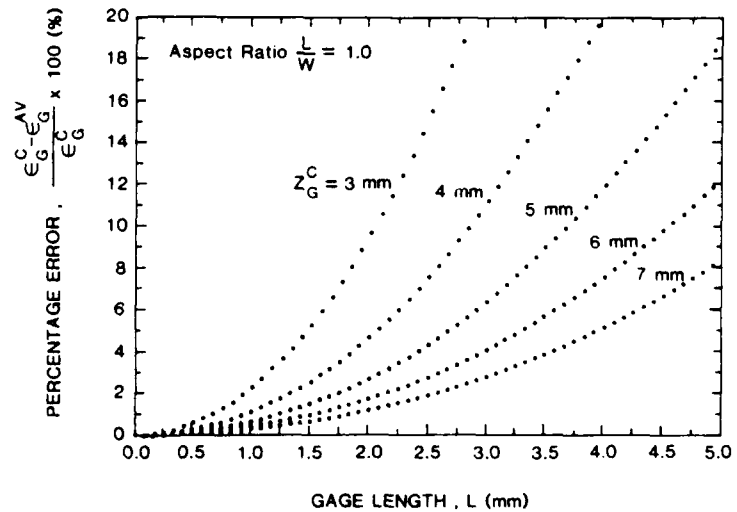


Fig 5. Averaging error as a function of the strain gage size.

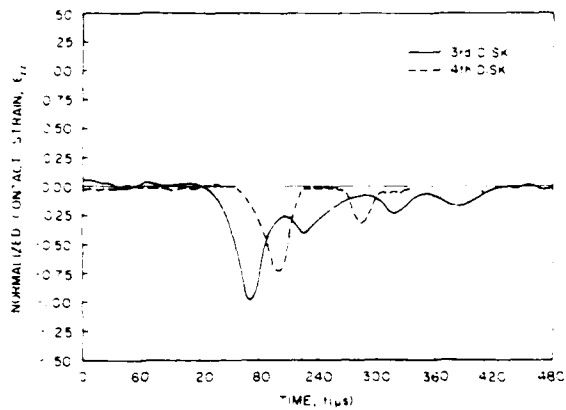


Fig 6. A typical strain profile obtained during experiment.

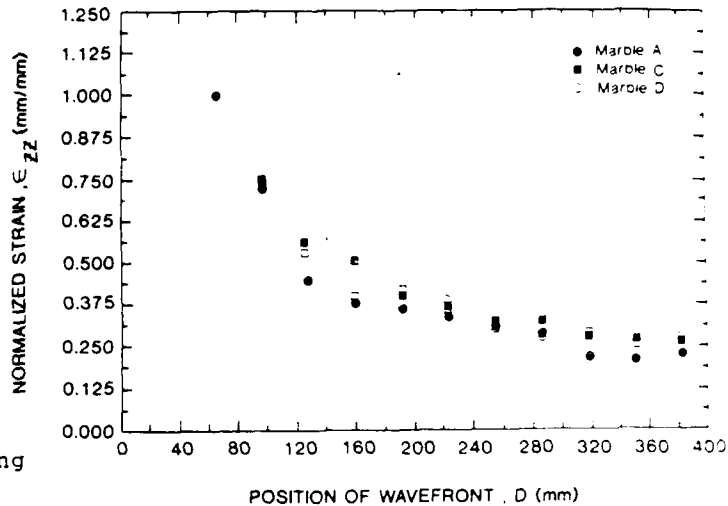


Fig 7. Normalized peak strain as a function of position from explosion.

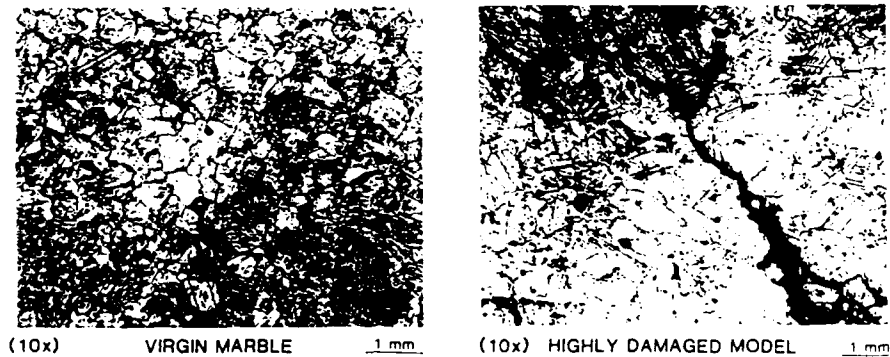


Fig 9. Damage as a result of stress wave propagation.

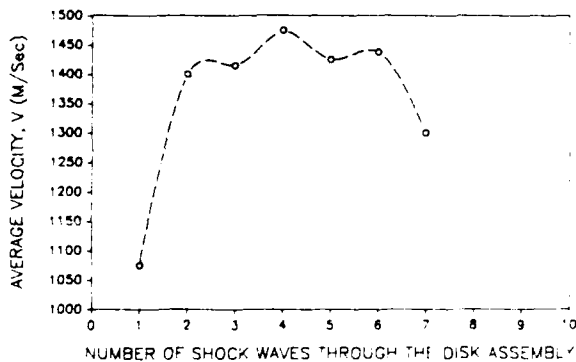


Fig 8. Change in wave velocity with repeated loading

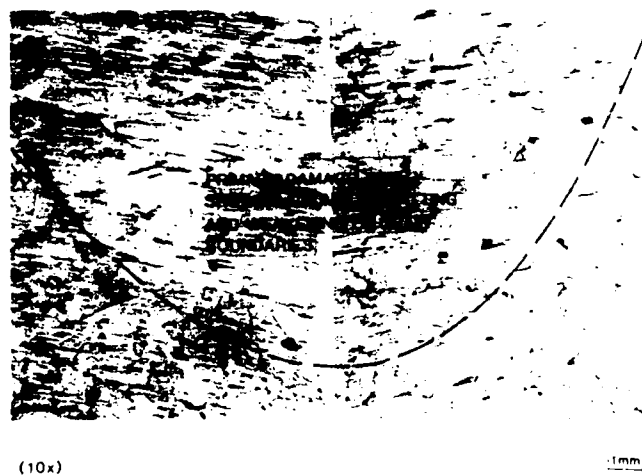


Fig 10. Photomicrograph showing damage near the contact zone.

TABLE A

TENSILE STRENGTH (N/m²) OBTAINED FROM TENSILE SPLITTING TEST

ROCK TYPE	1	2	3	4	AVERAGE STRENGTH
MARBLE A	1130	1040	1180	1180	1114
MARBLE B	1280	1020	1170	1070	1125
MARBLE C	1460	1540	1380	1385	1441
MARBLE D	800	1140	1120	670	932

TABLE B

NUMBER OF TIMES THE SHOCK WAVE PASSED THROUGH THE DISK CHAIN ASSEMBLY (15 mg OF LEAD AZIDE)	DISK NUMBER	RESIDUAL TENSILE STRENGTH (N/m ²)
1	1	610
	2	1160
2	1	610
	2	980
3	1	640
	2	1030
4	1	FRACTURED
	2	1030
5	1	670
	2	690

TABLE C

LEAD AZIDE (mg)	RESIDUAL TENSILE STRENGTH (N/m ²)	
	DISK #1	DISK #2
15	610	1160
20	fractured	1070
40	fractured	780
50	fractured	653